Metal-organic Frameworks as Drug Delivery System for Cancer Therapy

Von der Fakultät für Chemie und Mineralogie

der Universität Leipzig

genehmigte

D I S S E R T A T I O N

zur Erlangung des akademischen Grades

DOCTOR RERUM NATURALIUM

(Dr. rer. nat.)

vorgelegt

von

M.Sc. Rafaella Lima de Meneses Precker

geboren am 06.03.1986 in Campina Grande – PB, Brasilien

Angenommen aufgrund der Gutachten von: Prof. Dr. Evamarie Hey-Hawkins

Prof. Matti Haukka

Tag der Verleihung 28. Juni 2022

The practical part of this thesis was carried out from July 2015 to March 2020 at the Institute of Inorganic Chemistry, Faculty of Chemistry and Mineralogy of Leipzig University under the kind supervision of Prof. Dr. Dr. h.c. mult. Evamarie Hey-Hawkins.

Physical adsorption measurements were carried out by the author, at the Solution Chemistry of Advanced Materials and Technologies - SCAMT institute at ITMO University, in Saint Petersburg, Russia. The 3D samples were produced by the author, at the department of chemistry of Jyväskylä University, in Jyväskylä, Finland.

This thesis is written in the style of a monograph dissertation and parts of it have been published.

V. V. Vinogradov *et al.*, "Composites based on heparin and MIL-101(Fe): The drug releasing depot for anticoagulant therapy and advanced medical nanofabrication," *J. Mater. Chem. B*, vol. 6, no. 16, pp. 2450–2459, 2018, doi: 10.1039/c8tb00072g.

E. Lahtinen, R. L. M. Precker, M. Lahtinen, E. Hey-Hawkins, and M. Haukka, "Selective Laser Sintering of Metal-Organic Frameworks: Production of Highly Porous Filters by 3D Printing onto a Polymeric Matrix," *ChemPlusChem*, vol. 84, no. 2. pp. 222–225, 2019, doi: 10.1002/cplu.201900081.

A. Valente, R. L. M. Precker, and E. Hey-Hawkins, "Inorganic Polymers for Potential Medicinal Applications," *Smart Inorganic Polymers*. pp. 243–276, Apr. 22, 2019, doi: 10.1002/9783527819140.ch9
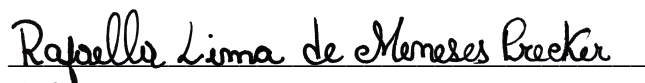
Selbständigkeitserklärung

Hiermit erkläre ich, die vorliegende Dissertation selbstständig und ohne unzulässige Hilfe angefertigt zu haben. Ich habe keine anderen als die im Literaturverzeichnis angeführten Quellen genutzt und sämtliche Textstellen, die wörtlich oder sinngemäß aus veröffentlichten oder unveröffentlichten Schriften entnommen wurden, sowie alle Angaben, die auf mündlichen Auskünften beruhen, als solche kenntlich gemacht. Ebenfalls sind alle von anderen Personen bereitgestellten Materialien oder erbrachten Dienstleistungen als solche gekennzeichnet. Unterstützungsleistungen bei der Auswahl und Auswertung des Materials, sowie bei der Erstellung der Manuskripte habe ich von Frau Prof. Dr. Dr. h.c. mult. E. Hey-Hawkins (Universität Leipzig) erhalten. Ich versichere, dass außer den in der Danksagung genannten Personen bei der geistigen Herstellung der vorliegenden Arbeit keine weiteren Personen, insbesondere kein Promotionsberater, beteiligt waren und dass weder unmittelbar noch mittelbar geldwerte Leistungen an Dritte vergeben wurden. Die vorgelegte Arbeit ist weder im Inland noch im Ausland in gleicher oder ähnlicher Form einer anderen Prüfungsbehörde zum Zweck einer Promotion oder eines anderen Prüfungsverfahrens vorgelegt worden. Ich habe keine früheren erfolglosen Promotionsversuche unternommen.

Leipzig, den 23.02.2022

Rafaella Lima de Meneses Precker

Bibliographische Beschreibung

Lima de Meneses Precker, Rafaella

Metal-organic Frameworks as Drug Delivery System for Cancer Therapy

Universität Leipzig, Dissertation

135 Seiten, 304 Literaturzitate, 95 Abbildungen, 9 Tabellen

Zusammenfassung

Die Forschung an porösen Hybridmaterialien hat sich rasch entwickelt, und in letzter Zeit ist die Anzahl neuer Strukturen und Zusammensetzungen aufgrund ihrer vielfältigen Anwendungsmöglichkeiten im Bereich des Kristall-Engineering von großem Interesse. Metall-organische Gerüste (metal-organic frameworks, MOFs) sind eine aufstrebende Klasse von Nanomaterialien, deren Eigenschaften durch Variation der Bausteine, die aus Metallionen und organischen Liganden bestehen und sich koordinativ zu einer dreidimensionale Struktur verbinden lassen, leicht angepasst werden können. Eigenschaften wie eine große Oberfläche und eine hohe Porosität verleihen diesen Materialien vielversprechende Eigenschaften, um als Wirtsmaterial verwendet zu werden.

Die vorliegende Arbeit konzentriert sich auf die Synthese der Verbindung $[Fe_3O(H_2O)_2(OH)(bdc)_3]n$ (bcd = 1,4-Benzoldicarboxylat; MIL-101(Fe), MIL = Materials of Institut Lavoisier), die aus einem carboxylato-verbrückten, oxido-zentriertem, dreikernigen Fe^{3+}-Komplex besteht. Die Struktur besitzt große Poren (Ø: 29 und 34 Å) und eine große Oberfläche mit der Fähigkeit, zahlreiche Moleküle einzuschließen. In der vorliegenden Arbeit wird MIL-101(Fe) als Arzneimittelabgabesystem verwendet.

Curcumin, Capecitabin und 5-Fluorouracil (5-FU) wurden als Modellarzneimittel für die Verkapselung in der MIL-101(Fe)-Struktur ausgewählt. Es wurden verschiedene Freisetzungsregime in unterschiedlichen biologischen Medien untersucht.

Nach vielversprechenden ersten Ergebnissen bei der Freisetzung dieser Medikamente aus der MIL-101(Fe)-Struktur wurde anschließend die selektive Lasersintertechnik (SLS) verwendet. Die SLS ist ein additives Schichtbauverfahren, das sich in dieser Arbeit als ressourcenschonende Technologie für die schnelle Herstellung erwiesen hat. Die Möglichkeit, die Größe, Form und Geometrie der hergestellten Proben individuell anzupassen, bot die Gelegenheit, die Wirkstofffreisetzung zu modulieren und den Freisetzungszeitraum zu verlängern.

Abstract

The field of porous hybrid materials has grown rapidly; recently the number of new structures and compositions are of great interest in the crystal-engineering field, due to their various possible applications. Metal-organic frameworks (MOFs) are an emerging class of nanomaterials, whose properties can be easily adjusted by varying the molecular building blocks, obtained from metal ions and organic ligands that can be combined to three-dimensional structures. Properties such as high surface area and high porosity give these materials promising characteristics to be used as host materials.

The present work focuses on the synthesis of $[Fe_3O(H_2O)_2(OH)(bdc)_3]_n$ (bcd = 1,4-benzenedicarboxylate; MIL-101(Fe), MIL = Materials of Institut Lavoisier), composed of carboxylate-bridged, oxido-centered, trinuclear Fe^{3+} complexes. The iron-based structure features large pore sizes (Ø: 29 and 34 Å) and high surface area with the ability to encapsulate numerous molecules, for use as a drug delivery system in the present work.

The curcumin, capecitabine, and 5-fluorouracil (5-FU) were chosen as model drugs for the encapsulation into the MIL-101(Fe) structure. Different delivery regimes were studied in different biological media.

After promising initial results with the release of these drugs from the MIL-101(Fe) structure, the selective laser sintering technique (SLS) was introduced subsequently. The SLS is an additive layer manufacturing technique that has emerged in this work as a resourceful technology for rapid manufacturing, the possibility to customize the size, shape, and geometry of the manufactured samples, thus providing the opportunity to modulate the drug release extending it for even longer periods of time.

Acknowledgements

To *Angela, Daniel, Divine, Reinhard, Robert, Toni and Sebastian* for their friendly and musically lively laboratory atmosphere.

To *Dr. Minghui Cong, Dr. Gizem Kahraman, and Liridona Useini* for their kindness and friendship, making the daily work cheerfully and lightened.

To Bogdan, Carlos, Elisabete, Gabriel, Indira, Katia, Lennart, Lukas, Mahsa, Marcela, Mariana, Mattias, Patrick, Thiago, Pedro, Suelyn for their friendship, love, and support during my Ph.D. time. I am a very lucky person to be able to call them friends, our time together in Leipzig are memories that I will always carry with me.

To my husband, Christian Precker who throughout our years together has always been one of my greatest supporters to reach further in my career, it is a great pleasure and honor to be able to share a life with you, especially now that we are welcoming our daughter.

My family, especially my parents and my siblings for their lifelong support, even from afar they made themselves present with their unconditional love and support.

Additionally, I would like to thank my husband's family, especially Antonia, Axel, Monika, and Sebastian for receiving me with open arms and making me feel that I also had a family here in Germany.

To my Family

Table of Contents

Chapter 1: Inorganic Polymers for Potential Medicinal Applications

1.1 Introduction

Although remarkable progress has been made in understanding the fundamental biology behind many diseases, major advances in their treatment are still to be made. The poor pharmacokinetics, the use of high drug concentrations, the non-specific drug distribution and the rapid metabolism led to an effort to develop suitable drug delivery systems. The drug delivery systems can be defined as a combination of technologies and methods for transporting a medicament throughout the body to a specific target, reducing undesirable side effects of their actions. Thus, they can be very useful in terms of improving the therapeutic efficiency of certain drugs.

This chapter gives an overview on the use of metal-organic frameworks (MOFs) in medicinal applications, mainly drug delivery, specifically addressing problems pertaining to instances when drugs must be administered in high concentrations and presenting possible solutions by developing systems that can modulate or prevent a faster release.

1.2 Emerging and Potential Applications for Metal-Organic Frameworks for Drug Delivery

MOFs are an emerging class of self-assembled nanoporous materials; their properties can be readily tuned by varying the molecular building blocks. Combining the properties of porous materials with the benefits of nanostructures is expected to improve the performance of the classical bulk crystalline MOFs, first reported by Yaghi in 1999.[1]

The design and construction of inorganic–organic hybrid framework materials are currently of great interest in the fields of crystal engineering and supramolecular chemistry, not only for their intriguing topological architectures, but also due to their potential applications in many fields that will be discussed in more details in the subsequent sections.

In the past decade, interest in ordered porous hybrid materials for medicinal applications has been growing very rapidly, not only as a result of the still increasing number of new structures and compositions (Figure 1.1), but also due to the significant efforts that have been undertaken to introduce new or optimized functionalities. For example, by functionalizing the organic linkers in MOFs with groups such as $-Br$, $-NH_2$, $-OC_3H_7$, $-OC_5H_{11}$, $-C_2H_4$ and $-C_4H_4$, demonstrating that its pore can be expanded with the long molecular struts biphenyl, tetrahydropyrene, pyrene, and terphenyl varying from 3.8 to 28.8 Å. [2]–[4]

Furthermore, inorganic and organic nanoparticles with sizes ranging from a few nanometers to several hundred nanometers are promising candidates for biomedical applications, such as active tumor targeting. Advantageous features are their adjustable size, a chemical surface adaptable to biochemical purposes, improvements

in terms of biocompatibility, possibility of high drug loading rates, kinetically controlled drug release, enhanced accumulation, and high permeability and retention effect.[5], [6]
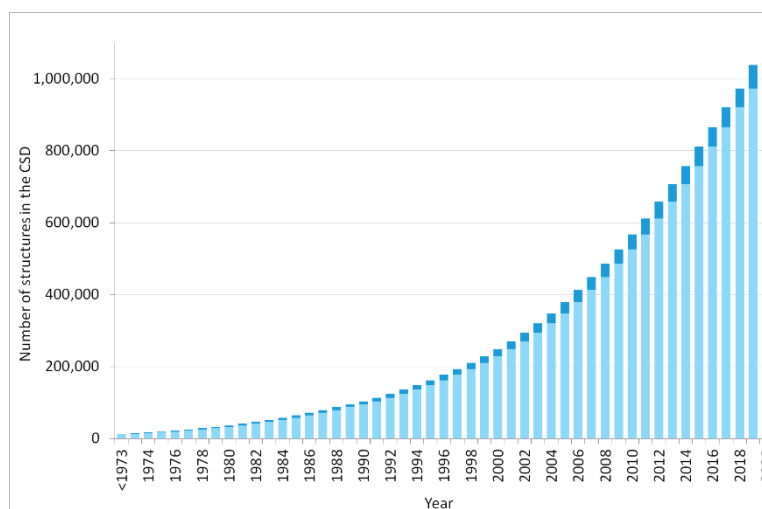
Figure 1.1. Metal-organic framework structures (1D, 2D, and 3D) reported in the Cambridge Structural Database (CSD) from 1970 to 2020.[7]

1.2.1 Metal-Organic Frameworks (MOFs)

MOFs[5] are a class of hybrid materials consisting of metal ions or clusters and bridging organic ligands (linkers) that form highly porous three-dimensional structures (Figure 1.2).[8]–[11] The high porosity (up to 90% of the crystal volume)[4] and high surface area (up to several thousand $m^2 \cdot g^{-1}$) of MOFs are highly interesting from a nanotechnological viewpoint.

These highly porous structures with pore diameters of up to 48 Å have promising applications, such as host materials for gas storage (H_2/CH_4),[1], [8], [12]–[15] adsorption and separation of molecules,[15] in catalysis [2], [16], and in the controlled release of drugs.[3], [5], [6], [17]–[22]
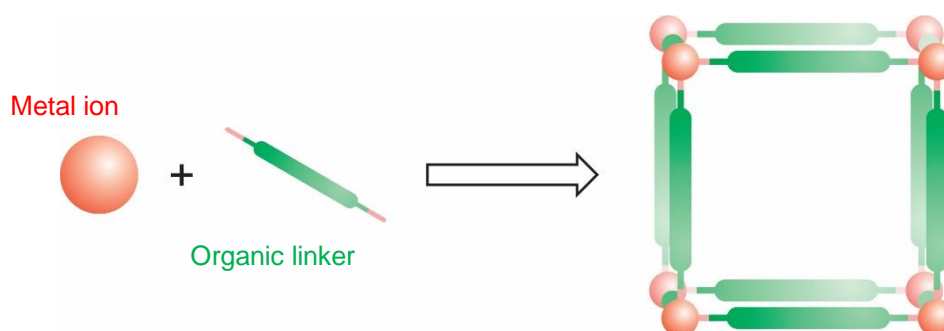
Figure 1.2. Simplified formation of a three-dimensional network through metal ions and organic linkers (only a section of the 3D network is shown).

As compared to inorganic systems, for example mesoporous silica and silicon that can deliver drugs in a more controlled manner due to their ordered network and porosity but have a limited load capacity, one of the advantages of MOFs is the possibility to adjust pore sizes and functional groups in the frameworks.[8], [19], [20], [22]–[28]

Primary Building Units

Metal ions and organic linkers used in the synthesis of MOFs are considered to be "primary building units". Transition metals are versatile connectors for building MOFs.

The transition metals commonly incorporated are Cr^{3+}, Fe^{3+}, Cu^{2+}, and Zn^{2+}; some alkaline and alkaline earth metal ions have also been used.[29], [30] Depending on the metal and the oxidation state, coordination numbers range from 2 to 7, giving rise to various geometries, such as linear or V shaped, T or Y shaped, square planar, tetrahedral, square pyramidal, or octahedral, which play an important role in targeting the diverse repertoire of MOF structures (Figure 1.3).[31]

Nº of functional sites	Connectors		Linkers	
2				
3				
4				
5				
6				
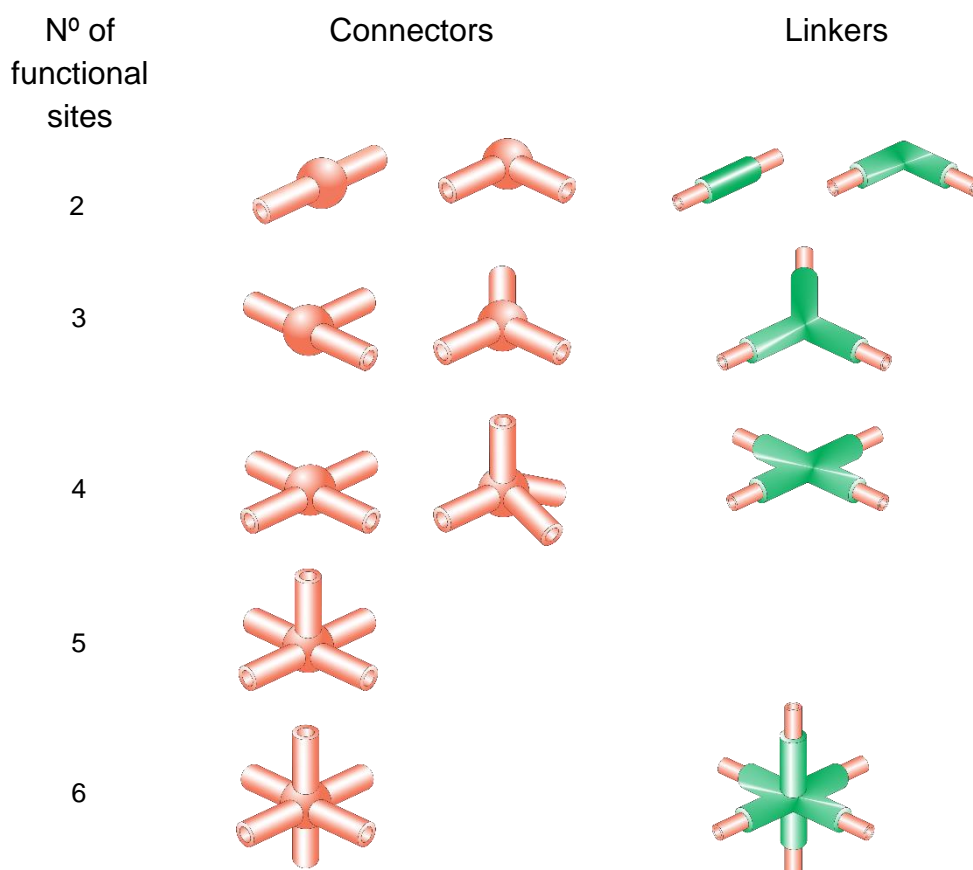
Figure 1.3. Examples of coordination geometries of metal ions; the corresponding numbers are related to the number of functional sites.

The organic ligands used in the construction of MOFs usually contain a functional group for coordination, such as carboxylate, phosphate, sulfonate, amine, or nitrile. (Figure 1.4) presents examples of these commonly used linkers. The ligand design can also improve the efficacy of the drug delivery system. Selective binding to targeted tissues can cause a conformational change, resulting in drug release. For example, the surface engineering method may improve the targeting, solubility or biodistribution of the drug delivery systems.[6], [32], [33]
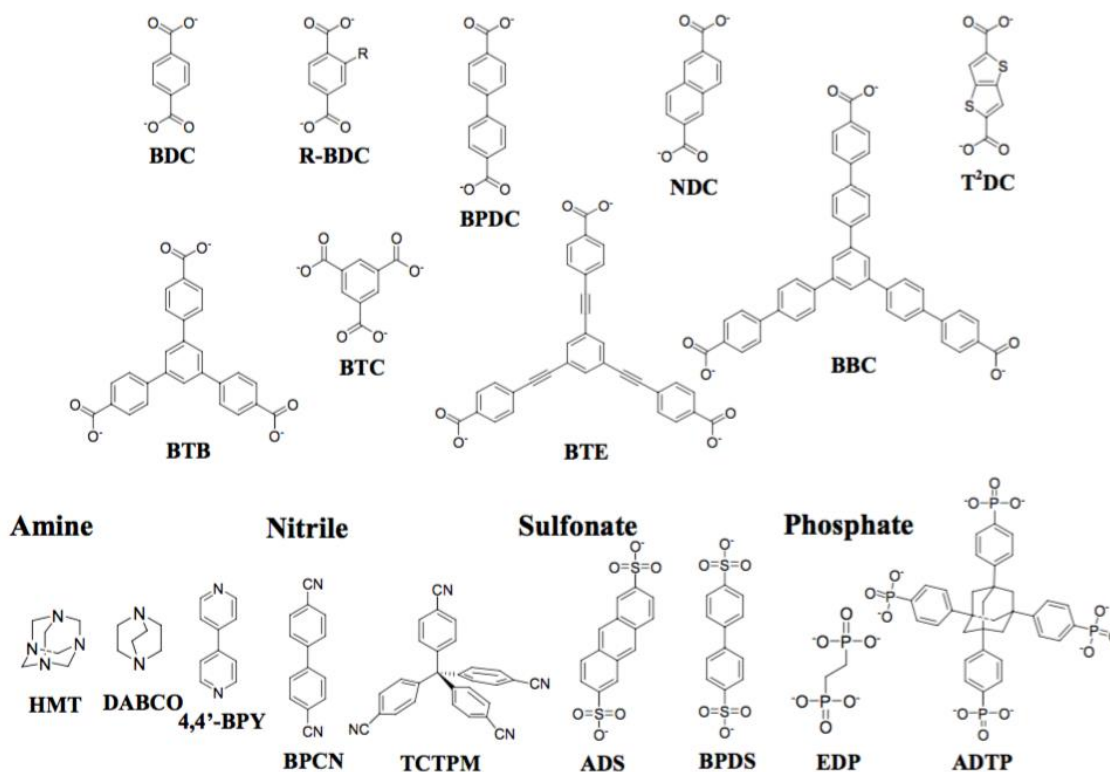
Figure 1.4. Examples of linkers used for the construction of MOFs.[31]

Secondary Building Units (SBU)

The secondary building units (SBUs) have intrinsic geometry, which plays an important role in view of the MOF topology. Some examples of geometries are shown in (

Figure 1.5). In 2009, Yaghi et al. described in detail the variety of SBU 131 geometries , which provides ample options for the design of MOF structures.[34] The MOFs built from SBUs exhibit a high structural stability. Metal-carboxylate bonds cause rigidity of these structures that is responsible for the thermal and chemical stability of the frameworks.[13], [35], [36]
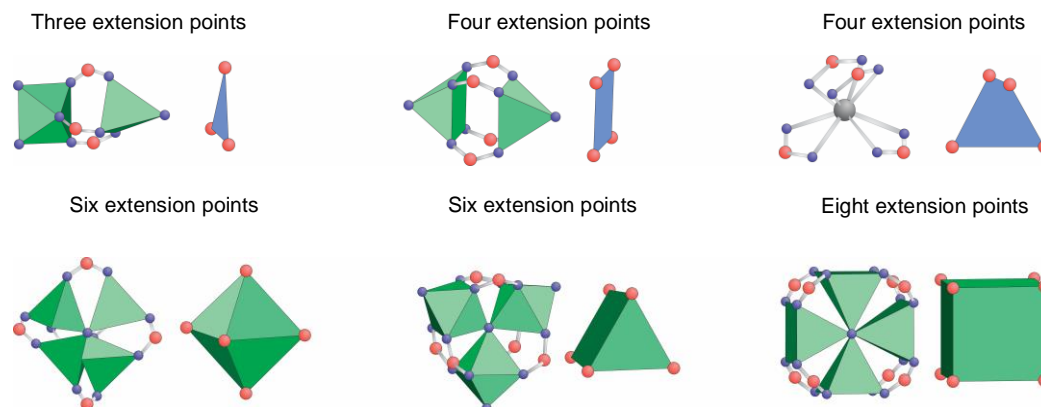
Figure 1.5. Examples of secondary building units. Atom labeling scheme: C (red), O (blue), metals (green polyhedral), H atoms are omitted for clarity.

1.2.2 MOF synthesis

The process of MOF synthesis relies on many parameters, such as compositional, for example, molar ratios of the starting materials, pH, and solvent, and process parameters, such as reaction time, temperature and pressure.[37] In addition to conventional methods for obtaining MOFs (hydro/solvothermal) other techniques have recently been developed to facilitate the crystal formation with adjustable sizes.

Hydro/Solvothermal synthesis

The most prevailing synthesis is based on the solvo- or hydrothermal method. High-throughput solvothermal syntheses are a powerful tool to accelerate the discovery of new MOF structures and to optimize synthesis protocols.[38] A large number of reported structures, such as MIL-88, their three-dimensional framework is constructed from trimers of oxocentered iron(III) octahedra and dicarboxylate aliphatic or aromatic linkers MIL-100 composed of iron(III) carboxylate or chromium (III) linked by 1,3,5-BTC = benzene tricarboxylic or trimesic acid, MIL-101 (chromic chloride hexahydrate or iron(III) chloride hexahydrate linked by H_2BDC = terephthalic acid), were produced through this technique that usually requires a longer reaction time, since some methods for obtaining crystals may vary from days to weeks, providing considerable yields at the end of the reactions.

In this method, the mixture of metal salt, ligand and solvent are placed into a teflon vessel (Figure 1.7a), sealed in an autoclave (Figure 1.7b) and heated at a specific temperature under pressure above 1 atm. According to Rabenau, the term solvothermal reactions can be defined as reactions taking place in closed vessels under autogenous pressure above the boiling point of the solvent.[37], [39] (Figure 1.6) shows an example of the solvothermal or hydrothermal synthesis of MOFs.[38]
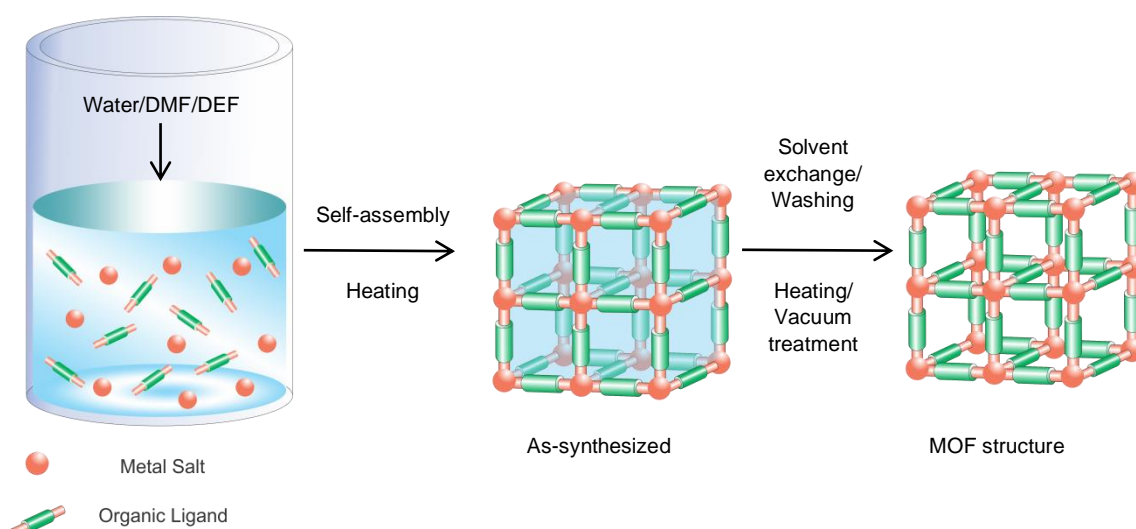
Figure 1.6. Metal-organic framework formation through solvothermal/hydrothermal synthesis; DMF = dimethylformamide; DEF = diethylformamide. Inspired by ref. [38].

Figure 1.7. (a) Teflon containers used in the synthesis of MOFs. (b) Stainless steel containers (autoclaves) used in the synthesis of MOFs.

Microwave-assisted synthesis

The microwave-assisted synthesis is another alternative for preparing MOFs. This technique is widely applied under hydrothermal conditions, due to its short reaction times. (Figure 1.8) shows an example. The starting materials are placed into a vessel, sealed and heated for an appropriate time at a specific temperature; the heat is generated internally within the reaction media by dielectric heating. Advantages of this method are a facile morphology control, phase selectivity and narrow particle size distribution. In energetic terms, this technique is more efficient when compared to the solvothermal method, but on the other hand does not always promote crystal growth where the single crystals have sufficient size for X-ray analysis.[38][40] The Zr-based MOFs, UiO-66 ($Zr_6(OH)_4O_4(BDC)_6$, BDC = benzene-1,4-dicarboxylate), on the other hand UiO-67 is obtained using the longer 4,4'-biphenyl-dicarboxylate (BPDC), are an example of structures prepared using this method. More recently, Taddei et al. optimized the synthesis of UiO-66 employing the microwave-assisted method.[41]
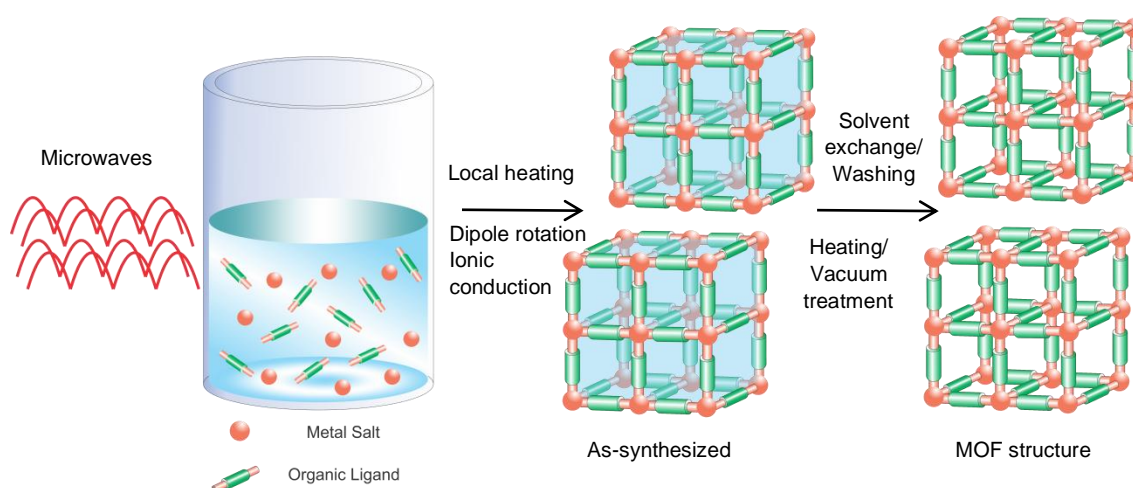
Figure 1.8. Microwave-assisted synthesis of MOFs. Inspired by ref. [38].

Sonochemical synthesis

In this synthesis procedure, the reaction takes place upon application of high-energy ultrasound to a reaction mixture. The sonochemical synthesis provides unusual reaction conditions, short duration of extremely high temperatures and pressures in liquids, that could not be achieved by other methods.[42] In this method, a mixture of

the metal salt, ligand and solvent is placed into a horn-type pyrex reactor fitted to a sonicator bar with an adjustable power output without external cooling. When the liquid is irradiated with ultrasound, the alternating expansive and compressive acoustic waves form bubbles in the acoustic cavitation that accumulate ultrasonic energy while growing and collapsing in a very short lifetime (Figure 1.9). Producing temperatures around ~5000 K and pressures around 987 atm , the energy is then dispersed to the surroundings, so the gas temperature in the hot spot quickly returns to the ambient value, therefore resulting in an extreme fast heating and cooling rates $>10^{10}$ K.s^{-1}, forming fine crystallites.[38][42] Li et al. reported the environmentally friendly synthesis of copper-based MOF with 1,3,5-benzenetricarboxylic acid as a ligand, HKUST-1 using the sonochemical method. Structures like MOF-5 ($Zn_4O(BDC)_3$, where BDC^{2-}=1,4-benzodicarboxylate) with high quality crystals ranging from 5-25 µm were obtained within 30 min through this method.[43][44]
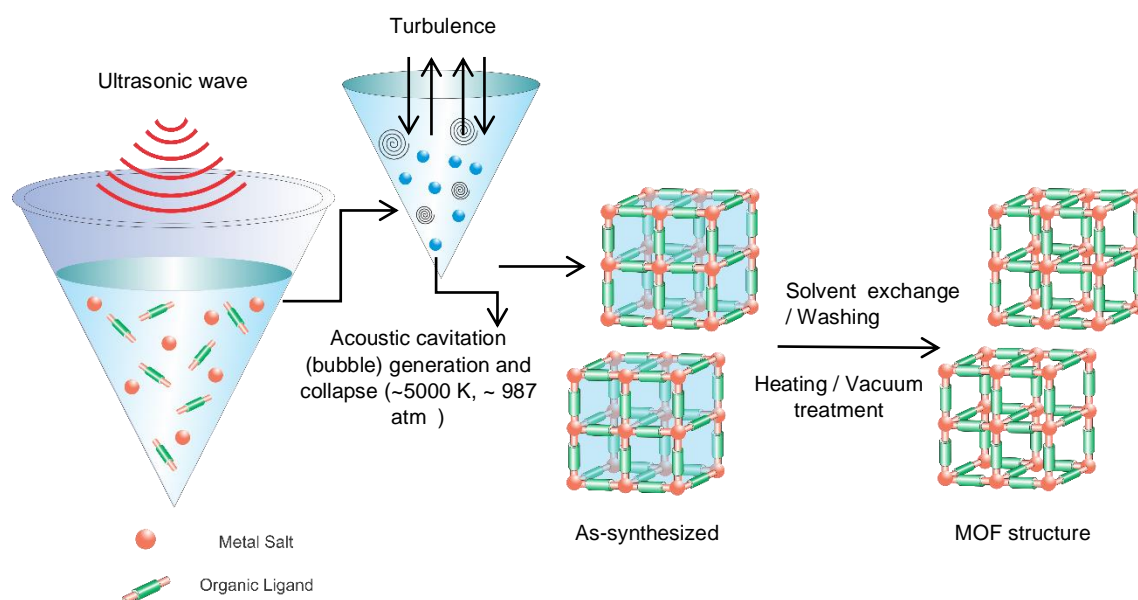
Figure 1.9. Sonochemical synthesis of MOFs. Inspired by ref. [38].

Electrochemical synthesis

First reported in 2005 by researchers at BASF,[45] rather than using metal salts, the metal ions are introduced through anodic dissolution to the reaction medium containing the dissolved ligand molecules and a conducting salt (Figure 1.10). The metal deposition on the cathode is prevented using protic solvents, although during the process resulting in the formation of H_2. Other alternatives could be the use of compounds like acrylonitrile, acrylic or maleic esters, that are preferentially reduced.[37] The advantage of this method compared to the solvothermal process are the reaction conditions. Reactions can be usually performed at ambient temperature and pressure, with short reaction times such as 2 hours and low energy consumption, combined with a simple operation where no special equipment is required.[37], [46]
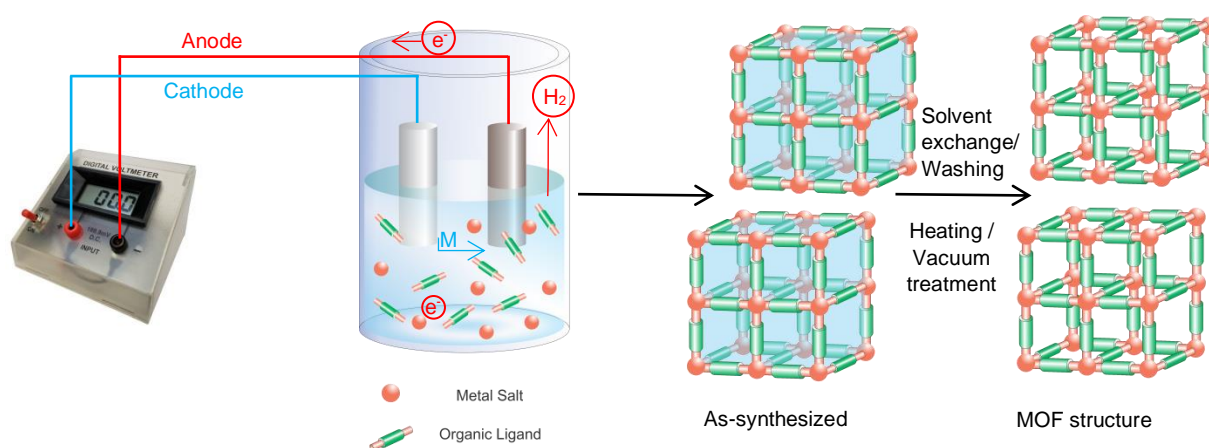
Figure 1.10. Electrochemical synthesis of MOFs. Inspired by ref. [38].

Mechanochemical synthesis

First reported in 2006, the mechanochemical synthesis sustained by mechanical force has been recently introduced as an alternative for synthesizing MOFs (Figure 1.11). This is a solvent-free process with a mechanical breakage of intramolecular bonds followed by a chemical transformation. The possibility to avoid organic solvents, working at room temperature with faster reaction times are advantages of this synthetic procedure.[38], [47]

Small amounts of solvent can be used as a liquid-assisted grinding, increasing the mobility of the reactants and promoting an acceleration of the mechanical reactions. However, this type of synthesis is limited to certain MOFs, such as the HKUST-1, UiO-66, MIL-100 and MOF-74 (in which structure is designated for isostructural compounds with metal species in composition of $M_2(dhtp)(H_2O)_2 \cdot 8H_2O$ (M = Zn, Mg, Ni, Co, Mn, Ca, and Sr; dhtp = 2,5-dihydroxyterephthalate) zeolitic azolate frameworks, and isoreticular metal-organic frameworks (IRMOFs).[47]–[53]
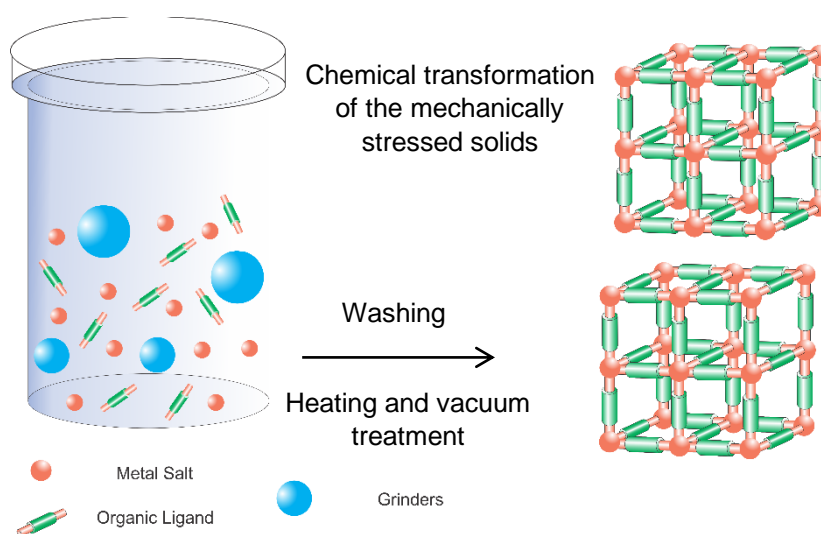
Figure 1.11. Mechanochemical synthesis of MOFs. Inspired by ref. [38].

Ionic liquids and deep eutectic solvents as synthesis medium

Usually, MOFs are synthesized either in organic solvents or in water. Ionic liquids have drawn interest as solvents in synthesis as their vapor pressure is essentially zero and they show distinguished solvating properties, easy recyclability, and high thermal stability (Figure 1.12). Most reports dealing with MOF synthesis have focused on ILs derived from 1-butyl 3-methylimidazolium L-aspartate; nonetheless, deep eutectic solvents (DESs), mixtures of two or more compounds with melting points lower than that of either of their constituents, are also known to exhibit solvent properties very similar to those of ILs and have been employed for MOF synthesis. They have advantages over ILs such as ease of preparation as pure phases from easily available components, low prices, and stability towards atmospheric moisture. Recently, HKUST-1 was prepared by sonochemical synthesis using choline chloride/dimethylurea as DES. Effects of various synthesis parameters on the crystallization process of HKUST-1 were examined, and the properties of the sample were compared to those of HKUST-1 prepared via a conventional ionothermal synthesis route in an oven.[38]
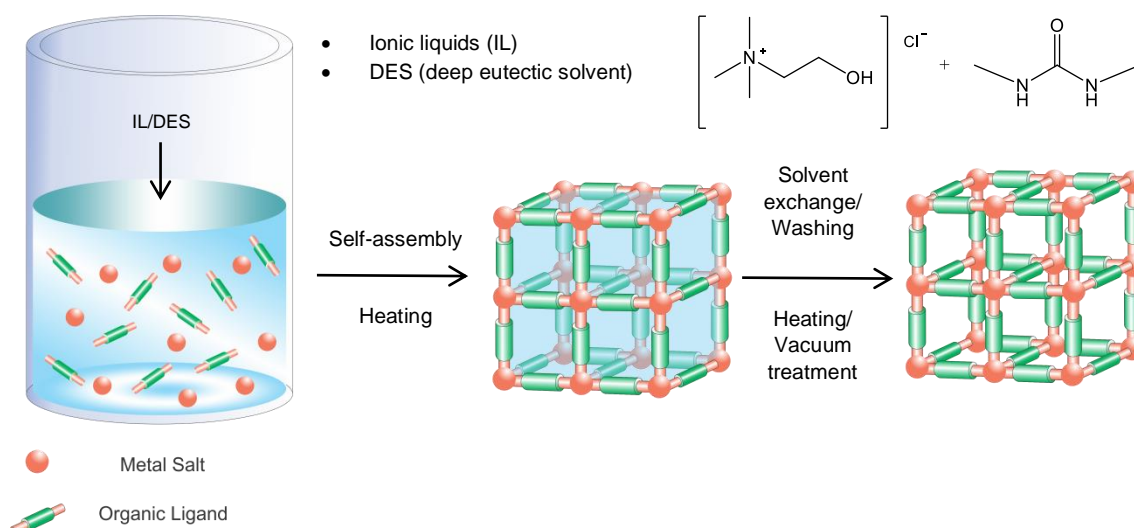
Figure 1.12. Ionothermal synthesis of MOFs. Inspired by ref. [38].

Microfluidic MOF Synthesis System

The microfluidic synthesis process was developed to meet the industrial requirements for MOF synthesis, HKUST-1 being an example of a MOF that was prepared using microfluidic equipment. The device is composed of two syringe pumps connected to a T-junction, where the formation of aqueous solution droplets in the continuous organic phase takes place (Figure 1.13). The capsule shell is formed at the liquid-liquid interface (emulsification step), while these droplets travel through hydrophobic tubing before collection takes place. The metal ion-containing aqueous solution (orange) flows through a tapered capillary centered in the tubing, and the ligand-containing organic solution (green) flows around it. Growing droplets detach when the force due to interfacial tension is exceeded by the drag force of the surrounding organic phase.[54]
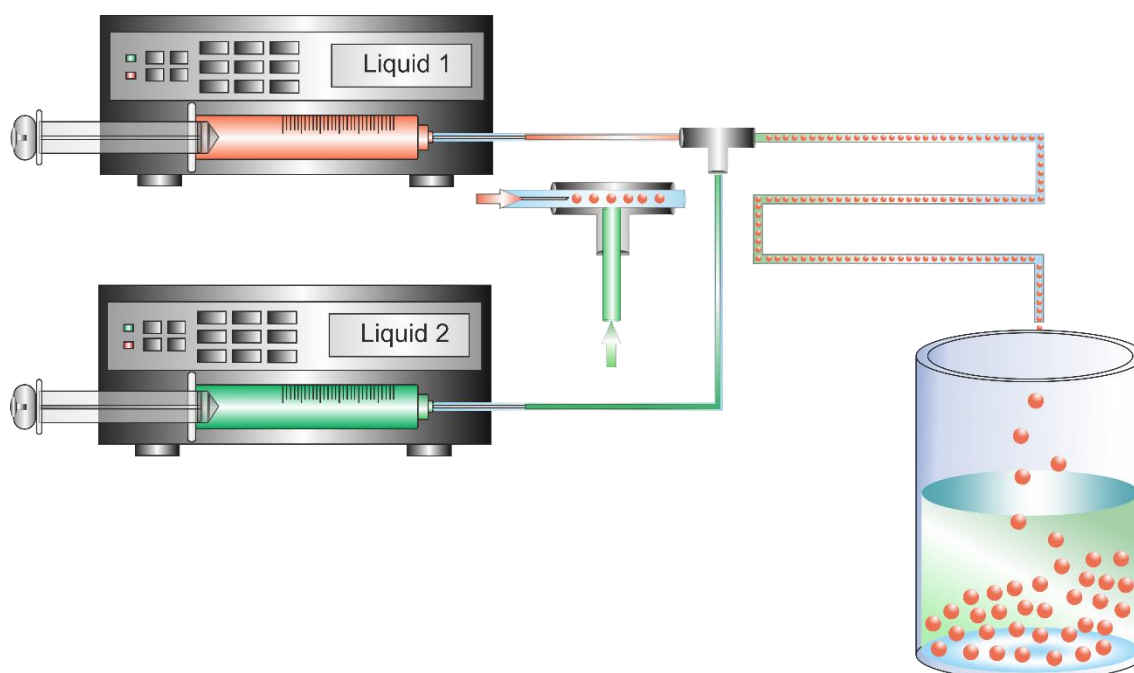
Figure 1.13. Representation of microfluidic synthesis of MOFs with a cut-away view of the T-junction showing details of the emulsification step. Inspired by: [54].

Dry-gel conversion method

Largely employed for the fabrication of zeolites, this method was later categorized into two methods: the vapor-phase transport (VPT) where a dry gel is crystallized in the vapor of water and volatile amine, and the steam-assisted crystallization (SAC) method where a dry gel containing a non-volatile amine is crystallized in the steam (Figure 1. 14). One of the benefits of applying this method relies on the minimization of waste disposal, reduction of reaction volume, and complete conversion of gel to uniform crystalline zeolites with a high yield.[38] The ZIF-8 ($Zn_6(mIm)_{12}$, mIm = 2-methylimidazole) and MIL-100(Fe) are examples of structures prepared according to the dry-gel conversion method.[55],[56]
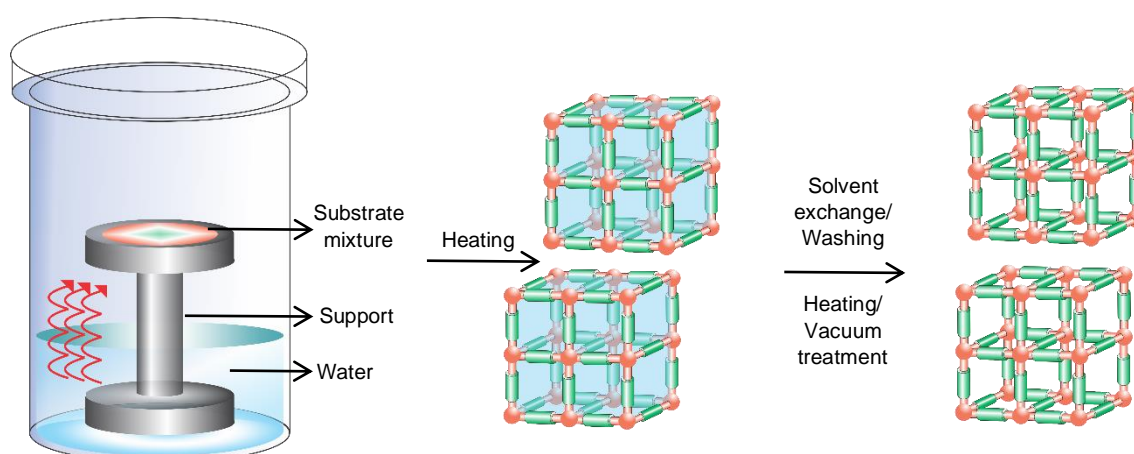
Figure 1. 14. Dry-gel conversion synthesis method. Inspired by:[38]

1.2.3 Post-Synthetic modification of MOFs (PSM)

Defined as a chemical modification of a MOF after is being synthesized, the introduction of organic functional groups into the MOF structure, or so called post-synthetic modification (PSM) it can be made to improve the host-guest chemistry between the MOF and other small molecules as guests. There are different ways that MOFs can be modified and the functionalization has the capacity to affect properties like crystallinity, porosity, flexibility, stability and topology of MOFs through induced structural changes and different types of secondary interactions. [57] The idea of PSM was first described by Hoskins and Robson in 1990, in which they have established the design and construction of 3D frameworks by using either tetrahedral or octahedral metal centers connected by rodlike linkers, these studies are considered to have laid the foundation for the larger body of work that followed.[58]

The PSM method was introduced by Cohen and collaborators in 2007 on their study on covalent modification of IRMOF-3, consisting of metal ions Zn as the central atom and the organic ligand benzene dicarboxylic (BDC) which has a group-NH_2 as a linker in the framework formation.[59], [60] Fujita and colleagues in 2008 also reported the reaction of acetaldehyde with amines to form acetaldehyde imines. It's essential to highlight that Cohen reported the PSM on the MOF linker, while Fujita involved the modification of a strongly bound guest molecule within the work structure.[61], [62]

Postsynthetic methods (Figure 1.15) most often associated with covalent modification of the ligand struts include postsynthetic modification (PSM), postsynthetic deprotection (PSD), and, more recently, postsynthetic polymerization (PSP).[62] In addition, there is an expanding topic related to post-synthetic rearrangement reactions, which can generally be categorized as rearrangement of functional groups in organic ligands, consisting of thermally activated ligand rearrangement reactions.[62]–[65]

The kinetically labile nature of metal-ligand coordination bonds in MOFs (compared to covalent bonds in organic materials) also enabled another set of post-synthetic methods.[62] Since then, numerous new PSM types have emerged, the possibility to shift chemical equilibrium has allowed for the swapping of metal or ligand components in and out of MOFs in a process known as post-synthetic ligand exchange (PSLE) or solvent-assisted linker exchange (SALE), which embodies the ligand substitution of a MOF.[66] The reactions involving metal ions exchange within the framework are known as transmetalation, a broad spectrum of metal binding groups can be incorporated into the ligand structure or be post synthetically constructed in the pores of the MOF, so-called post-synthetic metalation or post-synthetic metal exchange (PSME).[62], [67]–[70] Recently, the possibility to transform a low-connected MOF into another including high-connection numbers turned out to be possible through a process of solvent-assisted linker incorporation(SALI), or post-synthetic installation (PSI), this process is possible when symmetry, size, and coordination are compatible.[62], [66], [71], [72]
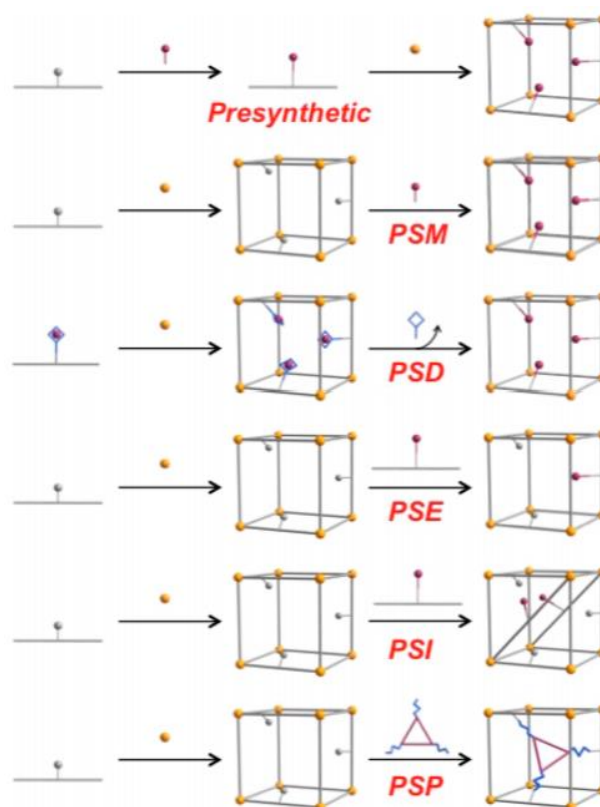
Figure 1.15. Generic schemes of presynthetic modification, postsynthetic modification (PSM), postsynthetic deprotection (PSD), postsynthetic exchange (PSE), postsynthetic insertion (PSI), and postsynthetic polymerization (PSP). SBUs are represented as gold spheres. Taken from: [62]

1.3 Application of MOFs in Drug Delivery Systems

When developing a controlled release system, one of the challenges is finding nontoxic carriers. Since each drug has a therapeutic range (Figure 1.16), with a toxic action above and below its ineffectiveness, the plasma levels are dependent on the dosage.

In the case of nanocarriers, some of the requirements for an effective therapy are:

(i) To control the drug release and prevent the "burst effect"; the burst effect is often related to high release rates reached in the initial stages after activation. As an example, when nanocarriers are associated they can improve the drug distribution over smaller volumes preventing this phenomena;[73]

(ii) To control the matrix degradation, improving the pharmacokinetics and increasing the biodistribution at the targeted organs resulting in an improved efficiency, the toxicity of the drug is then minimized once its accumulation happens on the targeted sites, as a consequence lower doses are required to reach its therapeutic effect, e.g. by using surface modification techniques; [74],[75],[76],[77]

(iii) Ability to reach a high loading capacity, improving the solubility of hydrophobic therapeutics in aqueous medium allowing parental administration.[78]
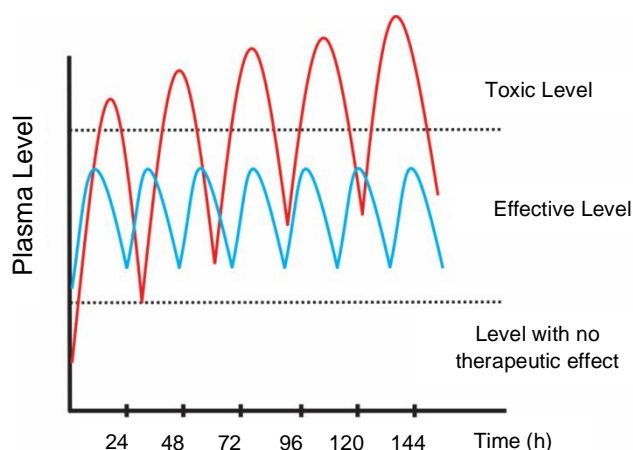
Figure 1.16. Comparison between the variation of drug concentration: (a) when administered by conventional multi-dosage method and (b) the controlled drug release system.

Additionally, when compared with other drug delivery systems e.g. liposomes, micelles, dendrimers the capacity of drug loading on inorganic nanocarriers such as MOFs are higher, even though certain instability is desirable when it comes to biological applications the organic systems present an inefficient drug loading, faster drug release and a shorter circulation time. [79][80]

1.3.1 Selected Examples of MIL-n Frameworks in Drug Delivery

The first example of encapsulation of a drug molecule was reported by Serre, Férey, and coworkers.[81] Ibuprofen (IBU) was used as a model drug in a chromium carboxylate MOF, an example of the cubic (Fd3m) zeotypic metal carboxylates, named MIL-100 and MIL-101 (MIL = Materials of Institut Lavoisier).[81] Composed of trimers of metal octahedra and di- or tricarboxylates, the structures exhibit large pores (with diameters of 25–34 Å) and a surface area of 3100–5900 $m^2.g^{-1}$. These frameworks exhibited a high loading capacity adsorbing different amount of ibuprofen, 35 wt% (for MIL-100) and 140 wt % (for MIL-101). The higher drug capacity of MIL-101 is related to its higher surface area, larger pore sizes (Ø: 29 and 34 Å), high pore volumes of 12,700 and 20,600 $Å^3$, and specific interactions between ibuprofen molecules and open metal sites and the organic spacers.[81]

While the comparatively lower capacity for MIL-100 (Cr) despite its large pore volumes (8200 and 12 700 $Å^3$) is probably due to its narrow pentagonal windows (5 Å).[81] With regard to the release, different behaviors were observed for MIL-100 within the first two hours, due to weakly bonded drug molecules probably located on the outer surface of the MOF. Release of the entire amount of ibuprofen took place over three days. In the case of MIL-101, the weakly bonded drug molecules were released in the first eight hours, and a complete release took six days, under physiological conditions (simulated body fluid (SBF) at 37 °C) (Figure 1.17a).[81]

Serre, Férey, and coworkers also demonstrated the controlled ibuprofen release in flexible, "breathing" MOFs, such as MIL-53, this MOF has a three-dimensional net-like structure composed of $CrO_4(OH)_2$ octahedrons bridged by terephthalic acid linkers. The structures of MIL-53(M) (M=Fe, Sc, Al) were built by replacing the Cr atoms of

13

MIL-53(Cr) with Fe, Sc and Al atoms. MIL-53 is flexible so that the coordination sites are rotatable.[82] To circumvent toxicity, chromium was replaced with iron. The MOFs MIL-53 (Cr) and MIL-53 (Fe) showed a high loading of ibuprofen (around 20 wt %) and a period of release of up to three weeks under physiological conditions (Figure 1.17b), in the first example of ibuprofen encapsulation the "rigid" structure was able to shown a release up to six days, now with the reversible "swelling" effect from the MIL -53(Cr) the release was prolonged up to 14 days with no apparent damage on the MOF structure.[83]
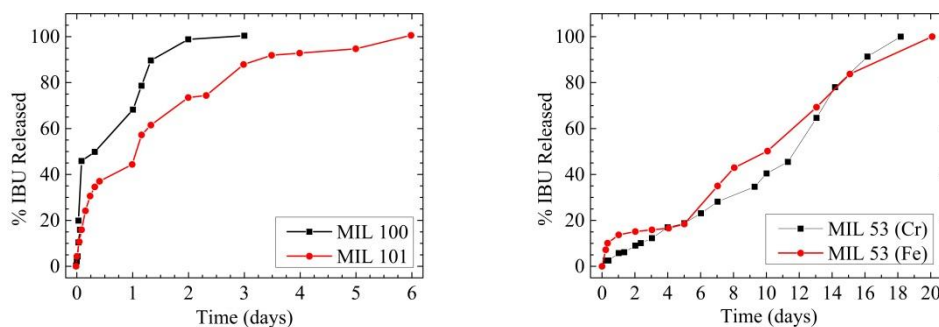
Figure 1.17. (a) Kinetics of delivery of ibuprofen from MIL-100 (Cr) and MIL-101 (Cr) in SBF at 37 ∘C. (b) Kinetics of delivery of ibuprofen from the MIL-53 (Cr) and MIL-53 (Fe) in SBF at 37°C. Taken from:[81][83]

Singco et al. described the aspirin entrapment in MIL-100 (Fe), in order to avoid the main side effects of aspirin following oral administration, especially when administered in high doses may include, gastrointestinal tract disorders (GI), stomach bleeding, hypersensitivity reactions (rash, edhema). In this investigation two drug loading strategies were reported through impregnation, where the MOF (MIL – 100(Fe)) is deposited into a saturated drug solution for a pre-determined time and a second method that incorporates the aspirin as a ligand during the MOF synthesis, called *de novo* synthesis, AH-series MOFs.

In the second case, the possibility to use aspirin as one of the building blocks of the metal-organic framework is a good strategy, once, factors such as pore size and pore volume (which are required to guarantee a higher drug loading when the impregnation method is used) are no longer critical.

The loading efficiency through the impregnation method after 24 hours was approximately 181wt% (1806 mg/mg MOF). This loading efficiency was the highest so far for MIL-100 (Fe), which showed until then had showed a loading efficiency of 35% for ibuprofen and 69% for urea. The release studies revealed a complete release in PBS (phosphate-buffered saline) at 37 °C in 14 days. [84]

The small molecular dimension of aspirin (0,41nm) facilitates the aspirin entrapment into the MIL-100(Fe) pores (1,8 and 2,3 nm), when compared to ibuprofen (1,3 x 0,6 nm), while the π –π interaction between the aromatic rings of the aspirin and the linker (trimesic acid) benefits the adsorption of aspirin stronger than urea.[84]

In the *de novo* synthesis different amounts of aspirin were added 10%, 20%, 30%, relative to H$_3$BTC, in the fabrication of the activated MOFs. SEM (Figure 1.18) presented serious framework damages of AH-10% immersed in basic medium

(pH=7,4), when compared to the acidic medium (pH=1,2). Suggesting that at high pH the aspirin is completely ionized (its pK_a is 3,5) increasing the rate of its dissolution as well as the trimesic acid. A slow degradation in acidic medium is beneficial protecting the drug in terms of unnecessary interactions with the stomach during its time of permanence approximately 2h before reaches the bloodstream.
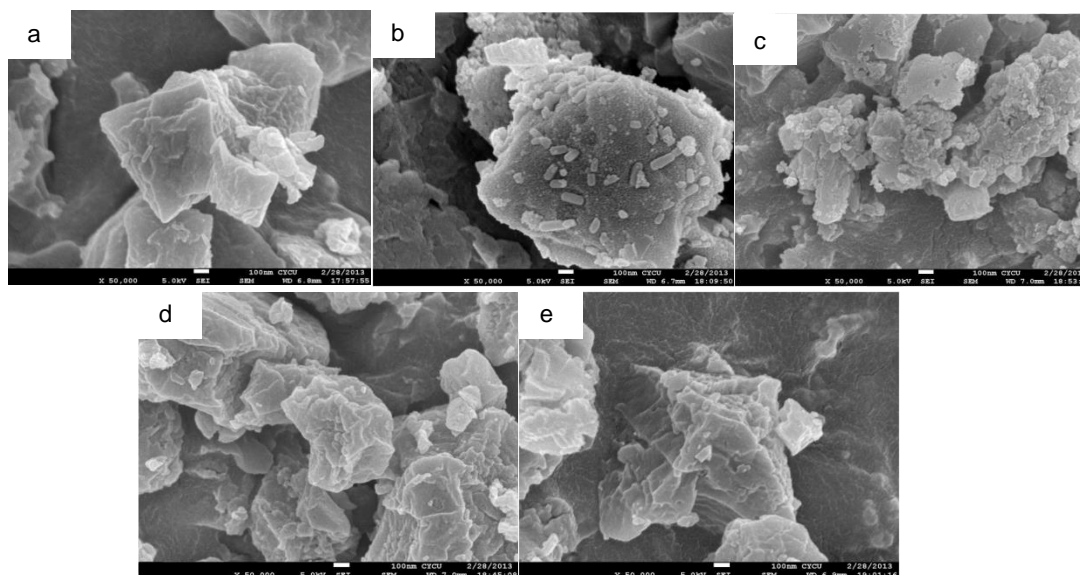
Figure 1.18. SEM images of AH-10% (a) as synthesized; (b) after immersion at 37°C in PBS (pH=7,4) for 24h, (c) and 3 days (d) and 0,1M HCl (pH = 1,2) for 24h, (e) and 3 days. Taken from: [84]

Other antitumor drugs such as doxorubicin (DOX) [85] [86], or busulfan [18] were encapsulated in MIL-100 (Fe). In the case of DOX, the drug–MOF interaction occurs through coordination of one or both deprotonated hydroxyl groups of the aglycone moiety of DOX with the unsaturated iron(III) centers, resulting in a highly stable binding, with a loading of 9 wt% and a release of up to two weeks. [85] For busulfan, the encapsulation (25 wt%) and delivery turned out to be a good alternative to avoid side effects, such as accumulation in the liver. However, 61% of the drug was released within the first 30 minutes[18], which could lead to adverse reactions such as the burst effect. In this case, a post-synthetic treatment with poly(ethylene glycol) could be used to modulate the release, therefore avoiding accumulation in liver.[18]

Adhikari and Chakraborty also reported a controlled release of DOX from iron- and zinc-based MOFs under different pH, the synthesis approach was performed at room temperature using water as a solvent, there have been already reported examples of MOF synthesis in the literature at the room temperature [87][88], a in order to turn the process environmentally friendly the solvent used was water. With an *in situ* drug encapsulation, during the synthesis of the MOF, this is a good example of avoiding any extra steps after the synthesis, such as, post-synthetic treatments discussed above; in this case the drug loading is also independent from the pore size, the DOX loading was higher for the iron-based MOF due to the stronger binding ≈ 92 wt% and ≈83 wt% for the Zn-based MOF.[86]

Agostoni et al. reported a "green" microwave-assisted hydrothermal synthesis of nontoxic MIL-100 (Fe) with large (29 Å) and small (24 Å) mesoporous cages. The two

types of cages are accessible through microporous pentagonal (5.6 Å) or hexagonal windows (8.6 Å).[89] This group used nanoscale MIL-100 (Fe) to entrap the antiretroviral agent azidothymidine triphosphate (AZT-TP). The interaction was attributed to the efficient coordination of the drug's phosphate groups to unsaturated iron (III) sites within the pores. Different incubation times (5 minutes, 30 minutes, 1 hour, 4 hours, and 24 hours) showed that encapsulation efficiencies reached 93 wt% and 98 wt% after 5 and 30 minutes, respectively. [90] It was shown that MIL-100 (Fe) can entrap 5 and 60 times more busulfan and 20 times more azidothymidine triphosphate, when compared to other nanosystems such as polymers or liposomes. [91][22][18]

Horcajada et al. demonstrated the use of other iron carboxylate MOFs (MIL-*n*), for example, MIL-53, MIL-88A, and MIL-89, also an Fe-based MOF composed of iron(III) chloride hexahydrate ($FeCl_3.6H_2O$) and trans, trans-muconic acid as ligand. besides MIL-100, in the encapsulation of antitumor (busulfan), antiretroviral (cidofovir and azidothymidine triphosphate), and cosmetic molecules, such as, caffeine (liporeductor), urea (hydratating agent), benzophenone 3 and benzophenone 4 (UVA and UVB filters). A high loading (up to 42 wt%), sustained release (3–14 days) and no burst effect were observed. [91]

In another study, Serre et al. considered the driving forces that governed the caffeine encapsulation and its delivery kinetics in the following frameworks: MIL-100(Fe), UiO-66(Zr) (later functionalized: - H, - Br, -NH2), MIL-53(Fe) (also functionalized afterward by - H, - Br, -NH2), MIL-127(Fe), composed of iron(III) cation and the 3,3′,5,5′-azobenzenetetracarboxylate (TazBz) as linker.[92] Reaching the highest loading with MIL-100(Fe) 49,5% due to its surface area and pore size in comparison to the other MOF structures: UiO66(Zr) with the loading of 22,4%, 29,2% for MIL-53(Fe) and 15,9% for MIL-127(Fe). The release studies in PBS solution revealed a burst effect where 79% and 93% of the active molecule were released in the first 30min from MIL-100 and UiO-66, respectively, this behavior, particularly from Zr-based structures, can be attributed to the stronger binding affinity between Zr and phosphate ions, leading to a faster release of caffeine.[93]

The possibility to combine molecular imaging and drug delivery in MOFs, is a good perspective in terms of diagnosing and treating of some diseases, up to now, surface modified architectures combining diverse functionalities have been developed as biosensing platforms for imaging, targeting and diagnostics.[94] Lin and coworkers encapsulated the prodrug ethoxysuccinato-cisplatin, *c,c,t*-[$PtCl_2(NH_3)_2(OEt)(O_2CCH_2CH_2CO_2H)$)] (ESCP) and an optical imaging contrast agent Br-BODIPY (1,3,5,7-tetramethyl-4,4-difluoro-8- bromomethyl-4-bora-3a,4a-diaza-s-indacene) in MIL-101 (Fe) by postsynthetic modifications, incorporating 2-aminoterephthalic acid (NH2-BDC). (Figure 1.19)

The incorporation of (NH2-BDC, around 17.4 mol%) enables a covalent attachment of ESCP (via formation of an amide bond), in this case, a load of 12.8 wt%, and slow release on MOF degradation A covalent grafting of the fluorescent dye BODIPY, (with a loading capacity of 5.6–11.6 wt %) via the amine group showed that both the dye and the prodrug were readily released, due to the instability of the nanosized MIL-101 (Fe). In the corresponding core–shell particles, in which the MOF was covered with a

thin silica layer, the release was then slowed to $t_{1/2}$ = 14 hours (BDC-NH-ESCP) and $t_{1/2}$ = 16 hours (BDC-NH-BODIPY) in PBS buffer at 37 °C.

Through laser scanning confocal microscopy images could be seen that BODIPY-loaded particles were able to cross the cell membrane and release the BODIPY dye inside of the cell, therefore the fluorescence was present in cells incubated with BODIPY-loaded particles but absent in cells incubated without nanoparticles, suggesting the MOF as an efficient platform for delivering an optical contrast agent. In addition, the modified BODIPY ligand was incubated with the cells, but no fluorescence was observed at all within the cells, indicating that the core–shell nanostructure was required for cell uptake. To increase the cytotoxicity, the silica shell was further functionalized with a targeting RGD (arginine, glycine, and aspartate) peptide resulting in an IC_{50} value comparable to that of cisplatin. This is a good example of how uncontrolled drug release can be avoided by covalent attachment of active molecules.[94][95]

The advantage of chemical stability in the rare earth family and the bridging ligands with the ability to latter stabilize the nanoparticles is one of the approaches for a sustained release. Related to this the development of nanoscale Pt-containing coordination polymers, namely NCP-1, consisting of Tb^{3+} ions and c,c,t-(diamminedichlorodisuccinato)platinum(IV),c,c,t-$[PtCl_2(NH_3)_2(O_2CCH_2CH_2CO_2H)]$ (DSCP, disuccinatocisplatin), as bridging ligand, which exhibited anticancer *in vitro* activity as demonstrated by Lin and coworkers.

The NCP-1, were precipitated from an aqueous solution of the components via the addition of a poor solvent, the polyvinylpyrollidone was added to the dispersion, after this process the PVP-NCPs were isolated through centrifugation, washed with methanol and ethanol, and redispersed in ethanol via ultrasonification. Precipitation from aqueous solution gave nanoparticles with diameters of 58.3±11.3 nm (by DLS measurements). In a similar approach as described above, The NCP-1 particles were coated with shells of amorphous silica, tetraethyl orthosilicate (TEOS), with varying thickness, e.g. according to the amount of TEOS, varying the reaction time and the release of the Pt drug studied. In order to enhance the cellular uptake of NCP-1´, the surface here was also modified with cyclo(Arg-Gly-Asp-D-Phe-Lys) [*c*(RGDfK)],which targets a type of integrin overexpressed in cancer. (Figure 1.20). These *c*(RGDfk)-functionalized particles showed improved cytotoxicity against human colon adenocarcinoma cells (HT-29), the targeted NCP-1′-a (silica shell thickness of ≈ 2nm) and NCP-1′-b (silica shell thickness of ≈ 7 nm) gave IC_{50} (50% Inhibitory Concentration) values of 9,7 and 11,9 µM, respectively, while the cisplatin standard had an IC_{50} value of only 13,0 µM. These results suggest the targeted NCPs are sufficiently internalized presumably via receptor-mediated endocytosis. Once inside the cells, the DSCP species released from the silica-coated NCPs could then be reduced to the active Pt(II) species by intracellular reductants that are present in high concentrations.[96]

The surface modification methods are being extensively used the iron-based water-stable MIL-101(Fe), through NH_2 post functionalization, was able to encapsulate and successfully delivery doxorubicin (DOX).[97] As demonstrated by Chen et al., where a mixed antitumor selenium/ruthenium where loaded into MIL−101(Fe) nanoparticles

17

combined with silencing small interfering RNAs (siRNAs) to improve therapy efficiency by silencing the multidrug resistance genes and interfere with microtubule dynamics in MC7/T(Taxol-ressistance) cell. While the cavities in the mesoporous framework would carry the drug as mentioned before, the metal ions on the external surfaces can bind to the siRNAs.[98]

In another study, Yin et al. described a multifunctional MOF-based nanoprobe developed for both tumor-targeted drug delivery and dual-mode therapeutic self-monitoring. The anticancer agent camptothecin (Cam) was loaded into NH_2-MIL-101(Fe) nanoparticles and conjugated with pegylated folate (FA), establishing this way the nanoprobe would be taken up selectively by FA receptor high-expressed cancer cells through endocytosis mediated by receptor−ligand interactions, and the encapsulated antitumor agent would be released from the nanoprobe in HepG2 cells (Figure 1.21). Ultimately, the released drugs initiated programmed death of cells and caspase-3 was activated as the main participant of cell apoptosis. Thus to monitor the treatment process, AuNCs were conjugated on to the MOFs through a peptide, which is the substrate of the apoptosis indicator (caspase-3). Once the peptide was enzymatically cleaved by caspase-3, the quenched fluorescence of AuNCs on MOFs was then recovered.[99]

The organometallic anticancer drug [Ru(p-cymene)Cl_2(pta)], where pta=1,3,5-Triaza-7-Phosphaadamantane,(RAPTA-C) was encapsulated in MIL-100 (Fe) (loading 42 wt%). The resulting system RAPTA-C@MIL-100 (Fe) combines all advantages described for MIL-100 (Fe) as a drug delivery system with the antimetastatic activity of RAPTA-C. In simulated body fluid (SBF), the RAPTA-C delivery process takes place in two steps exhibiting half-life periods of 1.9 and 30 hours. The first step could be related to weakly adsorbed molecules on the external nanoparticles surface as well as partial degradation of the MOF (10% of benzene-1,3,5-tricarboxylate (BTC) leaching after two days). Especially the long half-life of the second step of RAPTA-C delivery offers the possibility of achieving an adequately controlled release of the drug.[100]
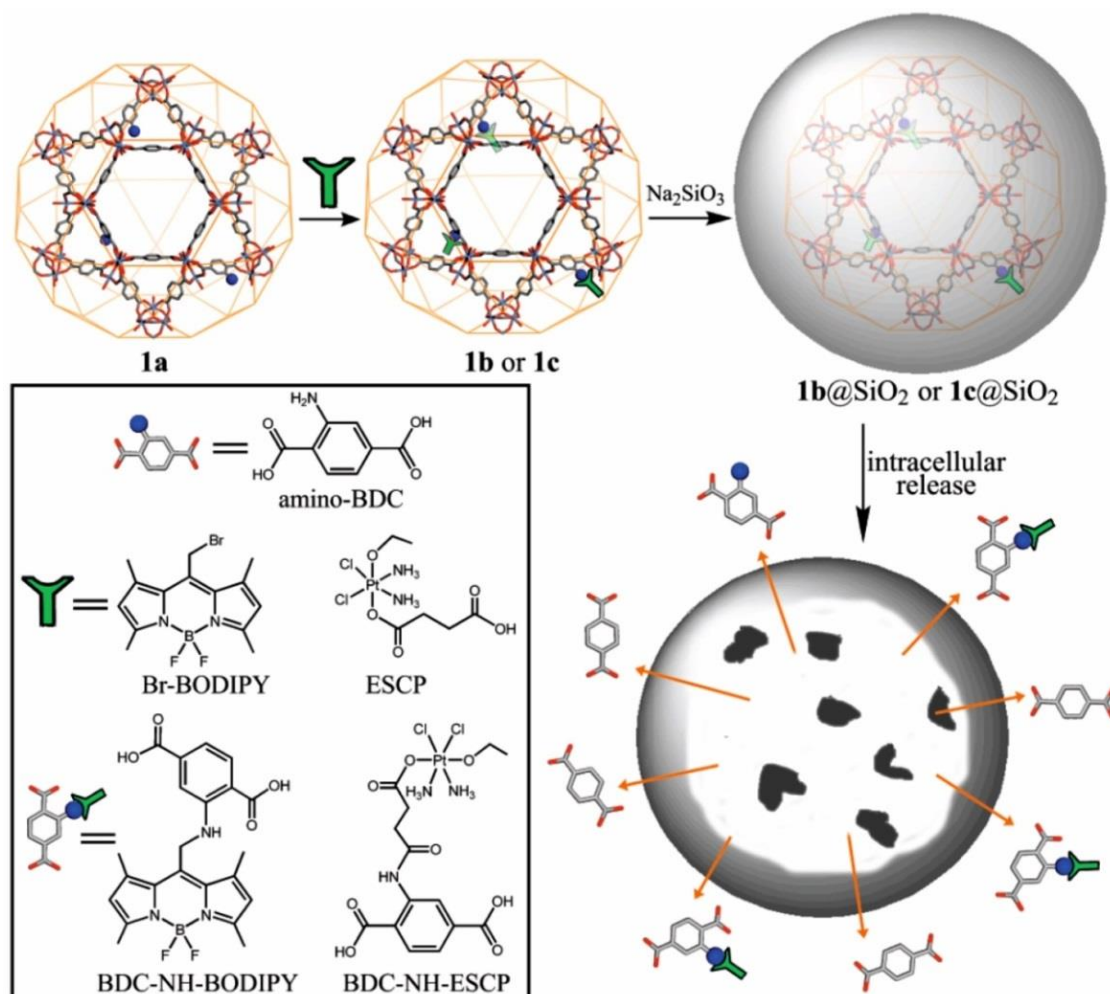
Figure 1.19. Schematic representations of the synthesis, modification, and drug release from amino-functionalized iron MIL-101 (Fe); 1a: amino-functionalized particles, 1b: BODIPY-loaded particles, 1c: ESCP-loaded particles. Taken from: [95]
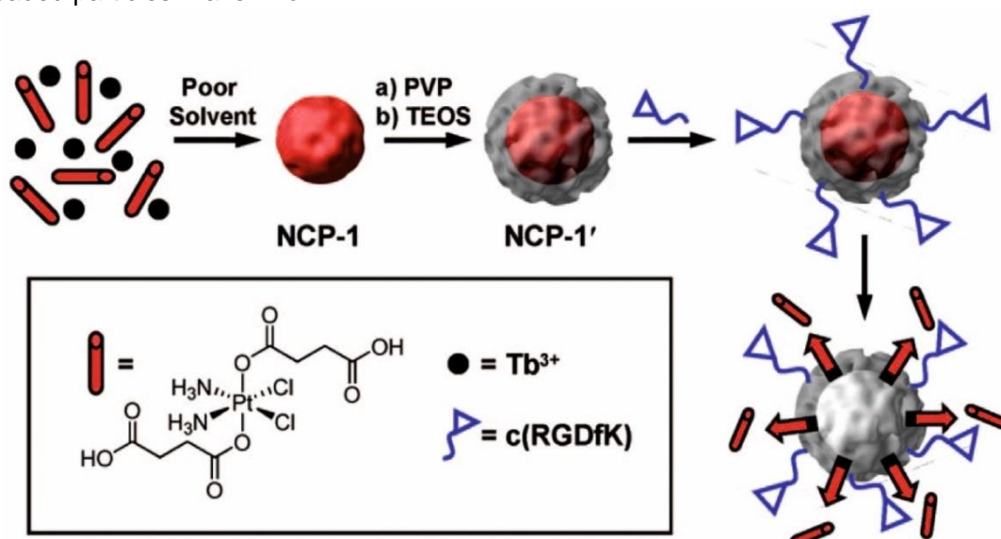
Figure 1.20. Construction of silica-coated NCP-1 particles and further functionalization with c(RGDfk).Taken From: [96].
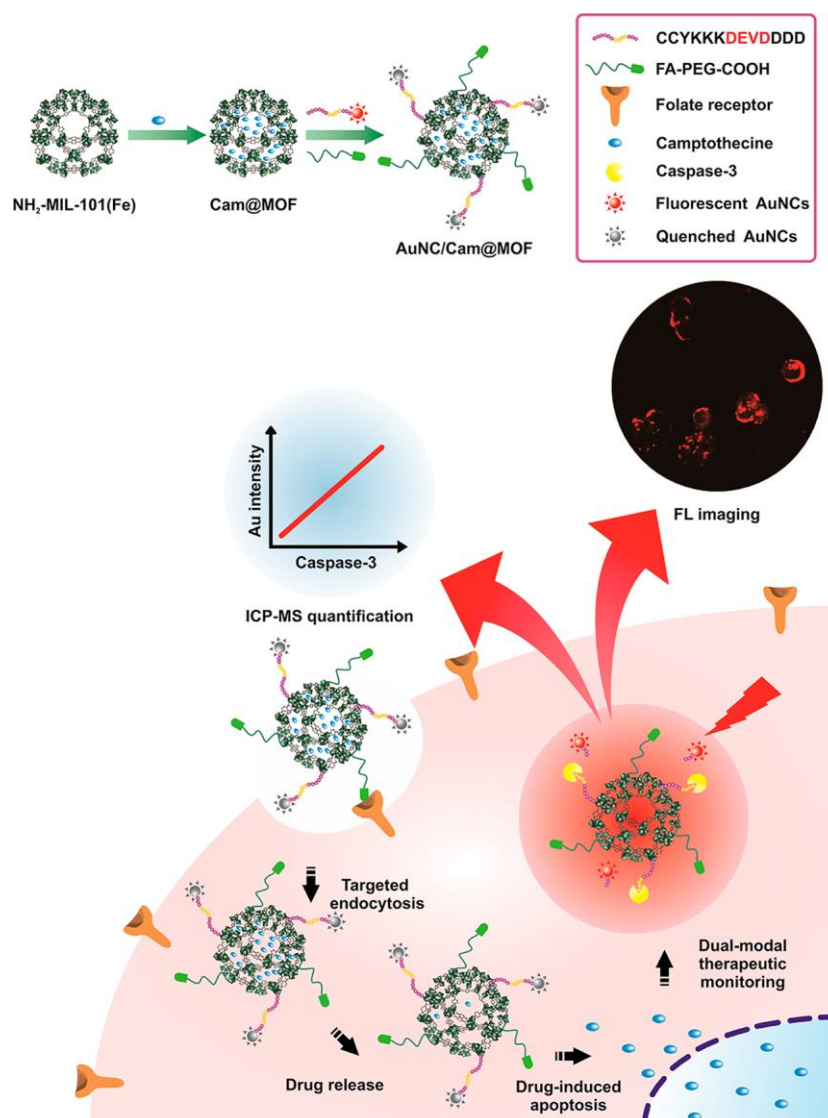
Figure 1.21. Schematic Illustration of Preparation of Multifunctional AuNC/Cam@MOF Nanoprobe and Experimental. Taken from: [99]

Wang et al. reported that MIL-101 (Fe) itself has the intrinsic ability to suppress angiogenesis processes in vitro, as well as the potential to effectively distinguish tumor cells, such as SKOV3 (ovary cancer), HeLa (human cervical carcinoma), and A549 (human lung carcinoma) from BABL-3T3 (normal mouse embryonic fibroblast) cells, encouraging the use of these MOFs as antitumor agents. Furthermore, MIL-101 (Fe) effectively induced apoptosis of human umbilical vein endothelial cells (HUVECs) through the mitochondrial pathway interfering with the G1/G0 cell division process, and in addition inhibited growth and migration of endothelial cells through processes such as downregulation, i.e. a process by which a cell decreases the amount of a cellular component, in this specific case the expression of the MMP-2/9 (MMP = matrix metalloproteinase).[101]

Recently, Taherzade et al. described two antibiotics with different solubility, tetracycline hydrochloride and doxycycline monohydrate, loaded separately on the nanosized MIL-100 (Fe). Through the release studies, the drug solubility in water was mediated by the MOF; in the case of tetracycline hydrochloride, the release was

sustained, and after 48 hours, it could be verified that 96% of the drug was released.[102]

There are numerous examples of porous iron carboxylate MOFs used for drug encapsulation, however the application of calcium-based MOFs are not so explored so far, Haydar described the loading of an anti-inflammatory drug flurbiprofen (FBP), into Ca-based MOFs and made a comparative study with the Fe–MILs (MIL–53, MIL–101, MIL–100).

The highest loading capacity was reached by the MIL–100 and MIL–101, 46 wt%, 37 wt%, respectively, that relates to the characteristics of those MOFs, high surface area and pore volume. Following by MIL–53 with a loading capacity of 20 wt% and Ca-MOF that reached only 10 wt% of loading. This phenomena can be explained by the high pore size ≈12,3 nm, for both MIL–53 and Ca–MOF, that allowed the flurbiprofen molecule to be loaded, but in a low percentage due to a low surface area around 26,20 and 34,72 m2/g, for MIL–53 and Ca–MOF, respectively, reaching a complete release after 48h.[103]

The physicochemical properties of MOFs, e.g, size, colloidal stability, and surface charge can influence the behavior of loaded MOFs in biological media, the particle size and shape are also important taking into consideration the administration routes, most studies have been targeting the intravenous route for delivering drug molecules Hidalgo et al. proposed a MOF nanocarrier (MIL–100) suitable for oral administration, which is covered on the outer surface with the biopolymer chitosan. This biocompatible polymer is widely used; because it is biodegradable and most importantly it show very low toxicity. The surface modification method improves the chemical and colloidal stability of the nano-MOF in oral fluids, as well to improve the intestinal barrier bypass, combined with a lower recognition by the immune system. Thus, these features make chitosan-coated MOFs promising candidates for the oral administration of potential drugs.[104]

Essentially, nanoparticles should interfere minimally with the function of the primary effector cells, this relates to the cells that will be directly in contact with the nanoparticles when introduced in the biological system, their physicochemical properties related to their small size, chemical composition, solubility, aggregation, can increase the interaction with biological tissues, MOFs have been studied by their *in vitro* toxicity in cancer cells, but there is still an open discussion about the adverse effects of those Wuttke et al., investigated the safety of these nanoparticles in terms of different fields of medical applications, for the purposes of this chapter only the drug delivery cases will be on focus in this chapter.[105][106]

Both chromium (MIL–101(Cr)) and iron based (MIL–100(Fe)) MOFs, were evaluated with and without supported lipid bilayers, 1,2-dioleoyl-sn-glycero-3-phosphocholine (DOPC) to enhance its biocompatibility, in endothelial cells, alveolar epithelial cells, and alveolar macrophages and their response was compared towards the non-lipid-coated control particles. Human umbilical cord vein cells (HUVEC) and human microvascular endothelial cells (HMEC) were exposed up to 72h to DOPC-coated Fe and Cr based MOFs in a dose range from 25 to 200 µg mL^{-1}. There were no signs of stress related rearrangement of actin fibers for the HMECs when exposed to the

studied nanoparticles for 24h. Further analysis revealed no induction of apoptosis for the MIL-101(Cr) nanoparticles coated with DOPC and uncoated MIL-101(Cr) nanoparticles in the full dose range when applied to HMECs for 72h. [106]

Both, Fe based nanoparticles coated with DOPC and the control MIL-100(Fe) at the highest dose 200 µg mL^{-1} presented an induction to apoptosis in endothelial cells (HMECs). [106]

Another strategy for targeted drug delivery is to assemble stimuli-responsive multifunctional MOFs combined with chemo-photothermal cancer therapy. These MOFs preloaded with a chemotherapeutic agent are latter coated with polydopamine (PDA), which is known to be an excellent photothermal transduction material, this surface treatment with PDA provides an advantage for the conjugation due to the PDA properties while promotes a combination of chemotherapy and photothermal therapy. Different types of MOFs including ZIF-8, MIL-101, and UiO-66 functionalized with PDA were successfully conjugated with targeting molecules such as aptamer, doxorubicin and folic acid (FA) for targeted drug delivery.[107]

1.3.2 Selected Other Metal-Organic Frameworks Used in Drug Delivery

Hu et al. described the synthesis of MOF-74-Fe(III), prepared through a post-oxidation procedure from neutral MOF-74-Fe(II) [containing Fe(II)$_2$(dobdc), where dobdc^{4-} = 2,5-dioxido-1,4-benzenedicarboxylate, as SBU], which proved to be a good carrier for the selective encapsulation of anionic drugs. [108] This cationic host material exhibits very low cytotoxicity for PC12 cells, which are derived from a pheochromocytoma of the rat adrenal medulla, used as a model to evaluate the cytotoxicity of nanomaterials, because they are vunerable to oxidative stress, given by the ferric compound in the MOF structure.[109]

The model drug was ibuprofen (IBU) and the loading capacity for the corresponding anions was around ≈15.5 wt% in the resulting composite. It was estimated that half the amount of the drug was released in four hours; the process presented different drug delivery rates due to the presence of two distinctive environments of IBU$^-$ anions in host channels, free and coordinated, resulting in distinctive different release behaviors, in the first stage the sodium ibuprofen and other coordinated free anions are released, the second stage involves the coordinated drug triggered by phosphate anions (PO$_4$ $^{3-}$) due to its preferential coordination with iron cation, followed by a gradual decomposition of the porous material in a later stage.[108]

Zhu et al. applied the zirconium-based MOF UiO-66 (based on linear 1,4-benzenedicarboxylate (BDC, terephthalate) ligands and Zr$_6$O$_4$(OH)$_4$ clusters as 12-connected nodes) for the delivery of alendronate (AL), an aminobisphosphonate, which is widely used for the treatment of osteoporosis and several other bone diseases, such as solid tumor bone metastases and myeloma bone disease. Owing to poor bioavailability of alendronate, high doses are usually required. Administration of a local, sustained AL delivery system with an enhanced loading capacity and delivery efficiency of AL into cancer cells allows tailoring the controlled capture and release of AL molecules based on the formation of strong Zr–O–P bonds. The time dependent release profile was studied in two different medias at pH 7.4, where 42,7% of AL were

released in 60 hours, and at pH 5.5 in this case 59% of the drug was released in the same interval.Thus, it was possible to encapsulate up to 51.4 wt% AL, in the UiO-66 nanoparticles. Around 42.7% of AL is released in 60 hours at pH 7.4, whereas more than 59% of the drug is released during the same time interval at pH 5.5, in acidic environments occurs, the protonation of phosphates weakening the interaction between AL and Zr–O clusters.[110]

Filippousi et al. developed a copolymer (poly(ε-caprolactone)–D-α-tocopheryl polyethylene-glycol-succinate (PCL–TPGS)) to modify the surface of two Zr-based MOFs, UiO-66 and UiO-67, to improve drug solubility of hydrophilic cisplatin and hydrophobic taxol. An amount of 140 mg taxol per g UiO-66 could be loaded and 100 mg on one gram of the UiO-67 framework. However, the loading of cisplatin on UiO-66 and UiO-67 (48 and 10 mg/g, respectively) was rather low, due to the hydrophilic nature of the drug as compared to the hydrophobic MOF linkers. It was found that the drug release depends on the MOF–drug interaction while the controlled release rates can be attributed to the hydrophilicity of the drug.[111] Through molecular dynamics simulations it was possible to visualize the predominant adsorption positions of the adsorbed molecules to get insight into the mobility and adsorption locations. The cisplatin molecules interact with the accessible basic site Zr–O–Zr of the inorganic framework, which is the case for both UiO-66 and UiO-67, while the taxol incorporation due to its size was possible through the introduction of linker defects into the UiO-67 structure. [111] The drug release profiles, under SBF at 37°C revealed when cisplatin was loaded into UiO-66 and UiO-67 a complete dissolution of the drug into the media was reached after 120 hours for both MOFs, only a higher release rate was observed for the UiO-67, probably due to the sample amorphisation, therefore the drug carriers were microencapsulated into PCL-block-TPGS copolymer. Three predominant steps on the release occur, a progressive release was observed for UiO-67 reaching a release rate of 35% for the first 100h, later between 24 and 120h, is possible to observe a lower increment in the release, presumably produced by diffusion of drugs from the interior of the microparticles and the erosion of the surface. Between 132 and 300h, another increment of the release rate is detected as a result of the collateral destruction of the polymer microparticles, after 400h the drug is dissolved completely.[111]

Is outstanding how post-synthetic modifications are a dynamic tool for building active tumor-targeted drug carriers, studied by Dong and collaborators that chosen two Zr-based MOFs, MOF-808 (composed of $ZrOCl_2 \cdot 8H_2O$ and H_3BTC = trimesic acid as ligand) and NH2-UiO-66 as DDS, thus the Zr_6 clusters on the surfaces of the nanoparticles were coordinated by the terminal carboxylate of FA molecules, substituting the original formate or terminal OH ligands and loaded with 5-fluorouracil (5-FU) showing efficient cytotoxic effects toward cancer cells and enhanced the intracellular uptake of nanoparticles within the cells.[112]

Drug resistance is a significant problem in the treatment of cancer, in this regard often a combination of different drugs is applied, however, each drug bears distinctive physicochemical properties, which leads to heterogeneous pharmacokinetics and tissue distribution. Addressing this challenge Engelke and co-workers developed liposome-coated metal-organic framework (MOF) nanoparticles. The prospect use of

MOFs for co-encapsulating multiple drugs thus synchronizing their delivery to the cancer cells and further functionalization with a lipid shell acting as a temporary seal is an alternative to control interactions with intracellular fluids. Therefore, nanoparticles of MIL-88A were loaded with irinotecan and floxuridine in a ratio of 1:1 and further coated with DOPC (1,2-dioleoyl-sn-glycero-3-phosphocholine)-derived liposomes, fluorescence measurements on non-coated and coated nanoparticles were investigated showing the coated nanoparticles had no premature leakage demonstrating the effectiveness of the DOPC coating.[113] In another investigation He et al. used Zr-based MOFs from the UiO series for the co-delivery of cisplatin and pooled small interfering RNAs to increase the therapeutic efficacy by silencing multiple drug resistance genes and resensitizing resistant ovarian cancer cells to cisplatin treatment.[114]

In a similar approach, Yang and colleagues designed a refined delivery of glucose-responsive insulin, a multi-enzyme metal-organic structure, using cobalt-doped ZIF-8 for the delivery of insulin and glucose oxidase, (named: Ins / GOx @ Co-ZIF-8) adopting the use of microneedles responsive to stimuli build from polyvinyl alcohol for transdermal administration displaying a good glucose concentration during the insulin release while preserved its function with no release of H_2O_2 and Co^{2+} ions from the structure.[115]

Tamames-Tabar et al. developed a biocompatible and bioactive MOF (BioMOF). BioMOFs present advantages, such as the active molecule can be a constitutive part of the MOF, in general, Ca^{2+}, Fe^{2+}, Fe^{3+}, Ag^+, or Zn^{2+} are used to construct BioMOFs, the active compounds may be also the linkers that are delivered via framework degradation, this avoids multistep procedures in loading the material. Both cation and ligand can be bioactive in order to achieve an additive and/or synergic therapeutic effect. BioMOFs could be also used for co-delivery of drugs; in this case, one drug integrates the framework, while the other is absorbed in the pores, this way the co-delivery can be achieved.[116][117]

The BioMIL-5 (Bioactive Materials from Institut Lavoisier), which is based on therapeutically active azelaic acid (exhibits antibacterial and anti-inflammatory properties) and bioactive Zn^{2+} cations (widely used as a cicatrizing agent, skin moisturizer, and antidandruff astringent) was prepared. In terms of drug delivery, the progressive release of the active Zn^{2+} and azelaic acid from BioMIL-5 in water or bacterial culture media allowed control of the growth of an S. *epidermidis* suspension, a Gram-positive bacterium, over seven days.[116]

Another type of BioMOF was reported by Rosi and coworkers. In bio-MOF-1, the anionic nature of the zinc-adeninate structure showed great potential for entrapment of cationic drugs. In this case, procainamide hydrochloride, an antiarrhythmic drug, was encapsulated (0.22 g drug per g material), and a steady release was observed in PBS buffer (pH 7.4) over 20 hours, and a complete release was reached after 72 hours. The crystalline integrity of the framework was maintained throughout the release process.[118]

Kim et al. proposed the NH_2-MIL-88(Fe) as a potential carrier to encapsulate brimonidine, an antiglaucoma drug, in order to improve its bioavailability. The NH_2-MIL-

88(Fe) can be fully degraded in biological fluid after 12 hours, the π–π bond interaction between linker (2-aminoterephtalic acid) and the drug results in a higher drug loading via chemical absorption, and ensure in the same time a sustained drug release. [119]

1.4 Toxicity

The concept of biocompatibility matured throughout the years, for the first generation of implantable devices (1940-1980), the criteria for an outstanding biological performance could be achieved when the material was least chemically reactive, and the basic criteria for implantable materials were based on non-toxic, nonimmunogenic, non-thrombogenic, non-carcinogenic, non-irritant and so onward. Nowadays, biocompatibility can be defined as the ability of a material to achieve its functionality without initiating an adverse biological response that affects the surrounding tissue or altering homeostasis, how those responses will influence the system relies on how the nanoparticles interact with proteins, immune cells, and lipids.[120][121][122]

Numerous studies focus on the in vitro evaluation of MOFs and their toxicity, however, it is important to set apart the studies performed on "healthy" cells, those coming from primary cell culture, from those conducted using cancer cell lines. In the first scenario is possible to evaluate the potential hazards of the material in the organism, in the second situation when you conduct studies using cancer cell lines, the anticancer activity is targeted. In most studies, authors only include toxicity evaluation in cell lines with a tumor origin, and the evaluation of the toxicity of the vector alone is often missing.[123]

The potential toxicity of MOFs and how they interact/affect with the living environment needs to be considered in terms of biocompatibility, as an example the particle diameter and conformation will determine the penetration inside the cells and potential interactions with membranes and organelles, until now the majority of studies have been focused on in vitro or ex vivo applications, therefore limiting the studies to a singular cell line. The characteristics amidst affecting MOFs safety (nano or micro) include chemical composition, structure, size, morphology, aggregation, purity and surface area properties (Figure 1.22).[106][120][123], [124]
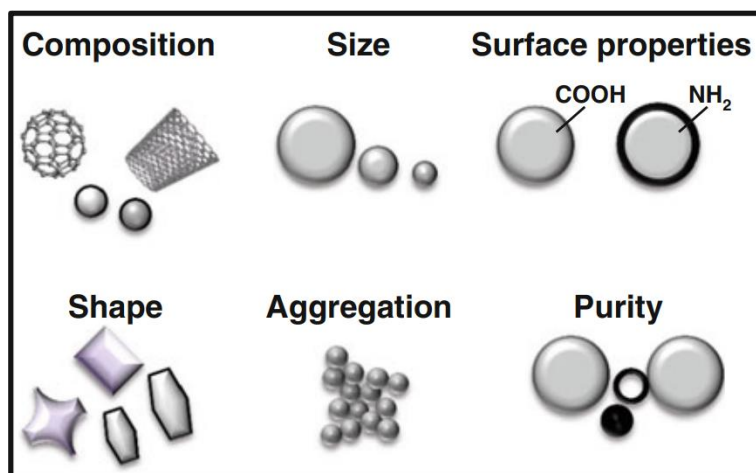
Figure 1.22. Properties that contribute to the biocompatibility of nanoparticles. Taken from: [121]

Recent studies on the toxicity of MOFs have been conducted, mainly because of their potential use as biomaterials. While chromium (LD50 1.8 g/kg), cadmium, nickel (LD50 0.2 g/kg), cobalt (LD50 0.5 g/kg), and other metals are not suitable as metal nodes in MOFs due to their high toxicity (even though some of them are essential elements, e.g. cobalt), are not considered suitable for biomedical applications.

The possible application of MOFs in humans as part of a pharmacological treatment involves the penetration of its components in the living organism, the health risks featured by those metals will be determined by the administration route chosen for the treatment, their extent, dose-dependent, along with how is distributed, accumulated, metabolized and eliminated by the system.[125]

The use of biocompatible metal nodes, such as metals that already exist in appreciable amounts in the body and/or biocompatible active molecules is a possibility to reach biocompatibility, as an example, iron is an important component of hemoglobin and is approximately 22 μM in blood plasma.

The diverse examples of metal species used in the treatment/diagnosis of several diseases concerning their toxicology are listed in (Table 1).

Table 1. Examples of metals and inorganic compounds used in medicine. Rat oral lethal dose 50 (LD_{50}) and composition in humans of the most appropriated metals in the synthesis of MOFs for biological applications. Metals are ordered by increasing LD_{50} value. Taken From:[117]

Element	Composition in humans (g)*	Oral LD50 in rats (mg.Kg^{-1})	Drug Active Compound Medical use
Pt	≤ 40 ng mL^{-1} (blood serum)	25 – 210 [$(NH_4)_2PtCl_4$]	Cisplatin Anticancer drug
Cu	0.072	30 $CuSO_4$	Cooper gluconate Supplement
Zn	2.3	100 – 600 $Zn(OAc)_2$	Zinc undecanoate Antifungal
Tc	No data reported	130 (all soluble compounds)	^{99m}Tc-pyrophosphate Bone X-ray
Ba	0.022	220 $BaCl_2$	$BaSO_4$ X-contrast
Fe	4 – 5	450 $FeCl_3$	Iron (II) formate and succinate dietary supplement
Gd	$7.2 \cdot 10^{-12}$ g·mL^{-1} (blood serum)	550 $GdCl_3$	[Gd(III)(DTPA)(H_2O)]$^{2-}$ ** MRI contrast agent
Li	0.007	590 Li_2CO_3	Li_2CO_3 Manic depression or bipolar disorder treatment
Co	0.003	691 $Co(NO_3)_2$	Vitamin B$_{12}$ Supplement
Mn	0.012	1484 $MnCl_2.3H_2O$	Manganese ascorbate Osteoarthritis treatment
Ca	1000	1940 $CaCl_2$	Calcium citrate-vitamin D Treatment of low blood Ca levels
Bi	0.0005	≥2000 Bi	K_3[Bi(III)(citrate)$_2$] Antiacid, Ulcer treatment
K	140	3020	Potassium citrate

		KCl	Treatment of kidney stone
In	0.0004	3300 $In(NO_3)_3$	Oxyquinoline In – 111 Diagnostic radiopharmaceuticals
Mg	1.9	5000 $MgSO_4$	MgO Antiacid, laxative
Sb	0.002	≥34.600 Sb_2O_3	Sodium Antimony (V) gluconate Antileishmaniasis
Au	42 – 420 ng mL^{-1} (blood serum)	No data reported	[Au(I)(PEt$_3$)(acetilthioglucose)] Arthritis treatment

* Average for a 70 kg adult human. Relative amounts of each element vary by individual, mainly due to differences in the proportion of fat, muscle and bone in their body. **DTPA: diethylenetriaminepentaacetic acid

As organic linkers, carboxylates and phosphonates can be used to build MOFs for biomedical applications. The most commonly used precursors for linkers showed LD_{50} values of 1.13 g/kg (1-methylimidazole), 1.4 g/kg (2-methylimidazole), 1.6 g/kg (5-aminoisophthalic acid), 5 g/kg (terephthalic acid, 2,6-napthalenedicarboxylic acid and isonicotinic acid), and 8.4 g/kg (trimesic acid), indicating that their toxicity is acceptable for bioapplication.[21] Furthermore, some organic linkers might be reused in the body, which would substantially reduce the risk of side effects, for example, amino acid-based MOFs, such as [Cu(L- or D-glutamic acid)(H$_2$O)]·H$_2$O,[126] or nucleobase-based MOFs, such as Zn$_8$(adeninate)$_4$(biphenyldicarboxylate)$_6$O·2Me$_2$NH$_2$, 8DMF, 11H$_2$O (bio-MOF-1). [118]

Horcajada et al. studied the cytotoxic potential of metal ions and organic linkers, and rated MOFs based on iron and zinc as the best candidates for use as biomaterials.[91] As mentioned before as an alternative to reach biocompatibility the metal nodes can be endogenous cations pre-existed in our body or exogenous elements that perform specific medical purposes, the medical compounds that are intended for medical applications, consequently holds the limitation of the Bertran diagram, which expresses the relationship among deficiency, optimum physiological response, and toxicity for the species in question according to dose.[117]

In vitro and in vivo toxicology studies for some iron carboxylate-based MOFs (iron(III) trimesate MIL-100, iron(III) fumarate MIL-88A and iron(III) tetramethylterephthalate MIL-88B_4CH$_3$) were conducted.[91][127] A high dose (up to 220 mg/kg) was administered intravenously in female Wistar rats. Indicators like water and food consumption, body and organ weights, absence of immune or inflammatory reactions, animal behavior, and serum parameters were evaluated up to three months after injection and showed no significant differences when compared to the control group.[91] The absorption, distribution, metabolism, and elimination, known as the ADME series, were also evaluated. MIL-100(Fe) seems to be the most promising regarding the stability, loading capacities, degradation/release profile, and in vitro and in vivo toxicity. Particle accumulation happened in the liver and spleen but no signs of histological or function alterations were observed with a progressive degradation and elimination of the excess of iron and the n-metabolized exogenous ligands by urines and feces. Accordingly, it was concluded that these MOFs are nontoxic. [91], [121], [127]. Kundu et al. further confirmed the nontoxic nature of Gd(III)-based MOF, in vivo in mice

through intravenous administration with only minor alterations associated with particle accumulation were described. [123], [128]

For comparison Simon-Yarza et al., studied the behavior of mesoporous iron (III) trimesate MIL-100 at early times after intravenous administration, by studying the organ accumulation and the blood circulating profile in 36 female Wistar rats, the animals were randomly divided in six different groups, each group composed of 6 animals related to the different administration times: 15 min, 30 min, 1, 3, 8 and 24h, respectively. The intravenous administration of a dose correspondent to 220 mg/kg of MIL–100. The pharmacokinetics studies revealed once the nanocarrier is in the organism act as a depot, reaching a maximal concentration after 30min of administration, but rapidly decreases after 3 h, the accumulation occurs mainly in the liver and spleen, but histological studies revealed no morphological alteration in without any alterations in these organs, the trimesate is progressively eliminated in urine. [129]

More recently, the zebrafish is being considered as a prominent model as it provides substantial information for the study of chemical toxicity of some nano MOFs, it is another approach to the classical acute fish toxicity test that nowadays is not suitable with most animal welfare legislation.[123], [130] Ruyra and coworkers reported combined in vitro (HepG2 and MCF-7 cells) and in vivo (zebrafish embryos) studies on the toxicity of 16 archetypical, uncoated nanoMOFs. MOF-74 (Mg), MOF-74 (Co), UiO-66, and UiO-67 presented very low or no toxicity, while MOF-74 (Zn), ZIF-7, and ZIF-8 showed high toxicity values, which is directly correlated with their composition and stability. The Zn^{2+}-based MOF (ZIF-8) showed high toxicity in the breast cancer cell line MCF-7 and human liver cancer cell line HepG2, due to release of Zn^{2+} ions into the cells. Nonetheless, the results of this toxicity study on MOFs were mainly to evaluate the environmental and health risks of these materials, rather than focus on their use for medical purposes. Further toxicologic studies on dose-dependent toxicity and the short/long term impact of these materials combined with different administration routes will imprint a breakthrough towards the bioapplication of these materials. [123], [131]

Liu et al. described the oral toxicity of the MIL-101(Cr), which possesses one of the highest surface areas, high porosity and therefore a high loading capacity among the MOFs many studies have been focused on other types of metal-organic frameworks, but the lack of toxicity studies involving the Cr based MOF and its possible risk to human health led to an investigation of 28 days dose dependent.[81], [132]

The 28-day oral toxicity test was evaluated on 96 mice of each sex that were randomly distributed into 4 different groups, once a day the groups received an oral administration of 0, 10, 100 and 1000 mg/Kg body weight of MIL-101, respectively.

There were no statistically significant effects on body weight, food consumption, organ weight, behavior, and mortality; Hematological analysis revealed no adverse changes in hematology parameters for both sexes treated with MIL101(Cr) in comparison to the control groups; As well the clinical biochemistry and histopathology were no adverse effects either present in mice treated with Cr based nanoparticles. Accordingly, the MIL-101(Cr) nanoparticles have no significant acute and subacute

toxicity, therefore the no observed adverse effect level of MIL-101(Cr) nanoparticle was defined as at least 1000 mg/kg/day orally for 28 days for male and female mice.[132]

Attempts in terms to design applicable in vitro cytotoxicity studies according to a distinctive MOF application have been made by Wuttke et al.using different primary healthy cell types according to the proposed bioapplication. They have studied MIL-100(Fe), MIL-101(Cr), also coated with DOPC (1,2-dioleoyl-sn-glycero-3-phosphocholine), named MIL-100(Fe)@DOPC, MIL-101(Cr)@DOPC, respectively, and evaluated their nanosafety as drug delivery, by lung cells (murine alveolar epithelial cells (MLE12) and mouse alveolar macrophages (MH-S). Both Fe and Cr-based MOFs could endure well endothelial cells, although the MIL-100(Fe)@DOPC caused some apoptotic cell death from a minimum dose of 100 µg mL−1 onward. The alveolar epithelial cells could tolerate only lipid-coated Fe and Cr-based MOFs at lower doses up to 50–100 µg mL−1, respectively. Considering the alveolar macrophages, which behaved quite sensitive to iron-based MOF nanoparticles, causing induction of a cellular stress response. Contrary to Cr-based MOFs that was well tolerated by these immune cells.[106], [125]

1.5 Biodegradation

Most MOFs exhibit intrinsic biodegradability under physiological conditions (PBS, pH 7.4 and PBS supplemented with albumin at 37 °C) as a result of relatively labile metal–ligand bonds. In biological applications, a certain amount of instability is desired in order to avoid endogenous accumulation, and the degradation products can be dealt with by the body's own systems.[10]

Studies investigating the degradability of MOFs such as MIL-88A (Fe), MIL-100 (Cr), MIL-101 (Cr), and MIL-53 (Fe, Cr), demonstrated that those solids degrade over days or even weeks. [91][84][85] The particle size composition and the crystalline MOF structure directly affect the degradation process, which in physiological media can be modulated from a few days up to several weeks.

Recently, Li et al. reported the effect of phosphates on nanoMOF degradation (MIL-100 (Fe)) the particles were incubated in PBS at 37 °C compared to water as a control. After six hours, considerable amounts of the constituting trimesate ligand (34±3 wt%) had been dissociated into PBS.[133] These data were consistent with previous reports where corresponding amounts of trimesate were dispersed under analogous conditions.[100] The phosphate concentration directly influenced the nanoMOF degradation mechanism–meaning a higher PBS concentration led to faster degradation.[133], [134] When the same nanoMOFs when analyzed in pure water at 37 °C, imperceptible amounts of their trimesate constituting ligand were dissociated after two days of incubation.[134] These results are in agreement with previous reports where less than 1 wt% trimesate was released after incubation for three days.[90], [135]

It was observed morphological changes by TEM investigations into nanoMOFs degradation on PBS, the sharp initial edges structures turned out into progressive round structures as disintegration occurs; Although this event takes place DLS measurements showed the particles essentially do not decrease drastically the diameter from 221 ± 24 nm to 187 ± 22 nm after two days incubation in PBS, even

though more than 30% of their constitutive ligand has left the particles. These studies confirm that these iron carboxylates based nanoMOFs are stable in water, but degrade in PBS with a progressive departure of the constitutive organic linkers associated with an amorphization. Noteworthy, although their very distinct morphological and structural changes in PBS, nanoMOFs maintain practically unchanged diameters over two days.[134] Same was observed for nanoparticles of MIL-100 (Fe) under similar conditions (in PBS).[134] In vivo MIL-100 (Fe) was degraded into its constitutive components and eliminated in urine and feces after intravenous administration in female Wistar rats, the nanoparticles were promptly sequestered by the liver and spleen, then further biodegraded and directly eliminated in urine or feces without metabolization and substantial toxicity.[127]

A counter effect happens with the microMOFs they degrade very slowly and therefore a concentration of 11,9 mM of PBS was used to accelerate the process. Raman-microscopy revealed that after 8 days of incubation in this medium the particles changed the color, with grey regions on the outer shell while its core remained red, the size of the particles standing unchanged, with less than 0.5% variation in all dimensions. Raman spectra gave useful information regarding MOFs degradation in PBS, suggesting that the most probable degradation mechanism is the competitive replacement of trimesate by phosphate ions in PBS solution. Additionally, Raman microscopy enabled obtaining spectra in different regions on the same particle.[134]

Nevertheless, an appropriate additional stability is still required in order to maintain the structure before reaching their target. Nanoscale MOFs (nanoMOFs) typically release their drug cargo in less than 24 hours. Surface modifications, e.g. coatings like silica, lipid layer, polymer, oligonucleotides, or nucleic acids, can also slow down the degradation of the nanomaterials.[10] Furthermore, cyclodextrin molecules were anchored to the nanoMOFs' surface in order to improve the physicochemical properties of drugs (stability, solubility, and bioavailability). The coatings are stable in body fluids and can be further functionalized with targeting ligands, highlighting the possibility of a versatile surface modification of nanoMOFs for targeted multifunctional drug delivery and other applications.[134]

Lin and coworkers stabilized nanoMOFs by encapsulating them within a silica shell. Silica coatings have been extensively used to modify inorganic and polymer nanoparticles. In order to make this type of coating, the nanomaterials are first coated with a polymer, for example, polyvinylpyrrolidone (PVP), and followed by treatment with tetraethyl orthosilicate (TEOS) in basic ethanol to afford silica coatings The silica shell coating allows improvements correspondent to biocompatibility, water dispersibility, and the ability to further functionalize the coreshell nanostructures, which is a viable method already demonstrates to reach encapsulation and modulate the release.[10][136]

Release is initiated after being internalized into cells, with the ability to induce apoptosis in both human breast and pancreatic cancer cells.

The Mn-bisphosphonate NCP developed by Lin and coworkers was coated with lipid and pegylated to achieve a controlled release and degradation.[96] These nanoparticles were further functionalized with anisamide (AA), which is a small

molecule that has been shown to target σ receptors that are overexpressed by many cancer cells. Release is initiated after being internalized into cells, with the ability to induce apoptosis in both human breast and pancreatic cancer cells. [137]

1.6 Final Remarks and Perspectives

Another approach in drug delivery uses metal-organic frameworks (MOFs), especially NMOFs or nanoMOFs, which have been shown to be well suited as nanocarriers for organic drug or metallodrug delivery. Mainly two approaches have been followed: adsorption of drugs in the porous network or use of drug as a MOF constituent. In both cases, tuning the drug release is the major issue. Nontoxic MOFs (so-called BioMOFs) have been developed and their degradation studied. In cases of limited stability, several approaches have been reported, e.g. core-shell particles. In some cases, modification of the shells can also be used to introduce a targeting unit, for example for specific cancer cells. The combination of a suitable drug carrier with a selective targeting unit also seems to be a very promising way here for improving stability as well as selectivity. The following chapter elucidates the possibility to combine different 3D printing techniques in the design of drug delivery systems and the possibility to incorporate metal-organic frameworks to modulate the drug release.

1.7 Bibliography

[1]   H. Li, M. Eddaoudi, M. O'Keeffe, and O. M. Yaghi, "Design and synthesis of an exceptionally stable and highly porous metal-organic framework," *Nature*, vol. 402, no. 6759, pp. 276–279, 1999, doi: 10.1038/46248.

[2]   J. Lee, O. K. Farha, J. Roberts, K. A. Scheidt, S. T. Nguyen, and J. T. Hupp, "Metal-organic framework materials as catalysts," *Chem. Soc. Rev.*, vol. 38, no. 5, pp. 1450–1459, 2009, doi: 10.1039/b807080f.

[3]   D. Peer, J. M. Karp, S. Hong, O. C. Farokhzad, R. Margalit, and R. Langer, "Nanocarriers as an emerging platform for cancer therapy," *Nat. Nanotechnol.*, vol. 2, no. 12, pp. 751–760, 2007, doi: 10.1038/nnano.2007.387.

[4]   W. Chen and C. Wu, "Synthesis, functionalization, and applications of metal-organic frameworks in biomedicine," *Dalt. Trans.*, vol. 47, no. 7, pp. 2114–2133, 2018, doi: 10.1039/c7dt04116k.

[5]   M. E. Davis, Z. G. Chen, and D. M. Shin, "Nrd2614," *Nat. Rev. Drug Discov.*, vol. 7, no. 9, pp. 771–782, 2008, doi: 10.1038/nrd2614.

[6]   C. S. Kim, B. Duncan, B. Creran, and V. M. Rotello, "Triggered nanoparticles as therapeutics," *Nano Today*, vol. 8, no. 4, pp. 439–447, 2013, doi: 10.1016/j.nantod.2013.07.004.

[7]   C. R. Groom, I. J. Bruno, M. P. Lightfoot, and S. C. Ward, "The Cambridge Structural Database," *Acta Crystallogr. Sect. B*, vol. 72, no. 2, pp. 171–179, 2016, doi: 10.1107/S2052520616003954.

[8]   A. D. Burrows, *The Chemistry of Metal–Organic Frameworks. Synthesis, Characterization, and Applications, 2 Volumes. Edited by Stefan Kaskel.*, vol. 56, no. 6. John Wiley & Sons, Ltd, 2017.

[9]   S. Kaskel, *Metal–Organic Frameworks. Design and Application. Edited by Leonard R. MacGillivray.*, vol. 49, no. 50. 2010.

[10] C. He, D. Liu, and W. Lin, "Nanomedicine Applications of Hybrid Nanomaterials Built from Metal-

Ligand Coordination Bonds: Nanoscale Metal-Organic Frameworks and Nanoscale Coordination Polymers," *Chem. Rev.*, vol. 115, no. 19, pp. 11079–11108, 2015, doi: 10.1021/acs.chemrev.5b00125.

[11] L. Wang, M. Zheng, and Z. Xie, "Nanoscale metal-organic frameworks for drug delivery: A conventional platform with new promise," *J. Mater. Chem. B*, vol. 6, no. 5, pp. 707–717, 2018, doi: 10.1039/c7tb02970e.

[12] R. E. Morris and P. S. Wheatley, "Gas storage in nanoporous materials," *Angew. Chemie - Int. Ed.*, vol. 47, no. 27, pp. 4966–4981, 2008, doi: 10.1002/anie.200703934.

[13] M. Eddaoudi *et al.*, "Systematic Design of Pore Size and Functionality in Isoreticular MOFs and Their Application in Methane Storage," *Science (80-.).*, vol. 295, no. 5554, pp. 469 LP – 472, Jan. 2002, doi: 10.1126/science.1067208.

[14] L. J. Murray, M. Dinc, and J. R. Long, "Hydrogen storage in metal-organic frameworks," *Chem. Soc. Rev.*, vol. 38, no. 5, pp. 1294–1314, 2009, doi: 10.1039/b802256a.

[15] J. R. Li, R. J. Kuppler, and H. C. Zhou, "Selective gas adsorption and separation in metal-organic frameworks," *Chem. Soc. Rev.*, vol. 38, no. 5, pp. 1477–1504, 2009, doi: 10.1039/b802426j.

[16] L. Ma, C. Abney, and W. Lin, "Enantioselective catalysis with homochiral metal-organic frameworks," *Chem. Soc. Rev.*, vol. 38, no. 5, pp. 1248–1256, 2009, doi: 10.1039/b807083k.

[17] L. Y. T. Chou, K. Ming, and W. C. W. Chan, "Strategies for the intracellular delivery of nanoparticles," *Chem. Soc. Rev.*, vol. 40, no. 1, pp. 233–245, 2011, doi: 10.1039/c0cs00003e.

[18] T. Chalati *et al.*, "Porous metal organic framework nanoparticles to address the challenges related to busulfan encapsulation," *Nanomedicine*, vol. 6, no. 10, pp. 1683–1695, Nov. 2011, doi: 10.2217/nnm.11.69.

[19] A. C. McKinlay *et al.*, "BioMOFs: Metal-organic frameworks for biological and medical applications," *Angew. Chemie - Int. Ed.*, vol. 49, no. 36, pp. 6260–6266, 2010, doi: 10.1002/anie.201000048.

[20] M. X. Wu and Y. W. Yang, "Metal–Organic Framework (MOF)-Based Drug/Cargo Delivery and Cancer Therapy," *Adv. Mater.*, vol. 29, no. 23, pp. 1–20, 2017, doi: 10.1002/adma.201606134.

[21] P. Horcajada, R. Gref, T. Baati, P. K. Allan, G. Maurin, and P. Couvreur, "Metal À Organic Frameworks in Biomedicine," pp. 1232–1268, 2012, doi: 10.1021/cr200256v.

[22] C.-Y. Sun, C. Qin, X.-L. Wang, and Z.-M. Su, "Metal-organic frameworks as potential drug delivery systems," *Expert Opin. Drug Deliv.*, vol. 10, no. 1, pp. 89–101, Jan. 2013, doi: 10.1517/17425247.2013.741583.

[23] O. M. Yaghi and H. Li, "Hydrothermal Synthesis of a Metal-Organic Framework Containing Large Rectangular Channels," *J. Am. Chem. Soc.*, vol. 117, no. 41, pp. 10401–10402, May 2002, doi: 10.1021/ja00146a033.

[24] C. Pettinari, F. Marchetti, N. Mosca, G. Tosi, and A. Drozdov, "Application of metal − organic frameworks," *Polym. Int.*, vol. 66, no. 6, pp. 731–744, 2017, doi: 10.1002/pi.5315.

[25] Y. Zhao, "Emerging applications of metal-organic frameworks and covalent organic frameworks," *Chem. Mater.*, vol. 28, no. 22, pp. 8079–8081, 2016, doi: 10.1021/acs.chemmater.6b04677.

[26] D. J. Xiao *et al.*, "Selective, Tunable O2 Binding in Cobalt(II)-Triazolate/Pyrazolate Metal-Organic Frameworks," *J. Am. Chem. Soc.*, vol. 138, no. 22, pp. 7161–7170, Jun. 2016, doi: 10.1021/jacs.6b03680.

[27] J. Li *et al.*, "Metal-organic framework-based materials: Superior adsorbents for the capture of toxic and radioactive metal ions," *Chem. Soc. Rev.*, vol. 47, no. 7, pp. 2322–2356, 2018, doi: 10.1039/c7cs00543a.

[28] M. A. Ward and T. K. Georgiou, *Thermoresponsive Polymers for Biomedical Applications*, vol. 3, no. 3. Molecular Diversity Preservation International, 2011, pp. 1215–1242.

[29] H. Wu, W. Zhou, and T. Yildirim, "High-capacity methane storage in metal-organic frameworks M2(dhtp): The important role of open metal sites," *J. Am. Chem. Soc.*, vol. 131, no. 13, pp. 4995–5000, 2009, doi: 10.1021/ja900258t.

[30] M. Stillman, *Biological Inorganic Chemistry. Structure and Reactivity. Edited by Ivano Bertini, Harry B. Gray, Edward I. Stiefel and Joan S. Valentine.*, vol. 46, no. 46. John Wiley & Sons, Ltd, 2007.

[31] S. Kitagawa, R. Kitaura, and S. I. Noro, "Functional porous coordination polymers," *Angew. Chemie - Int. Ed.*, vol. 43, no. 18, pp. 2334–2375, 2004, doi: 10.1002/anie.200300610.

[32] D. Peer, P. Zhu, C. V. Carman, J. Lieberman, and M. Shimaoka, "Selective gene silencing in activated leukocytes by targeting siRNAs to the integrin lymphocyte function-associated antigen-1," *Proc. Natl. Acad. Sci. U. S. A.*, vol. 104, no. 10, pp. 4095–4100, 2007, doi: 10.1073/pnas.0608491104.

[33] S. Kang *et al.*, "Tunable physiologic interactions of adhesion molecules for inflamed cell-selective drug delivery," *Biomaterials*, vol. 32, no. 13, pp. 3487–3498, 2011, doi: 10.1016/j.biomaterials.2011.01.046.

[34] D. J. Tranchemontagne, J. L. Mendoza-Cortés, M. O'Keeffe, and O. M. Yaghi, "Secondary building units, nets and bonding in the chemistry of metal-organic frameworks," *Chem. Soc. Rev.*, vol. 38, no. 5, pp. 1257–1283, 2009, doi: 10.1039/b817735j.

[35] B. Rungtaweevoranit, C. S. Diercks, M. J. Kalmutzki, and O. M. Yaghi, "Spiers Memorial Lecture:: Progress and prospects of reticular chemistry," *Faraday Discuss.*, vol. 201, no. September, pp. 9–45, 2017, doi: 10.1039/c7fd00160f.

[36] M. Eddaoudi, M. Eddaoudi, J. Kim, N. Rosi, and O. M. Yaghi, "Systematic Design of Pore Size and Functionality in Isoreticular MOFs," *Science (80-.).*, vol. 469, no. 2002, pp. 32–34, 2012, doi: 10.1126/science.1067208.

[37] N. Stock and S. Biswas, "Synthesis of metal-organic frameworks (MOFs): Routes to various MOF topologies, morphologies, and composites," *Chem. Rev.*, vol. 112, no. 2, pp. 933–969, 2012, doi: 10.1021/cr200304e.

[38] Y. R. Lee, J. Kim, and W. S. Ahn, "Synthesis of metal-organic frameworks: A mini review," *Korean J. Chem. Eng.*, vol. 30, no. 9, pp. 1667–1680, 2013, doi: 10.1007/s11814-013-0140-6.

[39] A. Rabenau, "The Role of Hydrothermal Synthesis in Preparative Chemistry," *Angew. Chemie Int. Ed. English*, vol. 24, no. 12, pp. 1026–1040, 1985, doi: 10.1002/anie.198510261.

[40] R. Vakili, S. Xu, N. Al-Janabi, P. Gorgojo, S. M. Holmes, and X. Fan, "Microwave-assisted synthesis of zirconium-based metal organic frameworks (MOFs): Optimization and gas adsorption," *Microporous Mesoporous Mater.*, vol. 260, no. October 2017, pp. 45–53, 2018, doi: 10.1016/j.micromeso.2017.10.028.

[41] M. Taddei *et al.*, "Efficient microwave assisted synthesis of metal-organic framework UiO-66: Optimization and scale up," *Dalt. Trans.*, vol. 44, no. 31, pp. 14019–14026, 2015, doi: 10.1039/c5dt01838b.

[42] V. Safarifard and A. Morsali, "Applications of ultrasound to the synthesis of nanoscale metal-organic coordination polymers," *Coord. Chem. Rev.*, vol. 292, pp. 1–14, 2015, doi: 10.1016/j.ccr.2015.02.014.

[43] Z. Q. Li *et al.*, "Ultrasonic synthesis of the microporous metal-organic framework Cu3(BTC)2 at ambient temperature and pressure: An efficient and environmentally friendly method," *Materials Letters*, vol. 63, no. 1. pp. 78–80, 2009, doi: 10.1016/j.matlet.2008.09.010.

[44] W. J. Son, J. Kim, J. Kim, and W. S. Ahn, "Sonochemical synthesis of MOF-5," *Chem. Commun.*, no. 47, pp. 6336–6338, 2008, doi: 10.1039/b814740j.

[45] M. S. Ulrich Muller, Hermann Putter, Michael Hesse, "Method For Electrochemical Production of A Crystalline Porous Material Organic Skeleton Material," 2007.

[46] O. J. De Lima Neto, A. C. de O. Frós, B. S. Barros, A. F. De Farias Monteiro, and J. Kulesza, "Rapid and efficient electrochemical synthesis of a zinc-based nano-MOF for Ibuprofen adsorption," *New J. Chem.*, vol. 43, no. 14, pp. 5518–5524, 2019, doi: 10.1039/C8NJ06420B.

[47] A. Pichon, A. Lazuen-Garay, and S. L. James, "Solvent-free synthesis of a microporous metal-organic framework," *CrystEngComm*, vol. 8, no. 3, pp. 211–214, 2006, doi: 10.1039/b513750k.

[48] H. Ali-Moussa, R. Navarro Amador, J. Martinez, F. Lamaty, M. Carboni, and X. Bantreil, "Synthesis and post-synthetic modification of UiO-67 type metal-organic frameworks by mechanochemistry," *Mater. Lett.*, vol. 197, pp. 171–174, 2017, doi: 10.1016/j.matlet.2017.03.140.

[49] K. Užarević *et al.*, "Mechanochemical and solvent-free assembly of zirconium-based metal-organic frameworks," *Chem. Commun.*, vol. 52, no. 10, pp. 2133–2136, 2016, doi: 10.1039/c5cc08972g.

[50] A. M. Fidelli *et al.*, "Green and rapid mechanosynthesis of high-porosity NU- and UiO-type metal-organic frameworks," *Chem. Commun.*, vol. 54, no. 51, pp. 6999–7002, 2018, doi: 10.1039/c8cc03189d.

[51] D. Prochowicz *et al.*, "A mechanochemical strategy for IRMOF assembly based on pre-designed oxo-zinc precursors," *Chem. Commun.*, vol. 51, no. 19, pp. 4032–4035, 2015, doi: 10.1039/c4cc09917f.

[52] M. Pilloni *et al.*, "Liquid-assisted mechanochemical synthesis of an iron carboxylate Metal Organic Framework and its evaluation in diesel fuel desulfurization," *Microporous Mesoporous Mater.*, vol. 213, pp. 14–21, 2015, doi: 10.1016/j.micromeso.2015.04.005.

[53] P. A. Julien *et al.*, "In Situ Monitoring and Mechanism of the Mechanochemical Formation of a Microporous MOF-74 Framework," *J. Am. Chem. Soc.*, vol. 138, no. 9, pp. 2929–2932, 2016, doi: 10.1021/jacs.5b13038.

[54] R. Ameloot, F. Vermoortele, W. Vanhove, M. B. J. Roeffaers, B. F. Sels, and D. E. De Vos, "Interfacial synthesis of hollow metalĝ€"organic framework capsules demonstrating selective permeability," *Nat. Chem.*, vol. 3, no. 5, pp. 382–387, 2011, doi: 10.1038/nchem.1026.

[55] Q. Shi, Z. Chen, Z. Song, J. Li, and J. Dong, "Synthesis of ZIF-8 and ZIF-67 by steam-assisted conversion and an investigation of their tribological behaviors," *Angew. Chemie - Int. Ed.*, vol. 50, no. 3, pp. 672–675, 2011, doi: 10.1002/anie.201004937.

[56] I. Ahmed, J. Jeon, N. A. Khan, and S. H. Jhung, "Synthesis of a metal-organic framework, iron-benzenetricarboxylate, from dry gels in the absence of acid and salt," *Cryst. Growth Des.*, vol. 12, no. 12, pp. 5878–5881, 2012, doi: 10.1021/cg3014317.

[57] S. Ali Akbar Razavi and A. Morsali, "Linker functionalized metal-organic frameworks," *Coord. Chem. Rev.*, vol. 399, p. 213023, 2019, doi: 10.1016/j.ccr.2019.213023.

[58] B. F. Hoskins and R. Robson, "Infinite Polymeric Frameworks Consisting of Three Dimensionally Linked Rod-like Segments," *J. Am. Chem. Soc.*, vol. 111, no. 15, pp. 5962–5964, 1989, doi: 10.1021/ja00197a079.

[59] Z. Wang and S. M. Cohen, "Postsynthetic covalent modification of a neutral metal-organic framework," *J. Am. Chem. Soc.*, vol. 129, no. 41, pp. 12368–12369, 2007, doi: 10.1021/ja074366o.

[60] P. T. Deka, R. Ediati, and D. Prasetyoko, "Crystal Growth of IRMOF-3 (Isoreticular Metal-Organic Frameworks-3) Synthesized using Solvothermal Method," *IPTEK J. Proc. Ser.*, vol. 0, no. 1, pp. 230–234, 2014, doi: 10.12962/j23546026.y2014i1.416.

[61] T. Haneda, M. Kawano, T. Kawamichi, and M. Fujita, "Direct observation of the labile imine formation through single-crystal-to-single-crystal reactions in the pores of a porous coordination network," *J. Am. Chem. Soc.*, vol. 130, no. 5, pp. 1578–1579, 2008, doi: 10.1021/ja7111564.

[62] S. M. Cohen, "The Postsynthetic Renaissance in Porous Solids," *J. Am. Chem. Soc.*, vol. 139, no. 8, pp. 2855–2863, 2017, doi: 10.1021/jacs.6b11259.

[63] A. Ferguson *et al.*, "Controlled partial interpenetration in metal-organic frameworks," *Nat. Chem.*, vol. 8, no. 3, pp. 250–257, 2016, doi: 10.1038/nchem.2430.

[64] Q. Chen *et al.*, "A Controllable Gate Effect in Cobalt(II) Organic Frameworks by Reversible Structure Transformations," *Angew. Chemie*, vol. 125, no. 44, pp. 11764–11767, 2013, doi: 10.1002/ange.201306304.

[65] H. Aggarwal *et al.*, "Direct evidence for single-crystal to single-crystal switching of degree of interpenetration in a metal-organic framework," *J. Am. Chem. Soc.*, vol. 136, no. 10, pp. 3776–3779, Feb. 2014, doi: 10.1021/ja500530y.

[66] O. Karagiaridi, W. Bury, J. E. Mondloch, J. T. Hupp, and O. K. Farha, "Solvent-assisted linker exchange: An alternative to the de novo synthesis of unattainable metal-organic frameworks," *Angew. Chemie - Int. Ed.*, vol. 53, no. 18, pp. 4530–4540, 2014, doi: 10.1002/anie.201306923.

[67] S. M. Cohen, "Postsynthetic methods for the functionalization of metal-organic frameworks," *Chem. Rev.*, vol. 112, no. 2, pp. 970–1000, 2012, doi: 10.1021/cr200179u.

[68] P. Deria, J. E. Mondloch, O. Karagiaridi, W. Bury, J. T. Hupp, and O. K. Farha, "Beyond post-synthesis modification: Evolution of metal-organic frameworks via building block replacement," *Chem. Soc. Rev.*, vol. 43, no. 16, pp. 5896–5912, 2014, doi: 10.1039/c4cs00067f.

[69] Z. Yin, S. Wan, J. Yang, M. Kurmoo, and M. H. Zeng, "Recent advances in post-synthetic modification of metal–organic frameworks: New types and tandem reactions," *Coord. Chem. Rev.*, vol. 378, pp. 500–512, 2019, doi: 10.1016/j.ccr.2017.11.015.

[70] J. D. Evans, C. J. Sumby, and C. J. Doonan, "Post-synthetic metalation of metal-organic frameworks," *Chem. Soc. Rev.*, vol. 43, no. 16, pp. 5933–5951, 2014, doi: 10.1039/c4cs00076e.

[71] M. Lalonde, W. Bury, O. Karagiaridi, Z. Brown, J. T. Hupp, and O. K. Farha, "Transmetalation: Routes to metal exchange within metal-organic frameworks," *J. Mater. Chem. A*, vol. 1, no. 18, pp. 5453–5468, 2013, doi: 10.1039/c3ta10784a.

[72] C. K. Brozek and M. Dincă, "Cation exchange at the secondary building units of metal-organic frameworks," *Chem. Soc. Rev.*, vol. 43, no. 16, pp. 5456–5467, 2014, doi: 10.1039/c4cs00002a.

[73] T. O. B. Olusanya, R. R. H. Ahmad, D. M. Ibegbu, J. R. Smith, and A. A. Elkordy, "Liposomal drug delivery systems and anticancer drugs," *Molecules*, vol. 23, no. 4, pp. 1–17, 2018, doi: 10.3390/molecules23040907.

[74] H. Wang *et al.*, "Preparation, pharmacokinetics, biodistribution, antitumor efficacy and safety of Lx2-32c-containing liposome," *PLoS One*, vol. 9, no. 12, pp. 1–13, 2014, doi: 10.1371/journal.pone.0114688.

[75] S. J. Wang *et al.*, "A phase 0 study of the pharmacokinetics, biodistribution, and dosimetry of 188Re-liposome in patients with metastatic tumors," *EJNMMI Res.*, vol. 9, 2019, doi: 10.1186/s13550-019-0509-6.

[76] V. Yurgel, T. Collares, and F. Seixas, "Developments in the use of nanocapsules in oncology," *Brazilian J. Med. Biol. Res.*, vol. 46, no. 6, pp. 486–501, 2013, doi: 10.1590/1414-431X20132643.

[77] H. K. and T. J. Das C, Lucia MS, "乳鼠心肌提取 HHS Public Access," *Physiol. Behav.*, vol. 176, no. 3, pp. 139–148, 2017, doi: 10.1016/j.physbeh.2017.03.040.

[78] F. U. Din *et al.*, "Effective use of nanocarriers as drug delivery systems for the treatment of selected tumors," *Int. J. Nanomedicine*, vol. 12, pp. 7291–7309, 2017, doi: 10.2147/IJN.S146315.

[79] S. Hossen, M. K. Hossain, M. K. Basher, M. N. H. Mia, M. T. Rahman, and M. J. Uddin, "Smart nanocarrier-based drug delivery systems for cancer therapy and toxicity studies: A review," *J. Adv. Res.*, vol. 15, pp. 1–18, 2019, doi: 10.1016/j.jare.2018.06.005.

[80] M. E. Grigore, "iMedPub Journals Organic and Inorganic Nano-Systems Used in Cancer Treatment Abstract Nano-Systems in Cancer Treatment," *J. Med. Res. Heal. Educ.*, vol. Vol. 1, no. October, pp. 1–8, 2017.

[81] P. Horcajada, C. Serre, M. Vallet-Regí, M. Sebban, F. Taulelle, and G. Férey, "Metal-organic frameworks as efficient materials for drug delivery," *Angew. Chemie - Int. Ed.*, vol. 45, no. 36, pp. 5974–5978, 2006, doi: 10.1002/anie.200601878.

[82] Y. Jiao, Z. Li, Y. Ma, G. Zhou, S. Wang, and G. Lu, "The studies on gas adsorption properties of MIL-53 series MOFs materials," *AIP Adv.*, vol. 7, no. 8, 2017, doi: 10.1063/1.4999914.

[83] P. Horcajada *et al.*, "Flexible Porous Metal-Organic Frameworks for a Controlled Drug Delivery," *Heal. (San Fr.*, pp. 6774–6780, 2008, doi: 10.1021/ja710973k.

[84] B. Singco, L. H. Liu, Y. T. Chen, Y. H. Shih, H. Y. Huang, and C. H. Lin, "Approaches to drug delivery: Confinement of aspirin in MIL-100(Fe) and aspirin in the de novo synthesis of metal-organic frameworks," *Microporous Mesoporous Mater.*, vol. 223, pp. 254–260, 2016, doi: 10.1016/j.micromeso.2015.08.017.

[85] R. Anand *et al.*, "Host–Guest Interactions in Fe(III)-Trimesate MOF Nanoparticles Loaded with Doxorubicin," *J. Phys. Chem. B*, vol. 118, no. 29, pp. 8532–8539, Jul. 2014, doi: 10.1021/jp503809w.

[86] C. Adhikari and A. Chakraborty, "Smart Approach for In Situ One-Step Encapsulation and Controlled Delivery of a Chemotherapeutic Drug using Metal–Organic Framework–Drug Composites in Aqueous Media," *ChemPhysChem*, vol. 17, no. 7, pp. 1070–1077, Apr. 2016, doi: 10.1002/cphc.201501012.

[87] N. Getachew, Y. Chebude, I. Diaz, and M. Sanchez-Sanchez, "Room temperature synthesis of metal organic framework MOF-2," *J. Porous Mater.*, vol. 21, no. 5, pp. 769–773, 2014, doi: 10.1007/s10934-014-9823-6.

[88] D. J. Tranchemontagne, J. R. Hunt, and O. M. Yaghi, "Room temperature synthesis of metal-organic frameworks: MOF-5, MOF-74, MOF-177, MOF-199, and IRMOF-0," *Tetrahedron*, vol. 64, no. 36, pp. 8553–8557, 2008, doi: 10.1016/j.tet.2008.06.036.

[89] V. Agostoni *et al.*, "A 'green' strategy to construct non-covalent, stable and bioactive coatings on porous MOF nanoparticles," *Sci. Rep.*, vol. 5, pp. 1–7, 2015, doi: 10.1038/srep07925.

[90] V. Agostoni *et al.*, "Towards an Improved anti-HIV Activity of NRTI via Metal–Organic Frameworks Nanoparticles," *Adv. Healthc. Mater.*, vol. 2, no. 12, pp. 1630–1637, Dec. 2013, doi: 10.1002/adhm.201200454.

[91] P. Horcajada *et al.*, "Porous metal-organic-framework nanoscale carriers as a potential platform for drug deliveryand imaging," *Nat. Mater.*, vol. 9, no. 2, pp. 172–178, 2010, doi: 10.1038/nmat2608.

[92] H. Chevreau *et al.*, "Synthesis of the biocompatible and highly stable MIL-127(Fe): From large scale synthesis to particle size control," *CrystEngComm*, vol. 18, no. 22, pp. 4094–4101, 2016, doi: 10.1039/c5ce01864a.

[93] D. Cunha *et al.*, "Rationale of drug encapsulation and release from biocompatible porous metal-organic frameworks," *Chem. Mater.*, vol. 25, no. 14, pp. 2767–2776, 2013, doi: 10.1021/cm400798p.

[94] S. Du and H. Zhang, *Metal-Organic Frameworks for Photonics Applications*. 2014.

[95] K. M. L. Taylor-Pashow, J. Della Rocca, Z. Xie, S. Tran, and W. Lin, "Postsynthetic modifications of iron-carboxylate nanoscale metal-organic frameworks for imaging and drug delivery," *J. Am. Chem. Soc.*, vol. 131, no. 40, pp. 14261–14263, 2009, doi: 10.1021/ja906198y.

[96] W. J. Rieter, K. M. Pott, K. M. Taylor, and W. Lin, "Nanoscale coordination polymers for platinum-based anticancer drug delivery. TL - 130," *J. Am. Chem. Soc.*, vol. 130 VN-, no. 35, pp. 11584–11585, 2008, doi: 10.1021/ja803383k.

[97] X. G. Wang *et al.*, "A multifunctional metal-organic framework based tumor targeting drug delivery system for cancer therapy," *Nanoscale*, vol. 7, no. 38, pp. 16061–16070, 2015, doi: 10.1039/c5nr04045k.

[98] Q. Chen, M. Xu, W. Zheng, T. Xu, H. Deng, and J. Liu, "Se/Ru-Decorated Porous Metal-Organic Framework Nanoparticles for the Delivery of Pooled siRNAs to Reversing Multidrug Resistance in Taxol-Resistant Breast Cancer Cells," *ACS Appl. Mater. Interfaces*, vol. 9, no. 8, pp. 6712–6724, Mar. 2017, doi: 10.1021/acsami.6b12792.

[99] X. Yin, B. Yang, B. Chen, M. He, and B. Hu, "Multifunctional gold nanocluster decorated metal-organic framework for real-time monitoring of targeted drug delivery and quantitative evaluation of cellular therapeutic response," *Anal. Chem.*, vol. 91, no. 16, pp. 10596–10603, 2019, doi: 10.1021/acs.analchem.9b01721.

[100] S. Rojas, F. J. Carmona, C. R. Maldonado, E. Barea, and J. A. R. Navarro, "RAPTA-C incorporation and controlled delivery from MIL-100(Fe) nanoparticles," *New J. Chem.*, vol. 40, no. 7, pp. 5690–5694, 2016, doi: 10.1039/c5nj02741a.

[101] J. Wang *et al.*, "Fe-MIL-101 exhibits selective cytotoxicity and inhibition of angiogenesis in ovarian cancer cells via downregulation of MMP," *Sci. Rep.*, vol. 6, no. April, pp. 1–13, 2016, doi: 10.1038/srep26126.

[102] S. D. Taherzade, J. Soleimannejad, and A. Tarlani, "Application of metal-organic framework Nano-MIL-100(Fe) for sustainable release of doxycycline and tetracycline," *Nanomaterials*, vol. 7, no. 8, Aug. 2017, doi: 10.3390/nano7080215.

[103] M. Al Haydar, H. R. Abid, B. Sunderland, and S. Wang, "Metal organic frameworks as a drug delivery system for flurbiprofen," *Drug Des. Devel. Ther.*, vol. 11, pp. 2685–2695, Sep. 2017, doi: 10.2147/DDDT.S145716.

[104] T. Hidalgo *et al.*, "Chitosan-coated mesoporous MIL-100(Fe) nanoparticles as improved bio-compatible oral nanocarriers," *Sci. Rep.*, vol. 7, no. January, pp. 1–14, Mar. 2017, doi: 10.1038/srep43099.

[105] A. Nel, T. Xia, L. Mädler, and N. Li, "Toxic potential of materials at the nanolevel," *Science (80-.).*, vol. 311, no. 5761, pp. 622–627, 2006, doi: 10.1126/science.1114397.

[106] S. Wuttke *et al.*, "Validating Metal-Organic Framework Nanoparticles for Their Nanosafety in Diverse Biomedical Applications," *Adv. Healthc. Mater.*, vol. 6, no. 2, pp. 1–11, 2017, doi: 10.1002/adhm.201600818.

[107] J. Feng *et al.*, "Stimuli-responsive multifunctional metal-organic framework nanoparticles for enhanced chemo-photothermal therapy," *J. Mater. Chem. B*, vol. 7, no. 6, pp. 994–1004, 2019, doi: 10.1039/c8tb02815j.

[108] Q. Hu, J. Yu, M. Liu, A. Liu, Z. Dou, and Y. Yang, "A low cytotoxic cationic metal-organic framework carrier for controllable drug release," *J. Med. Chem.*, vol. 57, no. 13, pp. 5679–5685, 2014, doi: 10.1021/jm5004107.

[109] R. Piga, Y. Saito, Y. Yoshida, and E. Niki, "Cytotoxic effects of various stressors on PC12 cells: Involvement of oxidative stress and effect of antioxidants," *Neurotoxicology*, vol. 28, no. 1, pp. 67–75, 2007, doi: 10.1016/j.neuro.2006.07.006.

[110] X. Zhu *et al.*, "Inherent anchorages in UiO-66 nanoparticles for efficient capture of alendronate and its mediated release," *Chem. Commun.*, vol. 50, no. 63, pp. 8779–8782, 2014, doi: 10.1039/c4cc02570a.

[111] M. Filippousi *et al.*, "Biocompatible Zr-based nanoscale MOFs coated with modi fi ed poly (e -caprolactone) as anticancer drug carriers," *Int. J. Pharm.*, vol. 509, no. 1–2, pp. 208–218, 2016, doi: 10.1016/j.ijpharm.2016.05.048.

[112] H. Dong *et al.*, "Folic Acid Functionalized Zirconium-Based Metal–Organic Frameworks as Drug Carriers for Active Tumor-Targeted Drug Delivery," *Chem. - A Eur. J.*, vol. 24, no. 64, pp. 17148–17154, 2018, doi: 10.1002/chem.201804153.

[113] B. Illes, S. Wuttke, and H. Engelke, "Liposome-coated iron fumarate metal-organic framework nanoparticles for combination therapy," *Nanomaterials*, vol. 7, no. 11, pp. 1–11, 2017, doi: 10.3390/nano7110351.

[114] C. He, K. Lu, D. Liu, and W. Lin, "Nanoscale metal-organic frameworks for the co-delivery of cisplatin and pooled siRNAs to enhance therapeutic efficacy in drug-resistant ovarian cancer cells," *J. Am. Chem. Soc.*, vol. 136, no. 14, pp. 5181–5184, 2014, doi: 10.1021/ja4098862.

[115] X.-X. Yang, P. Feng, J. Cao, W. Liu, and Y. Tang, "Composition-Engineered Metal–Organic Framework-Based Microneedles for Glucose-Mediated Transdermal Insulin Delivery," *ACS Appl. Mater. Interfaces*, 2020, doi: 10.1021/acsami.9b20774.

[116] C. Tamames-Tabar *et al.*, "A Zn azelate MOF: Combining antibacterial effect," *CrystEngComm*, vol. 17, no. 2, pp. 456–462, 2015, doi: 10.1039/c4ce00885e.

[117] S. Rojas, T. Devic, and P. Horcajada, "Metal organic frameworks based on bioactive components," *J. Mater. Chem. B*, vol. 5, no. 14, pp. 2560–2573, 2017, doi: 10.1039/C6TB03217F.

[118]   J. An, S. J. Geib, and N. L. Rosi, "Cation-triggered drug release from a porous zinc-adeninate metal-organic framework," *J. Am. Chem. Soc.*, vol. 131, no. 24, pp. 8376–8377, 2009, doi: 10.1021/ja902972w.

[119]   S. N. Kim *et al.*, "Metal-organic frameworks, NH2-MIL-88(Fe), as carriers for ophthalmic delivery of brimonidine," *Acta Biomater.*, vol. 79, pp. 344–353, Oct. 2018, doi: 10.1016/j.actbio.2018.08.023.

[120]   M. Hoop *et al.*, "Biocompatibility characteristics of the metal organic framework ZIF-8 for therapeutical applications," *Appl. Mater. Today*, vol. 11, pp. 13–21, 2018, doi: 10.1016/j.apmt.2017.12.014.

[121]   Z. Lu, *Nanomaterials in Pharmacology IN AND Series Editor*. .

[122]   D. F. Williams, "On the mechanisms of biocompatibility," *Biomaterials*, vol. 29, no. 20, pp. 2941–2953, 2008, doi: 10.1016/j.biomaterials.2008.04.023.

[123]   T. Simon-Yarza, S. Rojas, P. Horcajada, and C. Serre, "The situation of metal-organic frameworks in biomedicine," in *Comprehensive Biomaterials II*, vol. 4, no. April 2016, Elsevier, 2017, pp. 719–749.

[124]   M. Sajid, "Toxicity of nanoscale metal organic frameworks: a perspective," *Environ. Sci. Pollut. Res.*, vol. 23, no. 15, pp. 14805–14807, 2016, doi: 10.1007/s11356-016-7053-y.

[125]   T. Simon-Yarza, A. Mielcarek, P. Couvreur, and C. Serre, "Nanoparticles of Metal-Organic Frameworks: On the Road to In Vivo Efficacy in Biomedicine," *Adv. Mater.*, vol. 30, no. 37, Sep. 2018, doi: 10.1002/adma.201707365.

[126]   M. Mizutani, N. Maejima, K. Jitsukawa, H. Masuda, and H. Einaga, "An infinite chiral single-helical structure formed in Cu(II)-L-/D-glutamic acid system," *Inorganica Chim. Acta*, vol. 283, no. 1, pp. 105–110, 1998, doi: 10.1016/S0020-1693(98)00224-2.

[127]   T. Baati *et al.*, "In depth analysis of the in vivo toxicity of nanoparticles of porous iron(iii) metal–organic frameworks," *Chem. Sci.*, vol. 4, no. 4, pp. 1597–1607, 2013, doi: 10.1039/c3sc22116d.

[128]   T. Kundu, S. Mitra, P. Patra, A. Goswami, D. Díazdíaz, and R. Banerjee, "Mechanical downsizing of a gadolinium(III)-based metal-organic framework for anticancer drug delivery," *Chem. - A Eur. J.*, vol. 20, no. 33, pp. 10514–10518, 2014, doi: 10.1002/chem.201402244.

[129]   T. Simon-Yarza *et al.*, "In vivo behavior of MIL-100 nanoparticles at early times after intravenous administration," *Int. J. Pharm.*, vol. 511, no. 2, pp. 1042–1047, Sep. 2016, doi: 10.1016/j.ijpharm.2016.08.010.

[130]   E. Lammer, G. J. Carr, K. Wendler, J. M. Rawlings, S. E. Belanger, and T. Braunbeck, "Is the fish embryo toxicity test (FET) with the zebrafish (Danio rerio) a potential alternative for the fish acute toxicity test?," *Comp. Biochem. Physiol. - C Toxicol. Pharmacol.*, vol. 149, no. 2, pp. 196–209, 2009, doi: 10.1016/j.cbpc.2008.11.006.

[131]   A. Ruyra *et al.*, "Synthesis, culture medium stability, and in vitro and in vivo zebrafish embryo toxicity of metal-organic framework nanoparticles," *Chem. - A Eur. J.*, vol. 21, no. 6, pp. 2508–2518, 2015, doi: 10.1002/chem.201405380.

[132]   C.-H. Liu, H.-C. Chiu, H.-L. Sung, J.-Y. Yeh, K. C.-W. Wu, and S.-H. Liu, "Acute oral toxicity and repeated dose 28-day oral toxicity studies of MIL-101 nanoparticles," *Regul. Toxicol. Pharmacol.*, vol. 107, no. July, p. 104426, 2019, doi: 10.1016/j.yrtph.2019.104426.

[133]   E. Bellido, M. Guillevic, T. Hidalgo, M. J. Santander-Ortega, C. Serre, and P. Horcajada,

"Understanding the colloidal stability of the mesoporous MIL-100(Fe) nanoparticles in physiological media," *Langmuir*, vol. 30, no. 20, pp. 5911–5920, 2014, doi: 10.1021/la5012555.

[134]   X. Li *et al.*, "New insights into the degradation mechanism of metal-organic frameworks drug carriers," *Sci. Rep.*, vol. 7, no. 1, pp. 1–11, 2017, doi: 10.1038/s41598-017-13323-1.

[135]   V. Agostoni *et al.*, "Impact of phosphorylation on the encapsulation of nucleoside analogues within porous iron(iii) metal-organic framework MIL-100(Fe) nanoparticles," *J. Mater. Chem. B*, vol. 1, no. 34, pp. 4231–4242, 2013, doi: 10.1039/c3tb20653j.

[136]   W. J. Rieter, K. M. L. Taylor, and W. Lin, "Surface Modification and Functionalization of Nanoscale Metal-Organic Frameworks for Controlled Release and Luminescence Sensing Surface Modification and Functionalization of Nanoscale Metal-Organic Frameworks for Controlled Release and Luminescence Sensi," *J. Am. Chem. Soc.*, vol. 129, no. d, pp. 9852–9853, 2007, doi: 10.1021/ja073506r.

[137]   D. Liu, C. He, C. Poon, and W. Lin, "Theranostic nanoscale coordination polymers for magnetic resonance imaging and bisphosphonate delivery," *J. Mater. Chem. B*, vol. 2, no. 46, pp. 8249–8255, 2014, doi: 10.1039/c4t b00751d.

Chapter 2: The application of nanoscale MOF MIL-101(Fe) combined with 3D printing

2.1 Introduction to 3D printing

Developed in the mid-1980s, the additive manufacturing (AM), known as 3D printing, has emerged as a resourceful technology platform for rapid manufacturing. The equipment and materials were mostly applied in optics, chemistry, and robotics research.[1] The 3D printing was established as an additive layer manufacturing rapid prototyping technique that enables the production of a physical object from a computer-aided digital file.[2] One of the first to accomplish the development of a rapid prototyping technique using a single laser beam was Hideo Kodama in the early '80s. His published work relied on experiments to develop methods for automatic fabrication of three-dimensional models using UV rays and a photosensitive resin, using a mask to control the exposure of the UV source, describing techniques of solidifying thin consecutive layers of photopolymer that would later evolve to what we know today as stereolithography (SLA).[3]

In 1984, Hull invented stereolithography (SL), his patent issued in 1986 described a mechanism where liquid polymers were hardened under UV light to form cross-sections of a 3D model, using digital data and a computer-controlled beam of light to create each layer, one on top of the other. Afterward, he produced and sold stereolithography machinery by 3D Systems, founded by him where the first SLA printer was produced in 1988.[3], [4]

About the same time as Hull´s SLA patent, Deckhard developed the concept of the selective laser sintering (SLS) process, based on the selective solidification of powder using a laser beam. The first SLS printers were produced in 1992 by Desktop Manufacturing Corporation (DTM Corp), later acquired by 3D Systems. Deckhard went on another entrepreneur project, Sinterstation 2000, launching the SLS technology for industry in 2000.[3], [5]

In 1989, Scott and Crump filed a patent for the fused deposition modeling (FDM), another rapid prototyping technique in which a plastic filament or metal wire was heated in a nozzle and extruded. The deposition was commanded by a computer, based on a predetermined digital model, where each layer was kept in temperature just below the solidification point promoting a good interlayer adhesion. Eventually, Stratasys, a company founded by them, developed thermoplastic and printer systems for 3D printing.[3], [6], [7]

Later in 1994, the Massachusetts Institute of Technology (MIT) developed the 3D inkjet printing technology, named "three-dimensional printing techniques". Nowadays, the 3D printing technology mainly refers to the layer-by-layer processes.[8]–[10]

2.2 How does 3D printing work?

3D printing is an approach to produce a physical object, layer by layer, from a three-dimensional digital file of the object that will be printed. The prevailing way is to

create a digital model with Computer-Aided Design – CAD (Figure 2.1). Additionally, there is also the possibility to analyze a real-world object and through 3D scanning create its digital replica. The last approach is generally used for reverse engineering tasks by industry professionals.[11]

When the CAD design is finished, the file needs to be converted into an appropriate file extension, called STL (STereoLithography also Standard Tessellation Language), and sent to the printer. In other words, this file format carries a triangular mesh (polygons), describing the layout/surface of a three-dimensional object.[11]

The following operation, known as slicing, is based on translating the 3D file into instructions for the 3D printer. It consists of dividing or chopping the 3D model into hundreds or thousands of horizontal layers, telling the machine exactly what to do, step by step. Afterwards, a new file format is generated called G-code, with the file extension .gcode. G-code is the most widely used numerical code programming language and use to communicate with the machine. The machine will follow the automated G-code instructions and generate a path for the nozzle to follow based on the geometry of the part and user-specified settings (Figure 2.2). [11], [12]

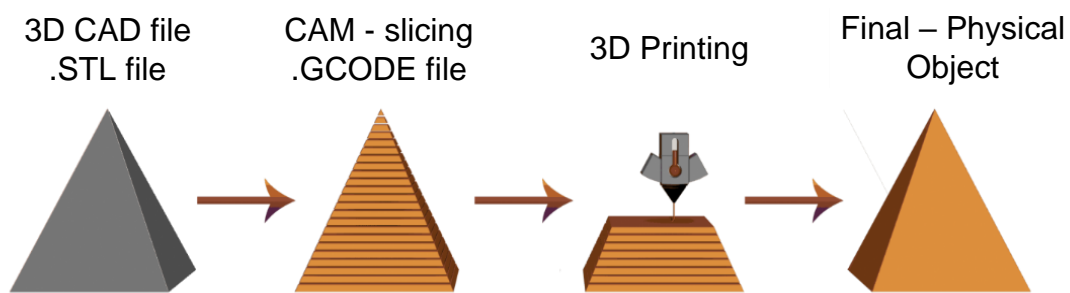| 3D CAD file .STL file	CAM - slicing .GCODE file	3D Printing	Final – Physical Object

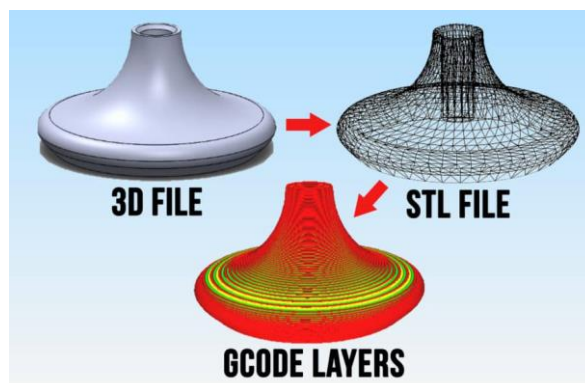Figure 2.1. Principles of 3D printing and how it works. Taken from ref. [11]

Figure 2.2. Representation of a software converting digital 3D files into G-code. Taken from ref. [12]

2.3 Types of 3D printing

In (Table 2.1) are listed types of 3D printing techniques, according to their methods.

Table 2.1. 3D printing techniques and their methods.

3D Method	Printing techniques
Extrusion:	Fused Deposition Modeling (FDM)
Light polymerization:	Stereolithography (SLA);
	Digital Light Processing (DLP);
Powder Bed:	Selective Laser Sintering (SLS);
	Selective laser melting (SLM);
	Electronic Beam Melting (EBM);
Lamination:	Laminated Object manufacturing (LOM)

Stereolithography

Contemplated as the first 3D printing process, stereolithography (SLA) remains one of the most utilized 3D printing methods today (Figure 2.3). It is a laser-based process that applies photopolymer resins reacting with the laser. The material is then is cured to form a solid in a precise way to produce objects. Naturally, there are some limitations to the materials and applications of this method since this method produces only non-porous solid objects.

The machine consists of a perforated build plate that is lowered to the vat surface containing a liquid photoresin and a UV laser beam. The UV laser beam traces the first layer of the object using the 3D model information, as the laser reaches the resin causing the photopolymerization reaction a thin layer of the photoresin is then solidified. When the layer is formed the build plate is lifted and lowered creating the layers until the whole object is constructed. This method has an outstanding surface finish, combining precision and fast manufacture.

The disadvantage of this method is the raw material cost, to form the object is needed to add supporting structures that are placed on the 3D model that will be then later manually removed, another factor is, after the printing the object has still some unpolymerized resin on its surface, even though is a imperceptible amount, adds the necessity of more steps such as, washing with organic solvents e.g. ethanol or isopropyl alcohol, followed by a cure in a UV-light chamber to complete the process.[13], [14]
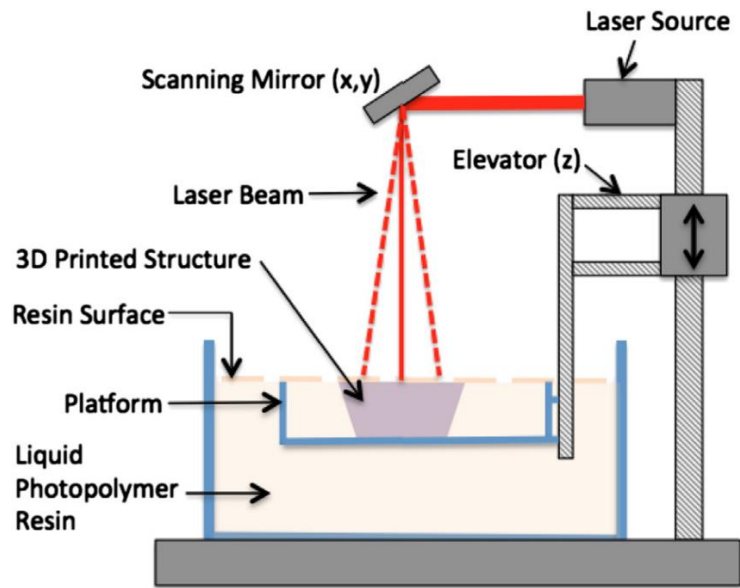
Figure 2.3. Diagram illustrating the components of a stereolithography system.Taken from: [3]

Fused Deposition Modeling

The principle of the FDM technique consists of an extrusion, where a movable heater head deposits the molten material on a substrate (Figure 2.4). The material used in this technique is a polymer filament that is pulled from a spool into a hot end (also called nose), by moving either the build plate or the hot end, the building material is heated to a temperature above its melting point to accelerate the solidification after extrusion, the polymers used in this process are made from a water-soluble material in order to be relatively easily washed away the excess of material once the print is completed.

The advantages of this method are the application of non-toxic inexpensive materials, such as polylactic acid (PLA), acrylonitrile butadiene styrene (ABS), medical grades ABS; although PLA is still the most applicable beginner-friendly, there are other types of polymers that had broadened the method, such as polyethylene terephthalate glycol (PETG), acrylonitrile styrene acrylate (ASA), and polyether ether ketone (PEEK). On the other hand, process fabrication may be slower in comparison with the SL method, the surface finishing of the parts is also not as good SL due to the fact the material extrusion may not be stopped quickly enough.
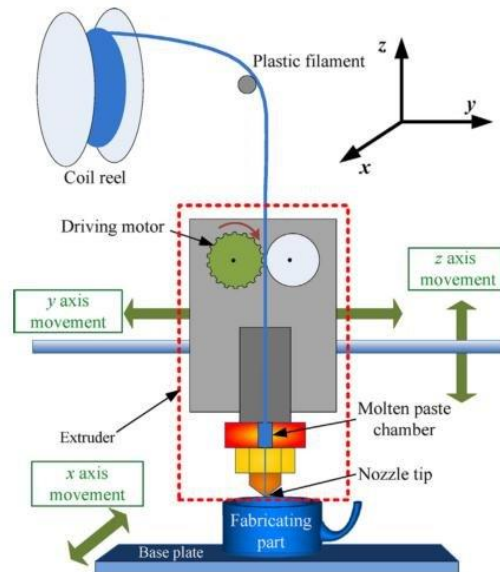
Figure 2.4. Fused Deposition Modeling system. Taken from:[15]

Selective Laser Sintering technique (SLS):

The powder bed fusion process consists of an electron beam melting (EBM), selective laser sintering (SLS), and selective heat sintering (SHS) printing technique. The SLS employs either a highly energized electron beam or laser, as a thermal source to melt or fuse the material powder together.[2]

This 3D printing technique consists of a powder bed fusion (PBF) method, (Figure 2.6) where a build plate with a polymer (approximately with 30–90 μm in dimension) that is preheated close to the melting transition and above the temperature necessary for recrystallization during the cooling cycle. A preheating on the build plate limits the energy input necessary from the laser to cause sintering, avoiding large thermal differentials that would otherwise result in part distortion.[16]

A thermal source a high-power CO_2 laser is applied to promote depending on the laser power chosen a partial or full fusion between the powder particles, followed by a recoater to add and smooth the next powder layer, the smoothing occurs between the sintering steps, that are interspersed with the application of an incremental layer of prepolymer powder of approximately 100μm applied by the recoater. The mechanism for binding applied here are mainly sintering and melting, the laser power (in a range up to 20–50W), beam size (typically about 0.5mm), beam speed and spacing between scans (both physical, known as hatch spacing, and temporal) needs to be carefully controlled to balance effective sintering while avoiding polymer property degradation that comes with overheating. [16], [17]

In this process the building material consists generally of a semi-crystalline, particulate thermoplastic, that is heated inside the building chamber, the temperature applied should be enough for the polymer chains to reach flexibility without reaching its melting point, as an example the polyamide -12 that is widely used in his method.

There is also polypropylene (PP), polyurethane (PU), poly(acrylonitrile/butadiene/styrene) (ABS), polycarbonate (PC), polystyrene (PS), and work continues to develop with high-density polyethylene, polyether ether ketone (PEEK) that needs considerably higher powder bed temperatures.[2], [14], [16]

When using this method, the particles must be free-flowing, considering the layers receive no further compaction. For this reason, particle size, shape, and free packing along with thermal behavior are critical factors in the material design. Typically, spherical particles have an easier flow and pack more densely in comparison with irregular shapes, therefore ground polymer processing is challenging since it creates irregular shape and a broad particle size distribution. On the other hand small particles also present process complications regarding their excessive cohesion or electrostatic repulsive forces.[16]

Afterward, the building chamber is gradually cooled down to maximize polymer crystallization while provides added strength as well as to reduce stress development and improve dimensional accuracy, which can be improved further by incorporation of shrinkage modeling into the initial part design. The free powder collected by the overflow containers can generally be reused in a new building process, in this case, there is the possibility of altering the material e.g. oxidation, therefore in order to avoid thermal degradation, the recycled powder is mixed with virgin powder for subsequent use. [16]

The model used to produce the 3D samples was the Sharebot's SnowWhite® (Figure 2.5) the (Figure 2.6) show the parts of the machine in details.

Figure 2.5. The SnowWhite® model used to produce the samples.

The machine works in two different modes: Environment mode, where the temperature is kept constant in the build chamber and the powder mode, where the heaters are controlled by the build platform temperature, the process can take twice as the amount of time needed in the environmental mode, but the mechanical resistance reached in the powder mode is higher.[10]
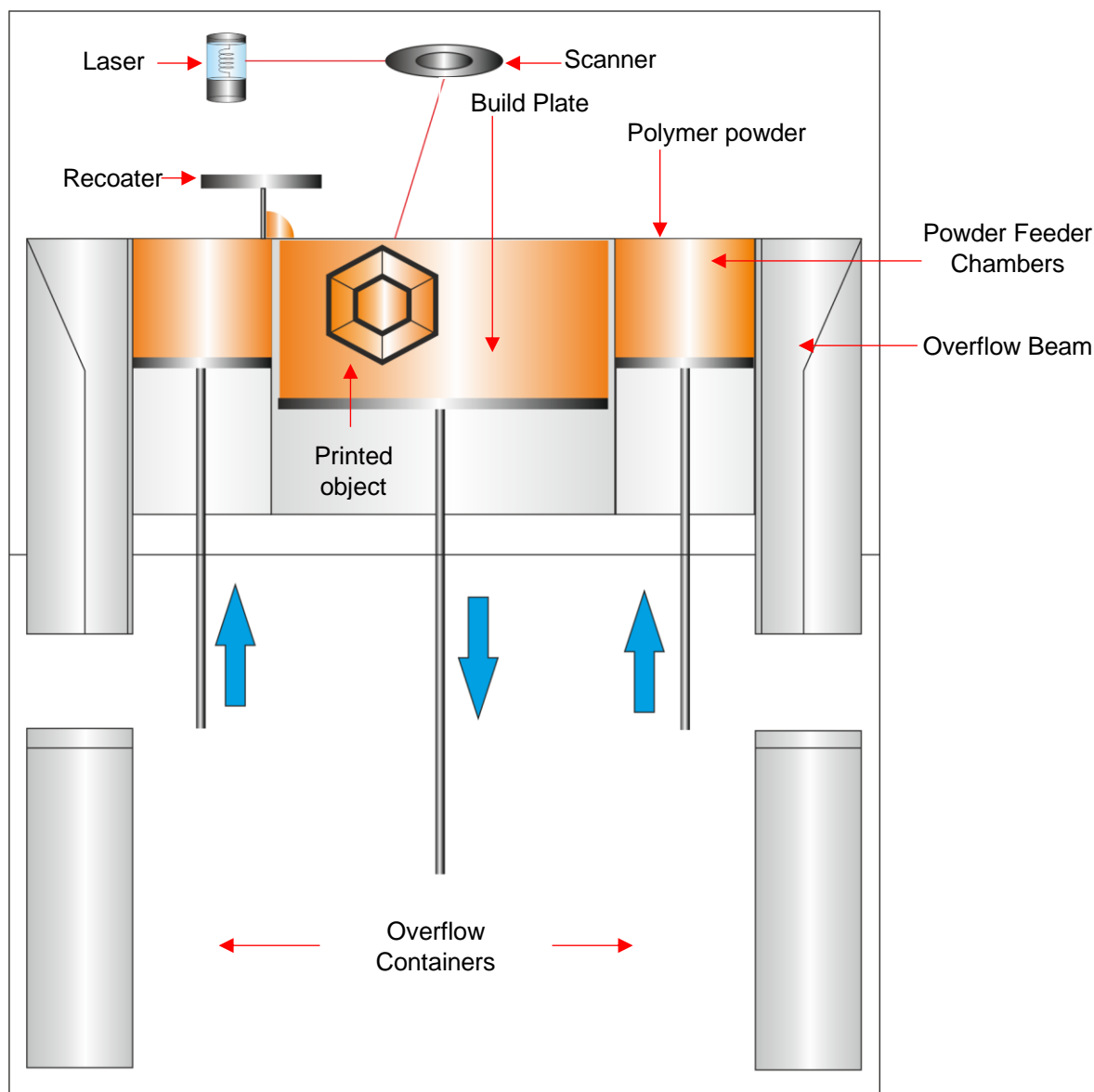
Figure 2.6. Representation of the SnowWhite® machine.

A significant advantage of the SLS technique is the possibility to customize different geometries, in terms of drug application when compared with the traditional process of manufacturing dosage forms, this way, different structures can be designed into the object with good mechanical properties especially if you intend to design prototypes or small production batches, allowing an even fiver level of control over the structure.

In order to do so, a series of parameters that will alter the sintering level is defined. For instance, parameters, like laser power and laser rate are defined as power applied in the inner part of the object, and the laser movement speed in points per second for the object border, respectively.

Those parameters will modify the melting degree within the material, as an example, by using a high laser power and high temperature, the energy density applied is also high, in a way that the object may be completely molten, producing a dense structure instead of a porous one.

Another prospect is the combination of different energy densities in the same structure, as an example is possible to modulate a drug release by applying a higher energy density for the outer sample section and a low energy density in the inner part structure, conferring a more dense sample to the outer section and a porous one in the inner structure (Figure 2.7).[8], [9], [14], [18]

Other parameters like *waiting time* (in seconds) refers to the time needed by the machine to wait before starting the heating process and after the end of the heating process. The *wait layer* (in seconds) is associated with the recoater movement, determining the time after the end of the layer until the recoater moves. The *warming layers* are related to the pre-heating that must be done before starting the printing. After all the parameters are defined the printing process begins.[10]

Altogether, the possibility to alter the inner structure of the samples by altering the parameters conceives an advantage in comparison with other 3D printed techniques mentioned above, as an example, in FDM the filament is completely molten excluding the possibility to design a solid porous sample, the same principle applies for the SL where polymerization mechanism leads to a completely dense structure, also the lack of supporting for producing a sample by the SLS is another advantage, once the object is supported by the surrounding powder, although the amounts necessary are relatively high, around 300g the excess of powder can often be recycled.[14], [19]
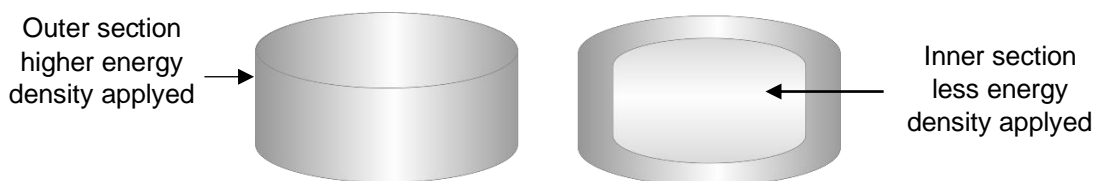
Figure 2.7. Representation of a 3D printed sample produced in a combination of different energy densities.

2.4 The process of sample fabrication

The following procedure is reproduced according to the Sharebot SnowWhite® user manual (2019).

I.   The 3D solid model (Figure 2.8) is designed with a stereolithography CAD software (computer-aided design), saved in the .stl file format and divided in slices by the software called *Slicer*. The slicer software then converts the file into G-code to be interpreted by the 3D printer. Additionally, the number of printed objects is selected, their shape, the number of layers, and the configuration of those layers, such as a concentric or parallel configuration. Those parameters, together with the laser power and the temperature inside the chamber, will directly influence properties, like porosity and mechanical strength. In the present work the software used was *Solidworks*.
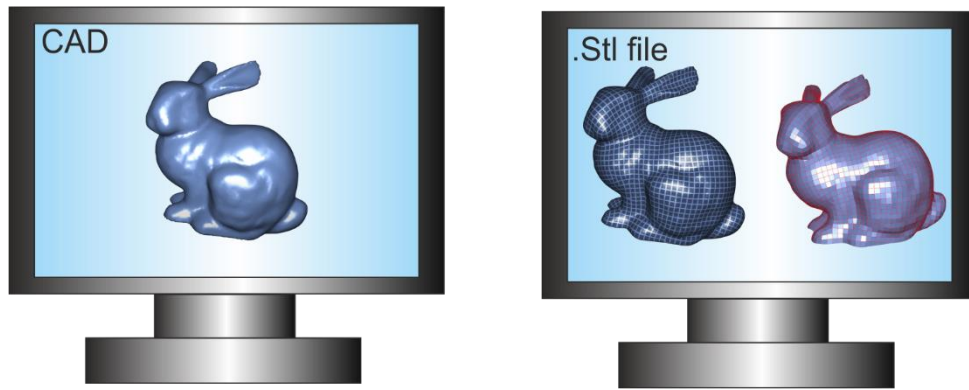
Figure 2.8. 3D Solid Model design representation.

II.   The powder feeder and the building platform shown in detail previous to the filling in (Figure 2.9) will be filled with the polymer that is supposed to be printed (Figure 2.10). Those areas will then be heated according to the temperature previously selected in the printer software (this temperature is just below the polymer melting point allowing the chains to reach a certain mobility facilitating layers adhesion).
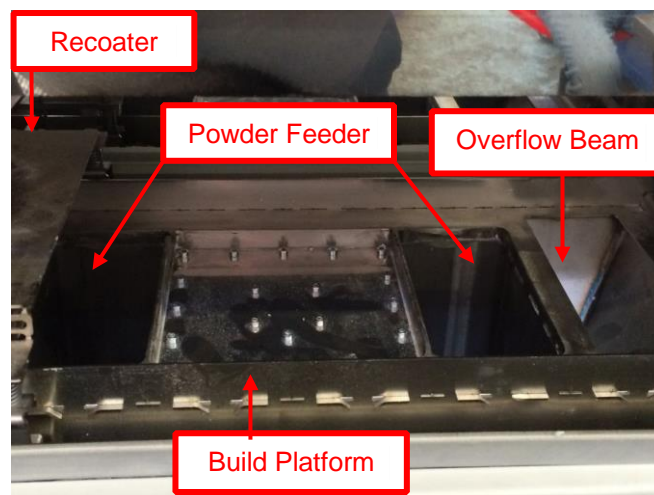
Figure 2.9. The module of sample preparation and its parts specified in detail.

Figure 2.10. The module of sample preparation filled with polymer.

III.   The recoater (Figure 2.11) deposits a very thin layer of the polymer on top of the building platform. After the layer deposition, the CO_2 laser beam (14 Watts)

starts to scan the surface selectively sintering the powder and solidifying a section of the part. After this process, the building platform moves down to create the other layer, in order to support the subsequent layers a small amount of unsintered powder still remains over the surface.

(a)   (b)
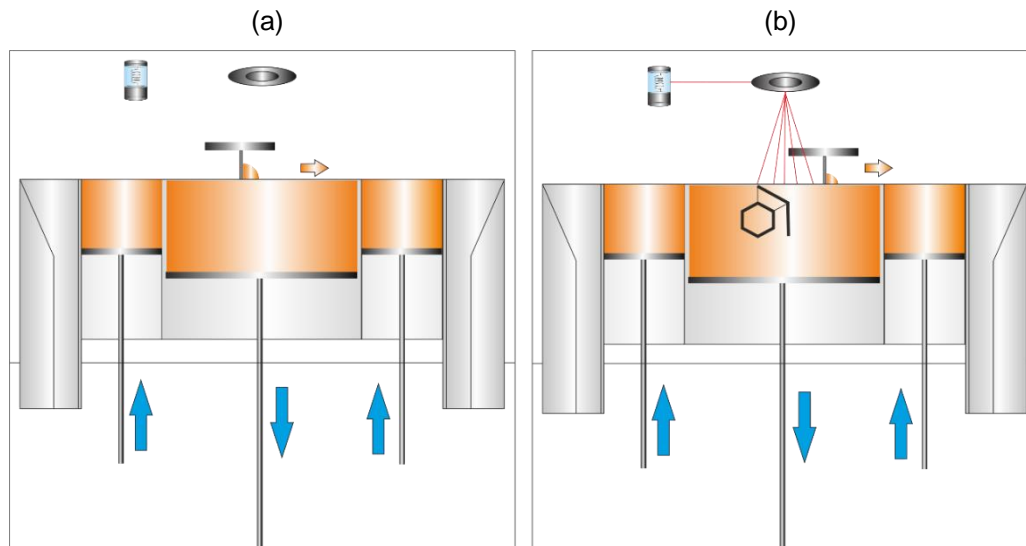

Figure 2.11. (a)The recoater layer deposition movement. (b) The laser selectively sintering and creating the objec.

IV.   A new layer is then deposited by the recoater on the top of the scanned layer; Followed by the laser beam that starts to sinter the successive part of the solid onto the previous layer. The recoater goes back to the initial position and the whole process is repeated until all parts are fully manufactured (Figure 2.12).

(a)   (b)
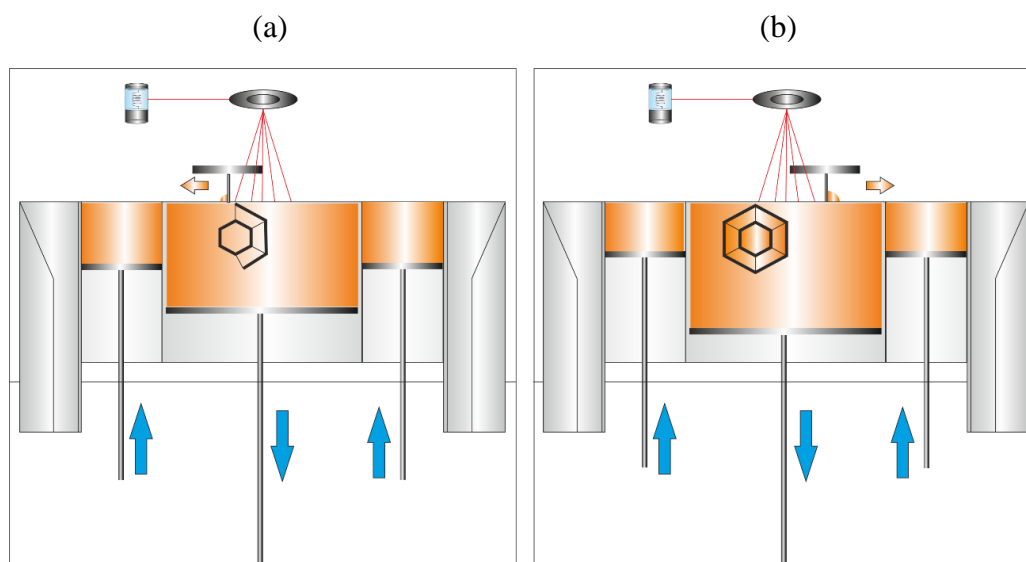
Figure 2.12. (a) The process of sample selectively sintering, (b) The finished sample process.

2.5 The incorporation of MIL-101(Fe) onto a porous solid matrix

In the last few years, the metal-organic framework MIL-101 (Fe), (MIL: Materials Institute Lavousier) by Férey et al. has been extensively studied as drug delivery

systems (see Chapter 1 of this thesis). The MIL family is built using trivalent metal ions and carboxylic acid-based bridging ligands, exhibiting a biocompatible and biodegradable crystalline structure which, due to its high porosity and regular stability, can act as a molecular sponge. [20][21][22]

Methods such as, oriented nucleation and oriented growth, dip-coating, sol-gel processing, step-by-step routes have been widely studied, [23][24] advancements in nanotechnology provided new ways to functionalize MOFs, but still, the research has focused on MOF growth from rigid substrates that narrows those, in terms of application. [25][26] New studies had been developed on the immobilization of MOFs, onto textiles through the deposition onto polymer solutions, as a way to fabricate functional textiles. [27][28]

The possibility to own tunable properties provides to the MOF chemistry a wide range of possible applications, as an example, a copper-base MOF embedding in a poly(vinyl acetate) as a polymer matrix, mixed matrix membranes (MMMs) are often used for gas separations, improving the gas transport properties over the pure polymer.[29] On the other hand, the functional applicability of polymeric surfaces for therapeutic applications in 3D printing is still unfolding. [2]

As a proof of concept was reported the possible application for SLS is 3D printed gas adsorbents, by studying the incorporation of a copper-based MOF, copper (II) benzene-1,3,5-tricarboxylate (HKUST-1) using the PA-12 as a supporting polymer matrix, by mixing the two components. The MOF crystals were capable to be unaltered and were uniformly distributed by the printing process, as it is demonstrated by the HIM images (Figure 2.13) .[30]

The possibility to combine the MOFs obtained by the solvothermal synthesis with the SLS technique, enabling at the end to have a solid porous structure, that will have the MOF incorporated is exhibited as a new MOF application.

Therefore, the aim of this investigation was to explore the applicability of the SLS technique as a method to produce a polyamide-12 matrix that will act as a support for the MIL-101(Fe).
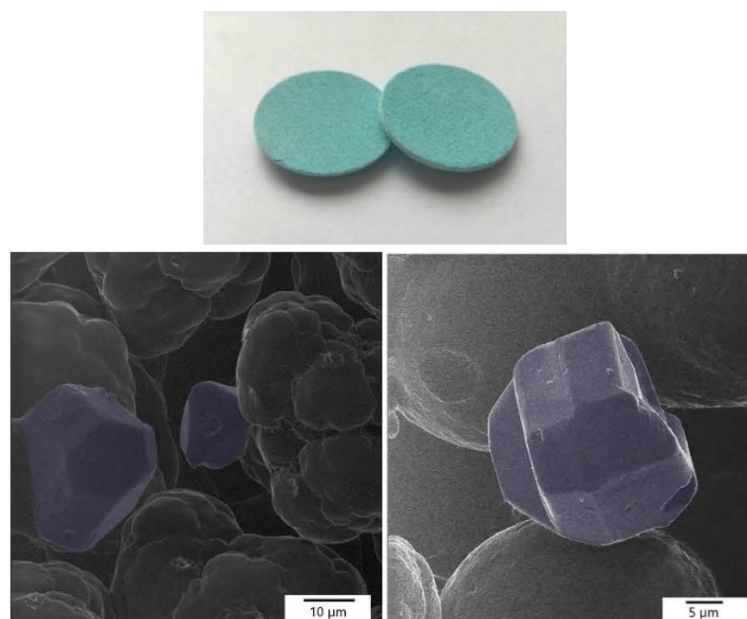

Figure 2.13. SLS 3D printed tablets and HIM of PA-12/HKNUST-1 images. Taken from:[30]

2.6 Experimental Section

The regular process for manufacturing 3D objects has been already discussed in detail, in sections 2.3 and 2.4 of this thesis chapter. Therefore, in this section, it will be discussed the experimental process of sample fabrication in terms of testing different polymers for 3D printing application and the blending of different materials in 3D printing.

Among the polyamide 12, a second biopolymer proposed for the 3D printing study was chitin (Figure 2.14), a linear polysaccharide composed of (1→4)-linked 2-acetamindo-2-deoxy-β-D-glucopyranose units, similar to cellulose, but it contains an additional acetamide group, $-NHCOCH_3$. Its properties such as, biocompatibility, non-toxicity, wound healing are very promising in terms of bio-applications.[31][32]
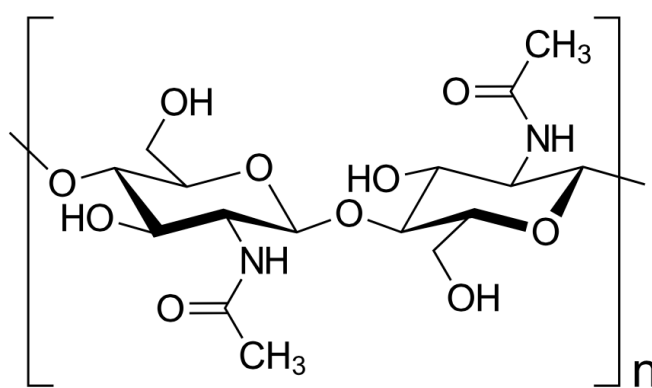
Figure 2.14. Chitin structure.

In terms of combining different materials using a polymer matrix as a supporting material, the process for sample preparation is relatively simple. Generally, when two components are being mixed is recommended that the properties of the additive are as close as possible from the supporting material.

The components are blended together in a defined ratio, there is a range of materials that can be blended and used in 3D printing processes, the only requirements are the melting point that must be near or higher to the melting point of the supporting polymer and the particle size, as mentioned on section 2.3 of this thesis the particle size employed for the SLS method is rather small. For this investigation, the polymanide-12 (PA-12) was applied as supporting material for the iron-based MOF MIL-101(Fe).

The following stage consists of identifying the suitable experimental parameters that will highly influence the physical characteristics of the object and therefore its importance in terms of doing some preliminary tests in terms of operating those parameters for a specific application.

For instance, parameters, like laser power and speed as well as the temperature and cooling rate, are altered to obtain chemically functional objects with the desired physical characteristics. After the printing, the unsintered powder is removed from the surface of the sample.

2.6.1 Characterization techniques

Scanning Electron Microscopy (SEM)

In order to analyze the structure morphology, integrity under the laser power, and the sample porosity the characterization was made by Scanning Electron Microscopy (SEM). The SEM employs the information of secondary electrons (SE), backscattered electrons (BSE), and emitted X-rays to visualize the sample morphology. The image of the topology is built up by raster scanning of the surface. In most cases, secondary electrons are detected as imaging signals. Thereby, a resolution up to a few nanometers is possible. Further, back-scattered electrons (BSE) can provide information about element distribution in the sample because the intensity of BSE is strongly related to the atomic number of the chemical elements. An X-ray can be applied to determine the elemental composition of the surface as the emitted frequencies are element dependent (EDX).

The printed tablets were covered with approximately 15 nm of gold, using the mini sputter SC7620 from Quorum Technologies and analyzed under the VEGA3, from Tescan.

Fourier Transform Infrared Spectroscopy (FTIR)

The IR spectroscopy was used to identify the functional groups present in MOF MIL-101 (Fe) and the tablets produced by the SLS technique.

IR spectroscopy is fundamentally the absorption of electromagnetic waves in the infrared area, in this area molecule vibrations and/or rotations are encouraged depending on the length and strength of the covalent bonds. The whole scope of infrared irradiation ranges over wave numbers from 10 cm^{-1} to 14000 cm^{-1}.

It can be categorized into three regions: near-infrared (14000 cm^{-1} - 4000 cm^{-1}), mid-infrared (4000 cm^{-1} - 400 cm^{-1}) and far-infrared (400 cm^{-1} - 10 cm^{-1}). Due to the typical stimulation energies, it is possible to determine different functional groups in molecules. To describe the transitions between different vibrational states, the quantum mechanical model of the anharmonic oscillator is applied (Figure 2.15).
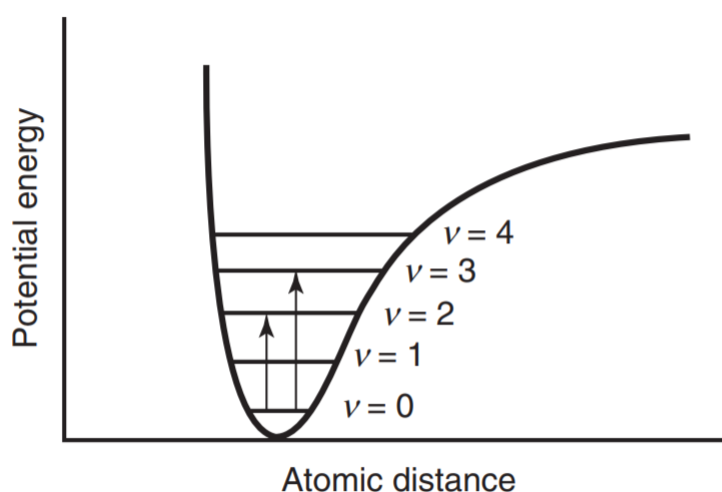

Figure 2.15. Potential of the anharmonic oscillator.

In case the wavelength of the infrared light fits the energy between different vibrational states it is absorbed, resulting in characteristic vibrational bands in the IR spectrum of the analyzed molecule or material, respectively.

Currently, IR spectroscopy is performed by a Fourier-Transform-IR (FTIR) spectrometer. In contrast to a classical scanning IR spectrometer using monochromatic irradiation, polychromatic light is guided through a Michelson interferometer. The resulting time-depending data is translated via Fourier-Transformation into the common infrared spectrum which is a function of the wavenumber.

FTIR spectroscopy has three major advantages compared to classical spectroscopy:

- time-saving aspect (multiplex of Fellgett's advantage)
- better signal to noise ratio (Jacquinot advantage)
- better wavelength accuracy (Cones advantage)

Nonetheless, IR spectroscopy is only applicable if the vibration is accompanied by a dipole moment change. Complementary to IR, Raman spectroscopy can be applied to investigate molecules missing vibrational modes with a change in dipole moment.

2.7 Results and discussion

The build of the 3D printed tablets using chitin as polymer was done according to the general 3D printing procedure described in section 2.4 of this thesis chapter. In order to identify suitable experimental parameters a series of tests were done, in which those could be optimized to achieve a solid porous structure with good mechanical properties.

Due to chitin´s, not well-defined melting point, rather than reaching a temperature that allows the mobility of the chains, the polymer was directly degradeted. Usually, chitin starts to degrade at 220-230°C, polymers with a rigid backbone, such as cellulose and chitin are acknowledged to involve a crystalline character, but the melting point cannot be easily detected considering they start to degrade even before the second-order transition temperature of these polymers.[33], [34] This is a possible explanation for the lack of chitin stability under the laser beam, therefore the 3D printing process for chitin was not a successful approach, as demonstrated in (Figure 2.16).
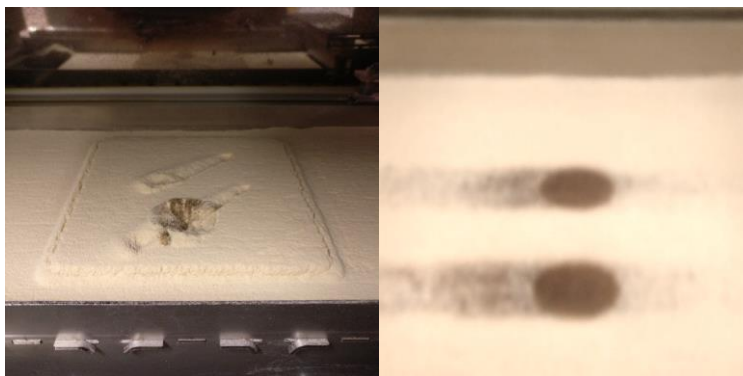

Figure 2.16. 3D SLS attempts of chitin printing

In the case of PA-12/MIL-101(Fe), before the components were blended together, a sequence of tests with the supporting polymer PA-12 was made with the same purpose as for the chitin tests, parameter optimization. Tablets with Ø 16,63 mm, were 3D printed.

Following the well-defined parameters for the PA -12, the iron-based MOF MIL-101(Fe), was incorporated into the structure, a mixture of PA-12/MIL- 101 (Fe) in a concentration of 0,5 wt% was then printed. Despite the fact that it was possible to achieve a porous solid 3D printed tablets, in all experiments the samples located in the front part of the building platform presented a bad layer's adhesion a recrystallization process seemed to take place, but this assumption was later discarded, as a result of MIL-101(Fe) stability being up to 350 °C.[8][35]

SEM microscopy was employed to characterize the tablets morphology, the material was covered with gold so the charging effect can be then reduced so that the tablet's surface could be analyzed.

Through SEM investigation in (Figure 2.17), the octahedral characteristic morphology described by Lin et al. (2009), for the MIL-101(Fe) is placed into the supporting polymer PA-12, demonstrating the crystal is stable under the laser power, in corroboration that is possible to produce 3D printing objects with the SLS technique, applying the PA-12 as a supporting polymer for the MIL -101(Fe).[36]
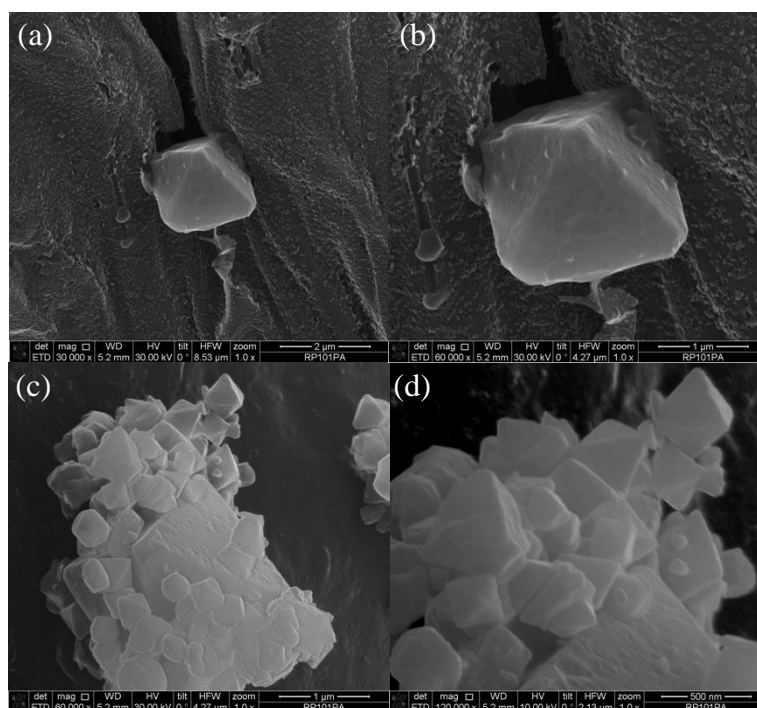
Figure 2.17. (a) SEM for the PA-12/MIL-101 (Fe) mixture with 2 µm magnification; (b) SEM PA-12/MIL-101 (Fe) mixture with 1 µm magnification; (c) SEM PA-12/MIL- 101 (Fe) the characteristic orthogonal shape with 1 µm magnification; (d) SEM PA-12/MIL-101 (Fe) with 500 nm magnification.

The FTIR spectra of the MIL-101(Fe) and PA-12/MIL-101(Fe) 3D printed samples are shown in (Figure 2.18). Analogous to MIL-101(Fe), characteristic bands of carboxylate groups of the peaks derived from terephthalic acid obtained from asymmetric and symmetrical C–O bonds at 1300–1700cm^{-1} and the benzene ring at

721cm^{-1} are found in PA-12/MIL-101(Fe). The two noticeable peaks found at 3313 and 3090 cm^{-1} are associated with stretching vibrations of the hydroxyl groups in MIL-101(Fe) and N-H groups in PA-12, respectively. In addition, the peaks at 551 cm^{-1} for MIL-101(Fe) and 538 cm^{-1} for PA-12/MIL-101(Fe) are related to the Fe–O vibration. It was seen that all characteristic peaks of the MIL-101(Fe) spectrum shifted slightly to the left for the PA-12/MIL-101(Fe) spectrum. This band-shifting provides spectroscopic evidence for the hydrogen bonding interactions, also the intensity of the peak at 3313 cm^{-1} is remarkably decreased in comparison with that of MIL-101(Fe), indicating the MIL-101(Fe) was successfully incorporated into the PA-12 3D printed supporting polymer matrix.[37]–[39]
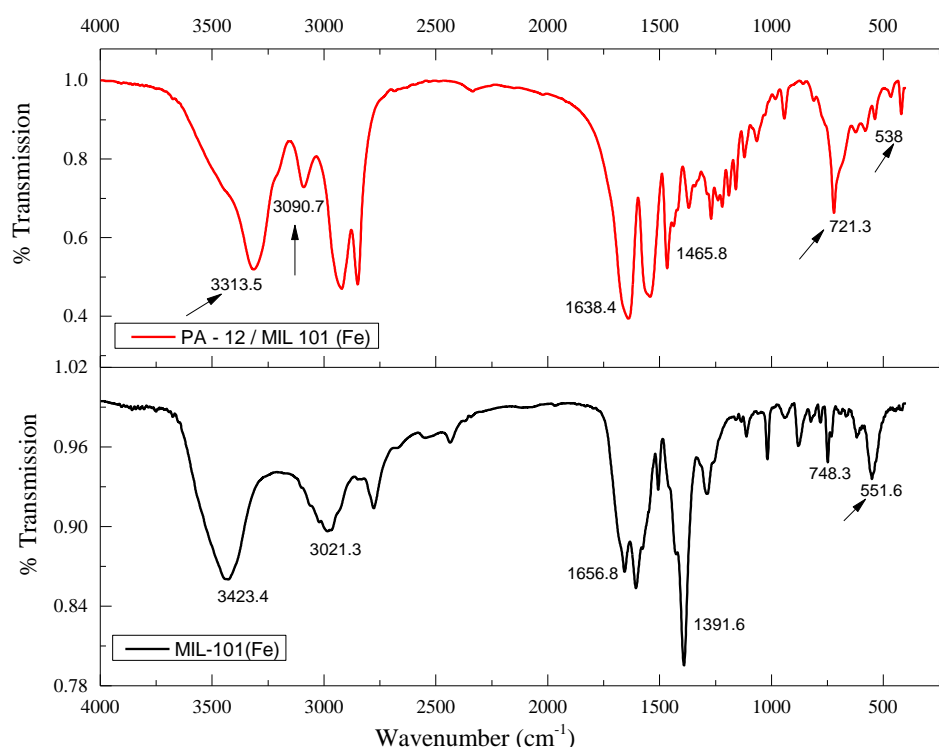
Figure 2.18. FTIR spectra of MIL-101 (Fe) (bottom) and the mixture PA-12/MIL-101 (Fe) (top).

2.8 Conclusion

The purpose of this investigation was to identify if processes of additive manufacturing, such as SLS, could be employed in fabricating chemically functional 3D printed objects. The potential to customize the size, shape, and geometry, by simply blending the components, on the SLS method altogether with the possibility to alter the physical properties by altering the parameters is a wide resourcefulness method of accessible applicability.

The SEM and FTIR studies confirmed the stability and incorporation of the iron-based MOF, MIL-101(Fe), for this purpose. In addition, it was demonstrated that the Selective Laser Sintering Technique can be used to incorporate a metal-organic framework, MIL-101 (Fe), into a PA-12 supporting polymer, producing a porous solid structure. Although chitin was ineligible for this method other biodegradable polymers such as polyvinylpyrrolidone (PVP), can be investigated in further studies. Chapter 3

explores the incorporation of curcumin into the MIL-101(Fe), as well as the application of SLS as a possible technique to modulate drug release to reach longer periods of releasing.

2.9 Bibliography

[1] A. International, *INTERNATIONAL STANDARD ISO / ASTM Additive manufacturing — General principles — Terminology*, vol. 5. 2015.

[2] K. Vithani, A. Goyanes, V. Jannin, A. W. Basit, S. Gaisford, and B. J. Boyd, "An Overview of 3D Printing Technologies for Soft Materials and Potential Opportunities for Lipid-based Drug Delivery Systems," *Pharm. Res.*, vol. 36, no. 1, 2019, doi: 10.1007/s11095-018-2531-1.

[3] A. Su and S. J. Al'Aref, *History of 3D printing*. Elsevier Inc., 2018.

[4] R. H. Crawford and J. J. Beaman, *Solid freeform fabrication*, vol. 36, no. 2. 2002.

[5] D. Composite, M. Layer, and P. E. L. Chiesa, "United States Patent (19)," 1997.

[6] Wohlers Associates Inc., "Wohler's report 2015 - 3D printing and additive manufacturing state of the industry. Annual Worldwide Progress Report.," *Wohlers Rep. 2012*, pp. 32–42, 2015.

[7] S. S. Crump, "Modeling apparatus for three-dimensional objects," 1994.

[8] G. V. Salmoria, R. A. Paggi, A. Lago, and V. E. Beal, "Microstructural and mechanical characterization of PA12/MWCNTs nanocomposite manufactured by selective laser sintering," *Polym. Test.*, vol. 30, no. 6, pp. 611–615, 2011, doi: 10.1016/j.polymertesting.2011.04.007.

[9] J. Zhang, X. Feng, H. Patil, R. V. Tiwari, and M. A. Repka, "Coupling 3D printing with hot-melt extrusion to produce controlled-release tablets," *Int. J. Pharm.*, vol. 519, no. 1–2, pp. 186–197, 2017, doi: 10.1016/j.ijpharm.2016.12.049.

[10] "Sharebot SnowWhite User Manual," *Sharebot srl*, 2017. https://www.sharebot.it/downloads/SnowWhite/EN_snowwhite_manuale.pdf.

[11] "How 3D Printing Works." http://my3dconcepts.com/explore/how-3d-printing-works/ (accessed Jun. 04, 2020).

[12] "3D Slicing Software – The Basics – The 3D Bros." https://the3dbros.com/3d-slicing-software-the-basics/ (accessed Jun. 05, 2020).

[13] M. Gao, "3D Printing of Nanostructures," in *Advanced Nano Deposition Methods*, 2016, pp. 209–221.

[14] E. Lahtinen, "Chemically Functional 3D Printing: Selective Laser Sintering of Customizable Metal Scavengers," 2019.

[15] P. I. Anakhu, C. A. Bolu, A. A. Abioye, and J. Azeta, "Fused Deposition Modeling Printed Patterns for Sand Casting in a Nigerian Foundry : A Review," *Ijaer*, vol. 13, no. 7, pp. 5113–5119, 2018.

[16] J. W. Stansbury and M. J. Idacavage, "3D printing with polymers: Challenges among expanding options and opportunities," *Dent. Mater.*, vol. 32, no. 1, pp. 54–64, 2016, doi: 10.1016/j.dental.2015.09.018.

[17] J. Y. Lee, J. An, and C. K. Chua, "Fundamentals and applications of 3D printing for novel materials," *Appl. Mater. Today*, vol. 7, pp. 120–133, 2017, doi: 10.1016/j.apmt.2017.02.004.

[18] G. Jonathan and A. Karim, "3D printing in pharmaceutics: A new tool for designing customized drug delivery systems," *Int. J. Pharm.*, vol. 499, no. 1–2, pp. 376–394, 2016, doi: 10.1016/j.ijpharm.2015.12.071.

[19] N. Shahrubudin, P. Koshy, J. Alipal, M. H. A. Kadir, and T. C. Lee, "Challenges of 3D printing technology for manufacturing biomedical products: A case study of Malaysian manufacturing firms," *Heliyon*, vol. 6, no. 4, p. e03734, 2020, doi: 10.1016/j.heliyon.2020.e03734.

[20] L. Wang, M. Zheng, and Z. Xie, "Nanoscale metal-organic frameworks for drug delivery: A conventional platform with new promise," *J. Mater. Chem. B*, vol. 6, no. 5, pp. 707–717, 2018, doi: 10.1039/c7tb02970e.

[21] C. He, D. Liu, and W. Lin, "Nanomedicine Applications of Hybrid Nanomaterials Built from Metal-Ligand Coordination Bonds: Nanoscale Metal-Organic Frameworks and Nanoscale Coordination Polymers," *Chem. Rev.*, vol. 115, no. 19, pp. 11079–11108, 2015, doi: 10.1021/acs.chemrev.5b00125.

[22] D. Peer, J. M. Karp, S. Hong, O. C. Farokhzad, R. Margalit, and R. Langer, "Nanocarriers as an emerging platform for cancer therapy," *Nat. Nanotechnol.*, vol. 2, no. 12, pp. 751–760, 2007, doi: 10.1038/nnano.2007.387.

[23] K. J. Kim *et al.*, "Nucleation and growth of oriented metal-organic framework thin films on thermal SiO2 surface," *Thin Solid Films*, vol. 659, no. November 2017, pp. 24–35, 2018, doi: 10.1016/j.tsf.2018.05.026.

[24] O. Shekhah *et al.*, "Step-by-step route for the synthesis of metal organic frameworks (Supporting Information)," *J. Am. Chem. Soc.*, vol. 129, no. 49, pp. S1–S5, 2007.

[25] J. K. Bristow, K. T. Butler, K. L. Svane, J. D. Gale, and A. Walsh, "Chemical bonding at the metal-organic framework/metal oxide interface: Simulated epitaxial growth of MOF-5 on rutile TiO2," *J. Mater. Chem. A*, vol. 5, no. 13, pp. 6226–6232, 2017, doi: 10.1039/c7ta00356k.

[26] S. Hermes, D. Zacher, A. Baunemann, C. Wöll, and R. A. Fischer, "Selective growth and MOCVD loading of small single crystals of MOF-5 at alumina and silica surfaces modified with organic self-assembled monolayers," *Chem. Mater.*, vol. 19, no. 9, pp. 2168–2173, 2007, doi: 10.1021/cm062854.

[27] M. J. Neufeld, J. L. Harding, and M. M. Reynolds, "Immobilization of Metal-Organic Framework Copper(II) Benzene-1,3,5-tricarboxylate (CuBTC) onto Cotton Fabric as a Nitric Oxide Release Catalyst," *ACS Appl. Mater. Interfaces*, vol. 7, no. 48, pp. 26742–26750, 2015, doi: 10.1021/acsami.5b08773.

[28] M. Yu *et al.*, "Covalent immobilization of metal-organic frameworks onto the surface of nylon - A new approach to the functionalization and coloration of textiles," *Sci. Rep.*, 2016, doi: 10.1038/srep22796.

[29] R. Adams, C. Carson, J. Ward, R. Tannenbaum, and W. Koros, "Metal organic framework mixed matrix membranes for gas separations," *Microporous Mesoporous Mater.*, vol. 131, no. 1–3, pp. 13–20, 2010, doi: 10.1016/j.micromeso.2009.11.035.

[30] E. Lahtinen, R. L. M. Precker, M. Lahtinen, E. Hey-Hawkins, and M. Haukka, "Selective Laser Sintering of Metal-Organic Frameworks: Production of Highly Porous Filters by 3D Printing onto a Polymeric Matrix," *ChemPlusChem*, vol. 84, no. 2. pp. 222–225, 2019, doi: 10.1002/cplu.201900081.

[31] M. Rinaudo, "Chitin and chitosan: Properties and applications," *Prog. Polym. Sci.*, vol. 31, no. 7, pp. 603–632, 2006, doi: 10.1016/j.progpolymsci.2006.06.001.

[32] V. Zargar, M. Asghari, and A. Dashti, "A Review on Chitin and Chitosan Polymers: Structure, Chemistry, Solubility, Derivatives, and Applications," *ChemBioEng Rev.*, vol. 2, no. 3, pp. 204–226, 2015, doi: 10.1002/cben.201400025.

[33] S. S. Kim, S. J. Kim, Y. D. Moon, and Y. M. Lee, "Thermal characteristics of chitin and hydroxypropyl chitin," *Polymer (Guildf).*, vol. 35, no. 15, pp. 3212–3216, 1994, doi: 10.1016/0032-3861(94)90124-4.

[34] A. Dufresne, S. Thomas, L. A. Pothan, R. F. Grossman, and D. Nwabunma, *Biopolymer Nanocomposites: Processing, Properties, and Applications*. Wiley, 2013.

[35] J. Tang, M. Yang, M. Yang, J. Wang, W. Dong, and G. Wang, "Heterogeneous Fe-MIL-101 catalysts for efficient one-pot four-component coupling synthesis of highly substituted pyrroles," *New J. Chem.*, vol. 39, no. 6, pp. 4919–4923, 2015, doi: 10.1039/c5nj00632e.

[36] K. M. L. Taylor-Pashow, J. Della Rocca, Z. Xie, S. Tran, and W. Lin, "Postsynthetic modifications of iron-carboxylate nanoscale metal-organic frameworks for imaging and drug delivery," *J. Am. Chem. Soc.*, vol. 131, no. 40, pp. 14261–14263, 2009, doi: 10.1021/ja906198y.

[37] S. Li, Y. Yang, X. Zha, Y. Zhou, W. Yang, and M. Yang, "Nanoscale morphology, interfacial hydrogen bonding, confined crystallization and greatly improved toughness of polyamide 12/polyketone blends," *Nanomaterials*, vol. 8, no. 11, 2018, doi: 10.3390/nano8110932.

[38] C. Gecgel, U. B. Simsek, B. Gozmen, and M. Turabik, "Comparison of MIL-101(Fe) and amine-functionalized MIL-101(Fe) as photocatalysts for the removal of imidacloprid in aqueous solution," *J. Iran. Chem. Soc.*, vol. 16, no. 8, pp. 1735–1748, 2019, doi: 10.1007/s13738-019-01647-w.

[39] Y. Wang, W. Guo, and X. Li, "Activation of persulfates by ferrocene-MIL-101(Fe) heterogeneous catalyst for degradation of bisphenol A," *RSC Adv.*, vol. 8, no. 64, pp. 36477–36483, 2018, doi: 10.1039/C8RA07007E.

Chapter 3: Curcumin encapsulation and 3D printing

3.1 Introduction

An important polyphenol extracted from the rhizomes of *Curcuma longa* (known as turmeric) is curcumin, which was first isolated in 1815 by Vogel and Pelletier[1], [2] from the Harvard College Laboratory in Cambridge, Massachusetts. Since then, the significant interest in curcumin has increased, and, more and more, its health benefits have been discovered.

Widely produced in India and China, curcumin has a long history of administration in the traditional medicine in those countries and has been used by different folks for treatment of many diseases, disorders and injuries, based on their antitumoral,[3], [4] anti-inflammatory,[5], [6] antiangiogenic,[7] neuroprotective,[8] anti-ischemic,[9] antidiabetic,[10] hepatoprotective,[11] analgesic,[12] antioxidant,[13] vasculoprotective,[14] anti-thrombotic,[15] cardioprotective,[16] pulmonoprotective[17] and immunomodulatory[18] effects. Curcurmin has been also employed as a coloring agent in food and beverages, as well as in the cosmetic industries.[19]–[21]

Established as part of the chemical class of polyphenols curcumin is known as 1,7-bis(4-hydroxy-3-methoxyphenyl)-1,6-heptadien-3,5-dione ($C_{21}H_{20}O_6$, 368.38 g mol^{-1}). The simple, symmetric molecular structure along with the relative density of functional groups in curcumin provide a versatile lead structure for derivatization studies and, thus, for drawing structure-activity relationships (SAR).[21]

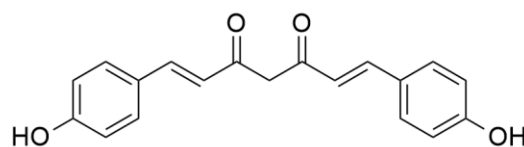The extract of *Curcuma longa* typically includes the following three molecules: diferuloylmethane/curcumin (**I**), demethoxycurcumin (**II**) and bis-de-methoxycurcumin (**III**) (Figure 3.1), with **I** as the most abundant one.[21]
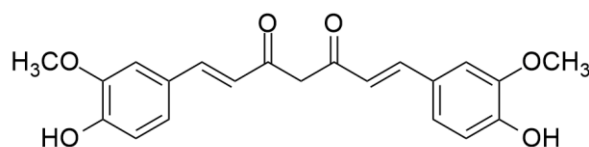
Curcumin (**I**):
60-70% of turmeric extract
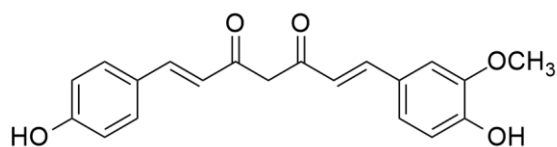
Demethoxycurcumin (**II**):
20-27% of turmeric extract

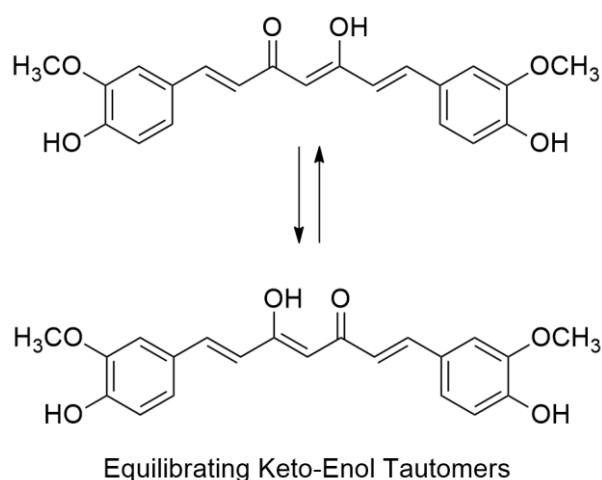Bis-demethoxycurcumin (**III**):
10-15% of turmeric extract

Equilibrating Keto-Enol Tautomers

Figure 3.1. Curcumin **I**, **II**, and **III** (curcumin, demethoxycurcumin, bis-demethyoxycurcumin), and curcumin keto-enol tautomers.

Curcumin, a lipophilic molecule, has various biological activities. Cancer cells when treated with curcumin displayed some features typical of apoptotic cell death, e.g. increased membrane permeability.[19], [22] Curcumin affects the function and structure of cell membranes and mimics typical events happening during the apoptosis process, such as loss of membrane integrity, from which, however, cells could recover in a relatively short time. Furthermore, curcumin had antiproliferative and apoptotic effects on human melanoma,[23], [24] human leukemia,[25]–[28] prostate cancer,[29]–[31] and non-small cell lung cancer in *in vitro* cell line experiments[32][33]. Preclinical studies on mice and phase I clinical trials on patients[34], [35] have confirmed that curcumin has minimal toxicity at relatively high doses (12 g per day).[21], [22]

Curcumin features seven chemical properties that facilitate intermolecular interactions, and thus, the association with biomolecular targets. These include (1) hydrogen bond donating and accepting capacity of the β-dicarbonyl moiety (and its keto-enol tautomeric form), (2) hydrogen bond accepting and donating capacity of the phenylic hydroxyl residues, (3) hydrogen bond accepting properties of the methoxy groups, (4) multivalent metal and non-metal cation binding properties, (5) relatively high octanol-water partition coefficient (log P), (6) rotation around multiple C–C bonds, and (7) behavior as a Michael acceptor (Figure 3.2). Although curcumin can induce apoptosis and inhibit proliferation and invasion of tumors by suppressing a variety of cellular signaling pathways, due to its distinct chemical properties, it is capable of interacting with a plethora of molecules such as fatty acyl chains of membrane lipids through hydrogen binding and hydrophobic interactions, resulting in low availability of curcumin inside the cytoplasm.[36]
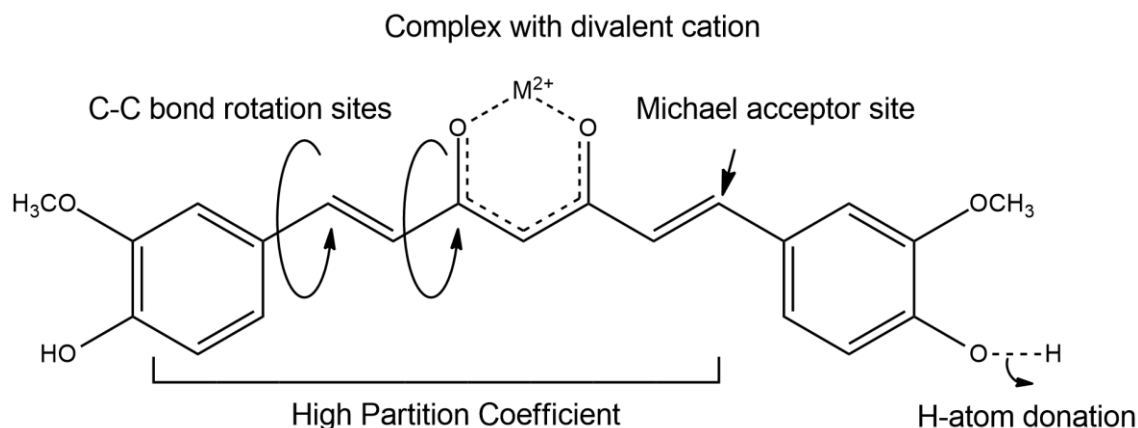
Complex with divalent cation

Figure 3.2. Chemical properties of curcumin.

To achieve an overall control in the biodistribution, cell targeting and *in vivo* stability of drugs, often biocompatible metal-organic frameworks (MOFs), like MILs (MILs = Materials Institute Lavoisier), PCNs (PCN = Polymeric Carbon Nitride), and ZIFs (ZIF = Zeolitic Imidazolate Framework), are applied as drug delivery vehicles. The usage of these drug carrier platforms then requires studies on the drug release kinetics and drug release mechanism. Current approaches for creating MOF-based, responsive drug carriers involve incorporation of stimuli-responsive fragments into MOFs or post-synthetic surface modification with sensitive molecules.

In the case of curcumin, due to its poor water solubility and low bioavailability, there is a need for the development of an effective drug-delivery system (DDS) capable of highly efficient drug delivery and selective cancer cell targeting.[37], [38]

Zou et al., for example, described a one-pot synthesis of anticancer drugs loaded into ZIF-8 nanocarriers, which release their payloads in the acidic microenvironment at tumor sites due to decomposition.[39] Yang et al. reported the MOF ZJU-101 (ZJU from: Zhejiang University), a pH-responsive, nanoscale, cationic, porous drug carrier, which can be easily loaded with negatively charged drugs due to electrostatic interactions.[38]–[40]

Glutathione (GSH) is the most abundant antioxidant found in living organisms; one important function is maintaining cellular redox homeostasis.[41] Lei et al. designed an intrinsic redox-responsive MOF-based carrier, namely MOF-M(DTBA), where M = Fe, Al, or Zr, and DTBA = 4,4'-dithiobisbenzoic acid.[38] The disulfide bond in DTBA is cleavable by GSH, which has an elevated concentration in tumor cells. Curcumin (CCM) loaded into MOF-Zr(DTBA) nanoparticles displayed a faster release *in vitro* and enhanced cell death in comparison with free curcumin. Similar results could be obtained by *in vivo* studies on cervical tumor-bearing BALB/c nude mice, which were treated with saline, free CCM, and CCM@MOF-Zr(DTBA). As a consequence of higher bioavailability of the loaded curcumin, CCM@MOF-Zr(DTBA) exhibited much higher antitumor activity than free CCM.[38] Nonetheless, is important to highlight studies evaluating the GSH levels in human tumors and healthy tissue (disease-free peritumoral). Glutathione levels tend to be elevated in breast, ovarian, head and neck, and lung cancers. Conversely, brain, and liver tumors, for the most part, exhibit lower tissue levels of glutathione compared to healthy tissue. As for other cancer types, there

is no clear trend as there is a significant number of studies reporting mixed results when comparing tumor tissue to disease-free peritumoral tissue or healthy tissue from cancer-free patients.[42], [43] Therefore, as Lei et al. did not describe which route was chosen for the injections (on tumor site or intravenously) in the *in vivo* tests performed on mice, taking into account the GSH levels throughout the body it is challenging to draw a conclusion whether this is a suitable approach to evaluate the MOF-based carrier.

Due to its minimal invasiveness photothermal therapy (PTT) has also been widely investigated. The conversion of light energy into heat, realized by photothermal agents after the absorption of nonhazardous light, which is usually in the near-infrared (NIR) range (650–900 nm), results in localized hyperthermia at tumor sites causing apoptosis and cancer tissue damage. However, tumor cells that are far from the hyperthermia region could be unaffected by a single PTT treatment, considering the limited penetration depth (a few centimeters) of NIR light, as well as the varied locations of tumors in humans. For this reason, PTT has been combined with chemotherapy to kill residual tumor cells with high efficacy. In order to improve the accumulation efficacy of drugs/photothermal agents at tumor sites and to achieve photoacoustic imaging (PAI)-guided chemo-/photothermal combinational tumor therapy, MIL-100(Fe) coated with polydopamine-modified hyaluronic acid (HA-PDA) was employed to load curcumin. This two-stage photothermal conversion capability boosted by HA-PDA improved the dispersibility, stability, as well as confered strong photothermal conversional efficiency to the system.[44]

Tiwari et al. could encapsulate curcumin in zeolitic imidazolate frameworks (ZIF-8) with high drug loadings (ca. 83.33 wt%). CCM@ZIF-8 displayed an enhanced therapeutic effect on HeLa cancer cells. It is intracellularly internalized through clathrin-mediated endocytosis in the lysosomal pathway, showing ZIF-8 as an adequate carrier shielding CCM against untimely degradation.[37]

This chapter seeks to explore the Selective Laser Sintering (SLS) technique extensively discussed in the previous chapter, by obtaining polymeric solid porous structures through PA-12 sintering.

(Table 3.1) below describes the available 3D printing parameters of the machine and what is the purpose of altering them for the sample production. The details about the sample production and how the machine works have been discussed on chapter 2, therefore in the methods section, the tables described in detail the production parameters for PA-12/CCM, PA-12/PVP and PA-12/PVP/CCM@MIL-101(Fe), respectively.

Table 3.1.. Definition of 3D printing parameters used in the sample production.

Power:	Refers to laser power for the inner part of the object, the value varies between 20 and 100%.
Rate:	this parameter is related to the speed at which the laser moves in points per second for the inner part of the object, this value is presented in a range of 1 and 64,000.
Env. Temp:	the temperature at which the build chamber is kept constant in this case the machine works on the 'Environment' mode; in the 'Powder' mode

	(Powder Temp.) it is the minimum temperature at which the build chamber should arrive at the end of the heating process.
Wait time:	seconds to wait after the recoater movement at the end of each layer.
Warming layers:	pre-heating layer which must be done before starting the printing process.
Layer thickness:	The thickness of each layer deposited in mm.
Add (%):	The amount of additive on wt% added to the polymer.
Sample size:	The size pre-established on the software (*Solidworks*) of the sample.

The already known properties of MIL-101(Fe) as a drug carrier and well-established application of PA-12 in SLS make them interesting candidates for the construction of a polymeric matrix. By encapsulating curcumin into MIL-101(Fe) it is possible to achieve a high loading and improve its bioavailability. Therefore, this chapter focuses on the generation of solid porous structures loaded with curcumin and the possibility to employ biodegradable polymers as polymer matrix.

3.2 Experimental
3.2.1. Materials
MIL-101(Fe) was synthesized according to the literature.[45] Curcumin was purchased from TCI chemicals purity >97.0%(T)(HPLC), nylon 12 powder (polyamide 12; PA-12) was purchased from Advanc3DMaterials, polyvinylpyrrolidone (PVP) powder from Alfa Aesar, bovine serum albumin (BSA) from Roth purity ≥98 %. All reagents and solvents purchased from commercial sources were used without further purification.

3.2.2. Methods
3D printing: The model used to produce the 3D samples was SnowWhite® from Sharebot.

Composition of the tablets:
PA-12/CCM: 12 g curcumin and 300 g PA-12 were placed in the printer build pate, with a final concentration of ca. 4 wt% curcumin (Table 3.2).

Table 3.2. Printing parameters for the PA-12/CCM

Sample name	Power (%)	Rate (pps)	Powder Temp (°C)	Wait time (s)	Warming layers	Add (%)	Layer thickness (mm)	Sample size (mm)
PA12E01	40/40	64k/64k	155	90	50	4	0.1	Ø16.6/Ø5
PA12E002	40/40	64k/64k	155	90	40	4	0.1	Ø16.6/Ø5
PA12E003	30/30	64k/64k	154	90	35	4	0.1	Ø16.6/Ø5
PA12E004	30/50	64k/50k	154	90	35	4	0.1	Ø16.6/Ø5
PA12E005	50/50	64k/64k	154	90	35	4	0.1	Ø16.6/Ø5

   PVP: 160 g of PVP were placed in the printer build plate, for printing tests. The printing parameters are listed on the (Table 3.3) below.

Table 3.3. Printing parameters for PVP only.

Sample name	Power (%)	Rate (pps)	Powder Temp. (°C)	Wait time (s)	Warming layers	Layer thickness (mm)	Sample size (mm)
PVP_001	40/40	64k/64k	130	300	10	0.1	Ø 16.6/Ø 5
PVP_002	70/70	64k/64k	130	300	10	0.1	Ø 5
PVP_003	100/100	64k/64k	135	300	10	0.1	Ø 5
PVP_004	100/100	32k/32k	138	300	10	0.1	Ø 5
PVP_005	80/80	64k/64k	150	300	10	0.1	Ø 5
PVP_006	80/80	64k/64k	155	300	10	0.1	Ø 5
PVP_007	90/90	50k/50k	163	300	10	0.1	Ø 5
PVP_008	100/100	40k/40k	168	300	10	0.1	Ø 5

   PA-12/PVP: 110g of *PVP and* 160 g of PA-12, were mixed and the homogeneous mixture was placed in the printer build plate. The concentration of PVP in the final mixture was ca. 40 wt% (Table 3.4).

Table 3.4. Printing parameters for the PA-12/PVP (40 wt%) mixtures.

Sample name	Power (%)	Rate (pps)	Env. Temp (°C)	Wait time (s)	Warming layers	Add (%)	Layer thickness (mm)	Sample size (mm)
PA12_T001	40/40	64k/64k	85	300	8	40	0.1	Ø 16.6
PA12_T002	40/40	64k/64k	160	300	8	40	0.1	Ø 16.6
PA12_T003	40/40	64k/64k	170	300	8	40	0.1	Ø 16.6
PA12_T004	40/40	64k/64k	150	300	8	40	0.1	Ø 16.6
PA12_T005	40/40	64k/64k	153	300	8	40	0.1	Ø 16.6
PA12_T006	40/40	64k/64k	158	300	8	40	0.1	Ø 16.6
PA12_T007	40/40	64k/64k	160	300	8	40	0.1	Ø 16.6

PA-12/PVP/CCM: 160 g PA-12, 110 g PVP and 8 g curcumin were mixed and placed in the printer. The concentration of PVP in the final mixture was ca. 40 wt% and the curcumin concentration was ca. 3 wt% (Table 3.5).

Table 3.5. Printing parameters for the PA-12/PVP (40%)/CCM (3%)

Sample name	Power (%)	Rate (pps)	Env. Temp (°C)	Wait time (s)	Warming layers	Add (%)	Layer thickness (mm)	Sample size (mm)
PA12_U001	40/40	64k/64k	153	300	8	40/3	0.1	Ø 16.6
PA12_U002	40/40	64k/64k	158	300	8	40/3	0.1	Ø 16.6
PA12_U003	40/40	64k/64k	158	300	8	40/3	0.1	Ø 16.6
PA12_U004	40/40	64k/64k	158	300	8	40/3	0.1	Ø 16.6

PA-12/CCM@MIL-101(Fe): 130 g PA-12 and 5.2 g CCM@MIL-101(Fe) were placed in the printer build plate, with a final concentration of ca. 4 wt% CCM@MIL-101(Fe) (Table 3.6).

Table 3.6. Printing parameters for the PA-12/CCM@MIL-101(Fe) (4%)

Sample name	Power (%)	Rate (pps)	Powder Temp (°C)	Wait time (s)	Warming layers	Add (%)	Layer thickness (mm)	Sample size (mm)
PA12_R001	40/40	64k/64k	174	300	8	4	0.1	Ø 16.6
PA12_R002	40/40	64k/64k	174	300	8	4	0.1	Ø 16.6
PA12_R003	40/40	64k/64k	170	300	8	4	0.1	Ø 16.6
PA12_R004	40/40	64k/64k	168	300	8	4	0.1	Ø 16.6
PA12_R005	40/40	64k/64k	165	300	8	4	0.1	Ø 16.6
PA12_R006	30/30	64k/64k	171	300	8	4	0.1	Ø 16.6
PA12_R007	30/30	64k/64k	169	300	8	4	0.1	Ø 16.6
PA12_R008	30/30	64k/64k	170	300	8	4	0.1	Ø 16.6

X-ray Diffraction (XRD)

The powder diffractograms were recorded on an X-ray powder diffractometer, Stoe Darmstadt PW 2373/00, with Cu Kα radiation (1.5418 Å, 60 kV, 0.02 step in the range of 2θ values from 2° to 50°). For sample preparation, the material was crushed in an agate mortar and placed in a capillary of 0.7 mm diameter.

Fourier-Transform Infrared Spectroscopy (FTIR)

Fourier-transform infrared spectroscopy method was conducted with the purpose to identify the functional groups present in the curcumin (CCM), MIL-101 (Fe), and in CCM encapsulated into the metalorganic framework CCM@MIL-101(Fe). FT-IR spectra were obtained with a PerkinElmer system 2000 FTIR spectrometer, scanning between 400 and 4000 cm^{-1} employing KBr pellets prepared in a glovebox under a nitrogen atmosphere.

Thermogravimetric Analysis

Simultaneous thermogravimetric/differential thermal analysis/mass spectrometry (TG/DTA-MS) studies were carried out on a Netzsch F1 Jupiter device connected to an Aeolos mass spectrometer. Samples were heated at a rate of 10 K min^{-1}.

UV-Vis absorption spectroscopy: studies of uptake into and release of curcumin from MIL-101(Fe)

The porous MIL-101(Fe) was evacuated in high vacuum at room temperature overnight before usage. For loading of curcumin, MIL-101(Fe) was soaked in a solution of curcumin in ethanol (0.006 mg/mL), stirred under exclusion of light for 48 h at room temperature, in different ratios 1:2 (w/w) and 1:3 (w/w) in order to determine the optimal loading of the drug into the MOF.

The UV-vis absorption spectra were measured with a PerkinElmer UV/VIS/NIR Lambda 900 spectrometer, equipped with a xenon arc lamp, using quartz cuvettes (V = 3 cm^3, l = 10 mm). All spectra were recorded at 25 °C in the range 300-600 nm at

1.0 nm resolution. For determination of the curcumin uptake kinetics, the calibration curve was obtained by measuring the concentration-dependent absorbance of curcumin in EtOH at 426 nm in triplicate (Figure 3.3). For determination of the release kinetics, the calibration curve was obtained by measuring the concentration-dependent absorbance of curcumin in PBS + 2 vol% DMSO + 5 wt% BSA (pH = 7.4) at 430 nm in triplicate (Figure 3.4).

The amount of adsorbed curcumin was calculated by determination of the amount of free curcumin still present in the supernatant solution after 24 h and 48 h from UV/Vis data (λ_{abs} = 426 nm). Each experiment was carried out in triplicate. The encapsulation efficiency (EE%) and loading capacity (LC%) was determined as follow:

$$EE\% = \left({(c_{i(CCM)} - c_{f(CCM)})} \Big/ {c_{i(CCM)}} \right) \times 100 \text{ (Equation 1)}$$

$$LC\% = \left({(c_{i(CCM)} - c_{f(CCM)})} \Big/ {c_{(MOF)}} \right) \times 100 \text{ (Equation 2)}$$

Where: $EE\%$ = encapsulation efficiency of the drug

$LC\%$ = loading capacity of the drug

$c_{i(CCM)}$ = initial concentration of curcumin

$c_{f(CCM)}$ = final curcumin concentration
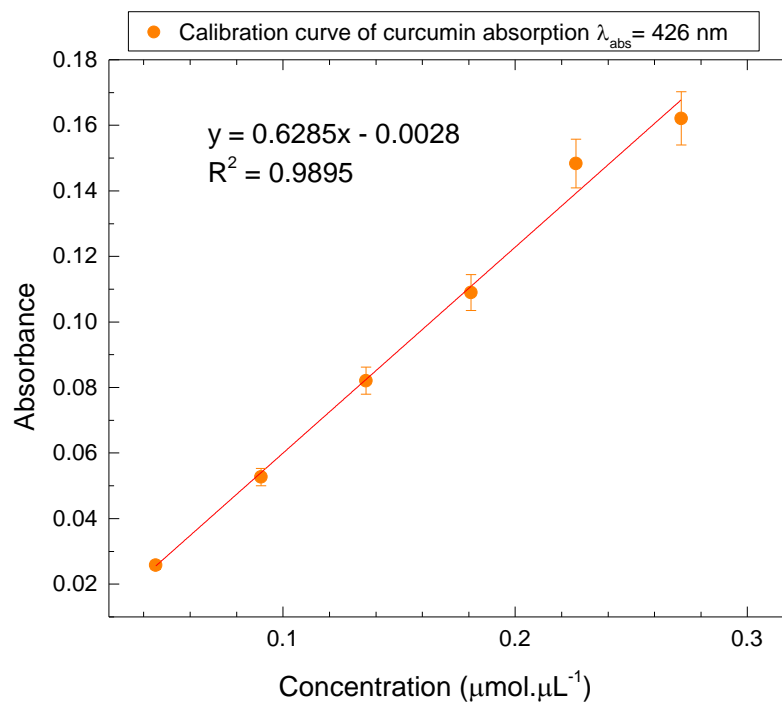
$c_{(MOF)}$ = concentration of the MOF

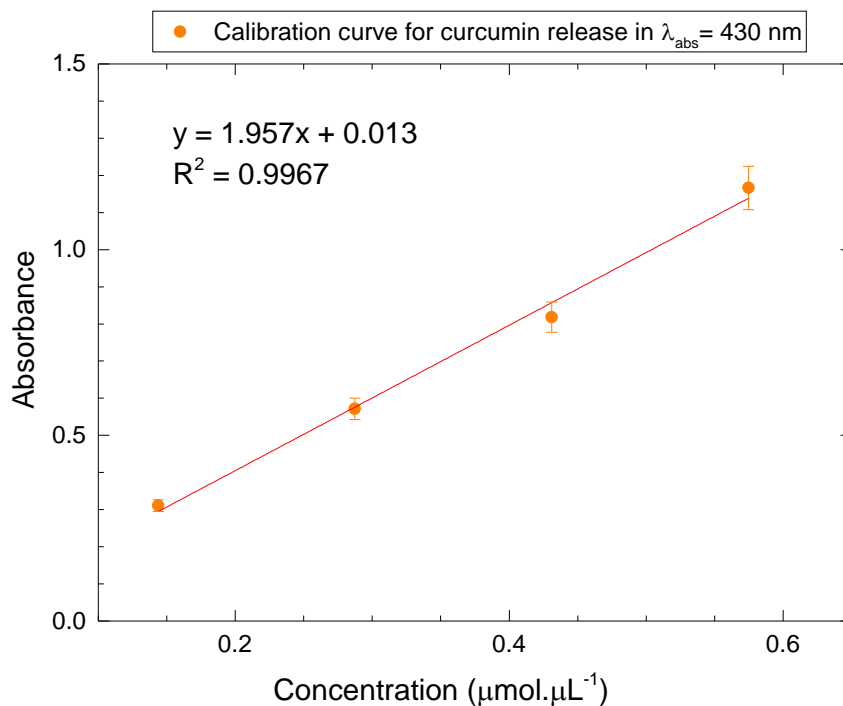Figure 3.3 Calibration curve of absorbance of curcumin in ethanol, λ_{abs} = 426 nm.

Figure 3.4 Calibration curve for release of curcumin in PBS/DMSO(2%)/BSA(5%), λ_{abs} = 430 nm.

3.3 Results and discussion

3.3.1 X-ray diffraction (XRD)

To investigate the crystallinity of MIL-101(Fe) before (a) and after loading of curcumin (b), XRD analysis was performed (Figure 3.5).

The reflections at 2θ = 3.26°, 5.81°, 8.34° and 8.96° demonstrate the high crystallinity of MIL-101(Fe) and corresponds to the previously reported data.[46] The intensive reflections at small angles (2θ) indicate that this porous material possesses abundant pores in the structure. Indeed, MIL-101(Fe) has two types of inner cages with internal diameters of 27 and 34 Å, respectively.[47] In the diffractogram of CCM@MIL-101(Fe), the reflections are observed at 2θ = 3.27°, 5.12°, 5.84°, 8.37° and 8.99°, also demonstrating a highly crystalline profile.[48] As the most intensive reflections in the XRD patterns of CCM@MIL-101(Fe) and MIL-101(Fe) hardly differ, framework stability and minimum impact on crystallinity on curcumin encapsulation can be implied.
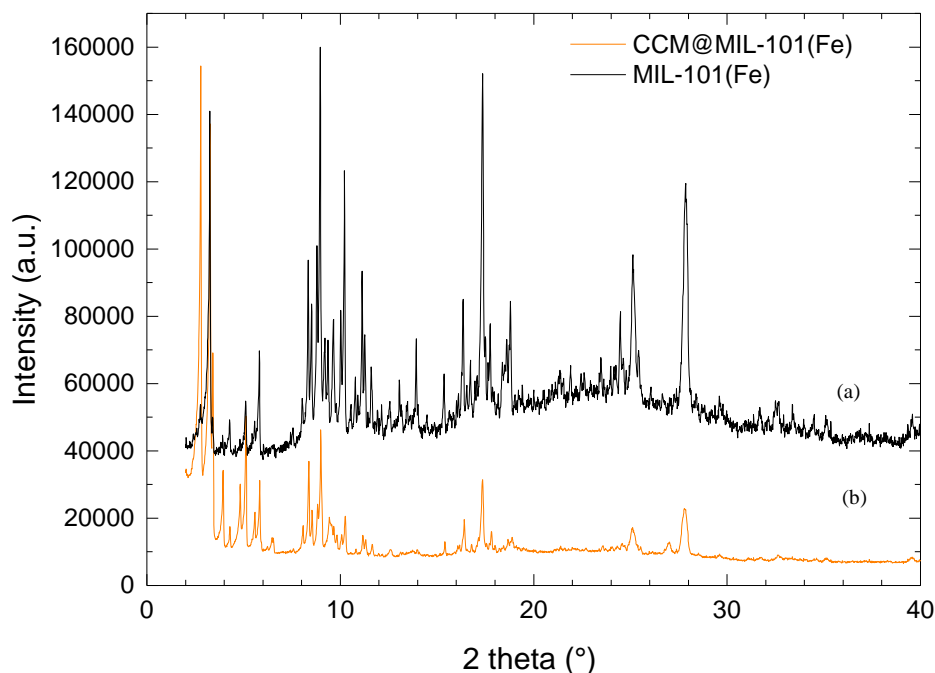
Figure 3.5. Powder diffractograms of MIL-101(Fe) (a) and CCM@MIL-101(Fe) (b).

3.3.2 Fourier-Transform Infrared (FTIR) Spectroscopy

FT-IR spectroscopy was used to identify the functional groups present in MIL-101(Fe), in the drug and in the combination of drug encapsulated in the metal-organic framework through the characteristic vibrations of the groups present in each material to evaluate possible interactions between the drug and the MOF. (Figure 3.6) shows the FT-IR spectra of curcumin (a), MIL-101(Fe) (b), and curcumin loaded into MIL-101(Fe) (CCM@MIL-101(Fe), c).

The FT-IR spectrum of curcumin showed its signature peaks at 3510 cm^{-1} corresponding to the phenolic O−H stretching vibration (Figure 3.6 (a)). The peak at 1628 cm^{-1}confirms the presence of aromatic moiety C=C stretching, following by the peak at 1602 cm^{-1}that confirms the benzene ring stretching vibrations. The band at 1510 cm^{-1} corresponds to the C=O stretch of the ketone. The band at 1400 cm^{-1} refers to the olefinic C−H bending vibrations vibrations. Around 1280 cm^{-1}, the C−O stretching vibration of the substituted phenyl ring is observed and 962 cm^{-1} is attributed to benzoate trans-C-H vibration. [37], [49]–[51] In the FT-IR spectrum of MIL-101(Fe) (Figure 3.6 (b)), the bands in the region 3500−2500 cm^{-1} are associated with the stretching vibrations of the OH groups of the absorbed water molecules; the bands in the region 1600−1670 cm^{-1} correspond to are assigned to the asymmetric and symmetric stretching vibrations of the carbonyl group of the ligand. .[52]

In the FT-IR spectrum of CCM@MIL-101(Fe) (Figure 3.6 (c)), bands in the 3500−2500 cm^{-1} region are associated with the stretching vibrations of adsorbed water. The vibration at 1510 cm^{-1} found in pure curcumin is also present in CCM@MIL-101(Fe). The interaction of curcumin and MIL-101(Fe) was evidenced by shifting of

characteristic peaks in MIL-101(Fe) from 1604 to 1593 cm^{-1} and from 1657 to 1686 cm^{-1}, as a result of intermolecular hydrogen bonding. Accordingly, the curcumin peak at 1280 cm^{-1} is shifted to 1288 cm^{-1}, which also suggests hydrogen bonding.
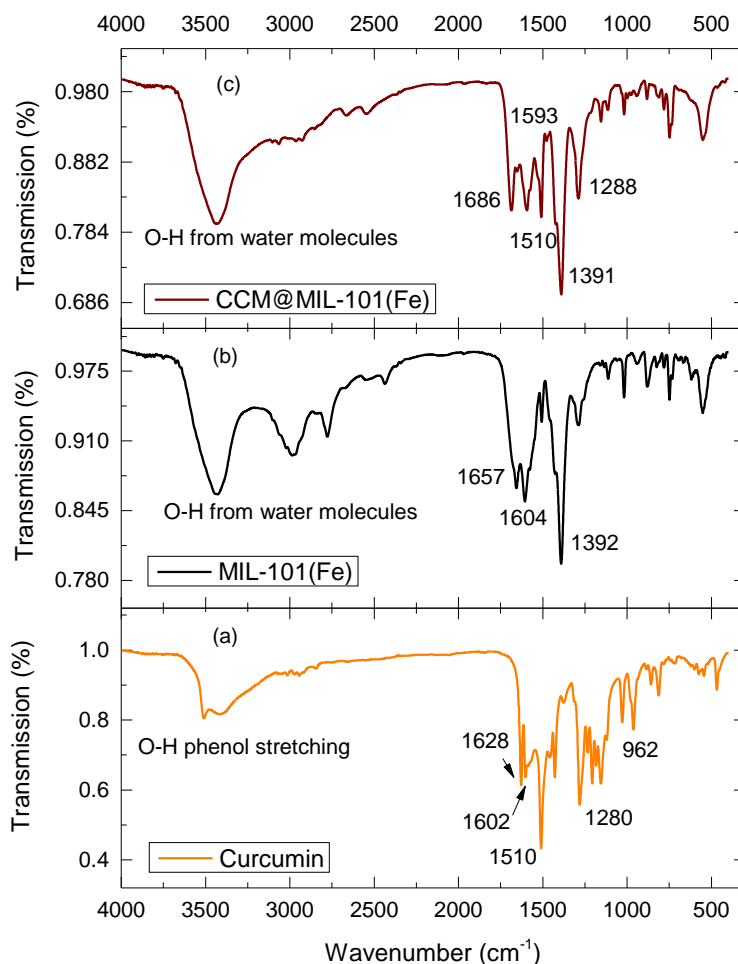

Figure 3.6. FT-IR spectra of curcumin (a), MIL-101(Fe) (b), and CCM@MIL101(Fe) (c).

3.3.3 TG/DTA

The thermal properties of the printed tablets and raw CCM were determined by thermogravimetric analysis (TGA) and differential thermal analysis (DTA). The samples were heated in an aluminum crucible from room temperature to 600 °C at a linear heating rate of 10 °C min^{-1}.

(Figure 3.7) shows the TG curves of raw CCM powder, PA-12 printed tablet, and the printed tablet of a CCM/PA-12 mixture. All samples showed a minor mass loss between 100 and 300 °C.

According to the literature, the PA-12 is thermally stable in an inert atmosphere up to ca. 400 °C, followed by an abrupt single mass loss step. The analysis of the PA-12 printed tablet produced by the SLS technique showed a single mass loss step of 98 wt% at 550 °C.[53]

Curcumin is known to thermally decompose below 600 °C in two stages. For the analyzed commercial curcumin used here, the curve looks like a single-step degradation; however, the two stages are better defined in the DTA curve (Figure 3.8). Curcumin is known to thermally decompose below 600 °C the observed mass loss in the TG curve is 60,4 wt%. The analyzed CCM was thermally stable up 170 °C due to the deshydroxylation of OH groups by the elimination of two water molecules. The DTG curve exhibits the decomposition of the curcumin in two consecutive rather overlapped unequal steps. The first step between 170 - 215 °C, which is within the principal step between 170 - 550 °C. The degradation of non-volatile intermediates resulted in the formation of amorphous carbon residue which is equivalent to 39,6 wt% of the sample weight.

The results are in agreement with those reported by Sun et al. (2013), Souguir et al. (2013), and Chen et al. (2014).[54]–[56]

The PA-12/CCM printed tablet mixture follows the weight-loss pattern of the PA-12 printed tablet. Decomposition starts at ca. 380 °C with a total weight loss of about 97 % at 550 °C. The enlarged TG curves show a decrease in stability when curcumin was introduced into the polymer matrix. Through DTA analysis, it can be seen that the exothermic peak with the incorporation of curcumin was broadened and slightly moved from 420 °C to 433 °C, followed by an endothermic peak at 469 °C that can be attributed to the decomposition of both curcumin and PA-12.

Analysis of a sample of composition PA-12/CCM@MIL101(Fe) showed that the printed tablet also follows the weight-loss pattern very similar to the PA-12 printed tablet. The TG curve suggests that curcumin encapsulation into the MOF prior to sintering can slightly increase the thermal stability of the matrix, in comparison to the PA-12/CCM sample. The thermal decomposition occurs at ca. 540 °C; this phenomenon is verified by the DTA data showing a large endothermic peak at 493 °C. It is known that the MIL-MOF family is thermally stable only up to 350 °C, but according to TG/DTA analysis the incorporation of CCM@MIL-101(Fe) into the PA-12 matrix increased the thermal stability of both components.[57]
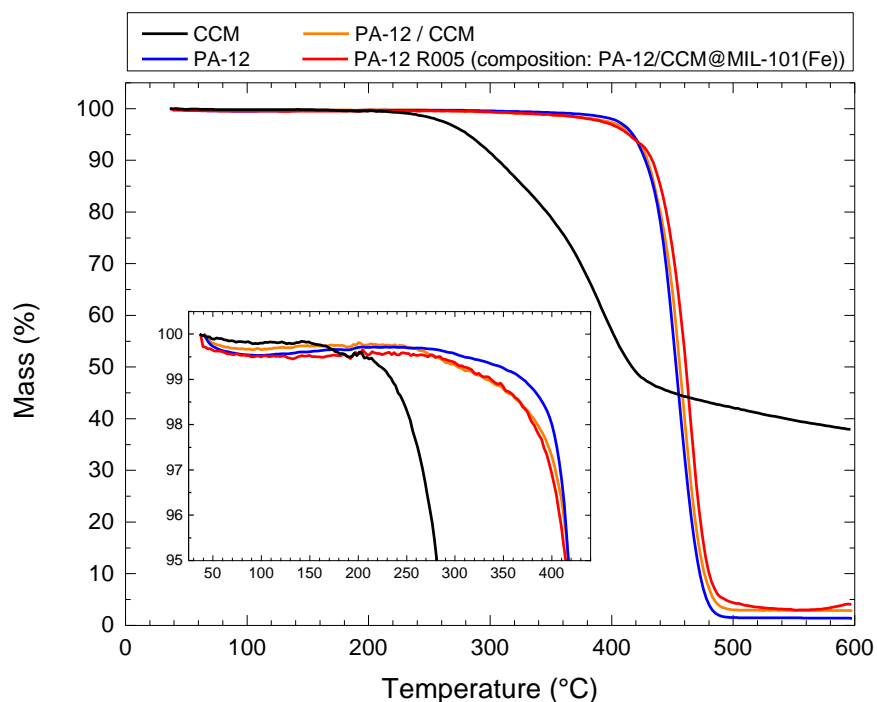
Figure 3.7. TG curves of curcumin (CCM), the printed PA-12 matrix, the mixture PA-12/CCM, and the PA-12 matrix with CCM@MIL101(Fe) incorporated. The inserted figure shows enlarged TG curves in the mass region from 95 to 100 %.
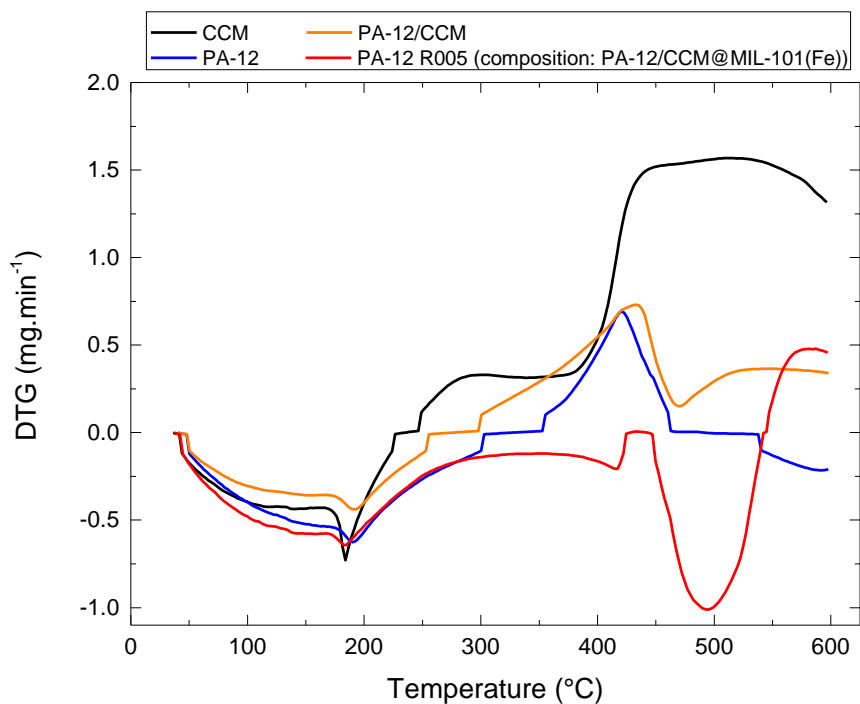

Figure 3.8. DTG curves of curcumin (CCM), the PA-12 printed matrix, the mixture PA-12/CCM, and the matrix PA-12 with CCM@MIL-101(Fe) incorporated.

3.3.4 Curcumin absorption kinetics in the metal-organic framework MIL-101(Fe)

The drug loading experiment was performed by measuring the UV-vis absorption spectra of free curcumin in ethanol at 426 nm. Additionally, the previously evacuated MIL-101(Fe) was soaked in a solution of curcumin in ethanol (6 x 10^{-3} mg mL^{-1}) in two different ratios 1:2 (w/w) and 1:3 (w/w), and the amount of encapsulated curcumin was determined by measuring the amount of free curcumin in the solution after 24 and 48 h by UV-vis spectroscopy. After 24 h, the 1:2 (w/w) samples showed an encapsulation efficiency of 65 wt% and a loading capacity of 32 wt%; these numbers increased slightly after 48 h to 68 wt% and 34 wt%, respectively (Figure 3.9). These values are similar to those of previously reported MOF-based carriers.[58]
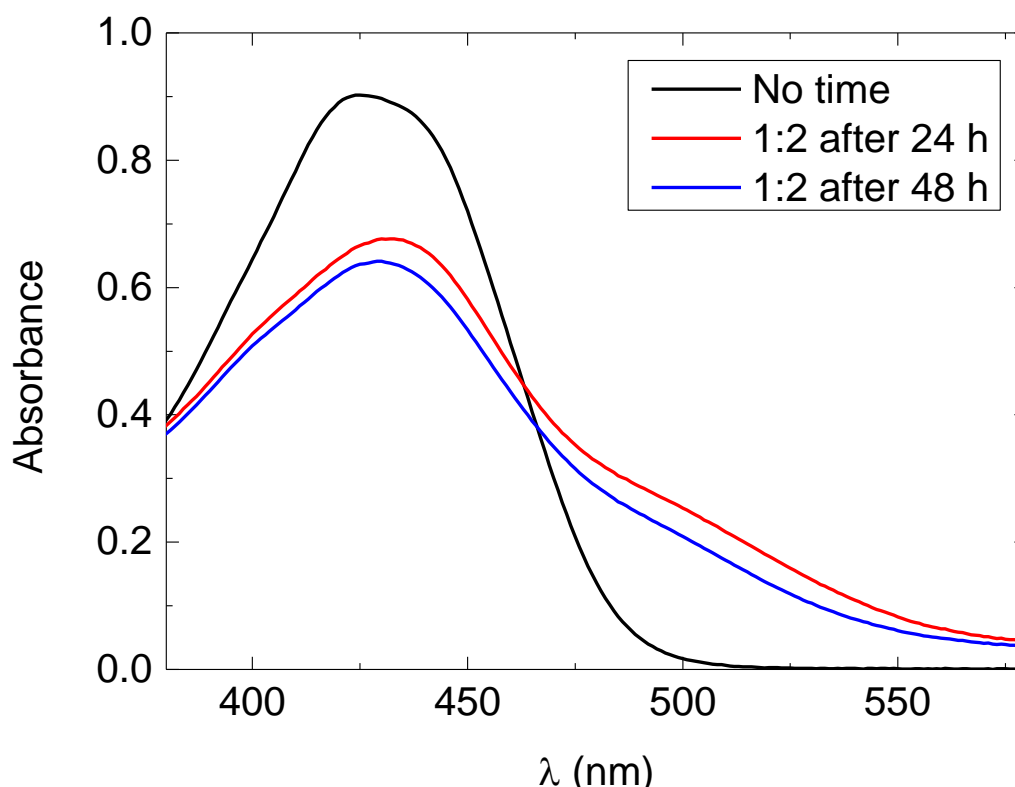

Figure 3.9. UV-vis spectra of free curcumin in ethanol (black) and after addition of MIL-101(Fe) (ratio CCM:MIL-101(Fe) = 1:2, after 24 h (red) and 48 h (blue)).

The same experiment was conducted with a curcumin:MIL-101(Fe) ratio of 1:3 (Figure 3.10). It was observed that the absorption peak of curcumin in ethanol was shifted after addition of MIL-101(Fe), namely to 431 nm after 24 h, and to 437 nm after 48 h. These shifts in the UV-vis spectra could be attributed to the formation of intermolecular hydrogen bonds between curcumin and MIL-101(Fe).[59], [60] On the basis of the UV-vis spectroscopic data, the encapsulation efficiency of 63 wt% and a loading capacity of 21 wt% of the drug after 24 h was determined. After 48 h, the encapsulation efficiency and loading capacity increased to 68 wt% and 23 wt%, respectively. The loading capacity of curcumin in the MIL-101(Fe) was increased first in the 1:2 (CCM@MIL-101(Fe)) ratio and then decreased when the level of MIL-101(Fe) in the solution was enhanced in the 1:3 ratio (CCM@MIL-101(Fe)). This outcome might be attributed to the fact that the LC value is defined as the concentration

percentage value (%) of encapsulated curcumin and concentration of MIL-101(Fe) nanoparticles according to eq.2, as the concentration ratio of CCM and MIL-101(Fe) changed from 1:2 to 1:3 the percentage increase of curcumin was lower than that of the MIL-101(Fe) nanoparticles and the LC value decreased.
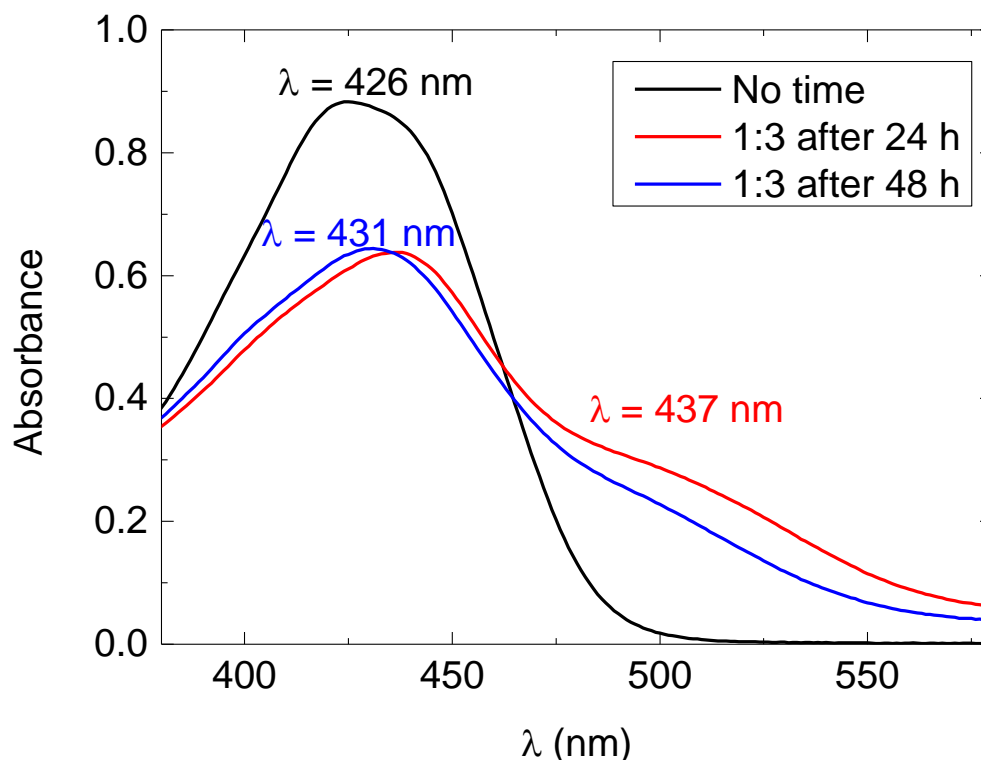

Figure 3.10. UV-vis spectra of free curcumin in ethanol (black) and after addition of MIL-101(Fe) (ratio CCM:MIL-101(Fe) = 1:3) after 24 h (red) and 48 h (blue).

3.3.5 Curcumin release studies

First, curcumin was encapsulated in MIL-101(Fe). Curcumin (0.625 g) was dissolved in DMSO (25 mL) and stirred at room temperature. Then, previously evacuated MIL-101(Fe) (0.625 g) was added and stirred in the dark at room temperature for 48 h. Afterwards, the solid was isolated, dried and placed into a solution containing phosphate buffered saline - PBS (30 mL), dimethyl sulfoxide -DMSO (2%) and bovine serum albumin - BSA (5%). The mixture was kept in the dark with stirring at 37 °C. Aliquots (2 mL) were withdrawn from the solution with an automatic micropipette at defined periods of time: 15 min, 30 min, 60 min, 120 min, 180 min, and 1440 min. After each sample collection, 2 ml of a fresh solution (PBS/DMSO (2%)/albumin (5%)) was added to retain the same volume. All experiments were performed in triplicate. In the first three hours, the MOF releases half of the amount of the loaded drug, but as a high amount of drug was released between 3 to 24 h (Figure 3.11), the experiment was repeated.
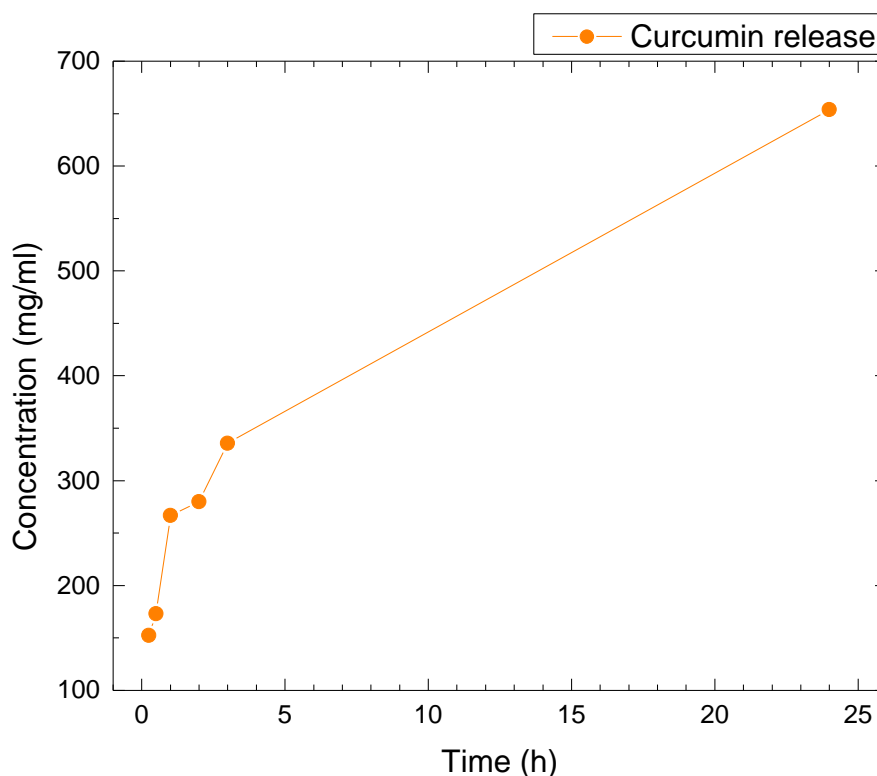
Figure 3.11. First experiment of curcumin release kinetics.

Curcumin (0.1 g) was loaded into previously evacuated metal-organic framework MIL-101(Fe) and kept under stirring in the dark for 48 h. The solid was isolated and dried, the particles of CCM@MIL-101(Fe) were then placed in a dialysis membrane and transferred to a solution of 10 ml of PBS / DMSO (2%) / albumin (5%) for the drug release experiments. The mixture was stirred in the dark at 37 °C. After the dialysis bag was submerged in PBS/DMSO (2%)/ albumin (5%) solution aliquots (2 mL) were collected from the medium at 15 min, 30 min, 60 min, 120 min, 180 min, 240 min, 300 min, 360 min, 12 h, 18 h, 24 h, 30 h, 36 h, 42 h, 48 h, 54 h, 60 h, 66 h, 72 h, 78 h, 84 h, and 90 h. After each sample collection the same amount of a fresh solution of PBS/DMSO (2%)/albumin (5%) was added to retain the total volume. The experiment was performed in triplicate (Figure 3.12).

The CCM@MIL-101(Fe) system displays a pulsatile release behavior, where the system releases finite amounts (or pulses) of a drug at distinct time intervals. In the first hour, 27 % of curcumin is released, reaching 40 % after 36 h, followed by subsequent pulses. After 96 h, 65% of curcumin has been already released.
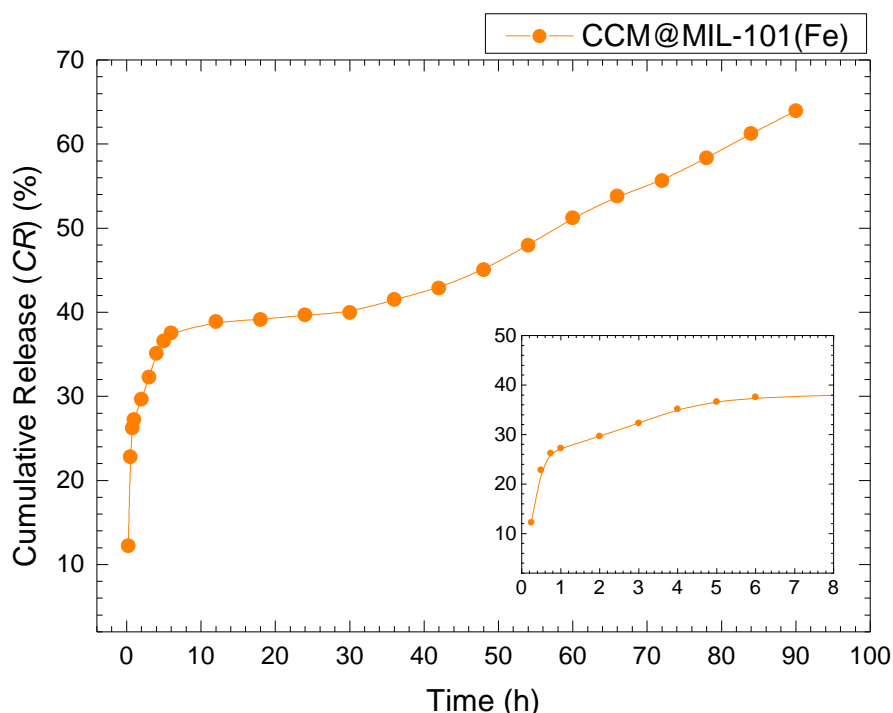
Figure 3.12. Cumulative kinetic release of curcumin from CCM@MIL-101(Fe).

In order to modulate this release behavior to achieve a slower and continuous release, the selective laser sintering (SLS) technique would be a possible approach to accomplish an extended release. Consequently, different types of matrices were proposed for sustained release investigations. The first is composed of only curcumin incorporated into a PA-12 matrix. The second category is a composition of two different polymers (PA-12 and the biodegradable polymer PVP) and curcumin. The third sample is composed of curcumin encapsulated in the MIL-101(Fe) framework and afterwards introduced into the PA-12 polymer matrix.

3.3.6 Curcumin release on samples produced by the selective laser sintering technique

Polyamide-12/Curcumin Samples

Tablets in two dimensions were prepared, one with approximately 16.63 mm diameter (PA-12 E01), a second one with a diameter of around 5 mm (PA-12 E005). To determine the estimated amount of curcumin in the tablets, an average mass of the samples was calculated and multiplied by the percentage amount of curcumin in the total initial mass, given the average concentration of curcumin in the tablets. We initially employed 12 g curcumin and 300 g polyamide-12, with 3.85 %(w/w) curcumin concentration, as a homogeneous mixture.

The curcumin release in a solution of PBS/DMSO (2%)/albumin (5 %) was studied at 37 °C in the dark. The cumulative release is calculated according to the formula:

$$C_n^{Corr} = C_n + \frac{v_s}{v_m}\sum_{i=1}^{n-1} C_i$$

Where C_n^{Corr} is the corrected concentration after sampling "n";

C_n and C_i are the observed concentration (uncorrected) in the "n" or "i" sample;

v_s = the volume of the sample taken;

v_m = the total volume that was taken from the sample

According to (Figure 3.13), in the first 6 h, the system releases around 20 % of curcumin into the simulated biological medium presenting an extended release. By having curcumin incorporated into the PA-12 matrix, the release rate is slowed down in comparison to the situation in which curcumin is loaded into MIL-101(Fe), where around 40 % of curcumin is releases in the first 6 h. The tablet continues to release small amounts of curcumin into the medium, displaying an extended release, where 50 % of the incorporated curcumin is released over 5 days.
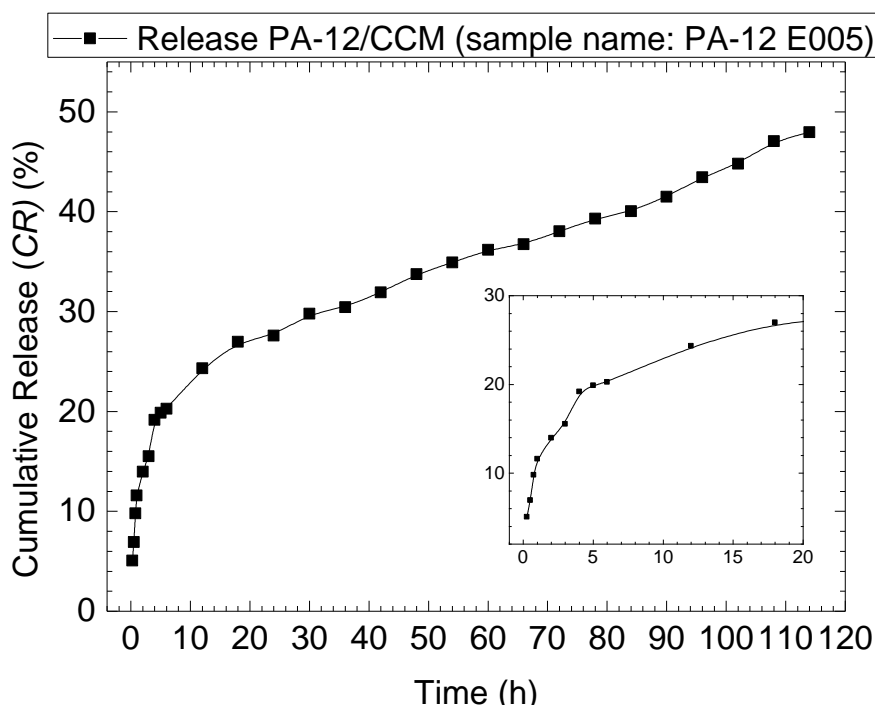

Figure 3.13. Cumulative release of a polyamide-12/curcumin sample (PA12 E005, tablet).

The following release study was conducted with tablets of 16.63 mm diameter (sample code PA-12 E01), in which the amount of curcumin was about six times higher than in the previous study performed on tablets of 5 mm diameter to allow study of the release for a longer period (Figure 3.14). In the first few hours, the curcumin is gradually released into the medium, reaching only about 4 % of its release in the first 24 h. The system keeps its diffusion-controlled release of small amounts of curcumin until 42 days, where about 20 % of the drug was released into the simulated biological medium. In this case, the incorporation of the drug in a polymer matrix allowed a slow curcumin release for a longer period of time in comparison with the metal-organic framework, CCM@MIL-101(Fe).
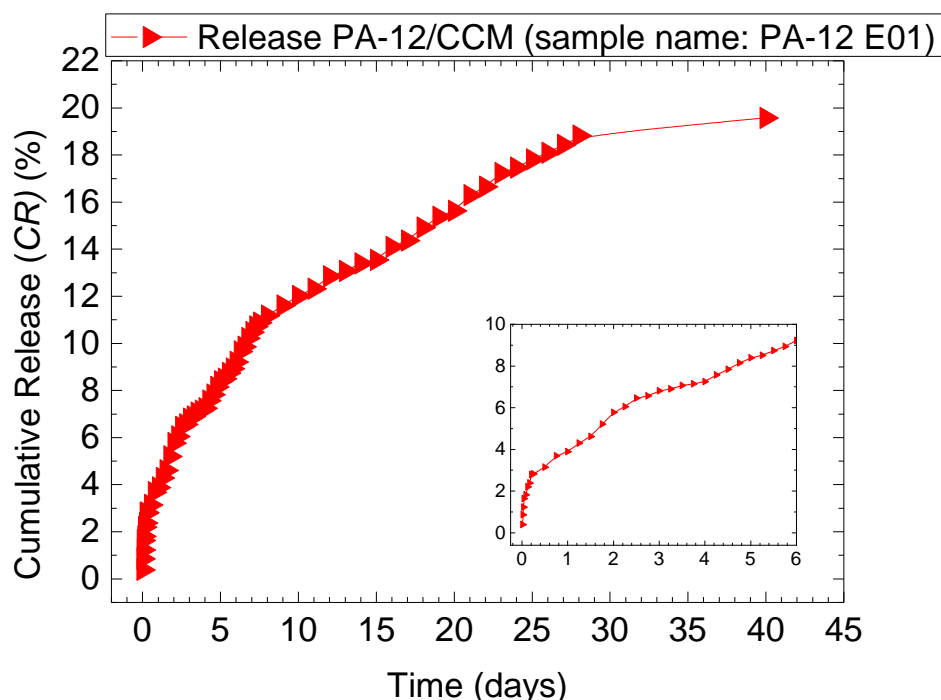
Figure 3.14. Cumulative release of sample PA12 E01.

Polyamide-12 / Polyvinylpyrrolidone / Curcumin Samples

The biocompatible polymer polyvinylpyrrolidone (PVP) is extensively applied in biomedical materials due to its environmental stability, bio- and chemocompatibility, low cytotoxicity, high chemical and thermal resistance, and good solubility in water and many organic solvents. The good water solubility is attributed to the presence of the polar lactam group in the pyrrolidone moiety which increases the hydrophilicity of the polymer (Figure 3.15). The non-polar methylene groups make PVP lipophilic. These outstanding properties of PVP have led to its ample applicability in pharmaceutical production in almost all dosage forms, for instance, in wet granulation in tablet production, in oral solutions, syrups and drops, in injectables and topical solutions, and in film coatings on tablets. [61]
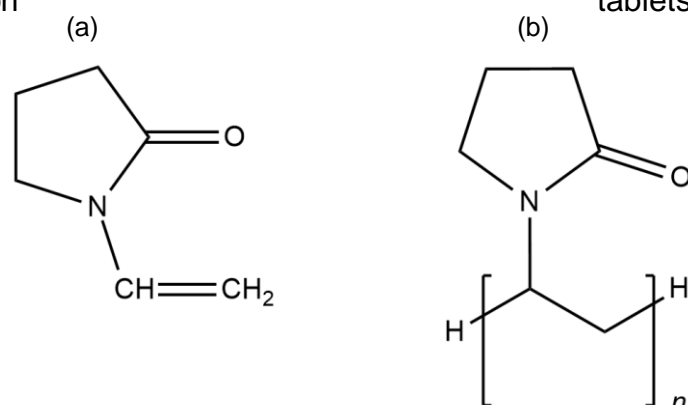

Figure 3.15. Molecular structure of the monomer N-vinylpyrrolidone (a); the repeating unit of PVP (b).

Incorporation of a drug in a polymeric matrix is one of the methods to develop controlled release dosage forms. The unlimited application of the matrix as a dosage form for non-conventional drug delivery is attributed to the simplicity, versatility, and

reproducibility of its fabrication method. Having a melting point that ranges from 150 to 180 °C, similar to the melting point of PA-12 (180 °C), the study of PVP using the SLS technique (for information on printing technology refer to Chapter 2) was proposed.[62] The printing tests for PVP only were not successful, because the tablets did not acquire good mechanical stability during the printing process. The laser power and the powder temperature were gradually increased in order to find the optimum printing parameters or so-called printing window, but all samples produced were very brittle (Figure 3.16 (a)). The next idea was to use a mixture of two polymers, one as the matrix, as another possible way to modulate drug release. For that reason, a mixture of PA-12 and PVP was prepared, where the PVP concentration was varied from 60 wt% to 50 wt% and 40 wt%; the optimal concentration turned out to be 40 wt% PVP (Figure 3.16 (b)). The most important criteria were good mechanical properties. For this batch, the printing mode was changed to the environmental mode, and for the printing tests, the temperature inside the chamber was in the range of 85 to 170 °C .
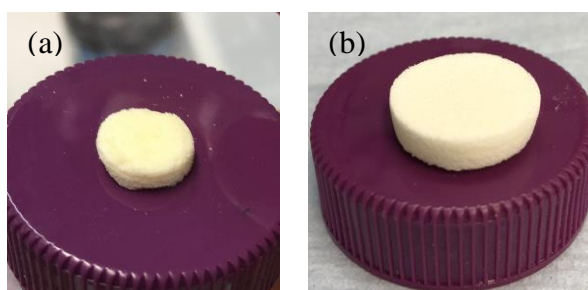
Figure 3.16. (a) Pellet of pure PVP; (b) Pellet of PA-12/PVP (40 wt%).

After finding the optimal parameters for printing PA-12/PVP, curcumin (3 wt%) was added to the mixture. Tablets of the curcumin/PVP/PA mixture were produced. The final tablets were then employed in drug release studies under the same condition as outlined above.[63]

The release characteristics of curcumin from a sample composed of PA-12/PVP/curcumin (Figure 3.17) demonstrates a sustained release that reaches 3 % of curcumin release within 24 h, typical for diffusion-controlled systems. As the drug is embedded in a dissolving matrix, in this case the slow dissolution of PVP permits controlled curcumin release up to 9 % in the course of 56 days.

Figure 3.17. Cumulative release of curcumin from a PA-12/PVP/curcumin system.

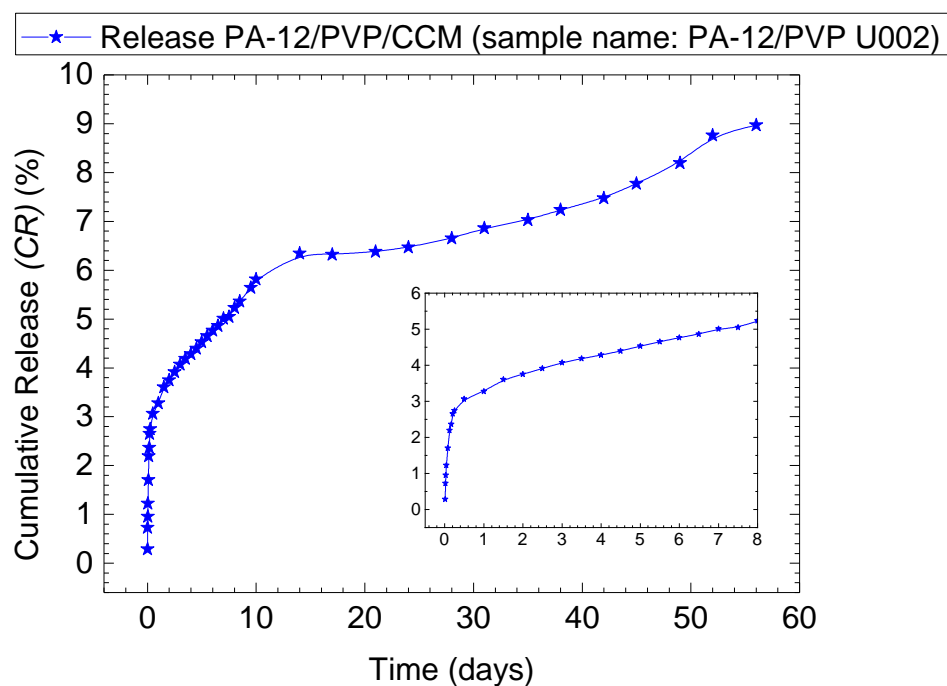As another alternative to modulate the drug release, curcumin was encapsulated into MIL-101(Fe) and the resulting CCM@MIL-101(Fe) was further incorporated into the polymer matrix (PA-12/PVP). The release characteristics of the PA-12/PVP/CCM@MIL-101(Fe) system also shows the pulsatile release characteristics observed for CCM@MIL-101(Fe), but differs from the last as two distinct release steps are observed (Figure 3.18). In the first stage up to 15 days, release of curcumin into the medium gradually increases to 14 % of curcumin. In the second stage, the system shows a sustained release of curcumin reaching 41 % after 56 days. In this scenario, the inclusion of curcumin in MIL-101(Fe) and the incorporation of CCM@MIL-101(Fe) into the polymer matrix allowed to modulate the release of the drug in the simulated biological medium, in contrast with the CCM@MIL-101(Fe), where around 40 % of curcumin is released in the first 10 h.
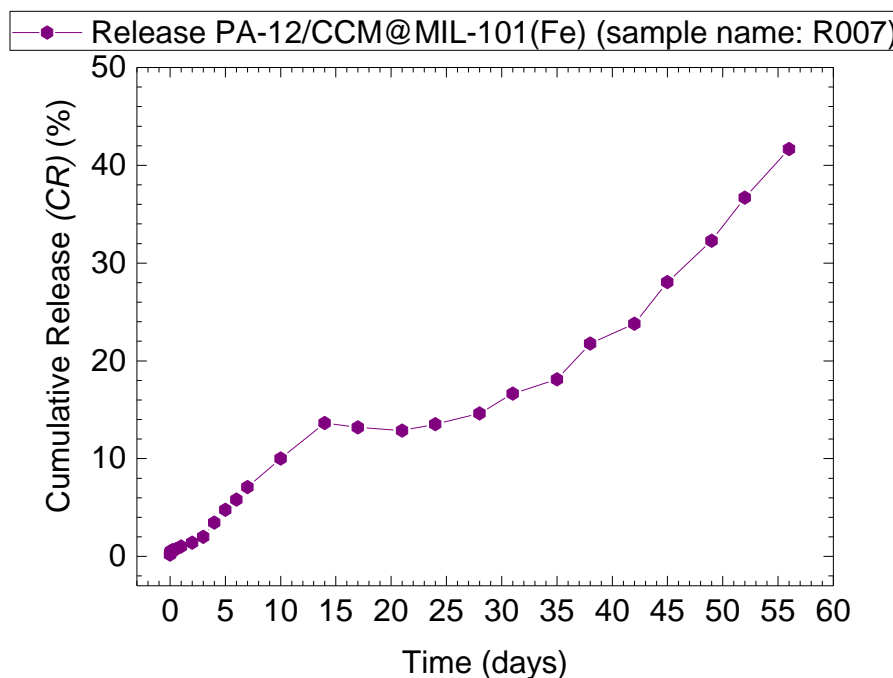
Figure 3.18. Cumulative release of curcumin from a PA-12/CCM@MIL-101(Fe) system.

3.4 Conclusion and outlook

The metal-organic framework MIL-101(Fe) was used successfully to encapsulate and release curcumin. Both processes were followed by UV-vis spectroscopy. Subsequently, the application of PA-12 as a polymer matrix for incorporation and release of curcumin was studied. The SLS technique applied here fulfilled the demands of finding a technique that was simple to use, customizable, and efficient to obtain PA-12/curcumin tablets. These tablets displayed a sustained extended release of curcumin over 5 days, confirming that modulation of drug release is possible by drug incorporation in a 3D printed polymer matrix. Furthermore, the incorporation of the biopolymer PVP together with PA-12 allowed to slightly reduce the release in the first 24 h. This could be beneficial for future applications *in vivo*, as it may prevent possible side effects due to its biocompatibility and slow release. Likewise, the encapsulation of curcumin into MIL-101(Fe) prior to 3D printing of the polymer mixture allowed reducing the drug release further in the first 24 h.

As 3D printing allows customization of the shape, size and geometry of an object according to the scientific and clinical needs, combining drugs or drug containers with suitable polymer matrices provides the potential to extend future studies to a large variety of drug@MOF−polymer combinations and, thus, is a versatile tool for the design of multifunctional nanoparticle systems.

A similar approach used here for curcumin is also applied in chapter 4 for the release studies of 5-Fluorouracil and capecitabine, altogether with the SLS technique presenting different directions in the drug delivery design.

3.5 Bibliography

[1]   A. Vogel and J. Pelletier, "Examen chimique de la racine de Curcuma," *J Pharm*, vol. 1, pp. 289–300, 1815.

[2]   H. A. Vogel and J. Pelletier, "Curcumin-biological and medicinal properties," *J Pharma*, vol. 2, no. 50, p. 24, 1815.

[3]   L. Hamzehzadeh, S. L. Atkin, M. Majeed, A. E. Butler, and A. Sahebkar, "The versatile role of curcumin in cancer prevention and treatment: A focus on PI3K/AKT pathway," *J. Cell. Physiol.*, vol. 233, no. 10, pp. 6530–6537, 2018, doi: 10.1002/jcp.26620.

[4]   M. Teymouri, M. Pirro, T. P. Johnston, and A. Sahebkar, "Curcumin as a multifaceted compound against human papilloma virus infection and cervical cancers: A review of chemistry, cellular, molecular, and preclinical features.," *Biofactors*, vol. 43, no. 3, pp. 331–346, May 2017, doi: 10.1002/biof.1344.

[5]   M. Ghandadi and A. Sahebkar, "Curcumin: An Effective Inhibitor of Interleukin-6.," *Curr. Pharm. Des.*, vol. 23, no. 6, pp. 921–931, 2017, doi: 10.2174/1381612822666161006151605.

[6]   A. Sahebkar, A. F. G. Cicero, L. E. Simental-Mendía, B. B. Aggarwal, and S. C. Gupta, "Curcumin downregulates human tumor necrosis factor-α levels: A systematic review and meta-analysis of randomized controlled trials.," *Pharmacol. Res.*, vol. 107, pp. 234–242, May 2016, doi: 10.1016/j.phrs.2016.03.026.

[7]   A. Shakeri, N. Ward, Y. Panahi, and A. Sahebkar, "Anti-Angiogenic Activity of Curcumin in Cancer Therapy: A Narrative Review.," *Curr. Vasc. Pharmacol.*, vol. 17, no. 3, pp. 262–269, 2019, doi: 10.2174/1570161116666180209113014.

[8]   S. Hu *et al.*, "HHS Public Access," vol. 15, no. 6, pp. 629–637, 2015, doi: doi:10.1586/14737175.2015.1044981.

[9]   K. Bavarsad, G. E. Barreto, M.-A.-R. Hadjzadeh, and A. Sahebkar, "Protective Effects of Curcumin Against Ischemia-Reperfusion Injury in the Nervous System.," *Mol. Neurobiol.*, vol. 56, no. 2, pp. 1391–1404, Feb. 2019, doi: 10.1007/s12035-018-1169-7.

[10]   Y. Panahi *et al.*, "Effects of Curcuminoids Plus Piperine on Glycemic, Hepatic and Inflammatory Biomarkers in Patients with Type 2 Diabetes Mellitus: A Randomized Double-Blind Placebo-Controlled Trial.," *Drug Res. (Stuttg).*, vol. 68, no. 7, pp. 403–409, Jul. 2018, doi: 10.1055/s-0044-101752.

[11]   N. A. Zabihi, M. Pirro, T. P. Johnston, and A. Sahebkar, "Is There a Role for Curcumin Supplementation in the Treatment of Non-Alcoholic Fatty Liver Disease? The Data Suggest Yes.," *Curr. Pharm. Des.*, vol. 23, no. 7, pp. 969–982, 2017, doi: 10.2174/1381612822666161010115235.

[12]   A. Shakeri and A. Sahebkar, "Optimized curcumin formulations for the treatment of Alzheimer's disease: A patent evaluation.," *J. Neurosci. Res.*, vol. 94, no. 2, pp. 111–113, Feb. 2016, doi: 10.1002/jnr.23696.

[13]   Y. Panahi *et al.*, "Antioxidant effects of curcuminoids in patients with type 2 diabetes mellitus: a randomized controlled trial.," *Inflammopharmacology*, vol. 25, no. 1, pp. 25–31, Feb. 2017, doi: 10.1007/s10787-016-0301-4.

[14]   V. Bianconi, M. R. Mannarino, A. Sahebkar, T. Cosentino, and M. Pirro, "Cholesterol-Lowering Nutraceuticals Affecting Vascular Function and Cardiovascular Disease Risk.," *Curr. Cardiol. Rep.*, vol. 20, no. 7, p. 53, May 2018, doi: 10.1007/s11886-018-0994-7.

[15] F. Keihanian, A. Saeidinia, R. K. Bagheri, T. P. Johnston, and A. Sahebkar, "Curcumin, hemostasis, thrombosis, and coagulation.," *J. Cell. Physiol.*, vol. 233, no. 6, pp. 4497–4511, Jun. 2018, doi: 10.1002/jcp.26249.

[16] A. Saeidinia, F. Keihanian, A. E. Butler, R. K. Bagheri, S. L. Atkin, and A. Sahebkar, "Curcumin in heart failure: A choice for complementary therapy?," *Pharmacol. Res.*, vol. 131, pp. 112–119, May 2018, doi: 10.1016/j.phrs.2018.03.009.

[17] D. Lelli, A. Sahebkar, T. P. Johnston, and C. Pedone, "Curcumin use in pulmonary diseases: State of the art and future perspectives.," *Pharmacol. Res.*, vol. 115, pp. 133–148, Jan. 2017, doi: 10.1016/j.phrs.2016.11.017.

[18] E. Abdollahi, A. A. Momtazi, T. P. Johnston, and A. Sahebkar, "Therapeutic effects of curcumin in inflammatory and immune-mediated diseases: A nature-made jack-of-all-trades?," *J. Cell. Physiol.*, vol. 233, no. 2, pp. 830–848, Feb. 2018, doi: 10.1002/jcp.25778.

[19] A. Giordano and G. Tommonaro, "Curcumin and cancer," *Nutrients*, vol. 11, no. 10, 2019, doi: 10.3390/nu11102376.

[20] F. Ghasemi, H. Bagheri, G. E. Barreto, M. I. Read, and A. Sahebkar, "Effects of Curcumin on Microglial Cells," *Neurotox. Res.*, vol. 36, no. 1, pp. 12–26, 2019, doi: 10.1007/s12640-019-00030-0.

[21] A. Noorafshan and S. Ashkani-Esfahani, "A Review of Therapeutic Effects of Curcumin," *Curr. Pharm. Des.*, vol. 19, no. 11, pp. 2032–2046, 2013, doi: 10.2174/138161213805289273.

[22] E. Jaruga *et al.*, "Apoptosis-like, reversible changes in plasma membrane asymmetry and permeability, and transient modifications in mitochondrial membrane potential induced by curcumin in rat thymocytes," *FEBS Lett.*, vol. 433, no. 3, pp. 287–293, 1998, doi: 10.1016/S0014-5793(98)00919-3.

[23] P. Anand, C. Sundaram, S. Jhurani, A. B. Kunnumakkara, and B. B. Aggarwal, "Curcumin and cancer: An 'old-age' disease with an 'age-old' solution," *Cancer Lett.*, vol. 267, no. 1, pp. 133–164, 2008, doi: 10.1016/j.canlet.2008.03.025.

[24] R. K. B. and U. B. Kausik Biswas, Ishita Chattopadhyay, "Biological and Medicinal Properties," *Curr. Sci.*, vol. 82, no. 11, pp. 1336–1345, 2002.

[25] M. Roy, S. Chakraborty, M. Siddiqi, and R. K. Bhattacharya, "Induction of apoptosis in tumor cells by natural phenolic compounds," *Asian Pacific J. Cancer Prev.*, vol. 3, no. 1, pp. 61–67, 2012.

[26] Y. Liu, R. L. Chang, X. X. Cui, H. L. Newmark, and A. H. Conney, "Synergistic effects of curcumin on all-trans retinoic acid- and 1 alpha,25-dihydroxyvitamin D3-induced differentiation in human promyelocytic leukemia HL-60 cells.," *Oncol. Res.*, vol. 9, no. 1, pp. 19–29, 1997.

[27] J. A. Sokoloski and A. C. Sartorelli, "Induction of the differentiation of HL-60 promyelocytic leukemia cells by nonsteroidal anti-inflammatory agents in combination with low levels of vitamin D3.," *Leuk. Res.*, vol. 22, no. 2, pp. 153–161, Feb. 1998, doi: 10.1016/s0145-2126(97)00156-2.

[28] M. H. Pan, W. L. Chang, S. Y. Lin-Shiau, C. T. Ho, and J. K. Lin, "Induction of apoptosis by garcinol and curcumin through cytochrome c release and activation of caspases in human leukemia HL-60 cells.," *J. Agric. Food Chem.*, vol. 49, no. 3, pp. 1464–1474, Mar. 2001, doi: 10.1021/jf001129v.

[29] Z. Mbese, V. Khwaza, and B. A. Aderibigbe, "Curcumin and Its Derivatives as Potential Therapeutic Agents in Prostate, Colon and Breast Cancers.," *Molecules*, vol. 24, no. 23, Nov. 2019, doi: 10.3390/molecules24234386.

[30] W. Zhao, X. Zhou, G. Qi, and Y. Guo, "Curcumin suppressed the prostate cancer by inhibiting JNK pathways via epigenetic regulation.," *J. Biochem. Mol. Toxicol.*, vol. 32, no. 5, p. e22049, May 2018, doi: 10.1002/jbt.22049.

[31] C. Yang *et al.*, "Curcumin induces apoptosis and protective autophagy in castration-resistant prostate cancer cells through iron chelation.," *Drug Des. Devel. Ther.*, vol. 11, pp. 431–439, 2017, doi: 10.2147/DDDT.S126964.

[32] S. Lev-Ari *et al.*, "Curcumin induces apoptosis and inhibits growth of orthotopic human non-small cell lung cancer xenografts.," *J. Nutr. Biochem.*, vol. 25, no. 8, pp. 843–850, Aug. 2014, doi: 10.1016/j.jnutbio.2014.03.014.

[33] Q. Chen *et al.*, "Curcumin inhibits proliferation-migration of NSCLC by steering crosstalk between a Wnt signaling pathway and an adherens junction via EGR-1.," *Mol. Biosyst.*, vol. 11, no. 3, pp. 859–868, Mar. 2015, doi: 10.1039/c4mb00336e.

[34] A. L. Cheng *et al.*, "Phase I clinical trial of curcumin, a chemopreventive agent, in patients with high-risk or pre-malignant lesions.," *Anticancer Res.*, vol. 21, no. 4B, pp. 2895–2900, 2001.

[35] R. Greil *et al.*, "A phase 1 dose-escalation study on the safety, tolerability and activity of liposomal curcumin (Lipocurc^{TM}) in patients with locally advanced or metastatic cancer," *Cancer Chemother. Pharmacol.*, vol. 82, no. 4, pp. 695–706, 2018, doi: 10.1007/s00280-018-3654-0.

[36] M. Heger, R. F. van Golen, M. Broekgaarden, and M. C. Michel, "The molecular basis for the pharmacokinetics and pharmacodynamics of curcumin and its metabolites in relation to cancers," *Pharmacol. Rev.*, vol. 66, no. 1, pp. 222–307, 2014, doi: 10.1124/pr.110.004044.

[37] A. Tiwari, A. Singh, N. Garg, and J. K. Randhawa, "Curcumin encapsulated zeolitic imidazolate frameworks as stimuli responsive drug delivery system and their interaction with biomimetic environment," *Sci. Rep.*, vol. 7, no. 1, pp. 1–12, 2017, doi: 10.1038/s41598-017-12786-6.

[38] B. Lei, M. Wang, Z. Jiang, W. Qi, R. Su, and Z. He, "Constructing Redox-Responsive Metal-Organic Framework Nanocarriers for Anticancer Drug Delivery," *ACS Applied Materials and Interfaces*, vol. 10, no. 19. pp. 16698–16706, 2018, doi: 10.1021/acsami.7b19693.

[39] H. Zheng *et al.*, "One-pot Synthesis of Metal-Organic Frameworks with Encapsulated Target Molecules and Their Applications for Controlled Drug Delivery," *Journal of the American Chemical Society*, vol. 138, no. 3. pp. 962–968, 2016, doi: 10.1021/jacs.5b11720.

[40] Y. Yang *et al.*, "A Large Capacity Cationic Metal-Organic Framework Nanocarrier for Physiological pH Responsive Drug Delivery.," *Mol. Pharm.*, vol. 13, no. 8, pp. 2782–2786, Aug. 2016, doi: 10.1021/acs.molpharmaceut.6b00374.

[41] A. Bansal and M. Celeste Simon, "Glutathione metabolism in cancer progression and treatment resistance," *J. Cell Biol.*, vol. 217, no. 7, pp. 2291–2298, 2018, doi: 10.1083/jcb.201804161.

[42] M. P. Gamcsik, M. S. Kasibhatla, S. D. Teeter, and O. M. Colvin, "Glutathione levels in human tumors," *Biomarkers*, vol. 17, no. 8, pp. 671–691, 2012, doi: 10.3109/1354750X.2012.715672.

[43] A. L. Ortega, S. Mena, and J. M. Estrela, "Glutathione in cancer cell death," *Cancers (Basel).*, vol. 3, no. 1, pp. 1285–1310, 2011, doi: 10.3390/cancers3011285.

[44] Y. Zhang *et al.*, "Engineering Metal-Organic Frameworks for Photoacoustic Imaging-Guided Chemo-/Photothermal Combinational Tumor Therapy.," *ACS Appl. Mater. Interfaces*, vol. 10, no. 48, pp. 41035–41045, Dec. 2018, doi: 10.1021/acsami.8b13492.

[45] J. Tang, M. Yang, M. Yang, J. Wang, W. Dong, and G. Wang, "Heterogeneous Fe-MIL-101

catalysts for efficient one-pot four-component coupling synthesis of highly substituted pyrroles," *New J. Chem.*, vol. 39, no. 6, pp. 4919–4923, 2015, doi: 10.1039/c5nj00632e.

[46] A. C. McKinlay *et al.*, "BioMOFs: Metal-organic frameworks for biological and medical applications," *Angew. Chemie - Int. Ed.*, vol. 49, no. 36, pp. 6260–6266, 2010, doi: 10.1002/anie.201000048.

[47] K. M. L. Taylor-Pashow, J. Della Rocca, Z. Xie, S. Tran, and W. Lin, "Postsynthetic modifications of iron-carboxylate nanoscale metal-organic frameworks for imaging and drug delivery," *J. Am. Chem. Soc.*, vol. 131, no. 40, pp. 14261–14263, 2009, doi: 10.1021/ja906198y.

[48] V. V. S. R. Karri *et al.*, "Curcumin loaded chitosan nanoparticles impregnated into collagen-alginate scaffolds for diabetic wound healing," *Int. J. Biol. Macromol.*, vol. 93, pp. 1519–1529, 2016, doi: 10.1016/j.ijbiomac.2016.05.038.

[49] A. Anitha, V. G. Deepagan, V. V. Divya Rani, D. Menon, S. V. Nair, and R. Jayakumar, "Preparation, characterization, in vitro drug release and biological studies of curcumin loaded dextran sulphate-chitosan nanoparticles," *Carbohydr. Polym.*, vol. 84, no. 3, pp. 1158–1164, 2011, doi: 10.1016/j.carbpol.2011.01.005.

[50] P. Ratanajiajaroen, A. Watthanaphanit, H. Tamura, S. Tokura, and R. Rujiravanit, "Release characteristic and stability of curcumin incorporated in β-chitin non-woven fibrous sheet using Tween 20 as an emulsifier," *Eur. Polym. J.*, vol. 48, no. 3, pp. 512–523, 2012, doi: 10.1016/j.eurpolymj.2011.11.020.

[51] V. R. Yadav, S. Suresh, K. Devi, and S. Yadav, "Effect of Cyclodextrin Complexation of Curcumin on its Solubility and Antiangiogenic and Anti-inflammatory Activity in Rat Colitis Model," *AAPS PharmSciTech*, vol. 10, no. 3, pp. 752–762, 2009, doi: 10.1208/s12249-009-9264-8.

[52] C. Li *et al.*, "Hierarchical hollow Fe2O3 @MIL-101(Fe)/C derived from metal-organic frameworks for superior sodium storage," *Sci. Rep.*, vol. 6, no. January, pp. 1–8, 2016, doi: 10.1038/srep25556.

[53] S. Ray and R. P. Cooney, *Thermal degradation of polymer and polymer composites*, Third Edit. Elsevier Inc., 2018.

[54] X.-Z. Sun, G. R. Williams, X.-X. Hou, and L.-M. Zhu, "Electrospun curcumin-loaded fibers with potential biomedical applications.," *Carbohydr. Polym.*, vol. 94, no. 1, pp. 147–153, Apr. 2013, doi: 10.1016/j.carbpol.2012.12.064.

[55] H. Souguir, F. Salaün, P. Douillet, I. Vroman, and S. Chatterjee, "Nanoencapsulation of curcumin in polyurethane and polyurea shells by an emulsion diffusion method," *Chem. Eng. J.*, vol. 221, pp. 133–145, 2013, doi: 10.1016/j.cej.2013.01.069.

[56] Z. Chen *et al.*, "Thermal degradation kinetics study of curcumin with nonlinear methods," *Food Chem.*, vol. 155, pp. 81–86, 2014, doi: 10.1016/j.foodchem.2014.01.034.

[57] H. Tian, J. Peng, Q. Du, X. Hui, and H. He, "One-pot sustainable synthesis of magnetic MIL-100(Fe) with novel Fe3O4 morphology and its application in heterogeneous degradation," *Dalt. Trans.*, vol. 47, no. 10, pp. 3417–3424, 2018, doi: 10.1039/c7dt04819j.

[58] M. Zheng, S. Liu, X. Guan, and Z. Xie, "One-Step Synthesis of Nanoscale Zeolitic Imidazolate Frameworks with High Curcumin Loading for Treatment of Cervical Cancer," *ACS Appl. Mater. Interfaces*, vol. 7, no. 40, pp. 22181–22187, Oct. 2015, doi: 10.1021/acsami.5b04315.

[59] Z. Moussa, M. Hmadeh, M. G. Abiad, O. H. Dib, and D. Patra, "Encapsulation of curcumin in cyclodextrin-metal organic frameworks: Dissociation of loaded CD-MOFs enhances stability of curcumin," *Food Chem.*, vol. 212, no. 2016, pp. 485–494, 2016, doi:

10.1016/j.foodchem.2016.06.013.

[60] K. I. Priyadarsini, "The chemistry of curcumin: From extraction to therapeutic agent," *Molecules*, vol. 19, no. 12, pp. 20091–20112, 2014, doi: 10.3390/molecules191220091.

[61] X. Liu, Y. Xu, Z. Wu, and H. Chen, "Poly(N-vinylpyrrolidone)-Modified surfaces for biomedical applications," *Macromol. Biosci.*, vol. 13, no. 2, pp. 147–154, 2013, doi: 10.1002/mabi.201200269.

[62] M. Teodorescu and M. Bercea, "Poly(vinylpyrrolidone) – A Versatile Polymer for Biomedical and Beyond Medical Applications," *Polym. - Plast. Technol. Eng.*, vol. 54, no. 9, pp. 923–943, 2015, doi: 10.1080/03602559.2014.979506.

[63] H. Rachmawati, L. Al Shaal, R. H. Müller, and C. M. Keck, "Development of curcumin nanocrystal: Physical aspects," *J. Pharm. Sci.*, 2013, doi: 10.1002/jps.23335.

Chapter 4: Other drugs, 5-Fluorouracil (5-FU), Capecitabine

4.1 Introduction

Antimetabolite drugs represent a class of anticancer drugs that mimic a metabolite and thus inhibit its use.[1–3] Such substances are often similar in structure to the metabolite that they interfere with. One example is 5-fluorouracil (5-FU) (Figure 4.1) a synthetic fluorinated pyrimidine analog of a DNA/RNA nucleobase, namely an analog of uracil with a fluorine atom at the C5 position in place of hydrogen. Consequently, it interferes with DNA or RNA replication processes by incorporation into DNA and RNA.[4] This cytostatic drug is administered i.v. and subsequently conversion intracellularly into their active forms. Among others it is used for treatment of the basal cell carcinoma (BCC), and is also broadly applied in treatment of colorectal,[5] breast cancers,[6] liver cancer,[7,8] pancreatic cancer,[9] esophageal cancer,[10] and gastric cancer.[11] Nevertheless, it is in colorectal cancer that 5-FU has had the greatest effect.[12,13] The mechanism of action of this drug, which has been known for more than 30 years now, was investigated in detail.[14] After administration and cellular uptake 5-FU is converted intracellularly to the following active metabolites: fluorodeoxyuridine monophosphate (FdUMP), fluorodeoxyuridine triphosphate (FdUTP) and fluorouridine triphosphate (FUTP); these active metabolites disrupt RNA synthesis and the action of thymidylate synthase (TS), which is the intended mechanism (ca. 20% of administered drug).[12] However, most of the prodrug is trapped in the liver (ca. 80%) where it is disactivated by the enzyme dihydropyrimidine dehydrogenase (DPD), which converts 5-FU to dihydrofluorouracil (DHFU) (Figure 4.1).[12,15] This is the reason for poor bioavailability of 5-FU.

One of the active metabolites of 5-FU, namely FdUMP, forms a covalent ternary complex with thymidylate synthase (TS) leading to prevention of the access of 2'-deoxyuridine-5'-monophosphate (dUMP), the natural substrate, to the nucleotide-binding site of TS and, in turn, inhibition of the 2'-deoxythymidine-5'-monophosphate (dTMP) synthesis, a necessary precursor in the DNA base thymidine production, which finally causes DNA strand breakage and eventually leading to cell death (Figure 4.1).[12]

A further metabolite of 5-FU, 5-fluoridine triphosphate (FUTP) can be incorporated into RNA, producing cytotoxicity by interfering with RNA processing and function.[1,12,17]

In more detail: 5-FU is activated by the conversion to fluorouridine monophosphate (FUMP), either directly by orotate phosphoribosyltransferase (OPRT) with phosphoribosyl pyrophosphate (PRPP) as the cofactor, or indirectly

via fluorouridine (FUR) through the sequential action of uridine phosphorylase (UP) and uridine kinase (UK). FUMP is then phosphorylated to fluorouridine diphosphate (FUDP), which can be either further phosphorylated to the active metabolite fluorouridine triphosphate (FUTP), or converted to fluorodeoxyuridine diphosphate (FdUDP) by ribonucleotide reductase (RR). In turn, FdUDP can either be phosphorylated or dephosphorylated to generate the active metabolites FdUTP or FdUMP, respectively. An alternative activation pathway involves the thymidine phosphorylase-catalyzed conversion of 5-FU to fluorodeoxyuridine (FUDR), which is then phosphorylated by thymidine kinase (TK) to FdUMP. Dihydropyrimidine dehydrogenase (DPD)-mediated disactivating of 5-FU to dihydrofluorouracil (DHFU) occurs also in normal and tumor cells (apart from the liver) (Figure 4.1).[12]
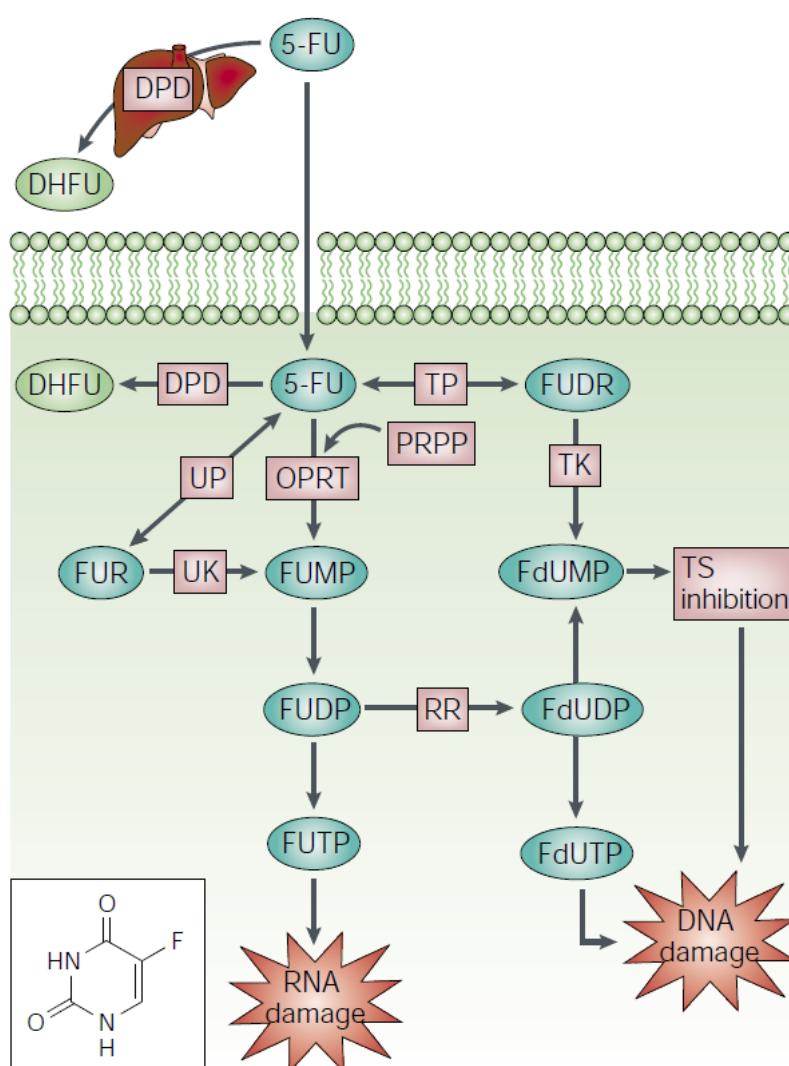

Figure 4.1. 5-FU mechanism of action in the human body. Taken from Longley et al.[12].FUMP = fluorouridine monophosphate; OPRT = orotate phosphoribosyltransferase; PRPP = phosphoribosyl pyrophosphate; FUR = fluorouridine; UP = uridine phosphorylase; UK = uridine kinase; FUDP = fluorouridine diphosphate; FUTP = fluorouridine triphosphate; FdUDP = fluorodeoxyuridine diphosphate; RR = ribonucleotide reductase; FUDR = fluorodeoxyuridine, TK = thymidine kinase; DPD = Dihydropyrimidine dehydrogenase; DHFU = dihydrofluorouracil.

Among all the malignancies cited above, such as breast, liver, pancreatic, esophageal, and gastric cancer 5-FU has been an essential component in the treatment of early-stage and advanced colorectal cancer; nonetheless, as a single agent, the overall response for advanced colorectal cancer is limited.[18,19]

Several modulation strategies including the implementation of 5-FU-based combination regimens with oxaliplatin, irinotecan and 5-FU pro-drugs, such as capecitabine, have been developed and tested to increase the antitumor activity of 5-FU and overcome the chemoresistance observed after a certain period of administration.[20–23]

Due to its gastrointestinal toxicity and poor oral absorption, the oral use of 5-FU as an isolated agent was abandoned early, and research has focused on the biomodulation approach, to improve therapeutic effectiveness of 5-FU. An example is leucovorin (LV, folinic acid), where high doses of FU were substituted with FU modulation by leucovorin which has been shown to improve patient's survival and the tumor response rate, acting as a chemoprotectant by inhibiting side effects caused by 5-FU.[23–25]

Another approach was to use a prodrug (capecitabine; Figure 4.2), which is administered orally, and after absorption through the gastrointestinal wall in intact form, is converted to the active form of 5-FU by thymidine phosphorylase, which is at higher concentrations in most tumor tissue than in most normal healthy tissue. This theoretically allows low systemic toxicity and should be more effective and much safer than 5-FU. [26]
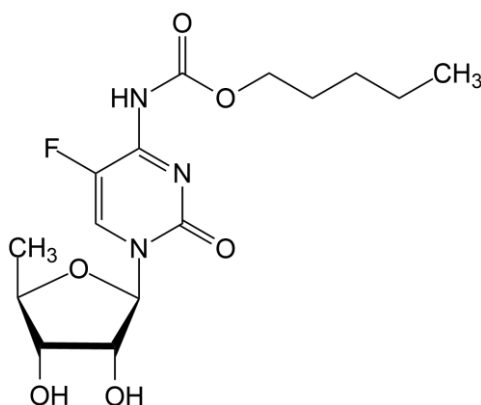

Figure 4.2. Schematic chemical structure of capecitabine.

In patients with dihydropyrimidine dehydrogenase (DPD) deficiency, the enzyme of (fluorinated) pyrimidine degradation, the administration of the same doses of 5-FU can lead to severe intoxications with symptoms such as neutropenia, diarrhea, and hand-foot syndromes. In this case the plasma level of the standard administered 5-FU dose exceeds the maximum tolerable dose.[27–29] These adverse drug reactions are as frequent as 10–30% and can lead to patient's death in around 1% of cases.[29] As a result, numerous attempts have been made in order to encapsulate 5-FU and diminish the adverse effects of its administration. The aim of this chapter was to exploit the encapsulation of 5-FU

and capecitabine into the metal-organic framework MIL-101(Fe), characterize and evaluate its release activity in biological media.[30]

4.2 Materials

MIL-101(Fe) was synthesized according to the literature.[31] 5-Fluorouracil (5-FU) was purchased from TCI chemicals (purity >99.0%, (HPLC)), capecitabine was purchased from TCI chemicals (purity >98.0%, (HPLC)), and nylon 12 powder (polyamide 12; PA-12) was purchased from Advanc3D Materials. All reagents and solvents were purchased from commercial sources and used without further purification.

4.3 Methods

Fourier-Transform Infrared Spectroscopy (FTIR)

Fourier-transform infrared spectroscopy was conducted to identify the functional groups present in 5-FU, MIL-101(Fe), and in 5-FU encapsulated in the metal-organic framework (MOF), named as 5-FU@MIL-101(Fe). FT-IR spectra were obtained with a PerkinElmer system 2000 FTIR spectrometer, scanning between 4000 and 400 cm^{-1} employing KBr pellets prepared in a glovebox under nitrogen atmosphere.

UV-Vis absorption spectroscopy: uptake and release studies of 5-FU and capecitabine in MIL-101(Fe)

The UV-vis absorption spectra were measured with a PerkinElmer UV/VIS/NIR Lambda 900 spectrometer, equipped with a xenon arc lamp, using quartz cuvettes (V = 3 cm^3, l = 10 mm). All spectra were recorded at 25 °C, in the range 200−400 nm, at 1.0 nm resolution.

The porous MIL-101(Fe) was evacuated under high vacuum at room temperature overnight before usage. For loading of 5-FU, MIL-101(Fe) was soaked in a solution of 5-FU in methanol (0.01 mg mL^{-1}), stirred under exclusion of light for 48 h at room temperature, in different weight ratios 1:2 (MOF:drug) and 1:3 (MOF:drug) in order to determine the optimal loading of the drug into the MOF.

For determination of the 5-FU uptake kinetics, the calibration curve was derived from concentration-dependent absorbance measurements of 5-FU in MeOH at 264 nm in triplicate (Figure 4.3).

For determination of the release kinetics, the calibration curve was obtained by measuring the concentration-dependent absorbance of 5-FU in phosphate buffered saline (PBS) (pH 7.4) (Figure 4.4) and (PBS/DMSO (2%)) (pH 7.4) at 266 nm, in triplicate (Figure 4.5).
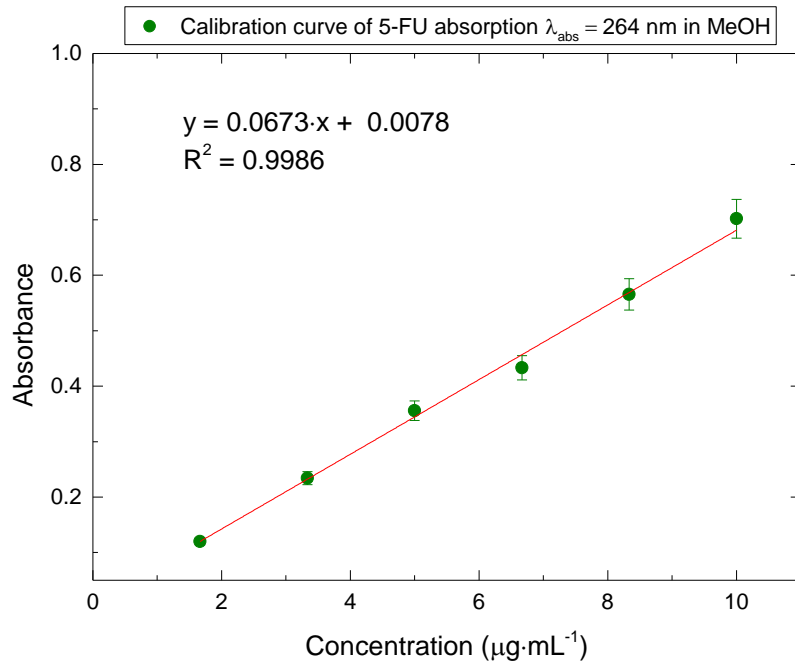
Figure 4.3. Calibration curve of 5-FU absorption or uptake in methanol, λ = 264 nm.
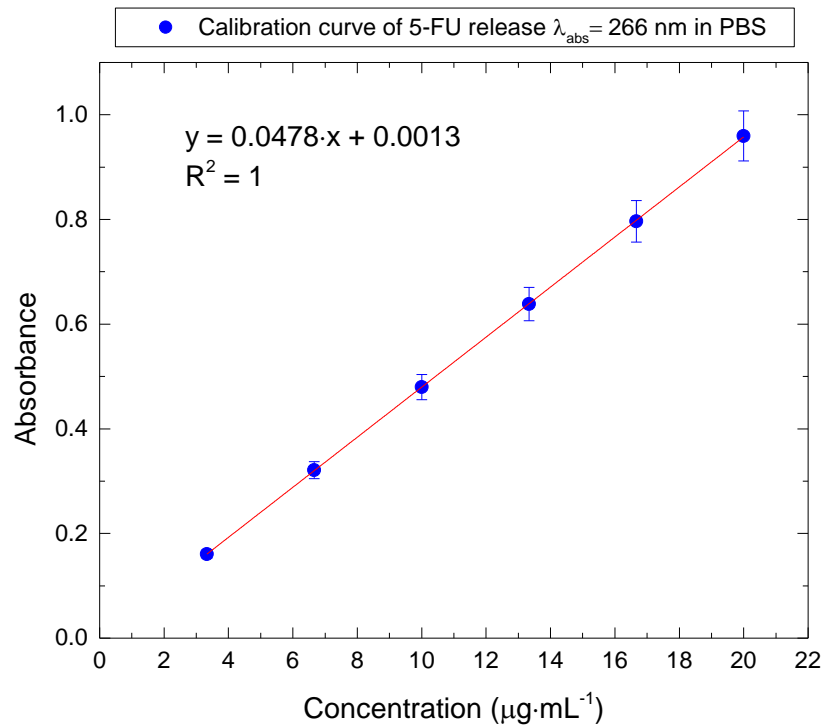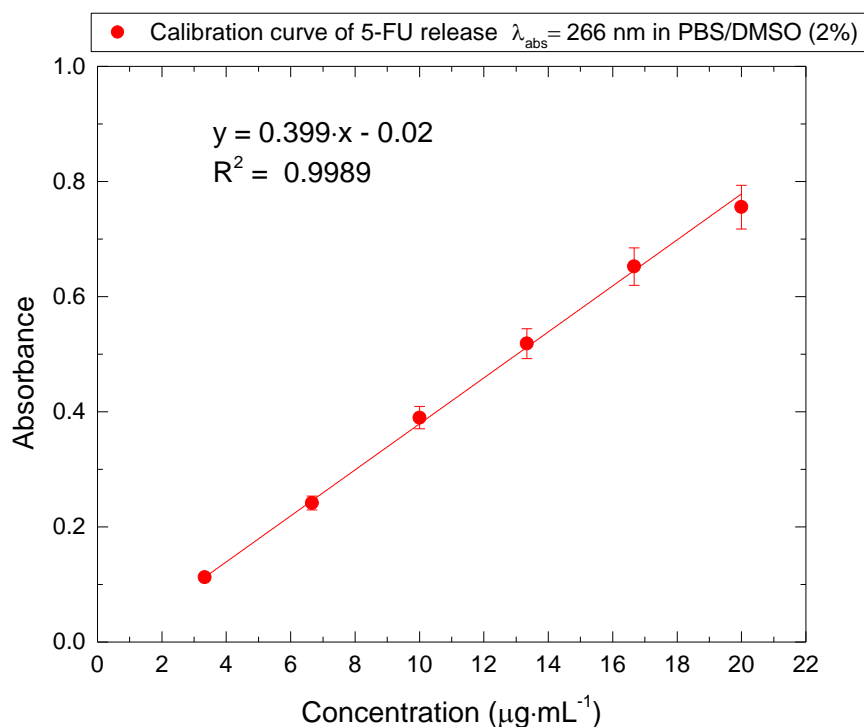

Figure 4.4. Calibration curve of 5-FU release in PBS, λ = 266 nm.

Figure 4.5. Calibration curve of 5-FU release in PBS/DMSO (2%), λ = 266 nm.

3D printing: The model used to produce the 3D samples was SnowWhite$^{®}$ from Sharebot.

Composition of the tablets:

PA-12/5-FU@MIL-101(Fe) (1:2, MOF:drug): 100 g PA-12 and 7.7 g 5-FU@MIL-101(Fe) (1:2, MOF:drug) were placed in the printer build plate, with a final concentration of 7.7% (w/w) PA-12/5-FU@MIL-101(Fe). Due to a bad layer adhesion in the first three produced samples, the concentration of 5FU@MIL-101(Fe) (1:2, MOF:drug) was lowered to 5% (w/w). The printing parameters are summarized in Table 4.1.

Table 4.1. Printing parameters for PA-12/5-FU@MIL-101(Fe)

Sample name	Power (%)	Rate (pps)	Powder Temp (°C)	Wait time (s)	Warming layers	Add (%)	Layer thickness (mm)	Sample size (mm)
PA12_Q001	40/40	64k/64k	170	300	2	7.7	0.1	Ø 16.63
PA12_Q002	40/40	64k/64k	174	300	2	7.7	0.1	Ø 16.63
PA12_Q003	40/40	64k/64k	176	300	3	7.7	0.1	Ø 16.63
PA12_Q004	40/40	64k/64k	174	300	8	5	0.1	Ø 16.63
PA12_Q005	40/40	64k/64k	174	300	8	5	0.1	Ø 16.63
PA12_Q006	40/40	64k/64k	174	300	8	5	0.1	Ø 16.63
PA12_Q007	40/40	64k/64k	174	300	8	5	0.1	Ø 16.63
PA12_Q008	40/40	64k/64k	174	300	8	5	0.1	Ø 16.63
PA12 Q009	40/40	64k/64k	174	300	8	5	0.1	Ø 16.63
PA12 Q010	40/40	64k/64k	174	300	8	5	0.1	Ø 16.63

For capecitabine

An analogous procedure was employed for the capecitabine loading in methanol (3 mg·mL^{-1}), stirred under exclusion of light for 48 h at room temperature, in different weight ratios 1:2 (MOF:drug) and 1:3 (MOF:drug) with regard to determining the capecitabine loading into the MIL-101(Fe).

Capecitabine exhibits UV absorption maxima at 214, 241 and 305 nm (Figure 4.6). The wavelength of 305 nm was selected as optimal for the determination of capecitabine. For the determination of the capecitabine uptake kinetics, the calibration curve was obtained by measuring the concentration-dependent absorbance of capecitabine in MeOH at 305 nm in triplicate (Figure 4.7).

The amount of adsorbed capecitabine was calculated by determination of the amount of free capecitabine still present in the supernatant solution after 24 h and 48 h from UV-Vis data (λ_{abs} = 305 nm). Each experiment was carried out in triplicate. The encapsulation efficiency (EE%) and loading capacity (LC%) were determined as follows:

$$EE\% = \left({(c_{i(Cap)} - c_{f(Cap)})} \Big/ {c_{i(Cap)}} \right) \times 100 \qquad \text{(Equation 3)}$$

$$LC\% = \left({(c_{i(Cap)} - c_{f(Cap)})} \Big/ {c_{(MOF)}} \right) \times 100 \qquad \text{(Equation 4)}$$

Where:

$EE\%$	= encapsulation efficiency of MIL-101(Fe) for capecitabine
$LC\%$	= loading capacity of MIL-101(Fe) for capecitabine
$c_{i(Cap)}$	= initial concentration of capecitabine
$c_{f(Cap)}$	= final concentration of capecitabine
$c_{(MIL-101(Fe))}$	= concentration of the MIL-101(Fe)

For the determination of the capecitabine release kinetics the calibration curve was obtained by measuring the concentration-dependent absorbance of capecitabine in PBS (pH 7.4) (Figure 4.8) and (PBS/DMSO (2%)) (pH 7.4) (Figure 4.9) at 305 nm in triplicate.
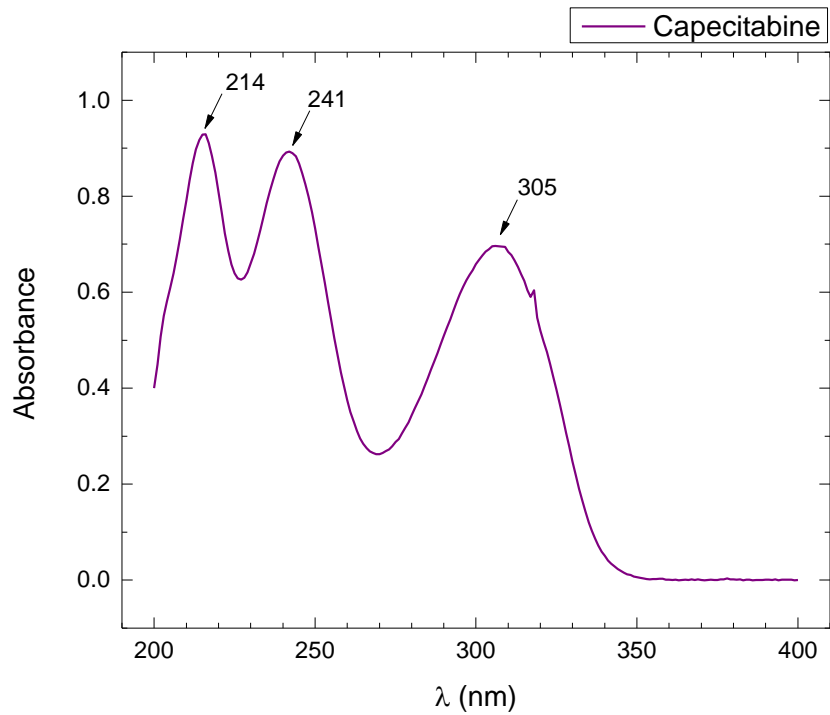
Figure 4.6. UV-vis spectrum of capecitabine in methanol (C_{MeOH}: 3 mg·mL^{-1})
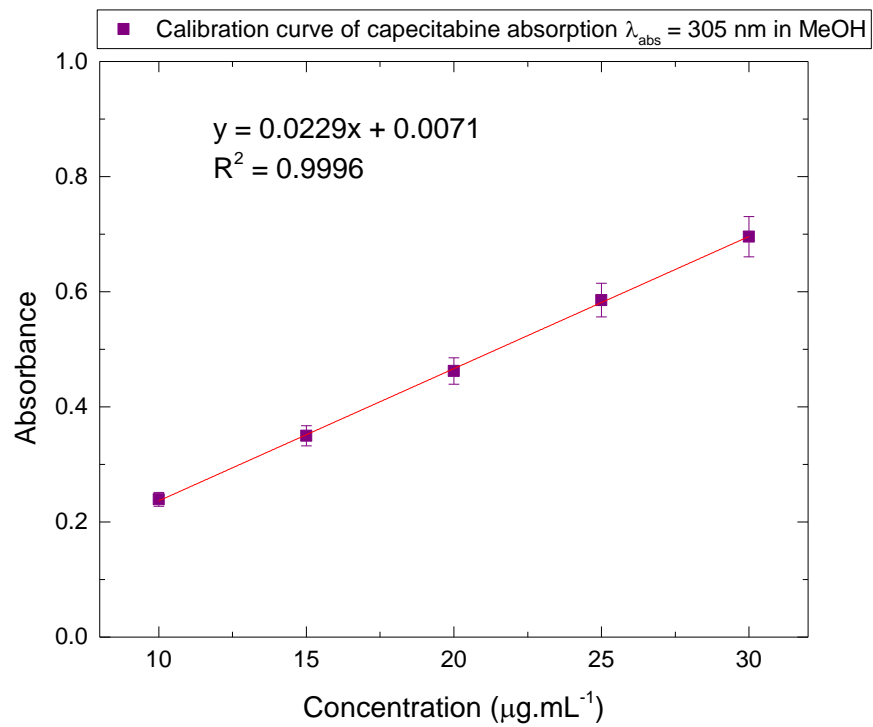

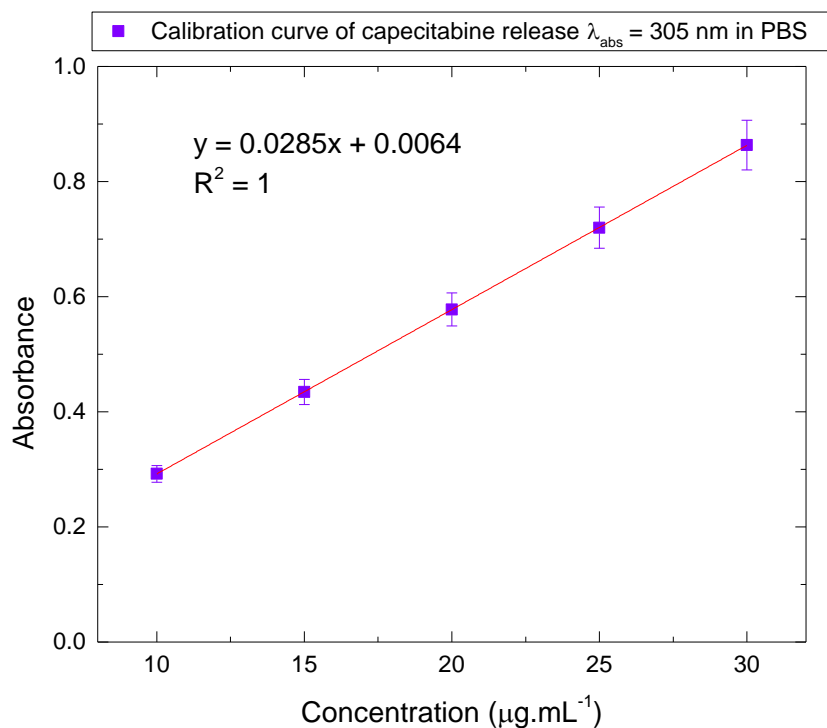Figure 4.7. Calibration curve of capecitabine uptake, in methanol at λ = 305 nm.

Figure 4.8. Calibration curve of capecitabine release in PBS, λ = 305 nm.
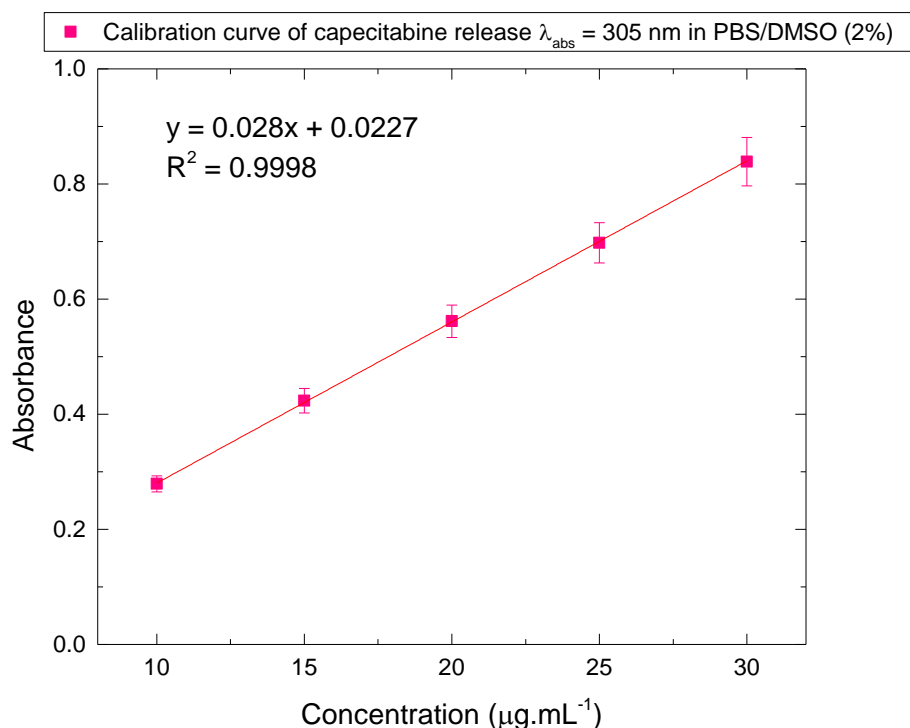

Figure 4.9. Calibration curve of capecitabine release in PBS/DMSO (2% v/v), λ = 305 nm.

Nuclear magnetic resonance (NMR) spectroscopy

The NMR spectra were recorded with a BRUKER Avance III HD 400 MHz NMR spectrometer at room temperature (^{1}H NMR 400.13 MHz, ^{13}C NMR 100.63 MHz). MeOH was used as the internal standard in the ^{1}H NMR spectra.

4.4 Results and discussion

4.4.1 Fourier Transform Infrared Spectroscopy (FTIR)

Figure 4.10 shows the FT-IR spectra of a) 5-FU, b) MIL-101(Fe) and c) 5-FU loaded into MIL-101(Fe) (sample named 5-FU@MIL-101(Fe)) in the weight ratio of 1:2 (MOF:drug) (c), and 5-FU loaded into MIL-101(Fe) in the weight ratio 1:3 (MOF:drug) (d).

The IR spectrum of the MOF (Figure 4.10 (a)) exhibits bands between 3500 and 2500 cm^{-1}, associated with the stretching vibrations of the −OH groups of the absorbed water molecules. The bands in the region 1300–1700 cm^{-1} correspond to the asymmetric and symmetric stretching vibrations of the carbonyl group of the ligand.[32]

The FTIR spectrum obtained for a 5-FU powder sample (Figure 4.10 (b)) shows the characteristic peaks of 5-FU at 1725 cm^{-1} and 1247 cm^{-1}, attributed to the stretching vibration of the C=O and C–N groups, respectively. The C–F deformation stretchings occur at 816–550 cm^{-1}.[32,33]

The FTIR spectra representing the 1:2 (MOF:drug) (Figure 4.10 (c)) and 1:3 (Figure 4.10 (d)) weight ratio of MOF:drug, 5-FU@MIL-101(Fe), have the characteristic bands related to the MIL-101(Fe) and 5-FU as a combination of both spectra, revealing the successful incorporation of the drug molecule into the MOF. When comparing the FTIR spectrum of pure 5-FU with that of 5-FU@MIL-101(Fe) (1:2, MOF:drug), an increase in the intensity of the vibrations in the region of 3500–2500 cm^{-1} (OH groups) and 1724–1247 cm^{-1} (C–N, C=O bond) is observed.

In addition, the intensity of the characteristic bands at 3500–2500 cm^{-1}, 1723–1247 cm^{-1}, and 816–529 cm^{-1} (C–F bond) in the 1:3 (MOF:drug) weight ratio of 5-FU@MIL-101(Fe) related to the C=O, C–N, and C–F band also confirmed the incorporation of the 5-FU molecule into the framework.[33–36]

In summary, the FT-IR results suggested that the 5-FU molecule was successfully incorporated in the MIL-101(Fe) framework, in the 5-FU@MIL-101(Fe) 1:2 ratio and 5-FU@MIL-101(Fe) 1:3 ratio.
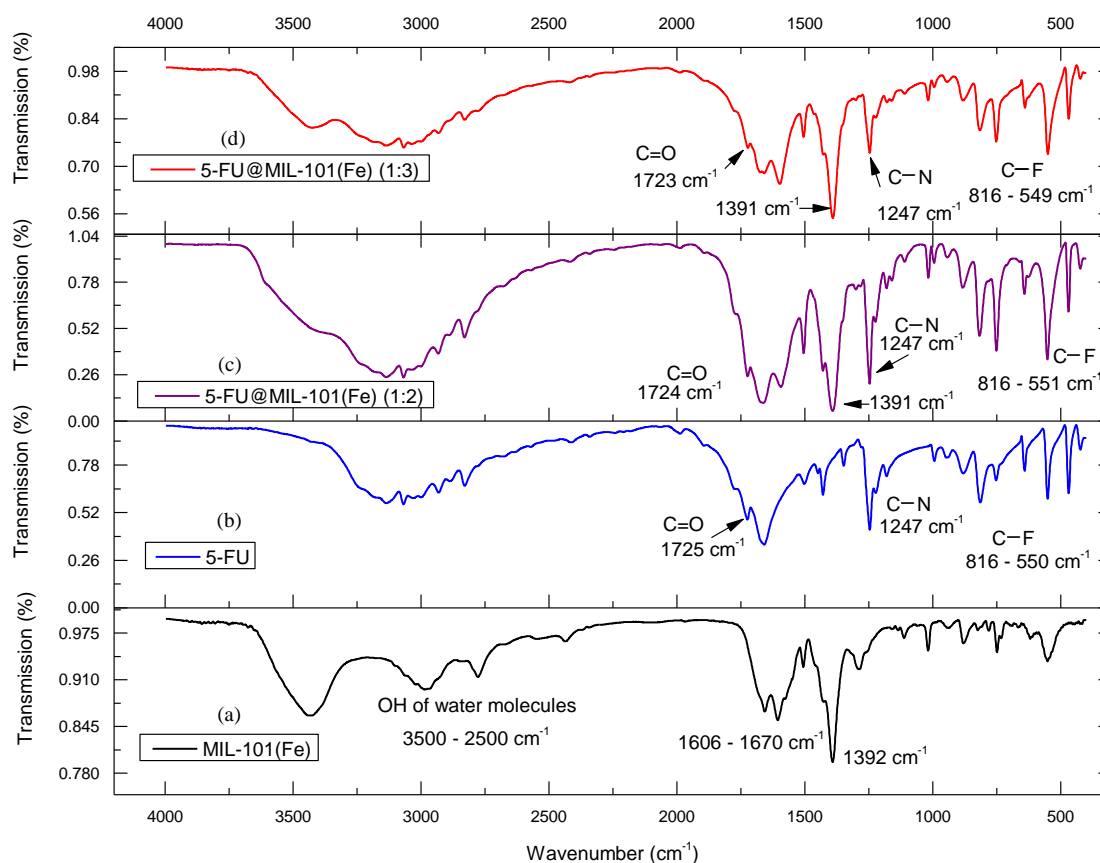
Figure 4.10. 5-FU (a), MIL-101(Fe) (b), 5-FU@MIL-101(Fe) (1:2 (MOF:drug) ratio, MIL-101(Fe):drug) (c), and 5-FU@MIL-101(Fe) (1:3 ratio) (d).

4.4.2 5-FU absorption kinetics in the metal-organic framework MIL-101(Fe)

The loading experiment of 5-FU was followed by measuring the UV-vis absorption spectra of free 5-FU in the supernatant methanol solution at 264 nm.

The evacuated MIL-101(Fe) was soaked in a solution of 5-FU in methanol (10^{-3} mg·mL^{-1}) in two different weight ratios for MOF:drug, namely 1:2 (Figure 4.11) and 1:3 (Figure 4.12), and stirred with exclusion of light for 48 hours.

The amount of encapsulated 5-FU was determined by measuring the amount of free 5-FU in the solution after 24 and 48 h by UV-vis spectroscopy.

For both samples, 1:2 (MOF:drug) and 1:3 (MOF:drug), the data obtained are inconclusive, showing the demand to repeat the experiments. After 48 h, a higher absorption in comparison with the pure 5-FU solution is observed. It is expected that once the MIL-101(Fe) is introduced in the drug solution the small molecules will slowly diffuse into the MIL-101(Fe) pores; As the opposite was observed, it can be assumed other MOF-drug interactions, governed by the strong interactions of hydrogen bonding between the drug and the ligand. Since more drug is present in the 1:2 (MOF:drug) ratio, the strong interaction is reflected as a higher absorption after 48 h.[37–39]

97

Therefore, an investigation through NMR spectroscopy was conducted, which will be discussed in section 4.4.4 of this chapter.

Figure 4.11. UV-vis spectra of free 5-FU in methanol (black) and after addition of MIL-101(Fe) weight ratio MOF:drug = 1:2, after 24 h (red) and 48 h (blue)).

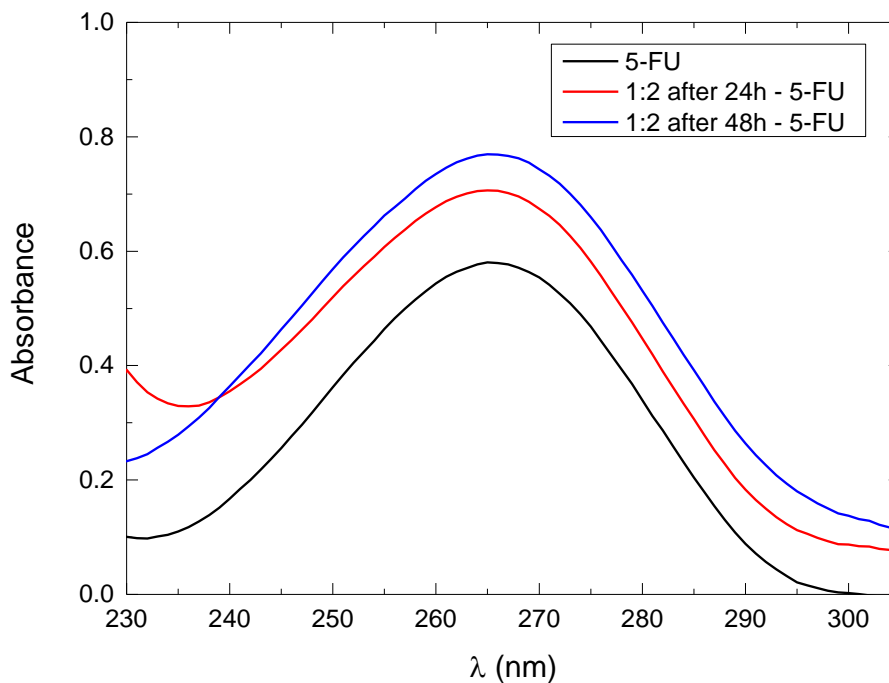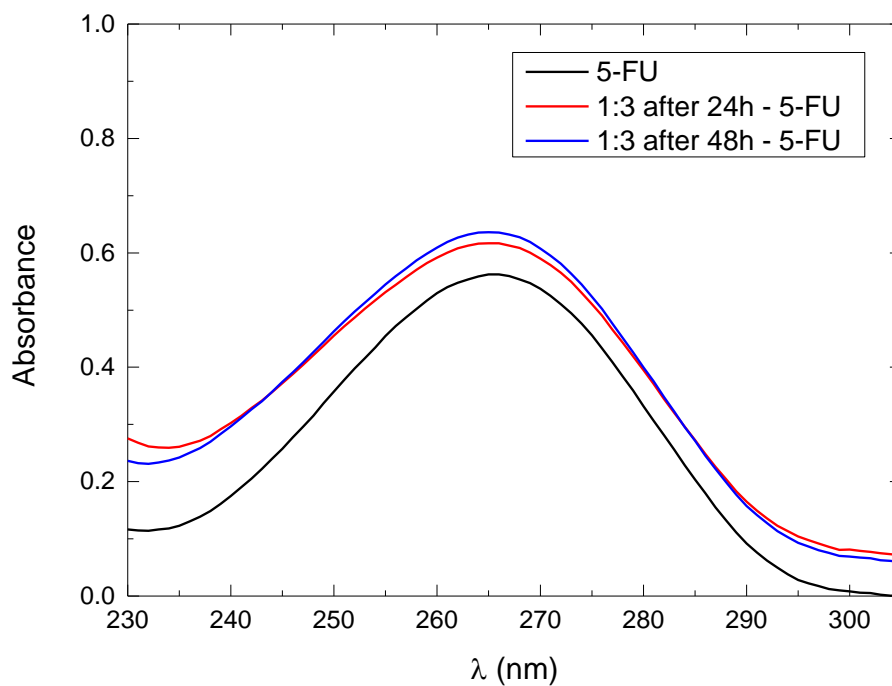Figure 4.12. UV-vis spectra of free 5-FU in methanol (black) and after addition of MIL-101(Fe) (weight ratio MOF:drug = 1:3, after 24 h (red) and 48 h (blue)).

4.4.3 Capecitabine absorption kinetics in the metal-organic framework MIL-101 (Fe)

The loading experiment of capecitabine was carried out by measuring the UV-vis absorption spectra of free capecitabine in methanol at 305 nm. The MIL-101(Fe) was kept under vacuum and then soaked in a solution of capecitabine in methanol in two different weight ratios, 1:2 (MOF:drug) with 1.5 mg of MIL-101(Fe) and 3 mg of capecitabine in 100 mL MeOH (Figure 4.13) and 1:3 (MOF:drug) with 1 mg of MIL-101(Fe) and 3 mg of capecitabine (Figure 4.14) in 100 mL of MeOH, and stirred with exclusion of light. The amount of encapsulated capecitabine was determined by measuring the amount of free capecitabine in the solution after 24 and 48 h by UV-vis spectroscopy.

The 1:2 (MOF:drug) samples after 24 h showed an encapsulation efficiency of 53 wt% and a loading capacity of 83 wt%; calculated according to (Equation 3) and (Equation 4) in methodology. After 48 h, the encapsulation efficiency and loading capacity did not increase significantly, reaching values of 54 wt% and 83.5 wt%, respectively (Figure 4.13). The encapsulation efficiency is the percentage of drug that is successfully entrapped into the framework, obtained by determining the amount of free capecitabine still present in the supernatant solution after 24 h and 48 h by UV-vis spectroscopy.

Loading capacity (LC%) can be calculated by determining the amount of total entrapped drug divided by the total weight of the metal-organic framework.[40]
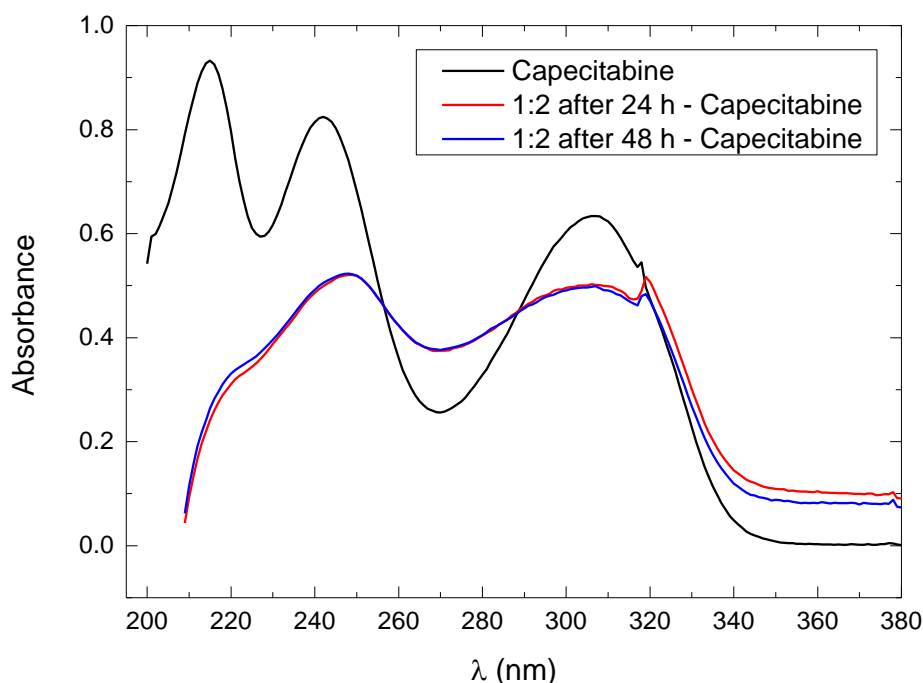

Figure 4.13. UV-vis spectra of free capecitabine in methanol (black) and after addition of MIL-101(Fe) (weight ratio MOF:drug = 1:2, after 24 h (red) and 48 h (blue)).

The same experiment was conducted with capecitabine in a weight ratio 1:3 (MOF:drug) (Figure 4.14). An encapsulation efficiency of 31 wt% and a loading capacity of 63 wt% were observed after 24 h. After 48 h, the values for encapsulation efficiency and loading capacity were significantly increased to 42 wt% and 77 wt%. Due to the considerably high surface area of MIL-101(Fe) that allows high drug loadings, the percentages reported here for the capecitabine encapsulation are higher in comparison with other drug@MOF systems described in the literature. [35,41–43] Moreover, the reduction of the amount of MIL-101(Fe) also means a reduction in the amount of the organic part represented by the ligand, apparently facilitating faster transport in the MOF and release of the drug to the neighboring aqueous medium resulting in lowering the drug content and entrapment efficiency.
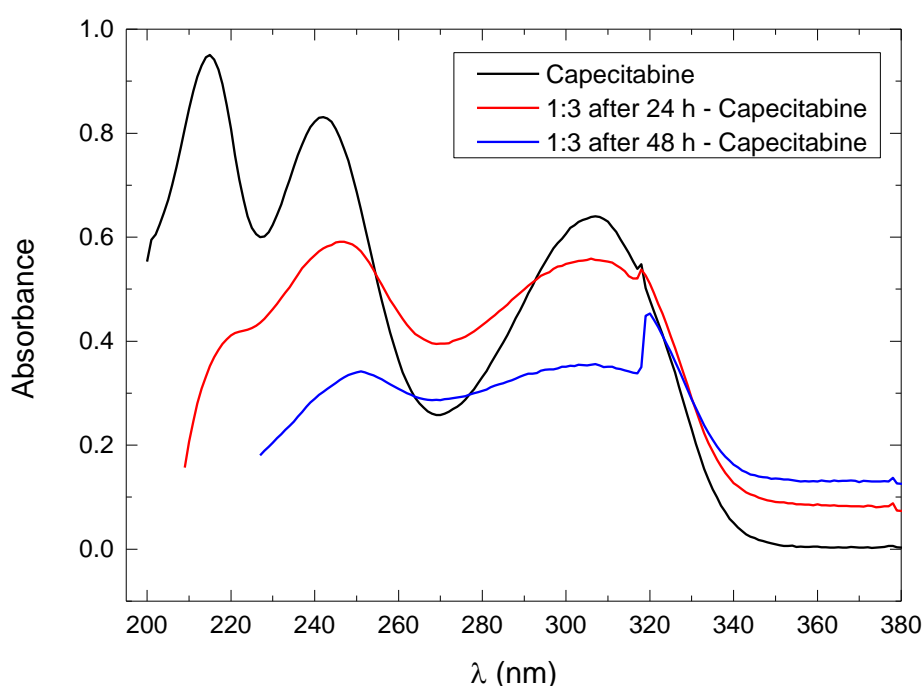

Figure 4.14. UV-vis spectra of free capecitabine in methanol (black) and after addition of MIL-101(Fe) (weight ratio MOF:drug = 1:3, after 24 h (red) and 48 h (blue)).

4.4.4 NMR Studies

One of the most efficient methods for the analysis of chemical transformation mechanisms in solution is through nuclear magnetic resonance (NMR) spectroscopy.[44] The high accuracy towards quantification of molecular mobility, diffusion, and exchange kinetics makes NMR a technique of choice to study pharmaceutical composites. Here, the aim was to define the molecular dynamics of the drug 5-FU within the MIL-101(Fe) structure at different time points.[44,45]

First, the ^{1}H NMR spectra of 5-FU (Figure 4.15 (b)) and MIL-101(Fe) (Figure 4.15 (a)) were recorded seperately in methanol-d_4, where the same sample weight was used as for the following encapsulation experiments.

In a second step, the mixtures for the encapsulation experiments (weight ratio of 1:2 (Figure 4.15) and 1:3 (MOF:drug) (Figure 4.17) were prepared and the [1]H

NMR spectra recorded in methanol-d_4 at 0 h, 24 h, 48 h, 120 h, 168 h after sample preparation.

The signal observed for 5-FU at 7.51 ppm (Figure 4.15) corresponds to the proton of the C−H group in the uracil ring and is split into a doublet due to the coupling with fluorine ($^3J_{HF}$ = 5.3 Hz). Both NH protons of 5-FU are chemically exchanging with the solvent and are not visible. After mixing both compounds (weight ratio 1:2 (MOF:drug)), there is no considerable difference compared with free 5-FU. With progressing time, it is possible to observe a sharpening of ^{1}H NMR signals. Generally, this means a slow exchange of protons on the NMR time scale (Figure 4.16), indicating slow exchange of protons bound to heteroatoms such as NH.[46] This might be interpreted as an indication of the interaction between the host and guest molecules. An analogous behavior was observed for the 1:3 (MOF:drug) samples (Figure 4.17).[47] Significant differences in the chemical shift of protons related to 5-FU (Figure 4.17 (b), Figure 4.18 (b)) were observed upon the encapsulation of 5-FU in the MIL-101(Fe) structure (5-FU@MIL-101 (Fe); Figure 4.17 (d,e,f,g), Figure 4.18 (d,e,f,g)). ^{1}H-NMR signals were shifted downfield of the H* signal of 5-FU, while the remaining protons retain their original position.

Figure 4.15. Section of the ^{1}H NMR spectra of (a) MIL-101(Fe), (b) 5-FU, and 1:2 (MOF:drug) samples (c) at 0 h, (d) after 24 h, (e) after 48 h, (f) after 120 h, and (g) after 168 h.
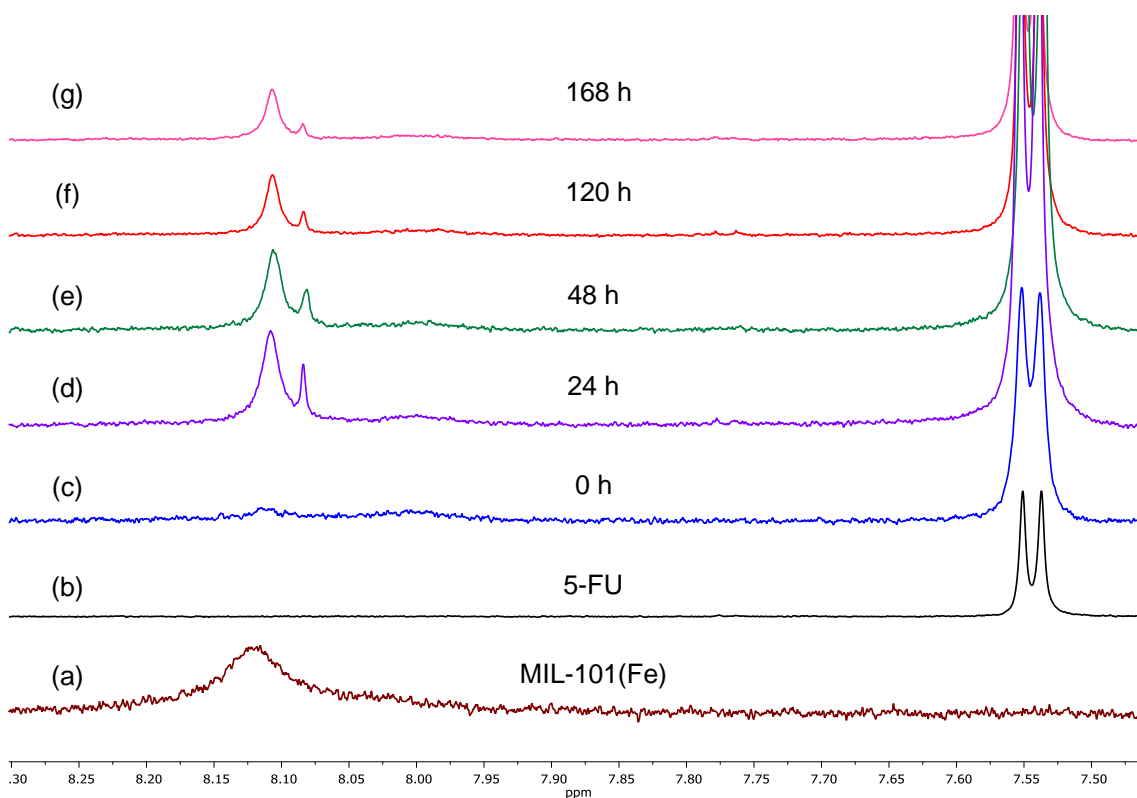
Figure 4.16. Enlarged region of the ^{1}H NMR spectra of (a) MIL-101(Fe), (b) 5-FU, and 1:2 (MOF:drug) samples (c) at 0 h, (d) after 24 h, (e) after 48 h, (f) after 120 h, and (g) after 168 h.

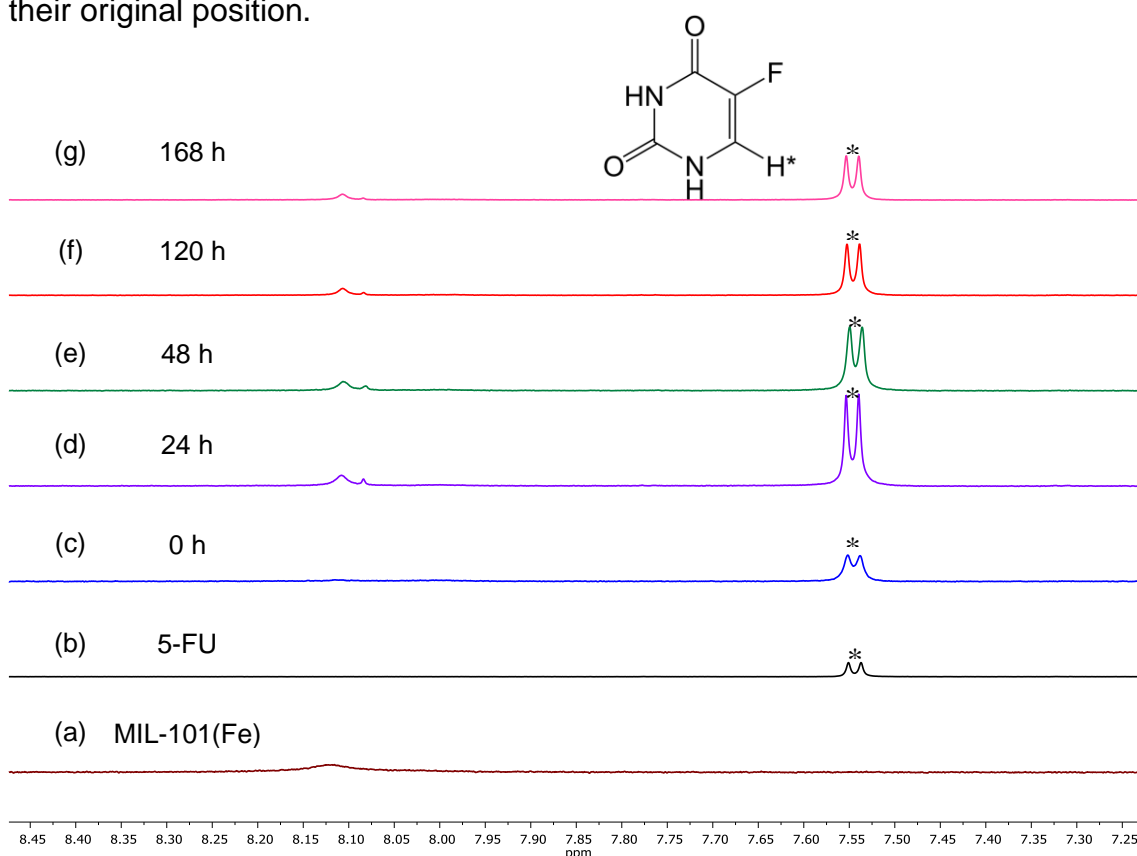Figure 4.17. Section of the ^{1}H NMR spectra of (a) MIL-101(Fe), (b) 5-FU, and 1:3 (MOF:drug) samples of (c) at 0 h, (d) after 24 h, (e) after 48 h, (f) after 120 h, and (g) after 168 h.

Figure 4.18. Enlarged region of ^{1}H NMR spectra of (a) MIL-101(Fe), (b) 5-FU, and 1:3 (MOF:drug) samples of (c) at 0 h, (d) after 24 h, (e) after 48 h, (f) after 120 h, and (g) after 168 h.
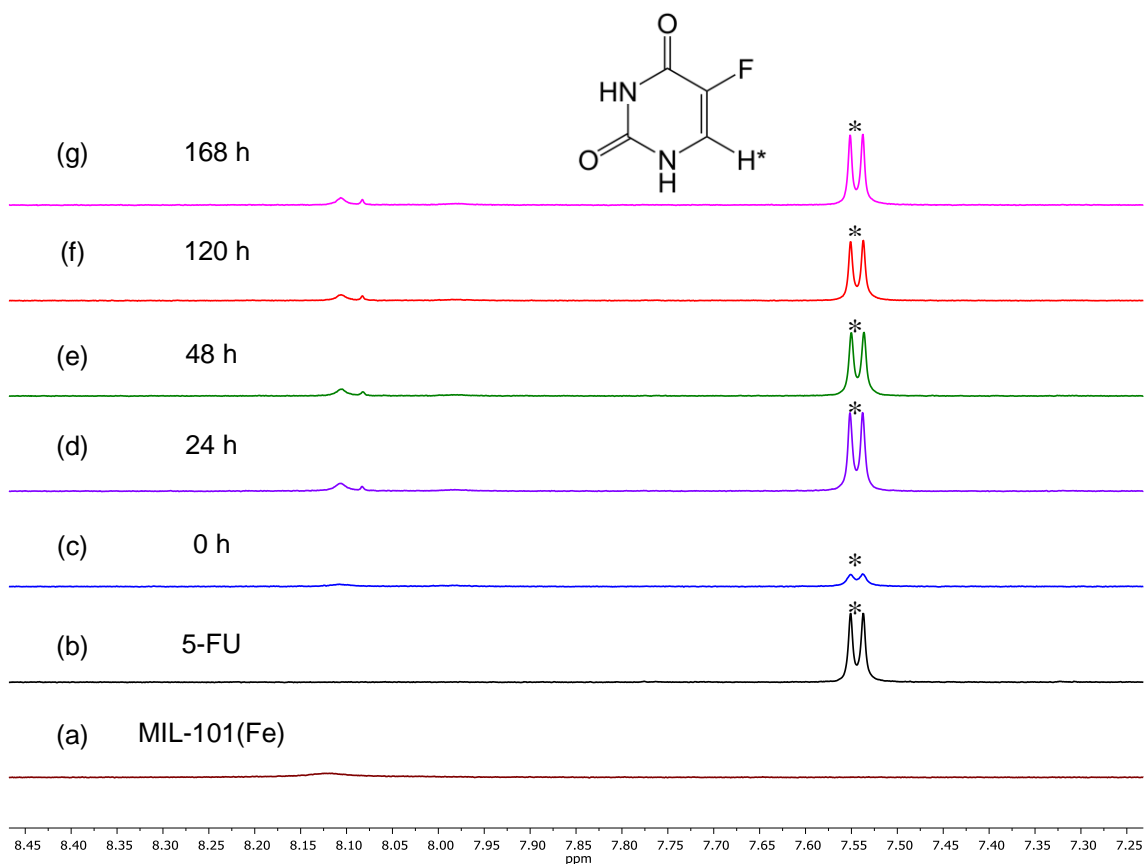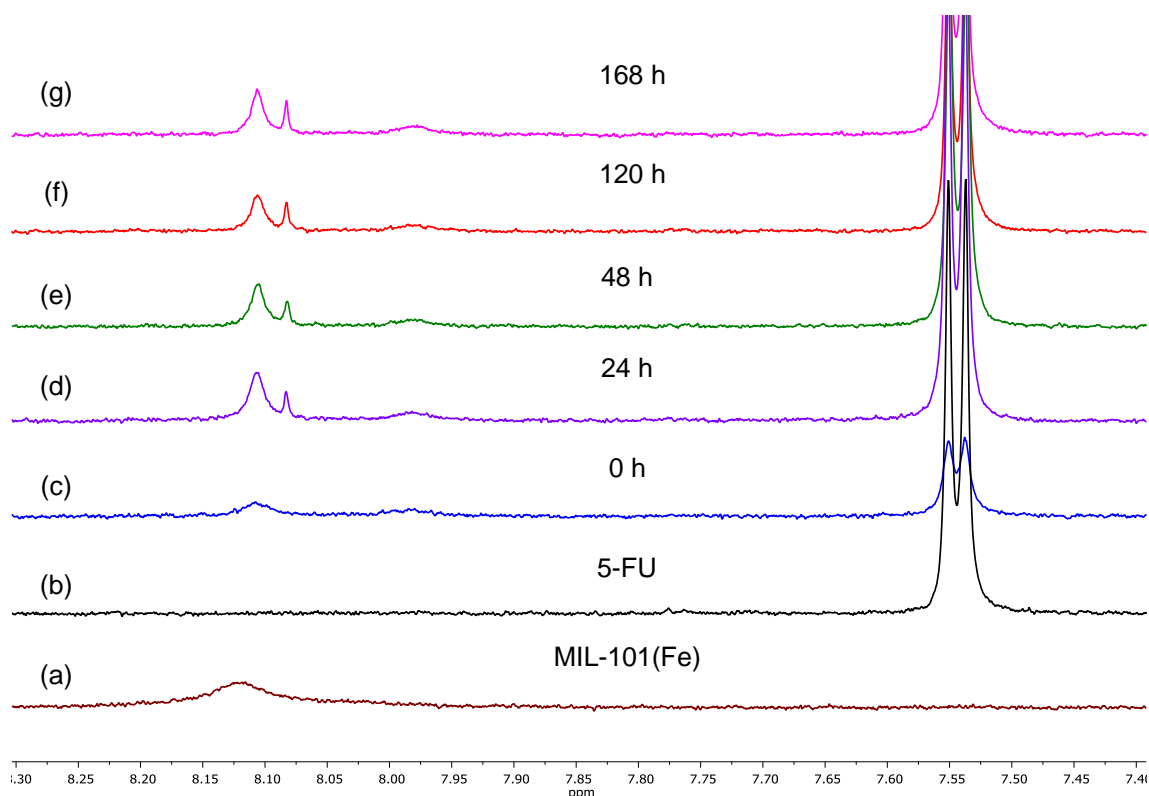
4.4.5 Release of 5-FU from 5-FU@MIL-101(Fe)

5-FU (5 mg) was encapsulated into previously evacuated metal-organic framework MIL-101(Fe) in two different weight ratios 1:2 (MOF:drug) and 1:3 (MOF:drug), in a methanol solution with stirring and exclusion of light for 48 h at room temperature in air.

The solid was isolated by filtration and dried under high vacuum for 48 h. The obtained powder of 5-FU@MIL-101(Fe) was then placed in a dialysis membrane and combined with different solutions 10 mL (PBS) and 10 mL (PBS/DMSO (2%v/v)) for the drug release experiments. The mixtures were stirred in the dark at 37 °C.

During the release process, aliquots of 2 mL were taken from the solution at different time points (15 min, 30 min, 45 min, 1 h, 2 h, 3 h, 4 h, 5 h, 6 h, 12 h, 24 h, 48 h, 72 h, 168 h). After each sampling point, the same amount of a fresh solution of (PBS) or (PBS/DMSO (2%v/v)) was added to retain the total volume. The experiments were performed in triplicate.

The system with a 5-FU@MIL-101(Fe) (1:2, (MOF:drug) weight ratio (Figure 4.19) exhibited a fast release behavior in PBS. In the first fifteen minutes, 16% of the drug (5-FU) is released, while after one hour, already 45% of the total 5-FU has been released. After 24 h, the MOF has released only up to 60% of 5-FU, after which a plateau is reached and only small amounts are released. Since almost half the amount of the loaded drug is released only in the first hour, this can be regarded as a burst effect.[48]

Figure 4.19. Cumulative release of 5-fluorouracil from 5-FU@MIL-101(Fe) (1:2, MOF:drug) weight ratio in PBS.

The release of 5-FU from 5-FU@MIL-101(Fe) (1:2, MOF:drug) weight ratio (Figure 4.20) in (PBS/DMSO(2%v/v)) was also fast. In the first fifteen minutes, 15% of the 5-FU was released, reaching a release of 43% in the first hour, followed by a release up to 74 % of 5-FU in 24 h and finally a plateau at about 80% is reached. By using 2 %(v/v) DMSO the amounts of drug being released could be increased by 20%. Those values are in accordance with similar 5-FU@MOF systems. Here, the fast release in the first hour indicates a burst effect.[49]

Figure 4.20. Cumulative kinetic release of 5-fluorouracil from 5-FU@MIL-101(Fe) (1:2, MOF:drug) weight ratio in PBS/DMSO (2%).

The 5-FU@MIL-101(Fe) (1:3, MOF:drug) weight ratio (Figure 4.21) system also presented a release behavior of releasing finite amounts of 5-FU at distinct time intervals in PBS. For 5-FU@MIL-101(Fe) (1:3, MOF:drug) weight ratio, 13% of 5-FU is released in the first fifteen minutes; this amount is slightly lower in comparison with the release observed for 5-FU@MIL-101(Fe) (1:2, MOF:drug) weight ratio in PBS.

In the first hour, 34 % of 5-FU is released, which is better (as it is slower) in comparison with 5-FU@MIL-101(Fe) (1:2, MOF:drug) weight ratio, but after 24 h, a total of 73 % of 5-FU has been already released. A possible explanation of a slower release for the 5-FU@MIL-101(Fe) (1:3, MOF:drug) weight ratio is a lower amount of encapsulated drug, as suggested by the FTIR results. For this case the particles of the drug are possibly located on the outer surface of the MIL-101(Fe) and not encapsulated in the pores of the MOF structure, therefore explaining a higher amount of release after 24 h.
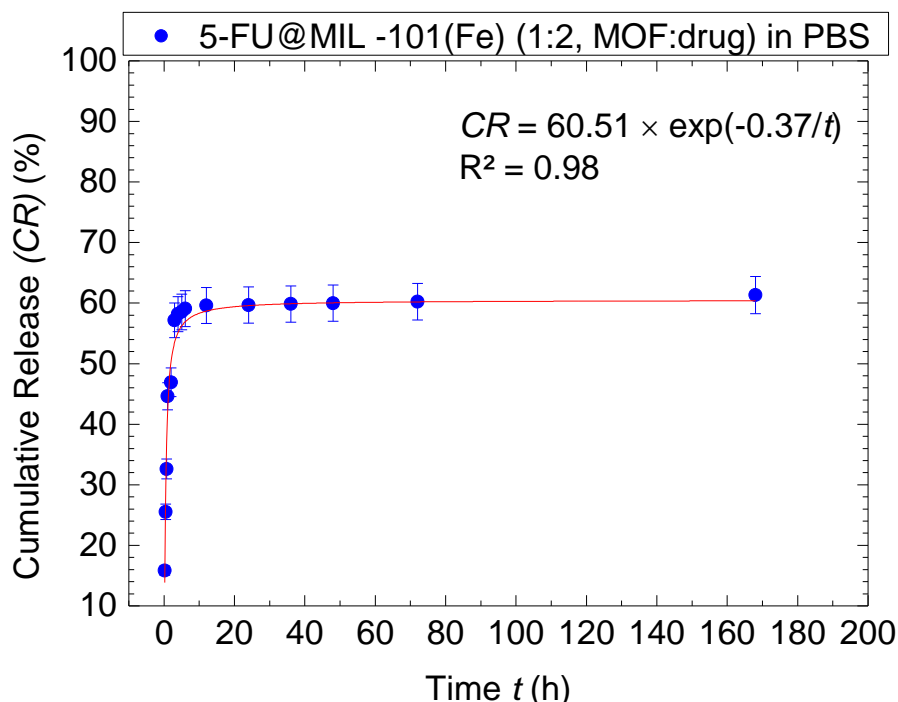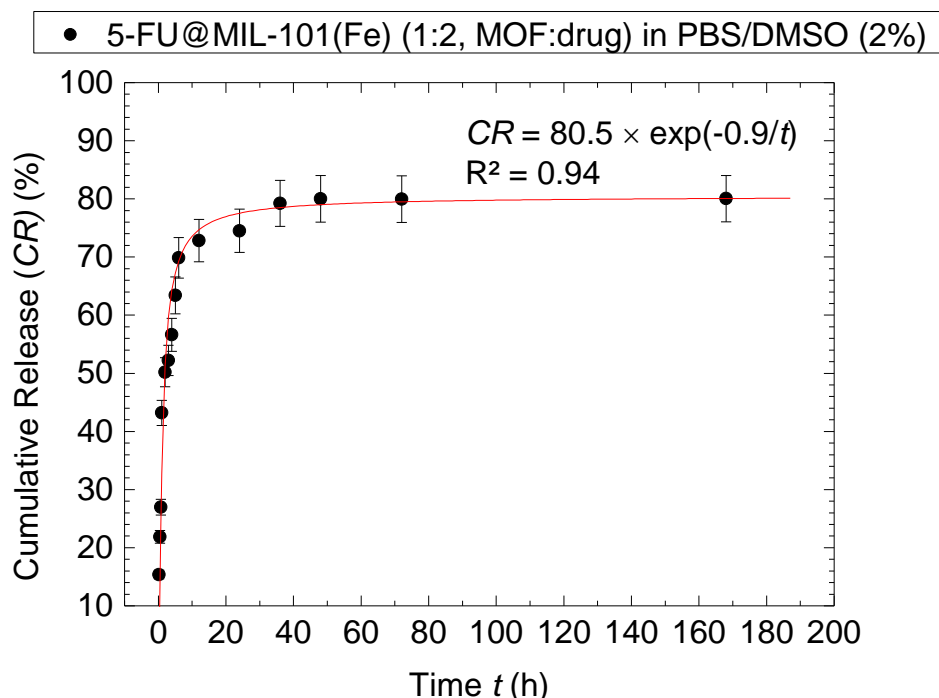
Figure 4.21 Cumulative kinetic release of 5-fluorouracil from 5-FU@MIL-101(Fe) (1:3, MOF:drug) weight ratio in PBS.

The 5-FU@MIL-101(Fe) (1:3, MOF:drug) weight ratio (Figure 4.22) system in (PBS/DMSO(2%)) , showed an analogous release behavior for 5-FU, of which 16% is released in the first 15 minutes and around 41% in the first hour. Those values are similar to the previously analyzed samples. A distinct behavior is observed after 24 h, where around 90% of 5-FU is released into (PBS/DMSO(2%)). This behavior may be attributed to the presence of DMSO, increasing the 5-FU solubility and consequently its release. This behavior where a high amount of 5-FU is released from the MIL-101(Fe) in the first 24 h is an indicator for a condition where the drug is not non-covalent interaction with the MOF in the pores, as a consequence of a high concentration of 5-FU. With the reduction of internal 5-FU concentration, the 5-FU release rate decreased but remained at a moderate level reaching an almost quantitative release within the following days. Apparently, after the initial burst release, the host−guest interactions between the MOF and 5-FU dominate the release performance.[38,39]
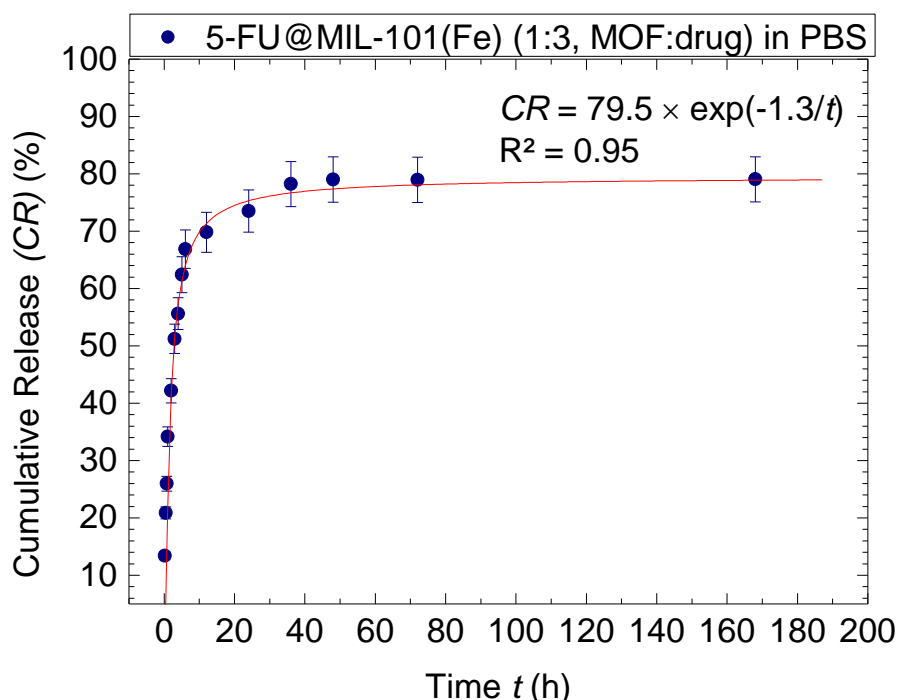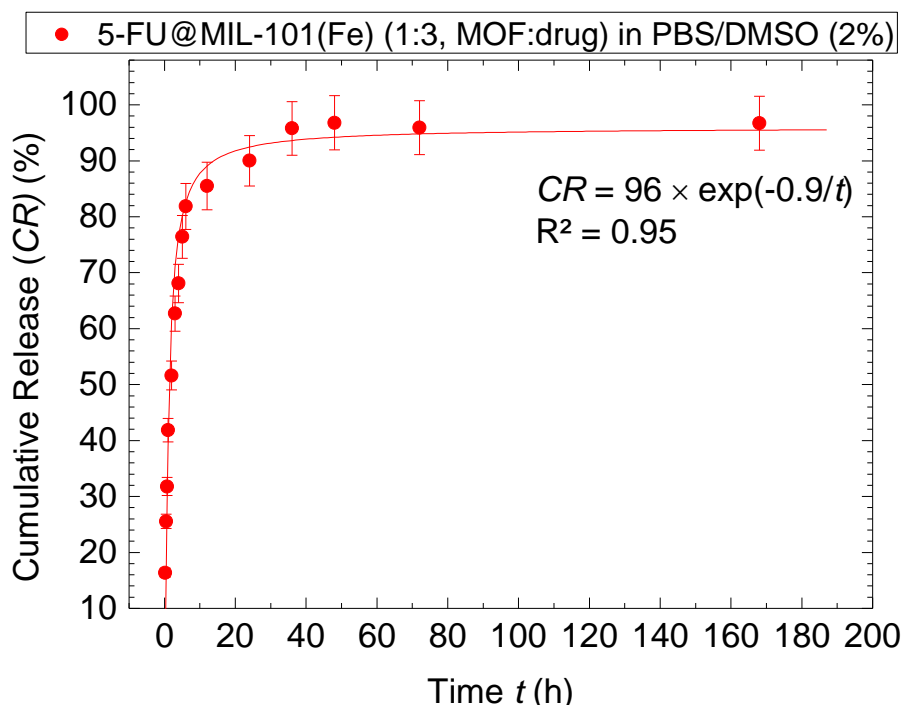
Figure 4.22. Cumulative kinetic release of 5-fluorouracil from 5-FU@MIL-101(Fe) (1:3, MOF:drug) weight ratio in PBS/DMSO (2%).

4.4.6 Release of Capecitabine from Capecitabine@MIL-101(Fe)

An analogous procedure was performed for the drug capecitabine (3×10^{-3} mg) for encapsulation in previously evacuated metal-organic framework MIL-101(Fe) employing two different weight ratios, namely 1:2 (MOF:drug) and 1:3 (MOF:drug). The samples were stirred in the dark for 48 h.

The particles of capecitabine@MIL-101(Fe) were isolated, dried, and then placed in a dialysis membrane and submerged in 10 mL solutions of PBS and (PBS/DMSO (2%v/v)) for the drug release experiments. The mixtures were stirred in the dark at 37 °C.

Aliquots of 2 mL were taken from the solutions at different times (15 min, 30 min, 45 min, 60 min, 120 min, 180 min, 240 min, 300 min, 360 min, 12 h, 24 h, 48 h, 72 h, 96 h). After each sample collection, the same amount of a fresh solution of PBS and (PBS/DMSO (2%)) was added to retain the total volume. The experiment was performed in triplicate.

The capecitabine@MIL-101(Fe) (1:2, MOF:drug) weight ratio (Figure 4.23) in (PBS) showed a release of finite amounts of capecitabine at distinct time intervals. In the first fifteen minutes, 15% of capecitabine was released, followed by 32% in the first hour. As a prodrug of 5-FU, this value is around ten percent lower compared with the release of 5-FU from 5-FU@MIL-101(Fe) (1:2, MOF:drug) weight ratio in (PBS) during the same time interval. The capecitabine was continuously released up to 59% in the first 24 h, followed by release of small amounts.

Figure 4.23. Cumulative kinetic release of capecitabine from capecitabine@MIL-101(Fe) (1:2, MOF:drug) weight ratio in PBS.

For capecitabine@MIL-101(Fe) (1:2, MOF:drug) weight ratio (Figure 4.24), immersed in (PBS/DMSO (2%)) , 21% of the drug were released in the first fifteen minutes, followed by 48% in the first hour; the system kept a sustainable release of capecitabine up to 71% in 24 h.

Figure 4.24. Cumulative kinetic release of capecitabine from capecitabine@MIL-101(Fe) (1:2, MOF:drug) weight ratio in PBS/DMSO (2%).

The capecitabine@MIL-101(Fe) (1:3, MOF:drug) weight ratio immersed in (PBS) (Figure 4.25) presented a lower capecitabine release in the first fifteen minutes of 6%, followed by a release of 27% in the first hour, reaching a constant release up to 77% in the first 24 h. Compared with capecitabine@MIL-101(Fe) (1:2, MOF:drug) weight ratio, the (1:3, MOF:drug) weight ratio showed a slower increase in drug release in the first 24 h, in accordance with the lower loading capacity (ca. 42%) in comparison with the (1:2, MOF:drug) weight ratio (ca. 54%). By definition, the loading capacity takes into consideration how many sites (pores) of the MOF have been presumably occupied by the drug.

Figure 4.25. Cumulative kinetic release of capecitabine from capecitabine@MIL-101(Fe) (1:3, MOF:drug) weight ratio in PBS.

Among all analyzed samples, capecitabine@MIL-101(Fe) (1:3, MOF:drug) weight ratio (Figure 4.26) immersed in (PBS/DMSO (2%)) , presented a very good release in terms of slow-release. In the first fifteen minutes, only 1.3% of capecitabine was released into the solution, which slowly increased in the first hour up to 25%, reaching 55% in 24 h.

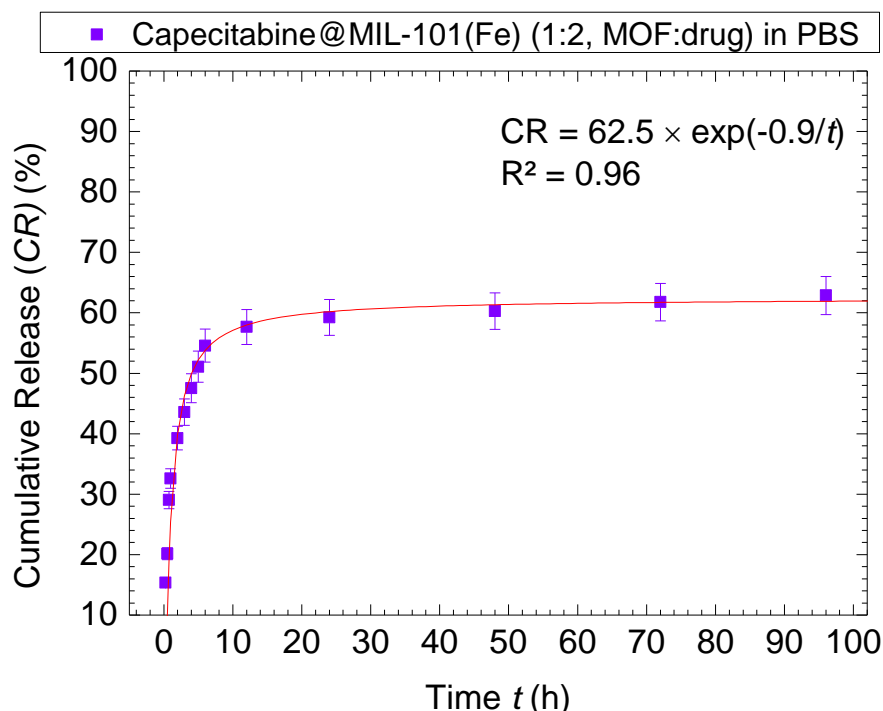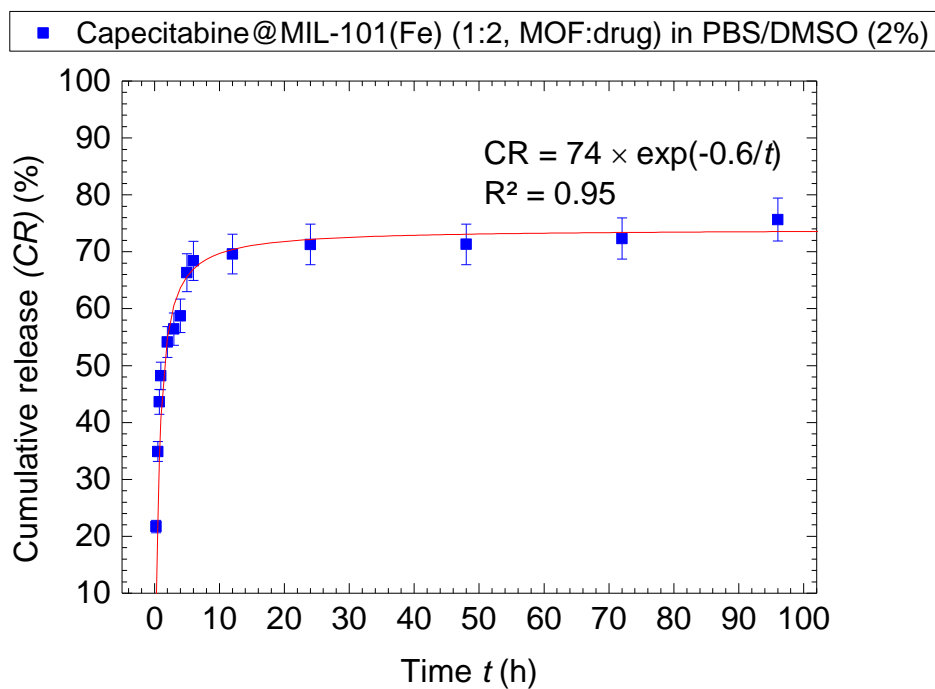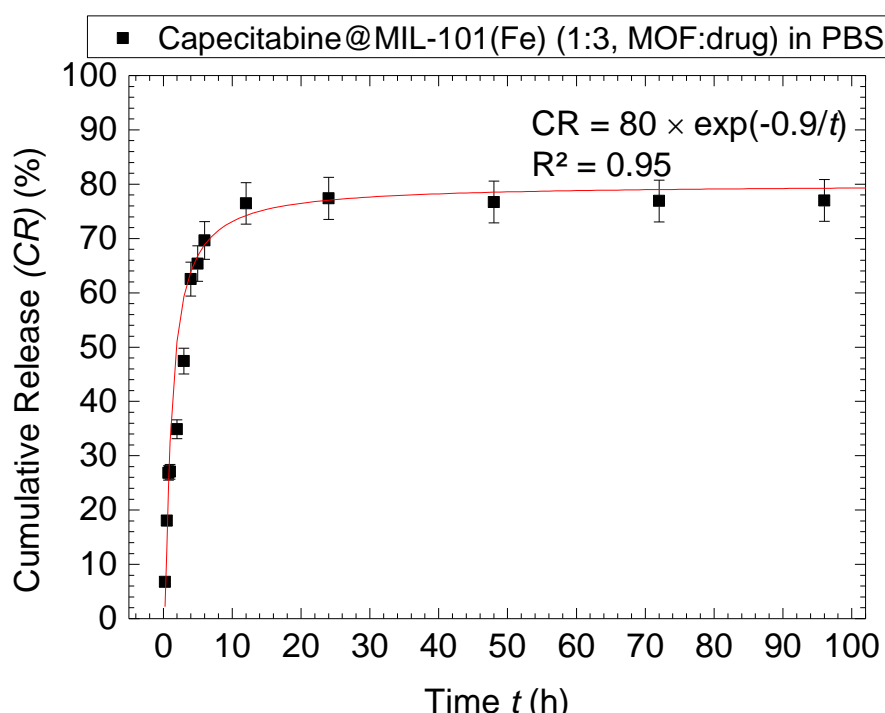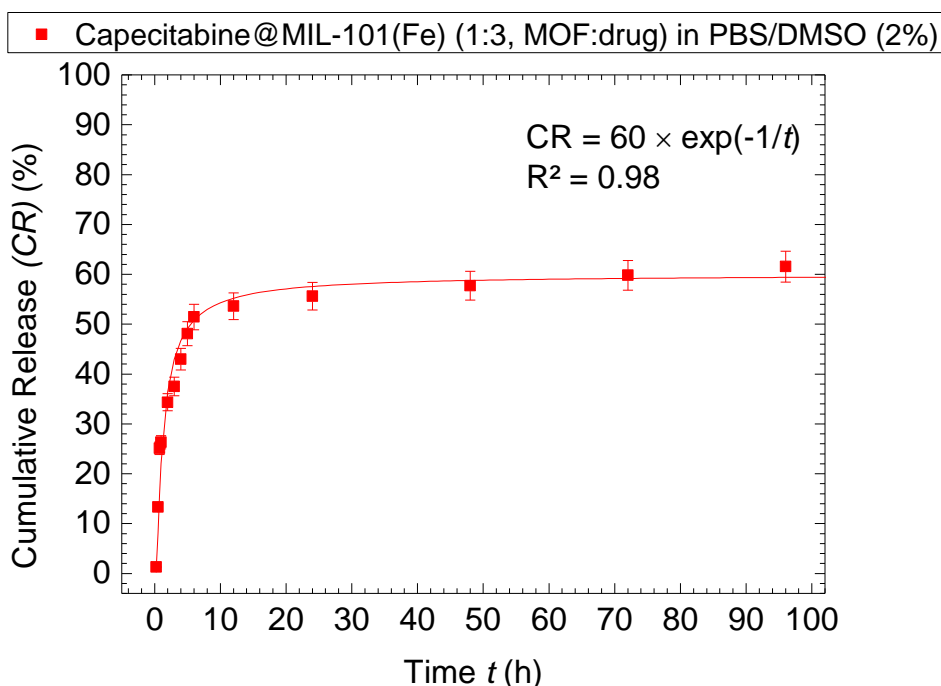Figure 4.26. Cumulative kinetic release of capecitabine from capecitabine@MIL-101(Fe) (1:3, MOF:drug) weight ratio in PBS/DMSO (2%).

4.4.7 Release of 5-FU from PA-12/5-FU@MIL-101(Fe) (1:2, MOF:drug) tablets.

3D printing is a technique based on the sequential deposition of layers of materials, where a computer-aided design (CAD) software is used; therefore, structures of various sizes and shapes can be produced. This method has found application in many sectors, from industrial engineering to personalized biomaterials and devices in medicine. [50–52] In the pharmaceutical field, 3D printing can produce small batches of medicinal products, with tailored dosages, shapes, sizes, and release characteristics.[50,53] For these reasons, the 3D printing technique is applied here to improve the drug release properties of the investigated drug@MIL-101(Fe) system aided by polymeric support.

Tablets based on polyamide-12 (PA-12) in dimensions of 16.63 mm diameter were prepared by SLS see Chapter 2. Their content of 5-FU@MIL-101(Fe) (1:2, MOF:drug) was determined by calculating the average mass of 5-FU@MOF (1:2, MOF:drug) in the produced tablet. Initially, 7% (w/w) of 5-FU@MIL-101(Fe) (1:2, MOF:drug) was used; however, it turned out that this mixture exhibited brittle samples. Consequently, the concentration of 5-FU@MIL-101(Fe) (1:2, MOF:drug) was changed to 5% (w/w) giving a homogeneous mixture with good mechanical properties, such as good layer adhesion (xx). The 5-fluorouracil release into a solution of (PBS) and (PBS/DMSO (2%)) was studied at 37 °C in a sealed vessel in the dark.

According to (Figure 4.27), in the first 60 min, around 13% of the encapsulated 5-FU was released into the (PBS) medium. In 24 h, 42% of 5-FU was released, followed by a slow release reaching 55% of 5-FU after 29 days.

By incorporating 5-FU@MIL-101(Fe) (1:2, MOF:drug) into the PA-12 matrix, the release of the drug was substantially slower compared with 5-FU@MIL-101(Fe) alone.

The tablets of PA-12/5-FU@MIL-101(Fe) (1:2, MOF:drug) system showed a 5-FU release of 7%, 13%, and 42%, in the first 15 min, 60 min, and 24 h; these values are 9%, 32%, and 18% lower in relation to the release of 5-FU from 5-FU@MIL-101(Fe) in (PBS), confirming that the 3D-printed tablets with a PA-12 matrix are able to provide an extended slow release.

The equation shown in the figure:

$$CR = 55.2 \times \exp(-0.25/t)$$
$$R^2 = 0.92$$

Figure 4.27. Cumulative release of 5-FU from a PA-12/5FU@MIL-101(Fe) (1:2, MOF:drug) sample in PBS (tablets of PA-12/5-FU@MIL-101(Fe) produced according to the parameters of the batch called Q008, see in 4.3).

As shown in (Figure 4.28), in the first 60 min, the system released around 20% of 5-FU into the (PBS/DMSO (2%)). The extended release was analyzed for up to 29 days. In 24 h, 57% of 5-FU was released, followed by a slow increase to 76% after 29 days.

By incorporating 5-FU@MIL-101(Fe) into the PA-12 matrix, it was possible to sustain an extended slow release of 5-FU into the (PBS/DMSO (2%)), in contrast to 5-FU@MIL-101(Fe), for which a rather fast release was observed.
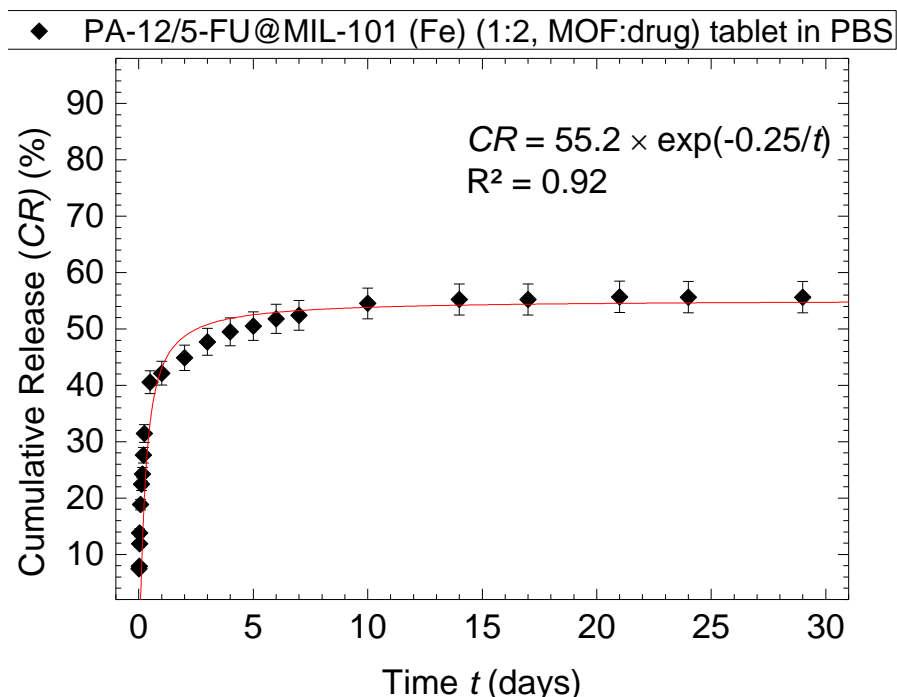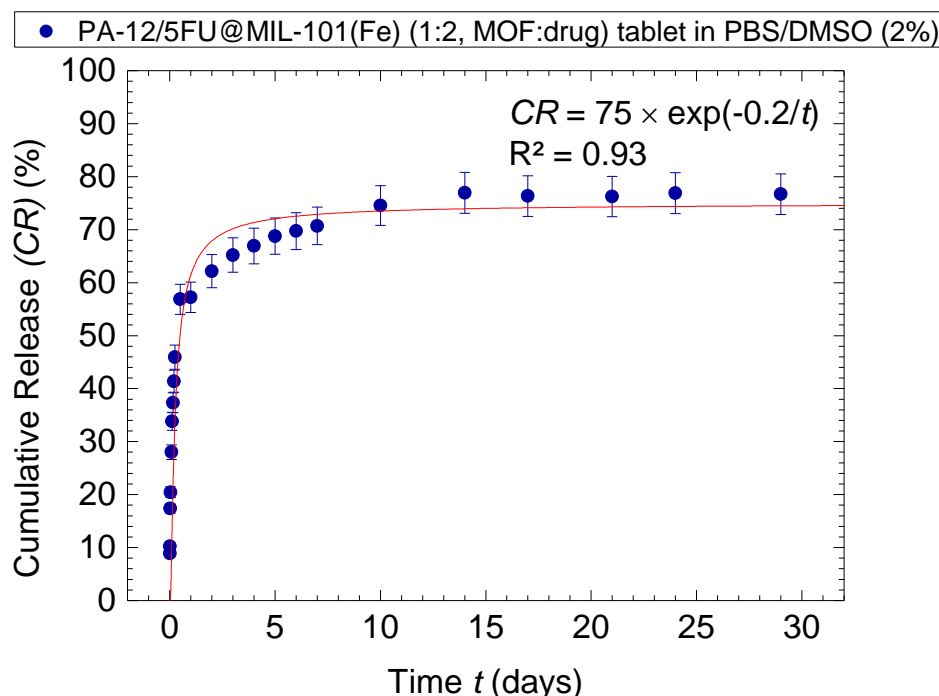
Figure 4.28. Cumulative release of a PA-12/5FU@MIL-101(Fe) (1:2, MOF:drug) sample in PBS/DMSO (2%) (tablets of PA-12/5-FU@MIL-101 (Fe) produced according to the parameters of the batch called Q009, see in 4.3).

4.5 Conclusion

Samples were prepared by loading the drugs 5-FU and capecitabine into the iron-based MOF MIL-101(Fe) and their release was investigated.
The results showed that both drugs presented a sustainable release over 4 days with a fast release (referred to as burst effect) in the first 24 h in all buffered media studied. This fast release of the drug in the first hours is also well described in the literature, where the release rate is determined by the host-guest interaction. This is why the Selective Laser Sintering (SLS) was introduced as a technique that could extend the period of release by diminishing the high drug concentration especially in the first hours. The tablets produced displayed a sustained extended release of 5-FU for an even longer period of 30 days, confirming that drug release modulation is possible by incorporation of a drug into a printed polymer matrix, therefore avoiding the burst effect characteristic of the first 24 h.

4.6 Summary

In this chapter, the iron-based MOF MIL-101(Fe) was applied successfully to encapsulate and release the drugs 5-FU and capecitabine. The release experiments were performed with 5-FU@MIL-101(Fe) for two different weight ratios, namely 1:2 and 1:3 (MOF:drug), in two different media (PBS and PBS/DMSO (2%)) over 180 h. Even though the samples presented an extended drug release over 180 h, the high amount of drug released into both media, (PBS and PBS/DMSO (2%)), indicated a burst effect. Therefore, 5-FU@MIL-101(Fe) was incorporated into a PA-12 matrix by SLS. In order to ensure the stability of

the drug 5-FU under the laser power, the drug was first encapsulated into the MOF and then PA-12 was employed as polymer matrix for the drug@MOF system. Through the SLS technique, also used in the third chapter for curcumin, it was possible to decrease the amount of 5-FU drug released into the system by extending its period of release up to 30 days, therefore being an effective way to overcome the burst effect. The same ratios and media, (PBS and PBS/DMSO (2%)) were applied for capecitabine, where an encapsulation efficiency of 53 wt% (1:2, MOF:drug) and 31 wt% (1:3, MOF:drug) was observed after 48 h in MIL-101(Fe).

In the next step, the release behavior for 5-FU from 5-FU@MIL-101(Fe) was studied. For the 1:2 (MOF:drug) ratio, in the first 24 h, a drug release of 59 wt% occurred in (PBS), and an even higher release of 71 wt% in (PBS/DMSO (2%) . For capecitabine@MIL-101(Fe), the 1:3 (MOF:drug) ratio showed a drug release of 77 wt% in (PBS) in the first 24 h, and a release of 55 wt% was observed in (PBS/DMSO (2%)) .

By incorporating the drug@MOF systems into a PA-12 matrix employing the SLS technique, it was possible to extend the release for longer periods of time (up to one month) avoiding high release rates of the respective drugs into the surrounding media within a few hours. This indicates that the PA-12/5-FU@MIL-101(Fe) can be applied as a drug release vehicle investigated here being effective in slowing down the release of 5-FU.

4.7 Bibliography

[1]   Cheung-Ong K, Giaever G, Nislow C. DNA-damaging agents in cancer chemotherapy: Serendipity and chemical biology. Chem Biol. 2013;20(5):648–59.

[2]   O'Connor MJ. Targeting the DNA Damage Response in Cancer. Mol Cell [Internet]. 2015;60(4):547–60.

[3]   Luengo A, Gui DY, Vander Heiden MG. Targeting Metabolism for Cancer Therapy. Cell Chem Biol. 2017;24(9):1161–80.

[4]   Blondy S, David V, Verdier M, Mathonnet M, Perraud A, Christou N. 5-Fluorouracil resistance mechanisms in colorectal cancer: From classical pathways to promising processes. Cancer Sci. 2020;111(9):3142–54.

[5]   Rossi L, Bonmassar E, Faraoni I. Modification of miR gene expression pattern in human colon cancer cells following exposure to 5-fluorouracil in vitro. Pharmacol Res. 2007;56(3):248–53.

[6]   Yao Y, Chen S, Zhou X, Xie L, Chen A. 5-FU and ixabepilone modify the microRNA expression profiles in MDA-MB-453 triple-negative breast cancer cells. Oncol Lett. 2014;7(2):541–7.

[7]   Cao Z, Zhang Z, Huang Z, Wang R, Yang A, Liao L, et al. Antitumor and immunomodulatory effects of low-dose 5-FU on hepatoma 22 tumor-bearing mice. Oncol Lett. 2014;7(4):1260–4.

[8]   Cheng M, He B, Wan T, Zhu W, Han J, Zha B, et al. 5-Fluorouracil Nanoparticles Inhibit Hepatocellular Carcinoma via Activation of the p53 Pathway in the Orthotopic Transplant

Mouse Model. PLoS One. 2012;7(10):1–12.

[9]   Phase II study of leucovorin , 5-fluorouracil metastatic pancreatic cancer (FOLFUGEM 2). 2004;645–50.

[10]   Liu Y, Wang X, Wang Y, Zhang Y, Zheng K, Yan H, et al. Combination of SNX-2112 with 5-FU exhibits antagonistic effect in esophageal cancer cells. Int J Oncol. 2015;46(1):299–307.

[11]   Mayr M, Becker K, Schulte N, Belle S, Hofheinz R, Krause A, et al. Phase I study of imatinib, cisplatin and 5-fluoruracil or capecitabine in advanced esophageal and gastric adenocarcinoma. BMC Cancer. 2012;12:0–6.

[12]   Longley DB, Harkin DP, Johnston PG. 5-Fluorouracil: Mechanisms of action and clinical strategies. Nat Rev Cancer. 2003;3(5):330–8.

[13]   Wei Y, Yang P, Cao S, Zhao L. The combination of curcumin and 5-fluorouracil in cancer therapy. Arch Pharm Res. 2018;41(1):1–13.

[14]   Heidelberger C, Chaudhuri NK, Danneberg P, Mooren D, Griesbach L, Duschinsky R, et al. Fluorinated Pyrimidines, A New Class of Tumour-Inhibitory Compounds. Nature. 1957;179(4561):663–6.

[15]   Diasio RB, Harris BE. Clinical Pharmacology of 5-Fluorouracil. Clin Pharmacokinet. 1989;16(4):215–37.

[16]   Asadi-Moghaddam K, Antonio Chiocca E. Prodrug-Activation Gene Therapy. Gene Ther Cent Nerv Syst From Bench to Bedside. 2006 Jan 1;291–301.

[17]   Wigmore PM, Mustafa S, El-Beltagy M, Lyons L, Umka J, Bennett G. Effects of 5-FU. Adv Exp Med Biol. 2010;678:157–64.

[18]   Del Rio M, Molina F, Bascoul-Mollevi C, Copois V, Bibeau F, Chalbos P, et al. Gene expression signature in advanced colorectal cancer patients select drugs and response for the use of leucovorin, fluorouracil, and irinotecan. J Clin Oncol Off J Am Soc Clin Oncol. 2007 Mar;25(7):773–80.

[19]   Cho YH, Ro EJ, Yoon JS, Mizutani T, Kang DW, Park JC, et al. 5-FU promotes stemness of colorectal cancer via p53-mediated WNT/β-catenin pathway activation. Nat Commun. 2020;11(1).

[20]   Shimma N. Case Study: Capecitabine: A Prodrug of 5-Fluorouracil. Prodrugs. 2008;1173–83.

[21]   Zhang N, Yin Y, Xu SJ, Chen WS. 5-Fluorouracil: Mechanisms of resistance and reversal strategies. Molecules. 2008;13(8):1551–69.

[22]   He L, Zhu H, Zhou S, Wu T, Wu H, Yang H, et al. Wnt pathway is involved in 5-FU drug resistance of colorectal cancer cells. Exp Mol Med. 2018;50(8).

[23]   Vodenkova S, Buchler T, Cervena K, Veskrnova V, Vodicka P, Vymetalkova V. 5-fluorouracil and other fluoropyrimidines in colorectal cancer: Past, present and future. Pharmacol Ther. 2020 Feb;206:107447.

[24]   Chionh F, Lau D, Yeung Y, Price T, Tebbutt N. Oral versus intravenous fluoropyrimidines for colorectal cancer. Cochrane database Syst Rev. 2017 Jul;7(7):CD008398.

[25] Wolpin BM, Mayer RJ. Systemic treatment of colorectal cancer. Gastroenterology. 2008 May;134(5):1296–310.

[26] Zhu J, Zeng W, Ge L, Yang X, Wang Q, Wang H. Capecitabine versus 5-fluorouracil in neoadjuvant chemoradiotherapy of locally advanced rectal cancer: A meta-analysis. Med (United States). 2019;98(17).

[27] Venerito M. S-1 in Patients with Advanced Esophagogastric Adenocarcinoma: Results from the Safety Compliance Observatory on Oral fluoroPyrimidines (SCOOP) Study. Drugs R D [Internet]. 2019;19(2):141–8.

[28] Zhang L, Xing X, Meng F, Wang Y, Zhong D. Oral fluoropyrimidine versus intravenous 5-fluorouracil for the treatment of advanced gastric and colorectal cancer: Meta-analysis. J Gastroenterol Hepatol. 2018 Jan;33(1):209–25.

[29] Latchman J, Guastella A, Tofthagen C. 5-Fluorouracil toxicity and dihydropyrimidine dehydrogenase enzyme: implications for practice. Clin J Oncol Nurs. 2014 Oct;18(5):581–5.

[30] Goirand F, Lemaitre F, Launay M, Tron C, Chatelut E, Boyer JC, et al. How can we best monitor 5-FU administration to maximize benefit to risk ratio? Expert Opin Drug Metab Toxicol. 2018;14(12):1303–13.

[31] Tang J, Yang M, Yang M, Wang J, Dong W, Wang G. Heterogeneous Fe-MIL-101 catalysts for efficient one-pot four-component coupling synthesis of highly substituted pyrroles. New J Chem. 2015;39(6):4919–23.

[32] Li C, Hu Q, Li Y, Zhou H, Lv Z, Yang X, et al. Hierarchical hollow Fe2O3 @MIL-101(Fe)/C derived from metal-organic frameworks for superior sodium storage. Sci Rep. 2016;6(January):1–8.

[33] Sun CY, Qin C, Wang XL, Yang GS, Shao KZ, Lan YQ, et al. Zeolitic imidazolate framework-8 as efficient pH-sensitive drug delivery vehicle. Dalt Trans. 2012;41(23):6906–9.

[34] Javanbakht S, Hemmati A, Namazi H, Heydari A. Carboxymethylcellulose-coated 5-fluorouracil@MOF-5 nano-hybrid as a bio-nanocomposite carrier for the anticancer oral delivery. Int J Biol Macromol. 2020;155:876–82.

[35] Ibrahim M, Sabouni R, Husseini G. Anti-cancer Drug Delivery Using Metal Organic Frameworks (MOFs). Curr Med Chem. 2016;24(2):193–214.

[36] Wang Y, Guo W, Li X. Activation of persulfates by ferrocene-MIL-101(Fe) heterogeneous catalyst for degradation of bisphenol A. RSC Adv. 2018;8(64):36477–83.

[37] Sha JQ, Zhong XH, Wu LH, Liu GD, Sheng N. Nontoxic and renewable metal-organic framework based on α-cyclodextrin with efficient drug delivery. RSC Adv. 2016;6(86):82977–83.

[38] Hu Z, Qiao C, Xia Z, Li F, Han J, Wei Q, et al. A Luminescent Mg-Metal-Organic Framework for Sustained Release of 5-Fluorouracil: Appropriate Host-Guest Interaction and Satisfied Acid-Base Resistance. ACS Appl Mater Interfaces. 2020;12(13):14914–23.

[39] Miri B, Motakef-Kazemi N, Shojaosadati SA, Morsali A. Application of a nanoporous metal organic framework based on iron carboxylate as drug delivery system. Iran J Pharm Res. 2018;17(4):1164–71.

[40] Rojas S, Colinet I, Cunha D, Hidalgo T, Salles F, Serre C, et al. Toward Understanding Drug Incorporation and Delivery from Biocompatible Metal-Organic Frameworks in View of Cutaneous Administration. ACS Omega. 2018;3(3):2994–3003.

[41] Horcajada P, Serre C, Vallet-Regí M, Sebban M, Taulelle F, Férey G. Metal-organic frameworks as efficient materials for drug delivery. Angew Chemie - Int Ed. 2006;45(36):5974–8.

[42] Hu Q, Yu J, Liu M, Liu A, Dou Z, Yang Y. A low cytotoxic cationic metal-organic framework carrier for controllable drug release. J Med Chem. 2014;57(13):5679–85.

[43] Pandey S, Vijayendra Swamy SM, Ubaid Ulla UM, Gupta A, Patel H, Yadav JS. Cell Line and Augment Cellular Uptake Study of Statistically Optimized Sustained Release Capecitabine Loaded Eudragit S100/PLGA(poly(lacticco- glycolic acid)) Nanoparticles for Colon Targeting. Curr Drug Deliv. 2016;14(6):887–99.

[44] Kumar D, Pal S. Solution dynamics of 5-fluorouracil entrapped in poly lactic-co-glycolic acid (PLGA) microsphere – A study with 1D selective NMR methods. Magn Reson Chem. 2019;57(2–3):118–28.

[45] Wang H, Huang T, Granick S. Using NMR to Test Molecular Mobility during a Chemical Reaction. J Phys Chem Lett. 2021;12(9):2370–5.

[46] Campos R. Experimental methodology. Fat Cryst Networks. 2004;267–348.

[47] Lee H, Ooya T. 19F-NMR, 1H-NMR, and fluorescence studies of interaction between 5-fluorouracil and polyglycerol dendrimers. J Phys Chem B. 2012 Oct;116(40):12263–7.

[48] Din FU, Aman W, Ullah I, Qureshi OS, Mustapha O, Shafique S, et al. Effective use of nanocarriers as drug delivery systems for the treatment of selected tumors. Int J Nanomedicine. 2017;12:7291–309.

[49] Li R, Liu S, Tang Q, Wang T, Xie Y, Zhai R. Encapsulation of 5-Fluorouracil in a Copper(II)-based Porous Metal-organic Framework: Drug Delivery and Inhibiting Human Spinal Cord Tumor Cells. Zeitschrift fur Anorg und Allg Chemie. 2018;644(5):317–21.

[50] Siamidi A, Tsintavi E, M. Rekkas D, Vlachou M. 3D-Printed Modified-Release Tablets: A Review of the Recent Advances. Mol Pharmacol. 2020;1–13.

[51] Trenfield SJ, Awad A, Goyanes A, Gaisford S, Basit AW. 3D Printing Pharmaceuticals: Drug Development to Frontline Care. Trends Pharmacol Sci. 2018;39(5):440–51.

[52] Chia HN, Wu BM. Recent advances in 3D printing of biomaterials. J Biol Eng. 2015;9(1):1–14.

[53] Norman J, Madurawe RD, Moore CMV, Khan MA, Khairuzzaman A. A new chapter in pharmaceutical manufacturing: 3D-printed drug products. Adv Drug Deliv Rev. 2017;108:39–50.

Chapter 5: Summary

5.1 Motivation

The present dissertation project aimed to deepen the understanding of the mechanisms involved in the release of different antitumor agents when encapsulated in the metal-organic structure [$Fe_3O(H_2O)_2(OH)(bdc)_3$]n (bcd = 1,4-benzene-dicarboxylate; MIL-101(Fe), MIL = Materials of Institut Lavoisier). To achieve this goal, a fusion of different methods covering various scientific areas of synthetic chemistry, bioanalytical chemistry, and biochemistry was required as a prerequisite to study the incorporation and release of the chosen antitumor agents, as well as to predict how those drugs will interact with biological systems. The establishment of a hassle-free manufacturing process involves the systematic development of drugs with minimal quality issues aiming to obtain highly robust products. These requirements when combined with printing techniques can transform healthcare applications.[1] In this dissertation project the drugs curcumin (CCM), capecitabine, and 5-fluorouracil (5-FU) were encapsulated into the MIL-101(Fe) metal-organic framework (MOF) structure. Furthermore, curcumin was also incorporated into a polyamide-12 (PA-12) polymer matrix as pure compound, and 5-FU and curcumin already incorporated in MIL-101(Fe) were incorporated into a PA-12 polymer matrix. The drug release properties of these systems was studied. The strategy in designing this drug delivery system was based on literature-known examples with the aim to get more information on the mechanisms responsible for the release of those drugs.

5.2 Results

The starting point of this dissertation is a chapter focusing on the various MOF structures, their synthesis methods, followed by the functionalization methods used to prepare them, and on the MOFs applied as drug delivery systems, as well as their toxicity and biodegradation. The second chapter is focused on different 3D printing techniques. The concept of additive manufacturing (AM) or rapid prototyping (RP) was first proposed during the late 1980s. Employing AM technology, it is possible to fabricate chemically functional 3D printed objects and customize them in terms of size, shape, and geometry, allowing the rapid design and development of personalized drug therapy.[2] Among the different 3D printing techniques presented, the selective laser sintering (SLS) was shown to be one of the techniques that could be used to incorporate the MIL-101(Fe) MOF structure applying PA-12 as a supporting polymer matrix. The MIL-101(Fe) incorporation into the polymer matrix was elucidated through scanning electron microscopy (SEM) and supported by spectroscopic data (FTIR). The FTIR spectra of MIL-101(Fe) and 3D printed samples of PA-12/MIL-101(Fe) show the characteristic bands of the carboxylate

groups derived from terephthalic acid present in MIL-101(Fe), as well as bands related to the Fe–O vibrations. The SEM investigation of the PA-12/MIL-101(Fe) samples showed the characteristic morphology of MIL-101(Fe).[3] Therefore, demonstrating the stability of the crystals when using laser power corroborates that is possible to produce 3D printed objects with the selective laser sintering (SLS) technique applying PA-12 as a supporting polymer for the MIL-101(Fe) (Figure 5.1). After the fundamental 3D printing techniques and the application of SLS in drug delivery were elucidated, studies concerning the incorporation and release of curcumin as a model drug from the MIL-101(Fe) structure in biological systems (Figure 5.2) were undertaken along with possibilities to modulate this release through 3D printing.
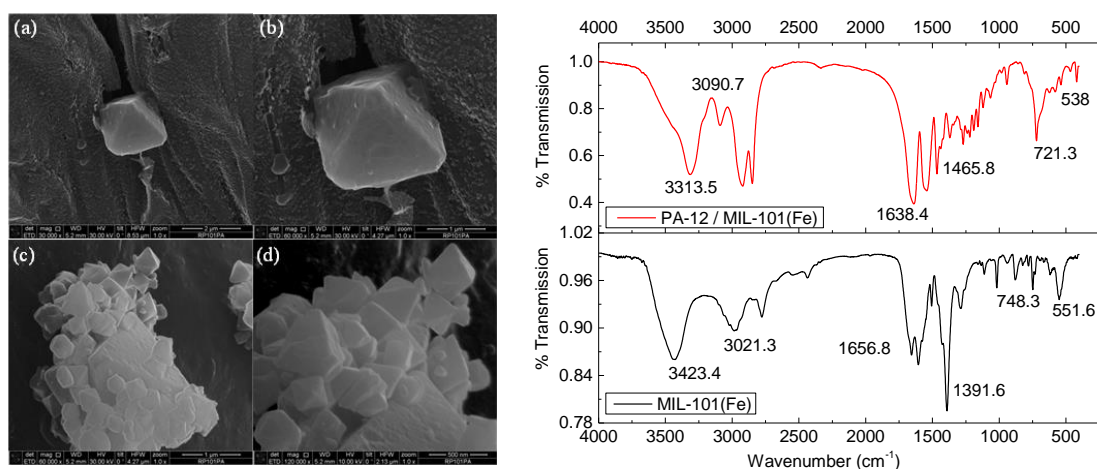
Figure 5.1. Left: SEM of the PA-12/MIL-101(Fe) mixture with (a) 2 μm magnification, (b) 1 μm magnification; (c) SEM of the PA-12/MIL-101(Fe) showing the characteristic octahedral shape with 1 μm magnification, and (d) with 500 nm magnification. Right: FTIR spectra of MIL-101(Fe) (bottom) and the mixture PA-12/MIL-101(Fe) (top).

Figure 5.2. Loading and release process: (a) Drug; (b) MOF; (c) loading process; (d) exposure to biological media; (e) release.

Consequently, Chapter 3 deals with finding the optimal conditions for encapsulation. The encapsulation experiment was conducted with two different ratios, 1:2 (w/w) and 1:3 (w/w) (CCM:MIL-101(Fe)) and followed by UV-vis

spectroscopy. After 24 h, the 1:2 (w/w) samples showed an encapsulation efficiency of 65 wt% and a loading capacity of 32 wt%; these numbers increased slightly after 48 h to 68 wt%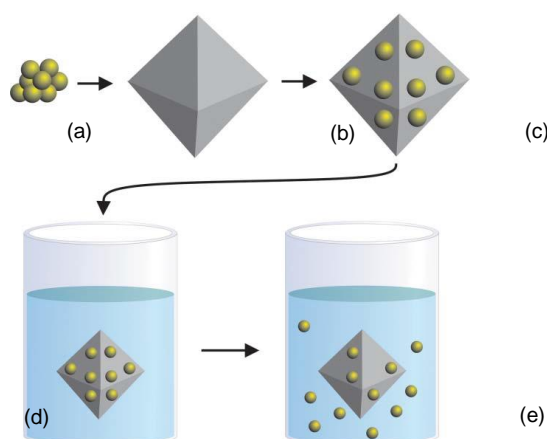 and 34 wt%, respectively (Figure 5.3, left). These values are similar to those of previously reported MOF-based carriers.[4] The same experiment was conducted with a curcumin:MIL-101(Fe) ratio of 1:3 (Figure 5.3, right). It was observed that the absorption peak of curcumin in ethanol was shifted after addition of MIL-101(Fe), namely to 431 nm after 24 h, and to 437 nm after 48 h. These shifts in the UV-vis spectra could be attributed to the formation of intermolecular hydrogen bonds between curcumin and MIL-101(Fe).[5], [6] The incorporation of the drug was also elucidated by FTIR and X-ray diffraction (Figure 5.4), the ultimate proof of a successful incorporation of the drug into the MIL-101(Fe) structure.[3], [7], [8]

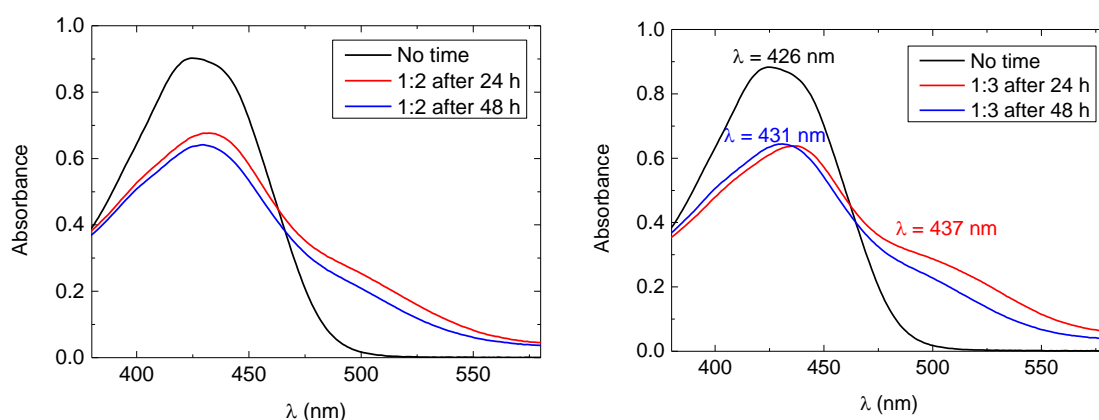Figure 5.3. Left: UV-vis spectra of free curcumin (CCM) in ethanol (black) and after addition of MIL-101(Fe) (ratio CCM:MIL-101(Fe) = 1:2, after 24 h (red) and 48 h (blue)). Right: UV-vis spectra of free curcumin in ethanol (black) and after addition of MIL-101(Fe) (ratio CCM:MIL-101(Fe) = 1:3, after 24 h (red) and 48 h (blue)).
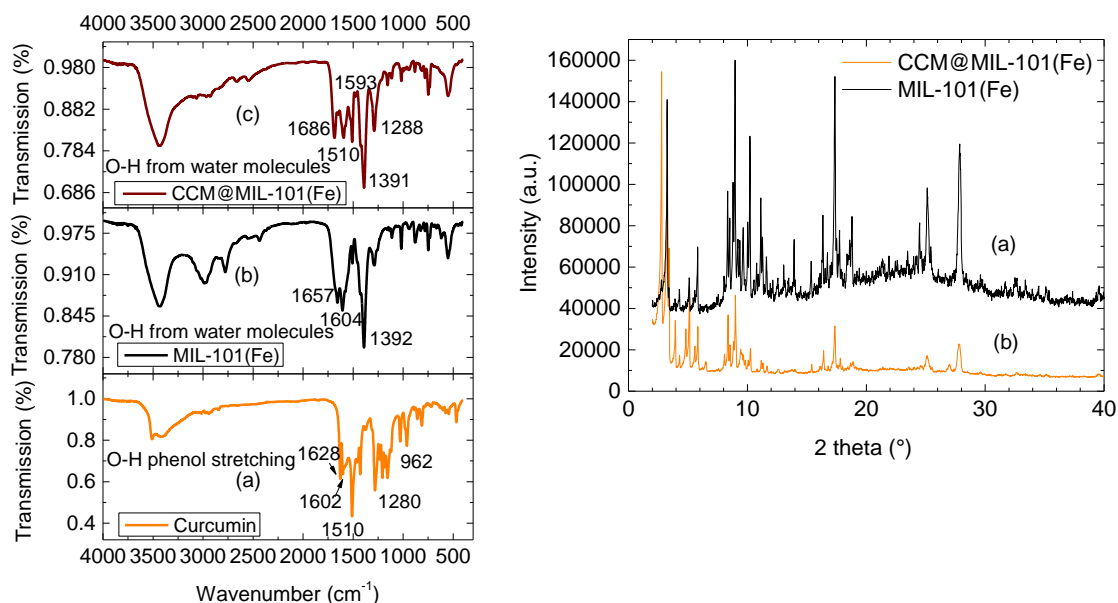

Figure 5.4. Left: FTIR spectra of (a) curcumin (CCM), (b) MIL-101(Fe), and (c) CCM@MIL101(Fe). Right: Powder diffractograms of (a) MIL-101(Fe) and (b) CCM@MIL-101(Fe).

Finally, the curcumin release studies were performed in phosphate-buffered saline/ dimethyl sulfoxide (2%)/ albumin (5%), phosphate-buffered saline (PBS)/DMSO (2%)/albumin (5%). The CCM@MIL-101(Fe) system released finite amounts of CCM at distinct time intervals; in the first hour, 27% of curcumin is released, reaching 40% after 36 h, followed by 65% after 96 h (Figure 5.5).
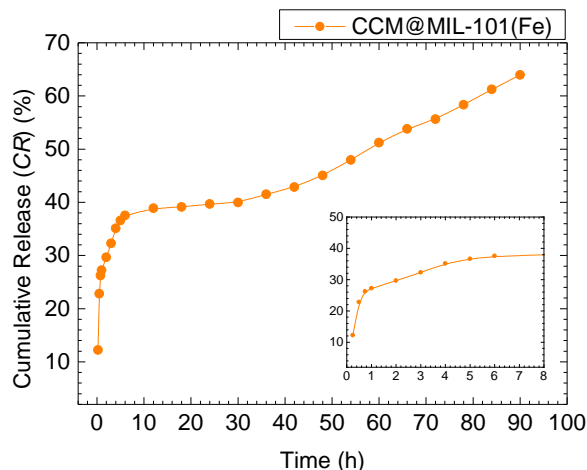

Figure 5.5. Cumulative kinetic release of curcumin from CCM@MIL-101(Fe).

In order to modulate this release behavior achieving a slower and continuous release, the selective laser sintering (SLS) technique was employed to accomplish an extended release. Consequently, different types of matrices were proposed for sustained release investigations. The first was composed of only curcumin incorporated into a PA-12 matrix. The second sample was a composition of two different polymers (PA-12 and the biodegradable polymer polyvinylpyrrolidone (PVP)) and curcumin. The third sample was composed of curcumin encapsulated in the MIL-101(Fe) framework and afterwards introduced into the PA-12 polymer matrix.

By having curcumin incorporated into the PA-12 matrix (Figure 5.6), the release rate is slowed down in comparison to the situation in which curcumin is loaded into MIL-101(Fe), where around 40% of curcumin is released in the first 6 h. The tablet continued to release small amounts of curcumin into the medium, displaying an extended release, where 50% of the incorporated curcumin is released over 5 days.

The release study was conducted on tablets of 16.63 mm diameter (sample code PA-12 E01, Figure 5.6 (b)) in which the amount of curcumin was about six times higher than in the previous study performed on tablets of 5 mm diameter (PA-12 E005), to allow the study of the release for a longer period (Figure 5.6 (a)). In the first few hours, the curcumin is gradually released into the medium, reaching only about 4% of its release in the first 24 h. The system keeps its diffusion-controlled release of small amounts of curcumin until 42 days, where about 20% of the drug was released into the simulated biological medium. In this case, the incorporation of the drug in a polymer matrix allowed a slow curcumin release for a longer period of time in comparison with the metal-organic framework, CCM@MIL-101(Fe).
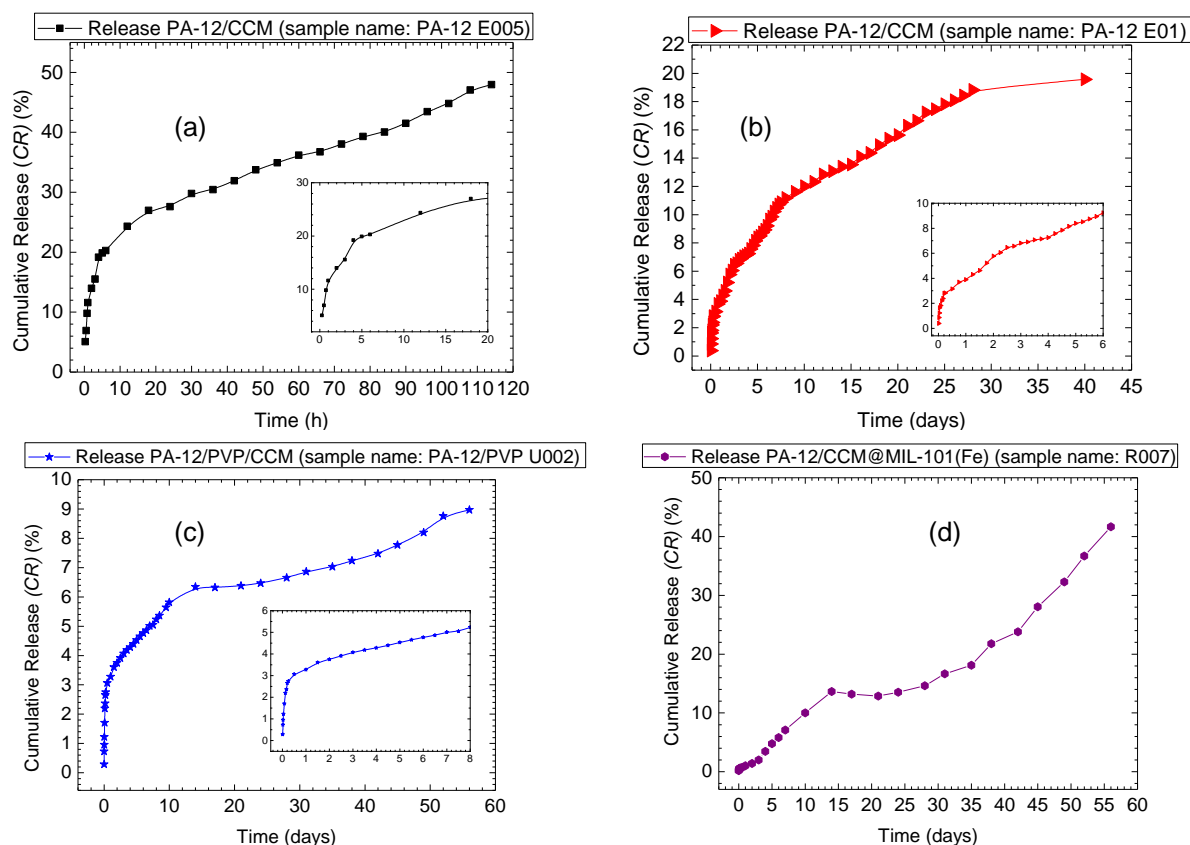
Figure 5.6. Cumulative release of curcumin from (a) a polyamide-12/curcumin sample (PA12 E005, tablet), (b) PA12/curcumin (PA12 E01), (c) a PA-12/PVP/curcumin system (PA-12/PVP U002), and (d) a PA-12/CCM@MIL-101(Fe) system (R007).

The biocompatible polymer polyvinylpyrrolidone (PVP) is extensively applied in biomedical materials due to its environmental stability, bio- and chemocompatibility, low cytotoxicity, high chemical and thermal resistance, and good solubility in water. Having a melting point that ranges from 150 to 180 °C, similar to the melting point of PA-12 (180 °C), the study of PA-12/PVP using the SLS technique was proposed.

The release characteristics of curcumin from a sample composed of PA-12/PVP/curcumin (sample name PA-12/PVP U002, Figure 5.6 (c)), demonstrated a sustained release that reached 3% of curcumin release within 24 h, typical for diffusion-controlled systems. As the drug is embedded in a dissolving matrix, in this case, the slow dissolution of PVP permitted controlled curcumin release up to 9% in the course of 56 days. As another alternative to modulate the drug release, curcumin was encapsulated into MIL-101(Fe) and the resulting CCM@MIL-101(Fe) was further incorporated into the polymer matrix (PA-12/PVP). The release characteristics of the PA-12/PVP/CCM@MIL-101(Fe) system also showed the pulsatile release characteristics observed for CCM@MIL-101(Fe), but differed from the last as two distinct release steps were observed (Figure 6 (d)). The release characteristics shown by PA-12/PVP/CCM@MIL-101(Fe) was composed of two distinct release steps; a first

stage that went up to 15 days (releasing 14% of CCM) and a second stage where 41% of CCM was released in the course of 56 days.

The highlighted results (FTIR, X-ray diffraction, and release studies) give strong evidence for a successfully developed strategy for a formulation concept that could be used as a new drug delivery method to extend the delivery of antitumor drugs.

The investigations in Chapter 4 were directed towards the incorporation of two other drugs into the MIL-101(Fe) structure, 5-FU and capecitabine. All following experiments aimed at collecting the release data were performed according to the methodology used in Chapter 3, namely two different weight ratios, 1:2 and 1:3 (MOF:drug), in two different media, PBS and PBS/DMSO (2%). All the samples studied presented an extended release over 180 h, however, indicating a possibility of a burst effect (Figure 5.7). This effect may lead to possible side effects and therefore should be avoided when drug delivery systems are designed.
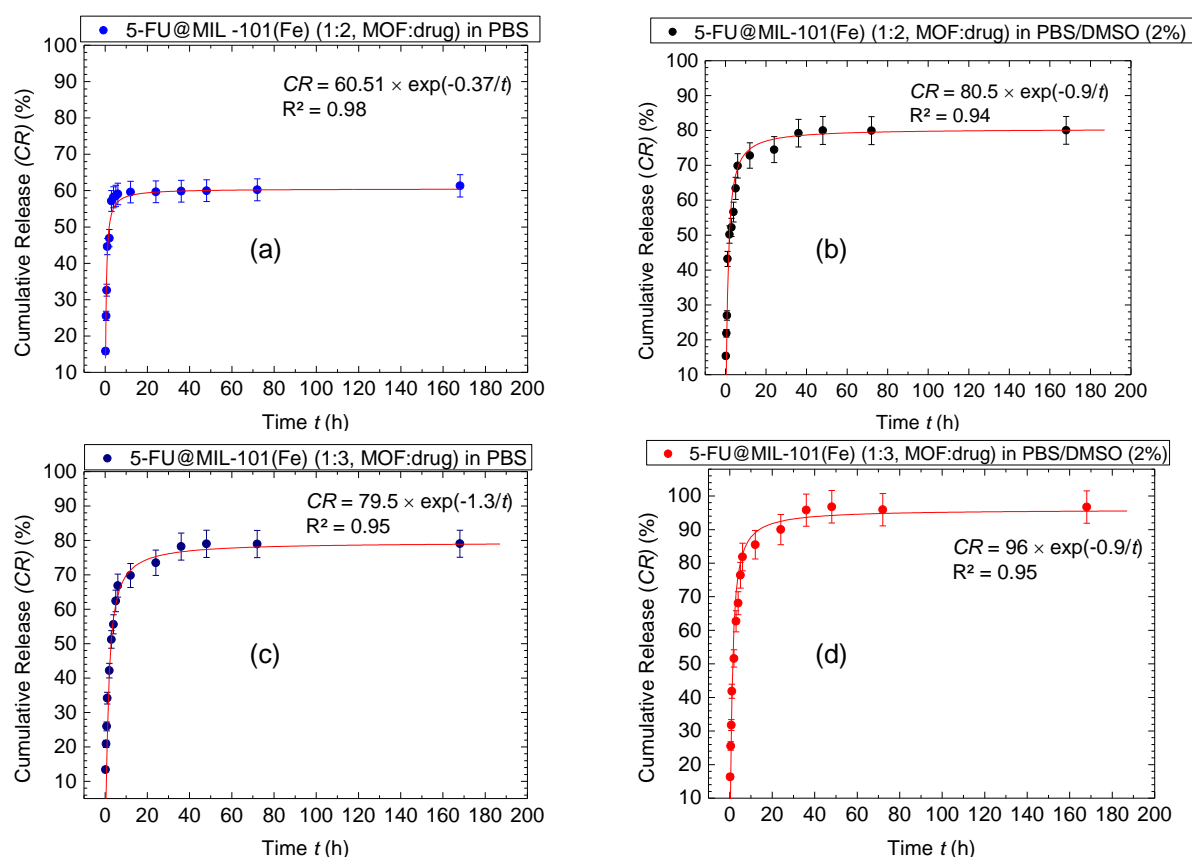
Figure 5.7. Cumulative release of 5-fluorouracil (5-FU) from (a) 5-FU@MIL-101(Fe) (1:2, MOF:drug) weight ratio in PBS, (b) 5-FU@MIL-101(Fe) (1:2, MOF:drug) weight ratio in PBS/DMSO (2%), (c) 5-FU@MIL-101(Fe) (1:3, MOF:drug) weight ratio in PBS, and (d) 5-FU@MIL-101(Fe) (1:3, MOF:drug) weight ratio in PBS/DMSO (2%).

As proposed in Chapter 3, the modulation with SLS was also proposed for the 5-FU@MIL-101(Fe) system which was incorporated into a PA-12 matrix. With the application of SLS, it was possible to decrease the amount of 5-FU released

into the system by extending its period of release up to 30 days, therefore being an effective way to overcome the burst effect (Figure 5.8).
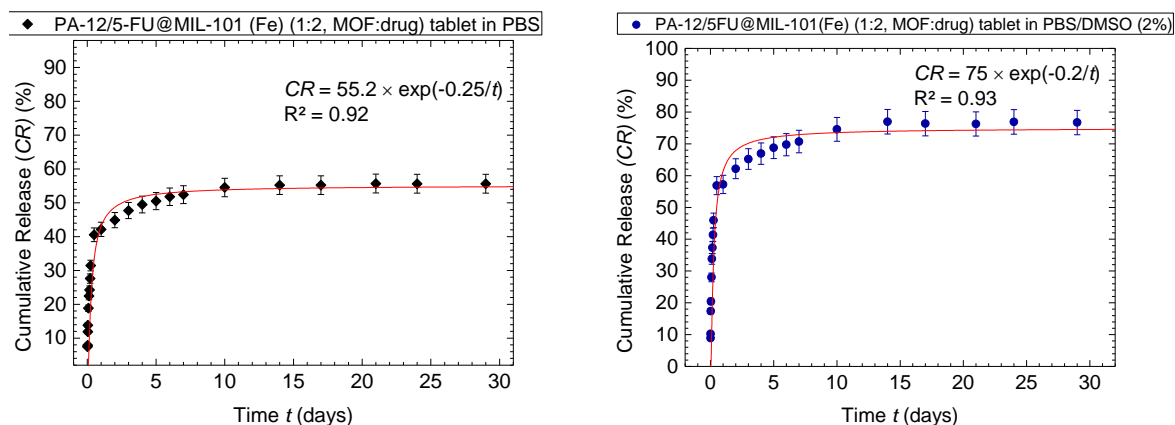
Figure 5.8. Left: Cumulative release of 5-FU from a PA-12/5FU@MIL-101(Fe) (1:2, MOF:drug) sample in PBS (tablets of PA-12/5-FU@MIL-101(Fe)). Right: Cumulative release of 5-FU from a PA-12/5FU@MIL-101(Fe) (1:2, MOF:drug) sample in PBS/DMSO (2%) (tablets of PA-12/5-FU@MIL-101(Fe).
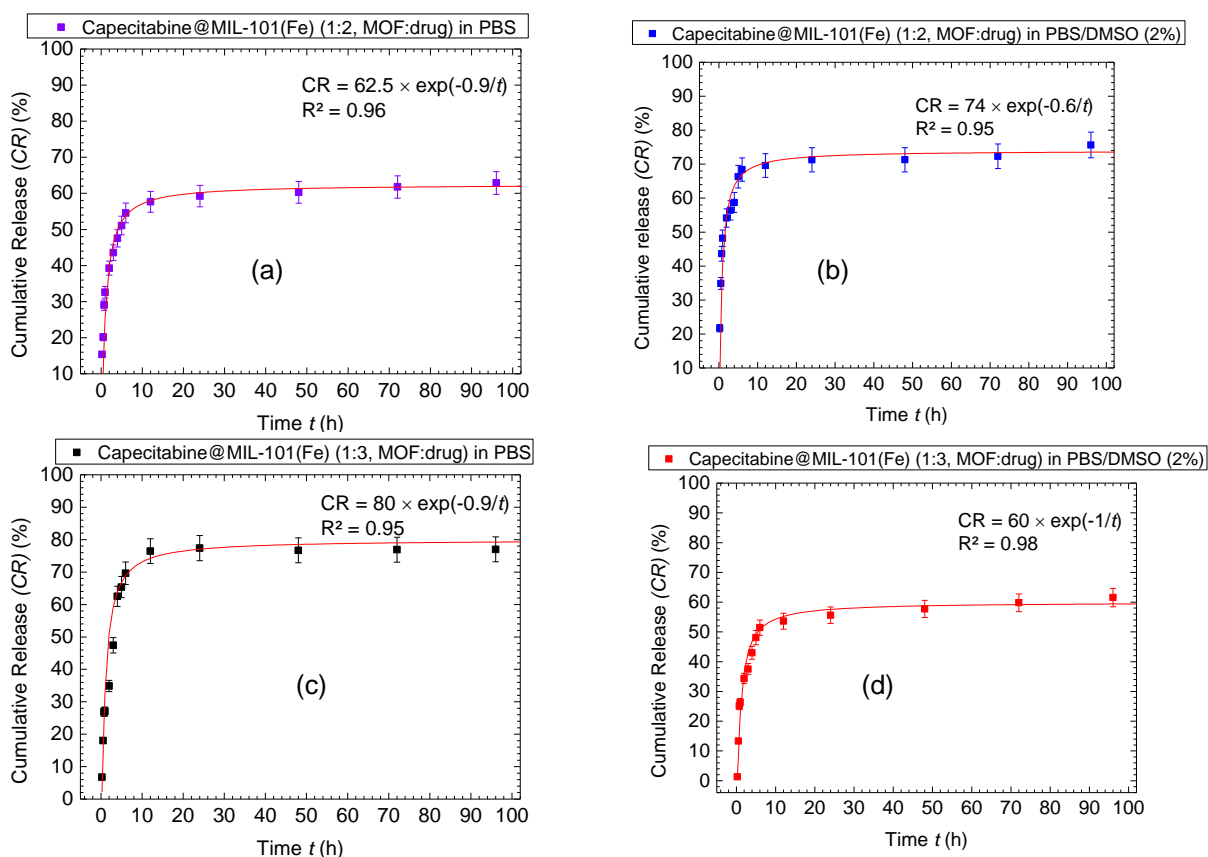
Figure 5.9. Cumulative kinetic release of capecitabine from (a) capecitabine@MIL-101(Fe) (1:2, MOF:drug) weight ratio in PBS, (b) capecitabine@MIL-101(Fe) (1:2, MOF:drug) weight ratio in PBS/DMSO (2%), (c) capecitabine@MIL-101(Fe) (1:3, MOF:drug) weight ratio in PBS, and (d) capecitabine@MIL-101(Fe) (1:3, MOF:drug) weight ratio in PBS/DMSO (2%).

The same ratios and media (PBS and PBS/DMSO (2%)) were applied for capecitabine, where an encapsulation efficiency of 53 wt% (1:2, MOF:drug) and

31 wt% (1:3, MOF:drug) was observed after 48 h in MIL-101(Fe). Nonetheless all the encapsulated capacetabine@MIL-101(Fe) samples also presented the possibility to develop a burst effect (Figure 5.9).

5.3 Conclusion

In conclusion, the main aspects of this dissertation project, i.e., synthesis, encapsulation and release studies of selected drugs, have revealed very promising results for future developments. By incorporating the drug@MOF systems into a PA-12 matrix employing the SLS technique, it was possible to extend the release for longer periods of time (up to one month) avoiding high release rates of the respective drugs into the surrounding media within a few hours. The potential to apply 3D printing in the design of drug delivery systems has revealed a promising new approach for drug delivery.

5.4 Bibliography

[1] M. Rahman *et al.*, "Three 'D's: Design approach, dimensional printing, and drug delivery systems as promising tools in healthcare applications," *Drug Discov. Today*, **2021**, *26*, 2726–2733; doi: https://doi.org/10.1016/j.drudis.2021.06.016.

[2] J. W. Stansbury and M. J. Idacavage, "3D printing with polymers: Challenges among expanding options and opportunities," *Dent. Mater.*, **2016**, *32*, 54–64; doi: 10.1016/j.dental.2015.09.018.

[3] K. M. L. Taylor-Pashow, J. Della Rocca, Z. Xie, S. Tran, and W. Lin, "Postsynthetic modifications of iron-carboxylate nanoscale metal-organic frameworks for imaging and drug delivery," *J. Am. Chem. Soc.*, **2009**, *131*, 14261–14263; doi: 10.1021/ja906198y.

[4] M. Zheng, S. Liu, X. Guan, and Z. Xie, "One-step synthesis of nanoscale zeolitic imidazolate frameworks with high curcumin loading for treatment of cervical cancer," *ACS Appl. Mater. Interfaces*, **2015**, *7*, 22181–22187; doi: 10.1021/acsami.5b04315.

[5] Z. Moussa, M. Hmadeh, M. G. Abiad, O. H. Dib, and D. Patra, "Encapsulation of curcumin in cyclodextrin-metal organic frameworks: Dissociation of loaded CD-MOFs enhances stability of curcumin," *Food Chem.*, **2016**, *212*, 485–494; doi: 10.1016/j.foodchem.2016.06.013.

[6] K. I. Priyadarsini, "The chemistry of curcumin: From extraction to therapeutic agent," *Molecules*, **2014**, *19*, 20091–20112; doi: 10.3390/molecules191220091.

[7] C. Li *et al.*, "Hierarchical hollow Fe_2O_3 @MIL-101(Fe)/C derived from metal-organic frameworks for superior sodium storage," *Sci. Rep.*, **2016**, *6*, 1–8; doi: 10.1038/srep25556.

[8] V. R. Yadav, S. Suresh, K. Devi, and S. Yadav, "Effect of cyclodextrin complexation of curcumin on its solubility and antiangiogenic and anti-inflammatory activity in rat colitis model," *AAPS PharmSciTech*, **2009**, *10*, 752–762; doi: 10.1208/s12249-009-9264-8.

5.5 Publications on the topic of the doctoral thesis

[1] Elmeri Lahtinen, **Rafaella L. M. Precker,** Manu Lahtinen, Evamarie Hey-Hawkins, Matti Haukka. Selective Laser Sintering of Metal-organic Frameworks: Production of Highly Porous Filters by 3D Printing onto a Polymeric Matrix, *ChemPlusChem*, **2019**, *84*, 222–225.

[2] Andreia Valente, **Rafaella L. M. Precker**, Evamarie Hey-Hawkins in: Smart Inorganic Polymers, Inorganic Polymers for Potential Medicinal Applications (Book Chapter), *Wiley-VCH Verlag GmbH & Co. KGaA*, **2019**, ISBN: 978-3-52781-914-0.

[3] Vladimir V. Vinogradov, Andrey S. Drozdov, Leila R. Mingabudinova, Emiliya M. Shabanova, Nina O. Kolchina, Elizaveta I. Anastasova, Alina A. Markova, Alexander A. Shtil, Valentin A. Milichko, Galina L. Starova, **Rafaella L. M. Precker**, Alexandr V. Vinogradov, Evamarie Hey-Hawkins and Evgeny A. Pidko. Composites Based on Heparin and MIL-101(Fe): The Drug Releasing Depot for Anticoagulant Therapy and Advanced Medical Nanofabrication, *J. Mater. Chem. B*, **2018**, *6*, 2450–2459.

Chapter 6: Appendices

6.1 Abbreviations

A549	human lung carcinoma cells
AA	anisamide
ABS	poly(acrylonitrile/butadiene/styrene)
ADME	absorption, distribution, metabolism, elimination
AL	alendronate
AM	additive manufacturing
ASA	acrylonitrile styrene acrylate
AZT-TP	azidothymidine triphosphate
BABL-3T3	normal mouse embryonic fibroblast cells
BCC	basal cell carcinoma
bdc	benzenedicarboxylate
BioMIL	bioactive Materials from Institut Lavoisier
bpdc	4,4'-biphenyldicarboxylate
bpy	bipyridine
BSA	bovine serum albumin
BSE	backscattered electrons
btb	4,4',4''-benzen-1,3,5-triyl-tribenzoate
btc	benzenetricarboxylate
CAD	computer-aided design
Cam	camptothecin
CCM	curcumin
CSD	Cambridge Structural Database
dabco	1,4-diazabicyclo[2.2.2]octane

DDS	drug delivery system
DEF	diethylformamide
DESs	deep eutectic solvents
DHFU	dihydrofluorouracil
dhtp	2,5-dihydroxyterephthalate
DLP	digital light processing
DLS	dynamic light scattering
DMF	dimethylformamide
DMSO	dimethyl sulfoxide
DNA	deoxyribonucleic acid
dobdc4−	2,5-dioxido-1,4-benzenedicarboxylate
DOPC	1,2-dioleoyl-sn-glycero-3-phosphocholine
DOX	doxorubicin
DPD	dihydropyrimidine dehydrogenase
DSCP	disuccinatocisplatin
DTA	differential thermal analysis
DTBA	4,4'-dithiobisbenzoic acid
DTM Corp	Desktop Manufacturing Corporation
dTMP	2'- deoxythymidine-5'- monophosphate
dUMP	2'- deoxyuridine-5'- monophosphate
EBM	electronic beam melting
EDX	energy-dispersive X-ray spectroscopy
EE	encapsulation efficiency
EtOH	ethanol
FA	pegylated folate
FA	folic acid
FDM	fused deposition modeling

FdUDP	fluorodeoxyuridine diphosphate
FdUMP	fluorodeoxyuridine monophosphate
FdUTP	fluorodeoxyuridine triphosphate
FTIR	Fourier Transform Infrared Spectroscopy
FUDP	fluorouridine diphosphate
FUDR	fluorodeoxyuridine
FUMP	fluorouridine monophosphate
FUR	fluorouridine
FUTP	fluorouridine triphosphate
GI	gastrointestinal tract disorders
GOx	glucose oxidase
GSH	glutathione
h	hour
HA-PDA	polydopamine-modified hyaluronic acid
HeLa	human cervical carcinoma
HepG2	human liver cancer cell line
HIM	helium ion microscope
HKUST	Hong Kong University of Science and Technology
HMEC	human microvascular endothelial cells
HUVEC	human umbilical cord vein cells
IBU	ibuprofen
ILs	ionic liquids
IR	infrared
LC	loading capacity
LD50	median lethal dose
LOM	laminated object manufacturing
LV	leucovorin

MCF-7	breast cancer cell line
MeOH	methanol
MH-S	mouse alveolar macrophages
MIL	Materials of Institut Lavoisier
mIm	2-methylimidazole
min	minutes
MIT	Massachusetts Institute of Technology
MLE12	murine alveolar epithelial cells
MMMs	mixed matrix membranes
MMP	matrix metalloproteinase
MOFs	metal-organic frameworks
MS	mass spectrometry
ndc	2,6-naphthalenedicarboxylate
NIR	near-infrared
NMR	nuclear magnetic resonance
OPRT	phosphoribosyltransferase
PA-12	polymanide-12
PAI	photoacoustic imaging
PBF	powder bed fusion
PBS	phosphate-buffered saline
PC	polycarbonate
PCL–TPGS	poly(ε-caprolactone)–d-α-tocopheryl polyethylene-glycol-succinate
PCN	polymeric carbon nitride
PDA	polydopamine
PEEK	polyether ether ketone
PETG	polyethylene terephthalate glycol

PLA	polylactic acid
PP	polypropylene
PRPP	phosphoribosyl pyrophosphate
PS	polystyrene
PSD	postsynthetic deprotection
PSE	postsynthetic exchange
PSI	post-synthetic installation
PSLE	post-synthetic ligand exchange
PSM	post-synthetic modification
PSME	post-synthetic metal exchange
PSP	postsynthetic polymerization
pta	1,3,5-triaza-7-Phosphaadamantane
PTT	photothermal therapy
PU	polyurethane
PVP	polyvinylpyrollidone
RNA	ribonucleic acid
RR	ribonucleotide reductase
SAC	steam-assisted crystallization
SALE	solvent-assisted linker exchange
SALI	solvent-assisted linker incorporation
SBF	simulated body fluid
SBUs	secondary building units
SE	secondary electrons
SEM	scanning electron microscope
SHS	selective heat sintering
SKOV3	ovary cancer cells
SL	stereolithography

SLA	stereolithography
SLM	selective laser melting
SLS	selective laser sintering
STL	stereolithography
TEM	transmission electron microscopy
TEOS	tetraethyl orthosilicate
TG	thermogravimetric analysis
TK	thymidine kinase
TS	thymidylate synthase
UK	uridine kinase
UP	uridine phosphorylase
UV	ultraviolet
vis	visible
VPT	vapor-phase transport
ZIF	zeolitic imidazolate framework
ZJU	Zhejiang University
λ	wavelength

6.2 Curriculum Vitae

Personal Data

First Name, Surname:	Rafaella Lima de Meneses Precker
Date of Birth:	06th March 1986
Place of Birth:	Campina Grande, Brazil
Gender:	Female
Position:	Doctoral student at Leipzig University

Education

Since 06/2015	**Doctoral student**
Supervisor	Prof. Dr. Dr. h.c. mult. Evamarie Hey-Hawkins
Title	*Metal-organic frameworks as drug delivery system for cancer therapy*
11/2012 – 10/2014	**Master of Science in Materials Science Engineering**, *Federal University of Campina Grande, UFCG*, Brazil.
Supervisor	Prof. Dr. Marcus Vinicius Lia Fook.
Title	*Development of Chitin Fibers for Application as Suture Wire*
10/2009 – 07/2012	**Bachelor of Science in Materials Science Engineering**, Federal University of Campina Grande, UFCG, Brazil
01/2001 – 12/2003	**High-School,** *Colégio Imaculada Conceição CIC Damas,* Campina Grande, Brazil

Work Experience

Since 06/2015	Doctoral project at Leipzig University, metal-organic frameworks (MOFs) for cancer therapy, under the supervision of Prof. Dr. Dr. h.c. mult. E. Hey-Hawkins, associated member of the Leipzig Graduate School of Natural Sciences – Building with molecules and Nano-objects (BuildMoNa)
2012 – 2014	Master in Materials Science Engineering on the biomaterials topic – Chitin Fibers for application as suture wire. Planning,

organizing, carrying out and interpreting experiments on biopolymers. The progressive working experience led to collaborations with Samaritan Hospital (SP, Brazil), ANVISA-National Health Surveillance Agency (Brasília, Brazil), and the University of Brescia (Brescia, Italy).

2012 – 2014	Technical Consultant at ANVISA, Brasília, Brazil. As a technical advisor, carried out activities on the issue of technical and scientific opinions collaborating with three teams on the use of materials, technology, and implants in health. According to ISO/IEC, ABNT, NBR regulations.
07/2011 – 03/2012	Intern at Acumuladores Moura S.A., Belo Jardim, Brazil. As a product engineer in the automotive industry, engaged in raw material/component material validations, quality control processes and improvements, supporting teams in technical choices in building new structures or processes on lead-acid batteries, working with cross-functional groups of different countries to meet the customer specifications.
10/2009 – 03/2010	Internship at Soft Matter Labs, Johannes Gutenberg University of Mainz, Institute of Physics, Germany. Responsible for assembling and handling ion-exchange circuits for advanced sample conditioning, in situ determination of particle concentrations, and conductometric control of the residual electrolyte concentration.

Further Activities

11-12/2019	Research stay – Department of Inorganic Chemistry, University of Jyväskylä, Finland.
11/2018	Research stay – Department of Inorganic Chemistry, University of Jyväskylä, Finland.

01/2018	Research Stay – Department of Inorganic Chemistry, University of Jyväskylä, Finland.
03/2017 – 06/2017	Research term at the International Laboratory Solution Chemistry of Advanced Materials and Technology, ITMO University, Saint Petersburg, Russia.
01/2014 – 03/2014	Research term at the Department of Mechanical and Industrial Engineering, University of Brescia, Brescia, Italy.

Scholarships and Awards

2015 – 2019	**Science Without Borders** fellowship for the doctoral studies.
03/2017 – 06/2017	**Erasmus+** fellowship for the doctoral project.
2018	**Travel Grant of the DAAD** (Deutscher Akademischer Austauschdienst)
2018	**Second Best Oral Presentation** at the annual conference of the Graduate School BuildMoNa, Leipzig School of Natural Sciences – Building with Molecules and Nano-objects.
2019	**Travel Grant of the DAAD** (Deutscher Akademischer Austausch Dienst)

Publications

[1] Elmeri Lahtinen, **Rafaella L. M. Precker,** Manu Lahtinen, Evamarie Hey-Hawkins, Matti Haukka. Selective Laser Sintering of Metal-organic Frameworks: Production of Highly Porous Filters by 3D Printing onto a Polymeric, *CHEMPLUSCHEM*. (2019), 84 (2), 222 – 225.

[2] Andreia Valente, **Rafaella L. M. Precker**, Evamarie Hey-Hawkins in: Smart Inorganic Polymers. Inorganic Polymers for Potential Medicinal Applications. (Book Chapter). *Wiley-VCH Verlag GmbH & Co. KGaA*, (2019), ISBN: 978-3-52781-914-0.

[3] Vladimir V. Vinogradov, Andrey S. Drozdov, Leila R. Mingabudinova, Emiliya M. Shabanova, Nina O. Kolchina, Elizaveta I. Anastasova, Alina A. Markova, Alexander A. Shtil, Valentin A. Milichko, Galina L. Starova, **Rafaella L. M. Precker**, Alexandr V. Vinogradov, Evamarie Hey-Hawkins and Evgeny A. Pidko.

Composites based on heparin and MIL-101(Fe): the drug releasing depot for anticoagulant therapy and advanced medical nanofabrication**. *JOURNAL OF MATERIALS CHEMISTRY B*, (2018), Apr 28; 6(16), 2450-2459.

[4] J. B. S. Wladymyr, E. P. Nascimento, K. V. Almeida, K. A. S. Farias, M. J. B. Cardoso, **R. L. Meneses**, M. V. L. Fook. Hybrid Membranes Development Made by Chitosan and Calcium Phosphate. *Materials Science Forum*, (2014), 798-799, 682-686.

[5] Andreas Engelbrecht, **Rafaella Meneses** and Hans Joachim Schöpe. Heterogeneous and homogeneous crystal nucleation in a colloidal model system of charged spheres at low metastabilities. *Soft Matter*, 2011, 7, 5685-5690.

Kurzfassung der wissenschaftlichen Ergebnisse zur Dissertation

Metal-organic Frameworks as Drug Delivery System for Cancer Therapy

Der Fakultät für Chemie und Mineralogie

der Universität Leipzig vorgelegt von

M.Sc. Rafaella Lima de Meneses Precker

im Februar 2022

Angefertigt am Institut für Anorganische Chemie

---

1. Motivation

The present dissertation project aimed to deepen the understanding of the mechanisms involved in the release of different antitumor agents when encapsulated in the metal-organic structure $[Fe_3O(H_2O)_2(OH)(bdc)_3]n$ (bcd = 1,4-benzene-dicarboxylate; MIL-101(Fe), MIL = Materials of Institut Lavoisier). To achieve this goal, a fusion of different methods covering various scientific areas of synthetic chemistry, bioanalytical chemistry, and biochemistry was required as a prerequisite to study the incorporation and release of the chosen antitumor agents, as well as to predict how those drugs will interact with biological systems. The establishment of a hassle-free manufacturing process involves the systematic development of drugs with minimal quality issues aiming to obtain highly robust products. These requirements when combined with printing techniques can transform healthcare applications.[1] In this dissertation project the drugs curcumin (CCM), capecitabine, and 5-fluorouracil (5-FU) were encapsulated into the MIL-101(Fe) metal-organic framework (MOF) structure. Furthermore, curcumin was also incorporated into a polyamide-12 (PA-12) polymer matrix as pure compound, and 5-FU and curcumin already incorporated in MIL-101(Fe) were incorporated into a PA-12 polymer matrix. The drug release properties of these systems was studied. The strategy in designing this drug delivery system was based

on literature-known examples with the aim to get more information on the mechanisms responsible for the release of those drugs.

2. Results

The starting point of this dissertation is a chapter focusing on the various MOF structures, their synthesis methods, followed by the functionalization methods used to prepare them, and on the MOFs applied as drug delivery systems, as well as their toxicity and biodegradation. The second chapter is focused on different 3D printing techniques. The concept of additive manufacturing (AM) or rapid prototyping (RP) was first proposed during the late 1980s. Employing AM technology, it is possible to fabricate chemically functional 3D printed objects and customize them in terms of size, shape, and geometry, allowing the rapid design and development of personalized drug therapy.[2] Among the different 3D printing techniques presented, the selective laser sintering (SLS) was shown to be one of the techniques that could be used to incorporate the MIL-101(Fe) MOF structure applying PA-12 as a supporting polymer matrix. The MIL-101(Fe) incorporation into the polymer matrix was elucidated through scanning electron microscopy (SEM) and supported by spectroscopic data (FTIR). The FTIR spectra of MIL-101(Fe) and 3D printed samples of PA-12/MIL-101(Fe) show the characteristic bands of the carboxylate groups derived from terephthalic acid present in MIL-101(Fe), as well as bands related to the Fe–O vibrations. The SEM investigation of the PA-12/MIL-101(Fe) samples showed the characteristic morphology of MIL-101(Fe).[3] Therefore, demonstrating the stability of the crystals when using laser power corroborates that is possible to produce 3D printed objects with the selective laser sintering (SLS) technique applying PA-12 as a supporting polymer for the MIL-101(Fe) (Figure 1). After the fundamental 3D printing techniques and the application of SLS in drug delivery were elucidated, studies concerning the incorporation and release of curcumin as a model drug from the MIL-101(Fe) structure in biological systems (Figure 2) were undertaken along with possibilities to modulate this release through 3D printing.
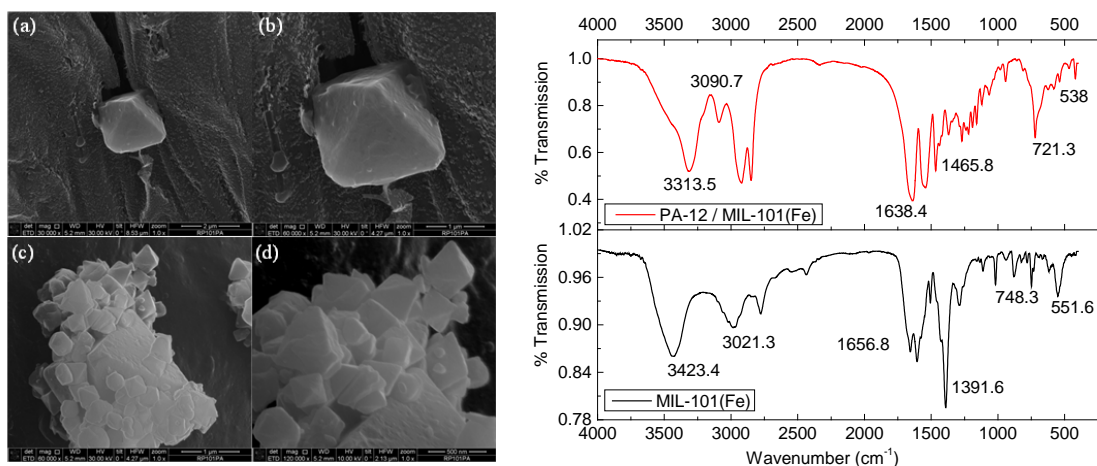
Figure 1. Left: SEM of the PA-12/MIL-101(Fe) mixture with (a) 2 μm magnification, (b) 1 μm magnification; (c) SEM of the PA-12/MIL-101(Fe) showing the characteristic octahedral shape with 1 μm magnification, and (d) with 500 nm magnification. Right: FTIR spectra of MIL-101(Fe) (bottom) and the mixture PA-12/MIL-101(Fe) (top).
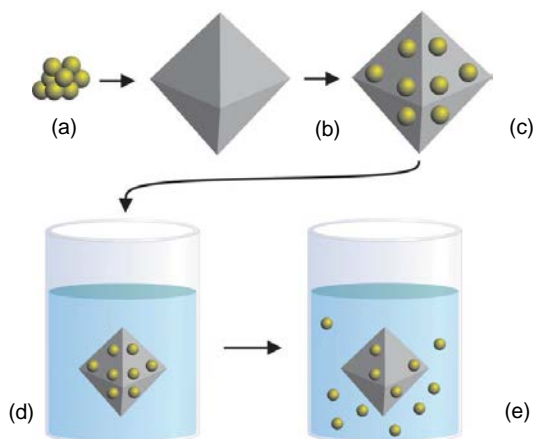

Figure 2. Loading and release process: (a) Drug; (b) MOF; (c) loading process; (d) exposure to biological media; (e) release.

Consequently, Chapter 3 deals with finding the optimal conditions for encapsulation. The encapsulation experiment was conducted with two different ratios, 1:2 (w/w) and 1:3 (w/w) (CCM:MIL-101(Fe)) and followed by UV-vis spectroscopy. After 24 h, the 1:2 (w/w) samples showed an encapsulation efficiency of 65 wt% and a loading capacity of 32 wt%; these numbers increased slightly after 48 h to 68 wt% and 34 wt%, respectively (Figure 3, left). These values are similar to those of previously reported MOF-based carriers.[4] The same experiment was conducted with a curcumin:MIL-101(Fe) ratio of 1:3 (Figure 3, right). It was observed that the absorption peak of curcumin in ethanol was shifted after addition of MIL-101(Fe), namely to 431 nm after 24 h, and to 437 nm after 48 h. These shifts in the UV-vis spectra could be attributed to the formation of intermolecular hydrogen bonds between curcumin and

MIL-101(Fe).[5], [6] The incorporation of the drug was also elucidated by FTIR and X-ray diffraction (Figure 4), the ultimate proof of a successful incorporation of the drug into the MIL-101(Fe) structure.[3], [7], [8]
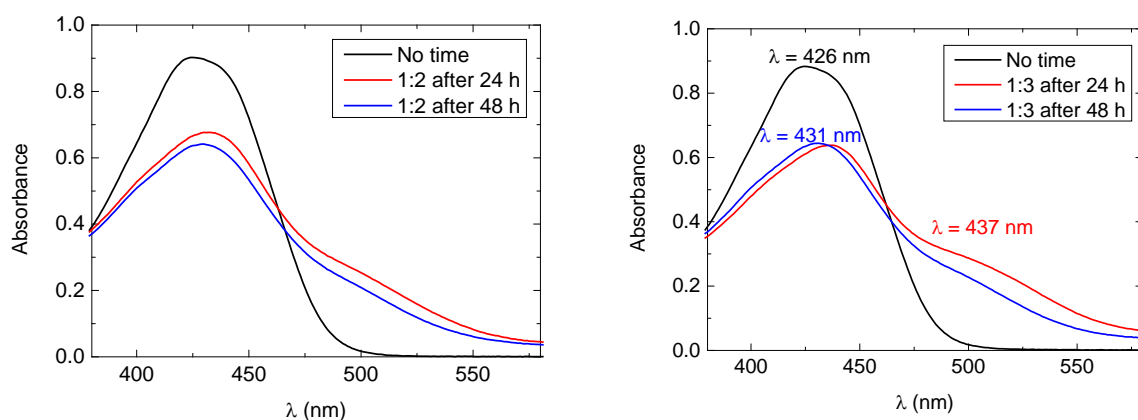

Figure 3. Left: UV-vis spectra of free curcumin (CCM) in ethanol (black) and after addition of MIL-101(Fe) (ratio CCM:MIL-101(Fe) = 1:2, after 24 h (red) and 48 h (blue)). Right: UV-vis spectra of free curcumin in ethanol (black) and after addition of MIL-101(Fe) (ratio CCM:MIL-101(Fe) = 1:3, after 24 h (red) and 48 h (blue)).
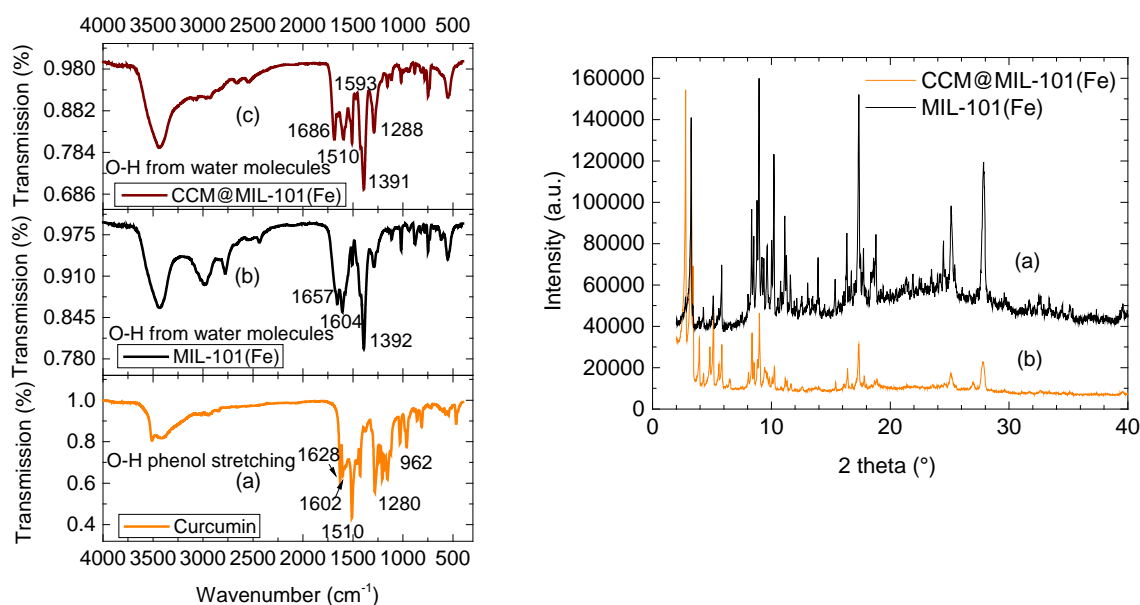

Figure 4. Left: FTIR spectra of (a) curcumin (CCM), (b) MIL-101(Fe), and (c) CCM@MIL101(Fe). Right: Powder diffractograms of (a) MIL-101(Fe) and (b) CCM@MIL-101(Fe).

Finally, the curcumin release studies were performed in phosphate-buffered saline/ dimethyl sulfoxide (2%)/ albumin (5%), phosphate-buffered saline (PBS)/DMSO (2%)/albumin (5%). The CCM@MIL-101(Fe) system released finite amounts of CCM at distinct time intervals; in the first hour, 27% of curcumin is released, reaching 40% after 36 h, followed by 65% after 96 h (Figure 5).
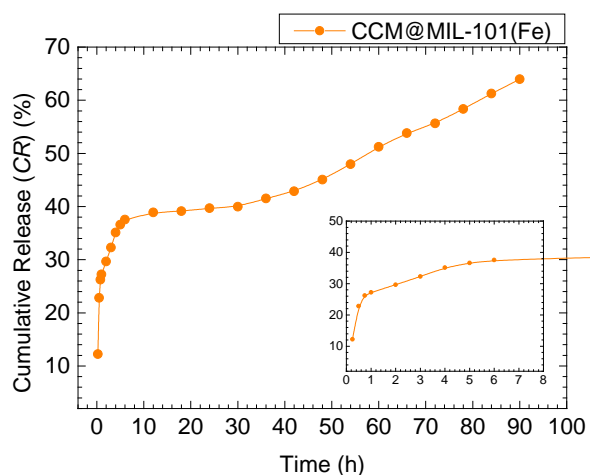
139

Figure 5. Cumulative kinetic release of curcumin from CCM@MIL-101(Fe).

In order to modulate this release behavior achieving a slower and continuous release, the selective laser sintering (SLS) technique was employed to accomplish an extended release. Consequently, different types of matrices were proposed for sustained release investigations. The first was composed of only curcumin incorporated into a PA-12 matrix. The second sample was a composition of two different polymers (PA-12 and the biodegradable polymer polyvinylpyrrolidone (PVP)) and curcumin. The third sample was composed of curcumin encapsulated in the MIL-101(Fe) framework and afterwards introduced into the PA-12 polymer matrix.

By having curcumin incorporated into the PA-12 matrix (Figure 6), the release rate is slowed down in comparison to the situation in which curcumin is loaded into MIL-101(Fe), where around 40% of curcumin is released in the first 6 h. The tablet continued to release small amounts of curcumin into the medium, displaying an extended release, where 50% of the incorporated curcumin is released over 5 days.

The release study was conducted on tablets of 16.63 mm diameter (sample code PA-12 E01, Figure 6 (b)) in which the amount of curcumin was about six times higher than in the previous study performed on tablets of 5 mm diameter (PA-12 E005), to allow the study of the release for a longer period (Figure 6 (a)). In the first few hours, the curcumin is gradually released into the medium, reaching only about 4% of its release in the first 24 h. The system keeps its diffusion-controlled release of small amounts of curcumin until 42 days, where about 20% of the drug was released into the simulated biological medium. In this case, the incorporation of the drug in a polymer matrix allowed a slow curcumin release for a longer period of time in comparison with the metal-organic framework, CCM@MIL-101(Fe).
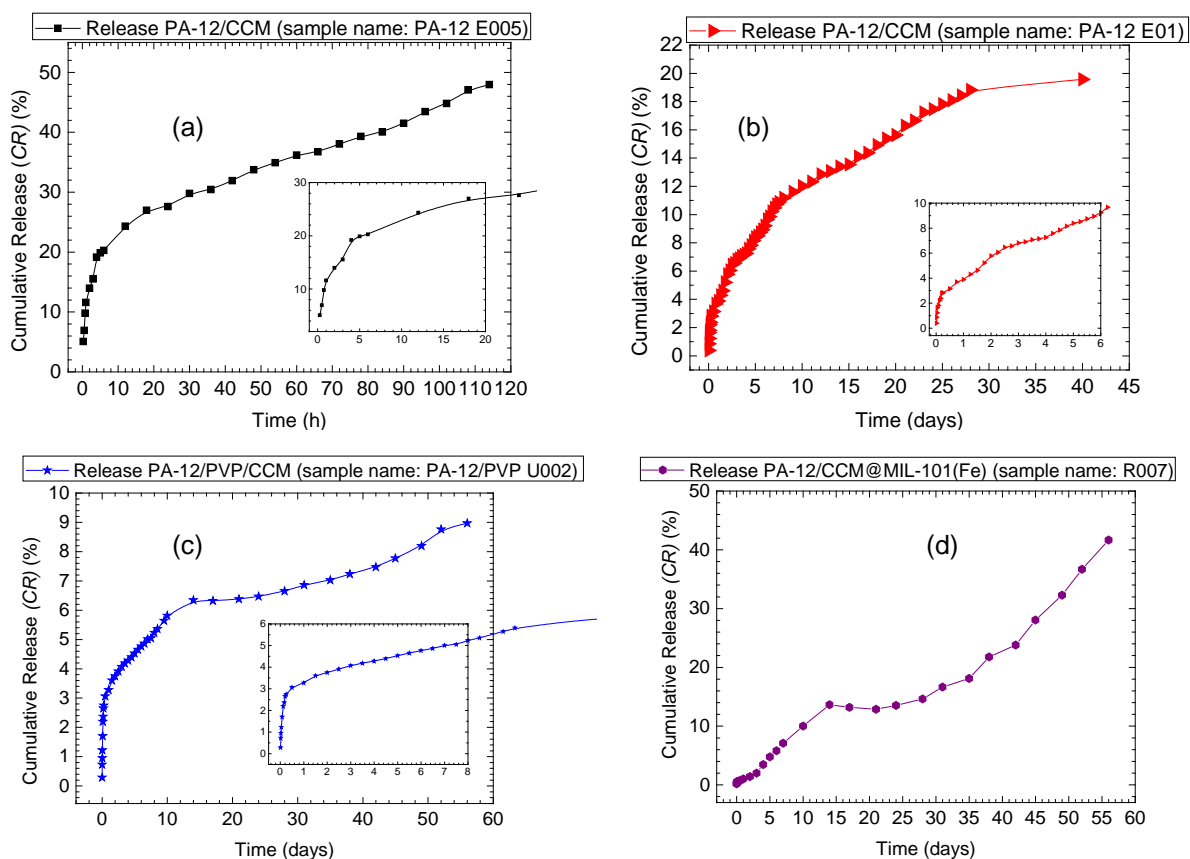
Figure 6. Cumulative release of curcumin from (a) a polyamide-12/curcumin sample (PA12 E005, tablet), (b) PA12/curcumin (PA12 E01), (c) a PA-12/PVP/curcumin system (PA-12/PVP U002), and (d) a PA-12/CCM@MIL-101(Fe) system (R007).

The biocompatible polymer polyvinylpyrrolidone (PVP) is extensively applied in biomedical materials due to its environmental stability, bio- and chemocompatibility, low cytotoxicity, high chemical and thermal resistance, and good solubility in water. Having a melting point that ranges from 150 to 180 °C, similar to the melting point of PA-12 (180 °C), the study of PA-12/PVP using the SLS technique was proposed.

The release characteristics of curcumin from a sample composed of PA-12/PVP/curcumin (sample name PA-12/PVP U002, Figure 6 (c)), demonstrated a sustained release that reached 3% of curcumin release within 24 h, typical for diffusion-controlled systems. As the drug is embedded in a dissolving matrix, in this case, the slow dissolution of PVP permitted controlled curcumin release up to 9% in the course of 56 days. As another alternative to modulate the drug release, curcumin was encapsulated into MIL-101(Fe) and the resulting CCM@MIL-101(Fe) was further incorporated into the polymer matrix (PA-12/PVP). The release characteristics of the PA-12/PVP/CCM@MIL-101(Fe) system also showed the pulsatile release characteristics observed for CCM@MIL-101(Fe), but differed from the last as two

distinct release steps were observed (Figure 6 (d)). The release characteristics shown by PA-12/PVP/CCM@MIL-101(Fe) was composed of two distinct release steps; a first stage that went up to 15 days (releasing 14% of CCM) and a second stage where 41% of CCM was released in the course of 56 days.

The highlighted results (FTIR, X-ray diffraction, and release studies) give strong evidence for a successfully developed strategy for a formulation concept that could be used as a new drug delivery method to extend the delivery of antitumor drugs.

The investigations in Chapter 4 were directed towards the incorporation of two other drugs into the MIL-101(Fe) structure, 5-FU and capecitabine. All following experiments aimed at collecting the release data were performed according to the methodology used in Chapter 3, namely two different weight ratios, 1:2 and 1:3 (MOF:drug), in two different media, PBS and PBS/DMSO (2%). All the samples studied presented an extended release over 180 h, however, indicating a possibility of a burst effect (Figure 7). This effect may lead to possible side effects and therefore should be avoided when drug delivery systems are designed.
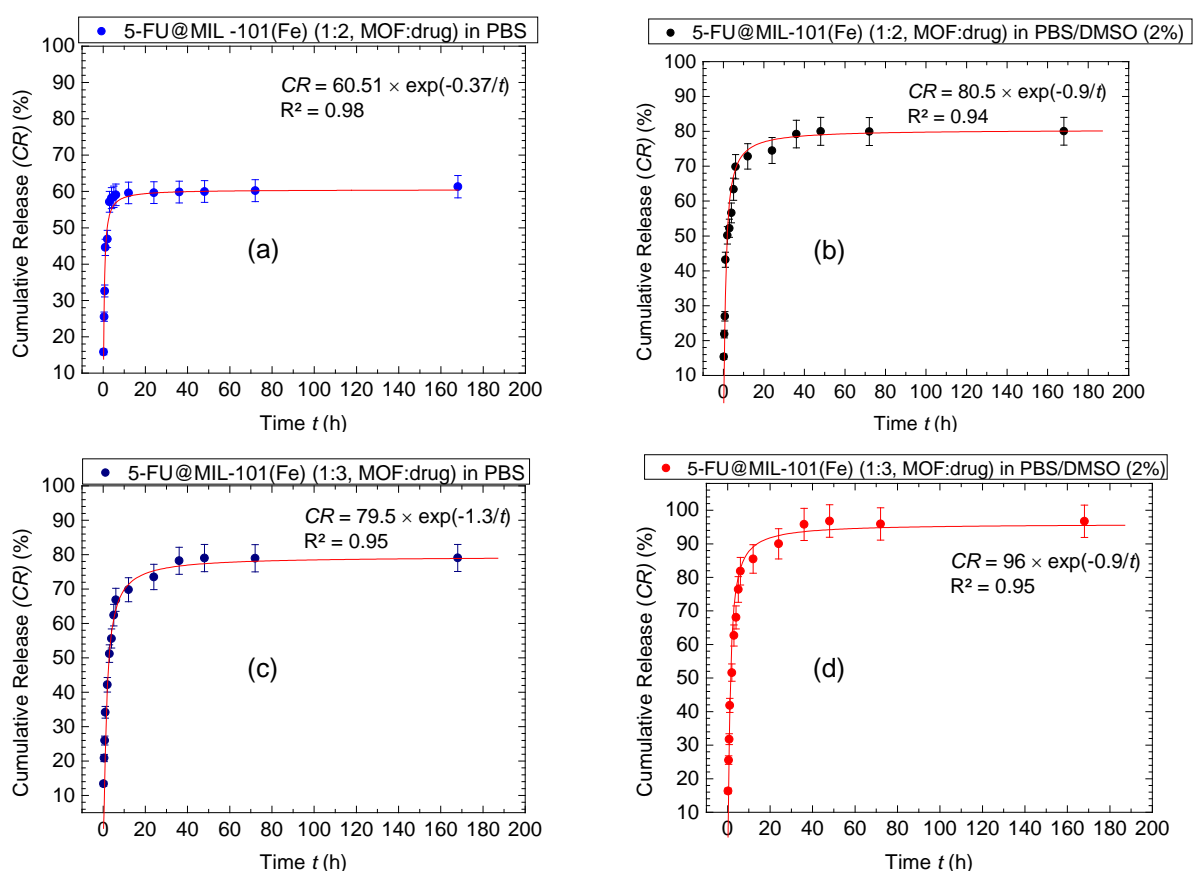

Figure 7. Cumulative release of 5-fluorouracil (5-FU) from (a) 5-FU@MIL-101(Fe) (1:2, MOF:drug) weight ratio in PBS, (b) 5-FU@MIL-101(Fe) (1:2, MOF:drug) weight ratio in PBS/DMSO (2%), (c) 5-FU@MIL-101(Fe) (1:3, MOF:drug) weight ratio in PBS, and (d) 5-FU@MIL-101(Fe) (1:3, MOF:drug) weight ratio in PBS/DMSO (2%).

As proposed in Chapter 3, the modulation with SLS was also proposed for the 5-FU@MIL-101(Fe) system which was incorporated into a PA-12 matrix. With the application of SLS, it was possible to decrease the amount of 5-FU released into the system by extending its period of release up to 30 days, therefore being an effective way to overcome the burst effect (Figure 8).
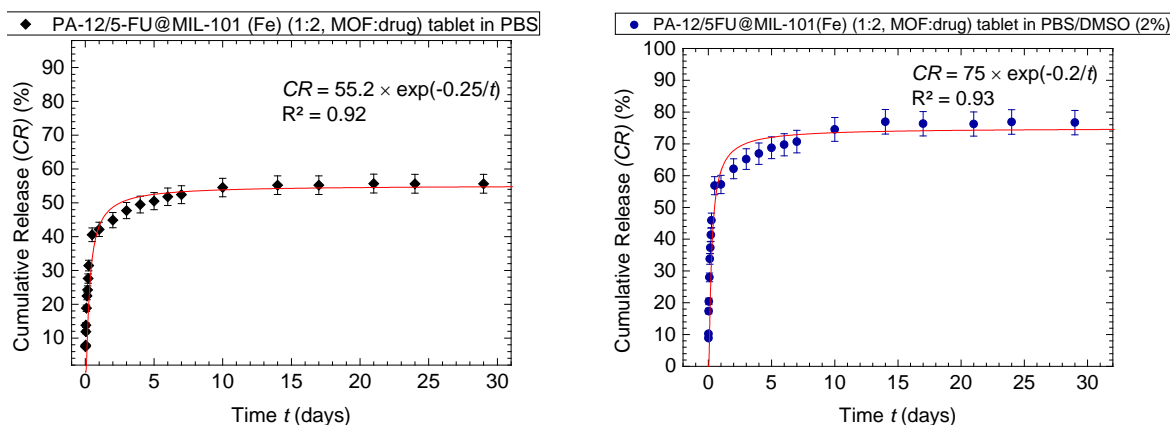

Figure 8. Left: Cumulative release of 5-FU from a PA-12/5FU@MIL-101(Fe) (1:2, MOF:drug) sample in PBS (tablets of PA-12/5-FU@MIL-101(Fe)). Right: Cumulative release of 5-FU from a PA-12/5FU@MIL-101(Fe) (1:2, MOF:drug) sample in PBS/DMSO (2%) (tablets of PA-12/5-FU@MIL-101(Fe).

The same ratios and media (PBS and PBS/DMSO (2%)) were applied for capecitabine, where an encapsulation efficiency of 53 wt% (1:2, MOF:drug) and 31 wt% (1:3, MOF:drug) was observed after 48 h in MIL-101(Fe). Nonetheless all the encapsulated capacetabine@MIL-101(Fe) samples also presented the possibility to develop a burst effect (Figure 9).
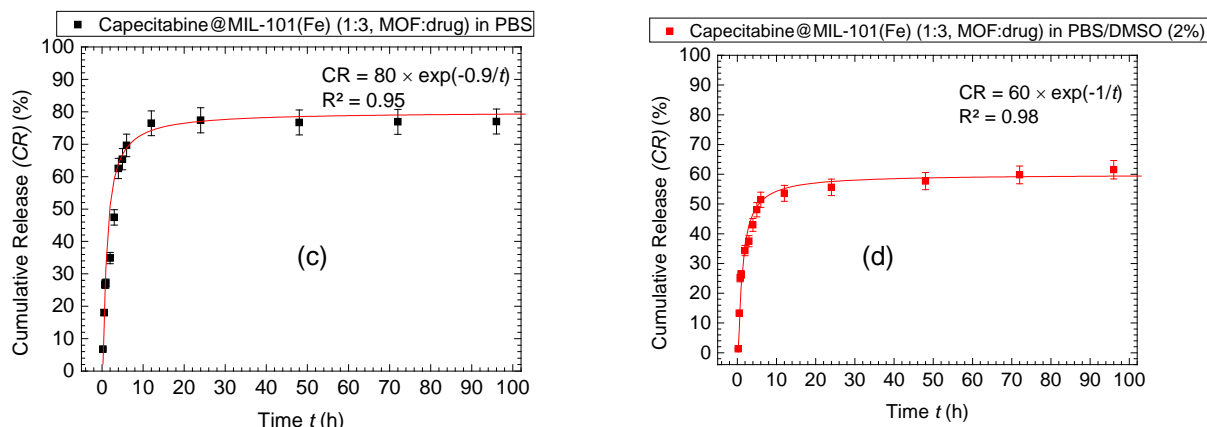

143
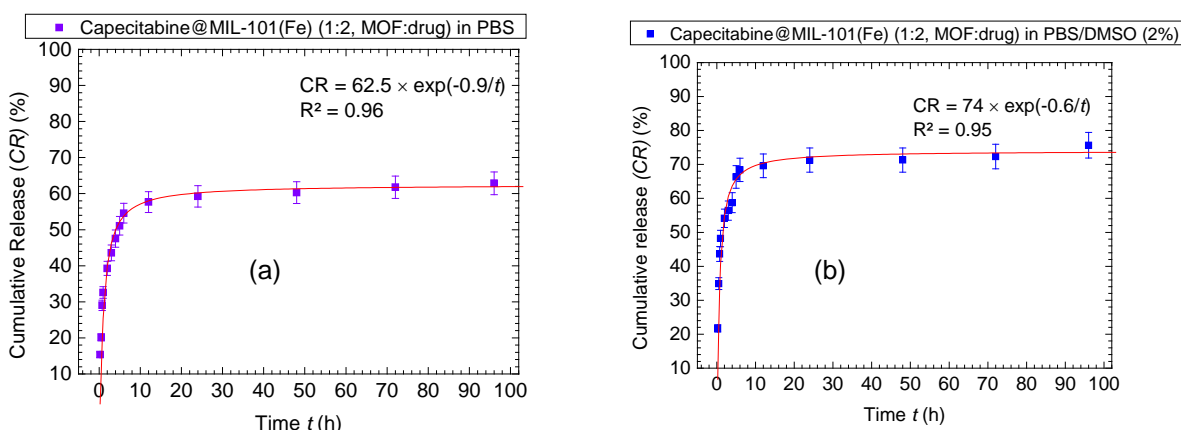
Figure 9. Cumulative kinetic release of capecitabine from (a) capecitabine@MIL-101(Fe) (1:2, MOF:drug) weight ratio in PBS, (b) capecitabine@MIL-101(Fe) (1:2, MOF:drug) weight ratio in PBS/DMSO (2%), (c) capecitabine@MIL-101(Fe) (1:3, MOF:drug) weight ratio in PBS, and (d) capecitabine@MIL-101(Fe) (1:3, MOF:drug) weight ratio in PBS/DMSO (2%).

3. Conclusion

In conclusion, the main aspects of this dissertation project, i.e., synthesis, encapsulation and release studies of selected drugs, have revealed very promising results for future developments. By incorporating the drug@MOF systems into a PA-12 matrix employing the SLS technique, it was possible to extend the release for longer periods of time (up to one month) avoiding high release rates of the respective drugs into the surrounding media within a few hours. The potential to apply 3D printing in the design of drug delivery systems has revealed a promising new approach for drug delivery.

4. Bibliography

[1] M. Rahman *et al.*, "Three 'D's: Design approach, dimensional printing, and drug delivery systems as promising tools in healthcare applications," *Drug Discov. Today*, **2021**, *26*, 2726–2733; doi: https://doi.org/10.1016/j.drudis.2021.06.016.

[2] J. W. Stansbury and M. J. Idacavage, "3D printing with polymers: Challenges among expanding options and opportunities," *Dent. Mater.*, **2016**, *32*, 54–64; doi: 10.1016/j.dental.2015.09.018.

[3] K. M. L. Taylor-Pashow, J. Della Rocca, Z. Xie, S. Tran, and W. Lin, "Postsynthetic modifications of iron-carboxylate nanoscale metal-organic frameworks for imaging and drug delivery," *J. Am. Chem. Soc.*, **2009**, *131*, 14261–14263; doi: 10.1021/ja906198y.

[4] M. Zheng, S. Liu, X. Guan, and Z. Xie, "One-step synthesis of nanoscale zeolitic imidazolate frameworks with high curcumin loading for treatment of cervical cancer," *ACS Appl. Mater. Interfaces*, **2015**, *7*, 22181–22187; doi: 10.1021/acsami.5b04315.

[5] Z. Moussa, M. Hmadeh, M. G. Abiad, O. H. Dib, and D. Patra, "Encapsulation of curcumin in cyclodextrin-metal organic frameworks: Dissociation of loaded CD-MOFs enhances stability of curcumin," *Food Chem.*, **2016**, *212*, 485–494; doi: 10.1016/j.foodchem.2016.06.013.

[6] K. I. Priyadarsini, "The chemistry of curcumin: From extraction to therapeutic agent," *Molecules*, **2014**, *19*, 20091–20112; doi: 10.3390/molecules191220091.

[7] C. Li *et al.*, "Hierarchical hollow Fe_2O_3 @MIL-101(Fe)/C derived from metal-organic frameworks for superior sodium storage," *Sci. Rep.*, **2016**, *6*, 1–8; doi: 10.1038/srep25556.

[8] V. R. Yadav, S. Suresh, K. Devi, and S. Yadav, "Effect of cyclodextrin complexation of curcumin on its solubility and antiangiogenic and anti-inflammatory activity in rat colitis model," *AAPS PharmSciTech*, **2009**, *10*, 752–762; doi: 10.1208/s12249-009-9264-8.

5. Publications on the topic of the doctoral thesis

[1] Elmeri Lahtinen, **Rafaella L. M. Precker,** Manu Lahtinen, Evamarie Hey-Hawkins, Matti Haukka. Selective Laser Sintering of Metal-organic Frameworks: Production of Highly Porous Filters by 3D Printing onto a Polymeric Matrix, *ChemPlusChem*, **2019**, *84*, 222–225.

[2] Andreia Valente, **Rafaella L. M. Precker**, Evamarie Hey-Hawkins in: Smart Inorganic Polymers, Inorganic Polymers for Potential Medicinal Applications (Book Chapter), *Wiley-VCH Verlag GmbH & Co. KGaA*, **2019**, ISBN: 978-3-52781-914-0.

[3] Vladimir V. Vinogradov, Andrey S. Drozdov, Leila R. Mingabudinova, Emiliya M. Shabanova, Nina O. Kolchina, Elizaveta I. Anastasova, Alina A. Markova, Alexander A. Shtil, Valentin A. Milichko, Galina L. Starova, **Rafaella L. M. Precker**, Alexandr V. Vinogradov, Evamarie Hey-Hawkins and Evgeny A. Pidko. Composites Based on Heparin and MIL-101(Fe): The Drug Releasing Depot for Anticoagulant Therapy and Advanced Medical Nanofabrication, *J. Mater. Chem. B*, **2018**, *6*, 2450–2459.